UNIVERSITÀ DEGLI STUDI DI TRIESTE

XXX CICLO DEL DOTTORATO DI RICERCA IN

Ambiente e Vita – Environmental Life Sciences

The role of atmospheric inputs in Dissolved Organic Matter dynamics: the Mediterranean Sea case

Settore scientifico-disciplinare: **BIO/07 Ecologia**

Ph.D. student
Yuri Galletti

Ph.D. program Coordinator
Prof. Giorgio Alberti

Thesis Supervisor
Dott.ssa Paola Del Negro

Thesis Co-Supervisor
Dott.ssa Chiara Santinelli

ANNO ACCADEMICO 2016/2017

UNIVERSITÀ DEGLI STUDI DI TRIESTE

XXX CICLO DEL DOTTORATO DI RICERCA IN

Ambiente e Vita – Environmental Life Sciences

The role of atmospheric inputs in Dissolved Organic Matter dynamics: the Mediterranean Sea case

Settore scientifico-disciplinare: **BIO/07 Ecologia**

Ph.D. student
Yuri Galletti

Ph.D. program Coordinator
Prof. Giorgio Alberti

Thesis Supervisor
Dott.ssa Paola Del Negro

Thesis Co-Supervisor
Dott.ssa Chiara Santinelli

ANNO ACCADEMICO 2016/2017

“Imagine a giant asteroid on a direct collision course with Earth. That is the equivalent of what we face now -the climate change-, yet we dither taking no action to divert the asteroid”.

James Hansen

Contents

General abstract

Marine dissolved organic matter (DOM) represents the largest and least understood reservoir of organic carbon on the Earth. It contains about 662 Pg C, a pool almost equivalent to the atmospheric CO_2. The Mediterranean Sea (Med Sea) is a low-nutrient-low chlorophyll (LNLC) area and receives different types of compounds (inorganic and organic) from the atmosphere via wet or dry deposition. In addition, it shows dissolved organic carbon (DOC) concentrations and distribution similar to those observed in the oceans, it can therefore be considered as a natural laboratory to gain information about the role of atmospheric deposition in DOM dynamics.

The main goals of this study are: (1) to investigate the optical properties (absorption and fluorescence) of the chromophoric DOM (CDOM) in a large open sea area of the Med Sea; (2) to quantify the annual fluxes of atmospheric DOC, DON and DOP, and the atmospheric C:N:P molar ratio at the island of Lampedusa, and to investigate the optical properties CDOM in the atmospheric depositions and compared with those of marine CDOM; (3) to assess the impact of atmospheric deposition in DOM dynamic, carrying out a dust addition experiment in the Northern Red Sea.

The first part of this work was devoted to study the CDOM dynamics in a large open sea area of the Med Sea and to compare these data with oceanic observations. The absorption and fluorescence data are the first ones reported for a vast open sea area of the Med Sea. In general, the CDOM optical properties and dynamics is similar in the Med Sea and in the oceans, even if some differences can be highlighted. The parallel factorial analysis (PARAFAC) applied to the 103 fluorescence excitation-emission matrixes allowed for the identification of five components: two terrestrial humic-like, one marine humic-like, one protein-like and one PAH-like. The humic-like substances dominated in the Med Sea with respect to the oceans and showed higher wavelengths of excitation and emission than in the oceans, suggesting a predominance of terrestrial substances in this basin. In agreement with oceanic observations, no relationship was observed between DOC and CDOM distribution. The protein-like fluorescence showed the highest intensity in the surface layer and a gradual decrease with depth, with vertical profiles similar to those of DOC. The occurrence of a PAH-like component was in agreement with the recent observation that there is an important net atmospheric input of PAHs to the open sea waters of the WM and the Ionian Sea - Sicily Region. The presence of terrestrial humic-like as well as PAH-like substances was relevant in the open sea waters of the Med Sea,

suggesting that the atmosphere can be an important external source of allocthonous (humic-like, yellow substances) material, in agreement with recent radiocarbon data for DOC in the Med Sea. The second part of the work was devoted to the study of atmospheric deposition collected at the ENEA Station for Climate Observations (35.52°N, 12.6°E, Lampedusa Island, Italy). Lampedusa is far from continental areas and from relevant pollutant sources and it is therefore located in an ideal position for the study of atmospheric DOM fluxes. DOC fluxes ranged between 0.06 and 1.78 mmol C m^{-2} day^{-1}, with a marked variability, these data were in the range of DOC atmospheric values reported in literature. The PARAFAC applied to 91 EEMs validated a seven-component model: four humic-like, two protein-like and one PAH-like mixture. The spectra of these components are similar to those observed in the open waters of the Med Sea and in the oceans. Atmospheric depositions of DOP and DON, and the C:N:P stoichiometric ratio were also studied. DON fluxes ranged between $1.5 \cdot 10^{-3}$ and 0.25 mmol m^{-2} d^{-1}, while DOP fluxes ranged between 0 and $2.7 \cdot 10^{-3}$ mmol m^{-2} d^{-1}. C:N:P molar ratios in atmospheric DOM showed a marked variability, with average values of 1909:292:1. The atmospheric fluxes and elemental ratios of DOM were in good agreement with depositions measured in the north-western Mediterranean Sea, although in different periods.

The preliminary results of a mesocosm experiment of dust addition, carried out in the Northern Red Sea in July 2017, showed an indirect effect of dust addition on DOM dynamics, the carbon content of dust was too low to determine an increase of DOC after the addition, but the changes in the ecosystems were responsible for a marked increase in DOC 20 hours after the dust addition. This observation can be explained by the release of DOC in situ by microbes stimulated by dust addition.

Milestones of my PhD project

- November 2014 - January 2015: I studied the basic processes occurring in the atmosphere with particular attention to organic aerosol. I followed some lectures on Atmospheric Chemistry by Prof. Maurizio Persico at Pisa University.
- March 2015: the first Italian atmospheric DOM deposition sampler was deployed at the Station for Climate Observations “Roberto Sarao” ENEA, Lampedusa Island.
- September - Dicember 2015: I won a 3.5 months fellowship (GORI) at the Woods Hole Oceanographic Institution (WHOI, US). In this period I worked under the supervision of Dr. Daniel Repeta, (Marine Chemistry & Geochemistry Department) on DOP. In the first period I learnt the orthophosphate quantification by using the molybdenum blue method with the persulfate oxidation, then I studied the Enzymatic hydrolysis of DOP by alkaline phosphatase (APase) using oceanic samples. The expertise, acquired thanks to this fellowship, allowed me to quantify DOP in atmospheric deposition.
- June 2016: I participated in the international oceanographic cruise “Argon” in the Western Mediterranean Sea. The cruise was carried out on-board of the Spanish Research Vessel *Garcia del Cid* (Chief scientist: Dr. Antonio Delgado Huertas, Spanish National Research Council). The work carried out was sampling and filtration of the samples for DOC, CDOM and FDOM analysis.
- September 2016: I participated in the 41st CIESM Congress Kiel with the presentation: *Total atmospheric deposition of dissolved organic carbon (DOC) at the Lampedusa Island*.
- May 2017: I won the *Progetto Professionalità Ivano Becchi*, funded by Fondazione Banca del Monte di Lombardia, an Institution of banking origin, that was established in 1992 in Pavia, Italy. The project aimes to give bright young professionals the opportunity to deepen their knowledge in their respective fields. This project gave me the funds to travel and all-inclusive financial support, including insurance expenses. My project, named “Sviluppare Resilienza”, concerned the field of scientific research. It had as main objective the study of air-sea interaction in order to improve the knowledge on atmospheric deposition of DOM.
- May 2017: Atmospheric samples were analyzed for DON and DOP at the Mediterranean Institute of Oceanography (MIO) (Marseille, France), thanks to the

project Atmospheric input of Dissolved ORganic mattEr to the Mediterranean Sea (ADORE), funded in the framework of the Galileo Program from the Università Italo Francese (Italian responsible C. Santinelli, French responsible E. Pulido-Villena). This project allowed me to work for 1 month at the MIO under the supervision of Dr. Elvira Pulido-Villena.

- June 2017: Dust addition experiment was carried out in Lampedusa (Italy, *Professionalità* project).
- July 2017: Dust addition experiment was carried out in Haifa (Israel, *Professionalità* project).

I devoted a lot of efforts to search for funds in order to cover my salary and to have the financial support for my PhD project.

Acknowledgments

I would like to thank my supervisor Chiara for her enthusiasm and dedication. She is my mentor, she supported me during all my experiences and, thanks to her, I discovered the beauty of scientific research. Thanks to the rest of the group, Simona, Margherita, Stefano and Giancarlo, and to the institute of biophysics (CNR, Italy) for having believed in me. Thanks to all of them, I became passionate about the study of DOM dynamics, I learned to work in a laboratory, to organize a research and to collaborate with international research groups.

I wish to express gratitude to three internationally renowned researchers that have been very helpful, honest, and transparent and worked with me with passion. To Daniel Repeta, that gave me the possibility to spend 3 months at his laboratory in Woods Hole. To Elvira Pulido-Villena, with whom I collaborated for the Galileo project funded by the Université Franco Italienne / Università Italo Francese and that allowed me to carry out the DOP and DON analysis, integrated in this present work, and to Eyal Rahav, with whom I carried out the dust addition experiment at Eilat, in Israel.

Many thanks to Damiano Sferlazzo, who performed the sampling of atmospheric DOM at the island of Lampedusa, making this study possible, to Alcide Giorgio di Sarra, head of the ENEA station, and Silvia Becagli, who made the metals analysis and PM_{10} measurement. They were always available for suggestions and advice.

Thanks to my two supervisors of Trieste: Serena Fonda Umani (Università di Trieste) and Paola Del Negro (Istituto Nazionale di Oceanografia e di Geofisica Sperimentale). Thanks for their availability.

This work would not have been possible without the contribution of the Banca del Monte di Lombardia foundation, which believed in me, and invested in my future. Thanks to Elisa Carraro, for supervising with enthusiasm the project funded by the foundation.

Glossary of abbreviations

a_{254} Absorption coefficient at 254 nm

a_{280} Absorption coefficient at 280 nm

BA bacterial abundance

BP bacterial production

BVOC biogenic volatile organic compound

CDOM Chromophoric Dissolved Organic Matter

Chl-a Chlorophyll-a

CTD Conductivity Temperature Density

DO Dissolved Oxygen

DOC Dissolved Organic Carbon

DOM Dissolved Organic Matter

DON Dissolved Organic Matter

DOP Dissolved Organic Matter

EEM Excitation-Emission Matrix

FDOM Fluorescent Dissolved Organic Matter

HULIC HUmic Like Substances

IPCC Intergovernmental Panel on Climate Change

IS Ionian Sea

LDOC Labile DOC

LNLC Low-Nutrient Low-Chlorophyll system

Med Sea Mediterranean Sea

NMR Nuclear Magnetic Resonance

OM Organic Matter

PAH Polycyclic Aromatic Hydrocarbon

PARAFAC PARAllel FACtor analysis

POC Particulate Organic Carbon

PP Primary Production

SLDOC Semi Labile DOC

$S_{275\text{-}295}$ Spectral slope calculated between 275 and 295 nm.

$S_{350\text{-}400}$ Spectral slope calculated between 350 and 400 nm.

S_r the ratio between $S_{275\text{-}295}$ and $S_{350\text{-}400}$

TDP Total Dissolved Phosphorous

TS Tyrrhenian Sea

TSN Total Soluble Nitrogen

WM Western Mediterranean Sea

WSOC Water-soluble organic carbon

INTRODUCTION

“Earth and sky, woods and fields, lakes and rivers, the mountain and the sea, are excellent schoolmasters, and teach some of us more than we can ever learn from books”.

John Lubbock

Introduction

Since the middle of the last century, the scientific community devoted a lot of efforts to understand the human impact on natural systems. In 1972 the report "*The Limits to Growth*" was presented by the Massachusetts Institute of Technology (MIT). This study was commissioned by the Club of Rome, an international think-tank founded by the Italian economist Aurelio Peccei. The report developed a theory which stated that every phase of strong economic growth would inevitably be followed by a major collapse of the system. This research showed that in the hypothesis of unaltered growth in population, industrialization, pollution, food production and consumption of natural resources, humanity would be constrained to live in the most basic conditions well before the year 2100. The report also recommended to reach a condition of ecological and economic equilibrium.

Despite this important study and the incredible debate around it, 46 years later the effects of human pressure on the Earth system is dramatically increased. We are actors of global change, we are triggering it, but at the same time we are suffering the consequences of our actions. In a few generations, humanity will exhaust the fossil fuels, that were generated over several hundred million years, causing large emissions of carbon dioxide (CO_2) and pollutants. We live in a new geological era: the Anthropocene. Every second, humanity consumes about 1,000 barrels of oil, 93,000 cubic meters of natural gas and 221 tons of coal. Today, global warming is unequivocal and its consequences are already manifesting on the natural environment.

In the marine environment, ocean acidification is one of the most alarming consequences of climate change. The oceans absorb a large fraction of the atmospheric CO_2 produced by the burning of fossil fuels. This absorption results in the build-up of carbonic acid in the water, and in the gradual acidification of the oceans. The decrease in pH affects corals and fish larvae as well as bivals and snails which produce calcareous shells, with a direct economic impact on fishery. The global carbon cycle is significantly impacted by the global consumption of fossil fuels. It is necessary to understand our imprint on this natural cycle, in particular at the microscopic level, in order to understand how humans can influence the dissolved organic matter (DOM) dynamics and composition. Williams et al. (2016) found that the quality of DOM in waters nearby or flowing through highly populated areas is strongly altered and this may have an impact on carbon cycles at a larger scale. Little is known about atmospheric deposition of DOM,

although it represents the main mechanism of carbon removal from the atmosphere. Therefore, it is crucial to study and comprehend the transfer of organic matter (OM) from atmosphere to the sea, and its impact on the marine ecosystem and food web.

1. Anthropocene

Earth is strongly impacted by human activities, that are significantly altering the environment at the global scale. Over the past few decades, evidence has mounted that planetary-scale changes are occurring rapidly (Steffen et al., 2006; Zalasiewicz et al., 2011). Human changes to the Earth System are multiple, complex and affect all the terrestrial sphere: the geosphere, the hydrosphere, the atmosphere and the biosphere. The magnitude and spatial scale of human-induced changes are unprecedented in the history of the Earth. The speed of these changes is on the order of decades to centuries (Steffen et al., 2006, 2011), and the impacts on the environment are outclassing natural processes (Crutzen, 2006). The impact of human activities on the Earth's made the scientists to introduce another geological epoch, the Anthropocene Era, a term proposed by Paul Crutzen and Eugene Stoermer (Crutzen and Stormer, 2000). The milestones of Anthropocene are:

- In the last 150 years humankind has exhausted 40% of the known oil reserves that took several hundred million years to generate;
- Nearly 50% of the land surface has been transformed by direct human action, with significant consequences for biodiversity, nutrient cycling, soil structure and climate;
- The production of nitrogen fertilizers and the N release by fossil fuel combustion are higher than its natural fixation in all terrestrial ecosystems;
- Underground water resources are being depleted rapidly in many areas;
- The concentrations of several climatically important greenhouse gases (e.g CO_2, CH_4 and N_2O), in addition to CO_2 and CH_4, have substantially increased in the atmosphere;
- Coastal and marine habitats are dramatically altered;
- About 22% of recognized marine fisheries are overused or already depleted, and 44% are at their limit of exploitation;
- Extinction rates are increasing quickly in marine and terrestrial ecosystems around the world; the Earth is now in the midst of its first great extinction event caused by the activities of a single biological species (mankind).

Anthropocene is also termed the “great acceleration” of human activity since the industrial revolution in 1750. Recently, Ellis et al. (2016) identified the deep roots of this new era, trying to bring together both environmental and socio-cultural changes, that are closely connected (Fig. 1).

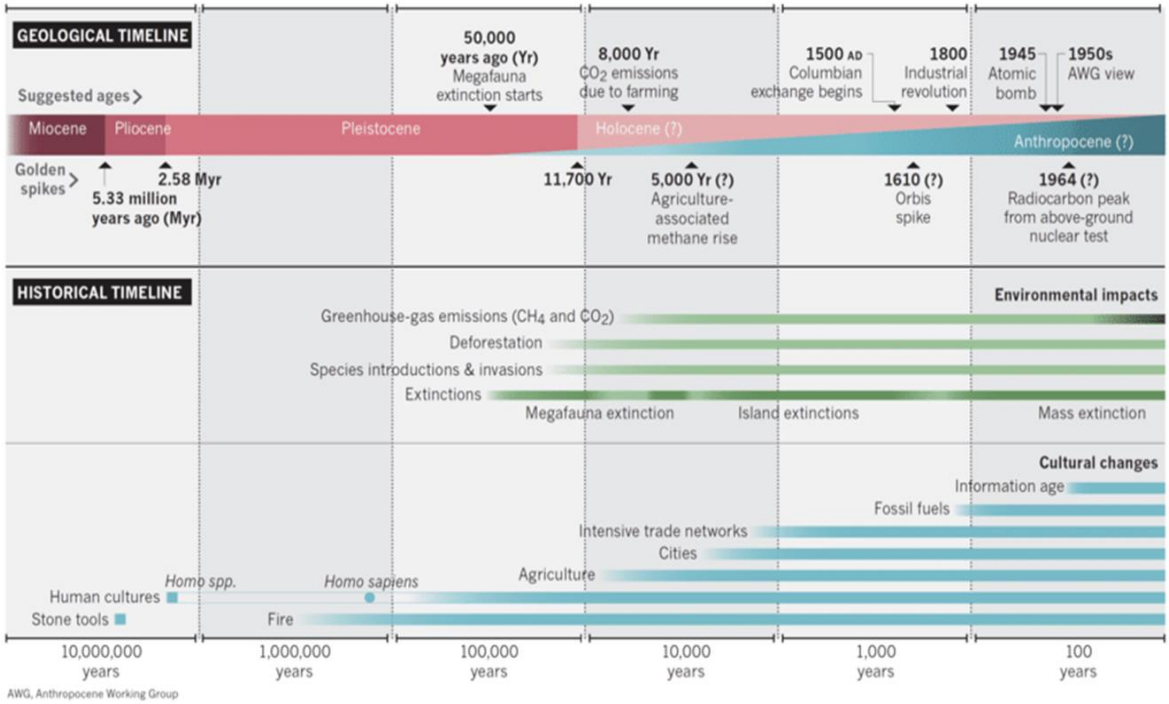

Figure 1. The deep roots of the Anthropocene (Ellis et al., 2016).

1.1 Climate change

The concentration of atmospheric CO_2 is increasing dramatically, mainly as a result of human activities (Seinfeld and Pandis, 2016). In recent years, CO_2 has received much attention because its concentration in the atmosphere has risen to ~30% above natural background levels and is expected to rise more in the near future. Scientists have shown that this increase is the result of human activities that occurred over the last 150 years (Seinfeld and Pandis, 2016). The carbon fluxes involve natural processes that have regulated the carbon cycle and atmospheric CO_2 levels for millions of years. The modern-day carbon cycle also includes several relevant fluxes developed from human activities, such as the combustion of fossil fuels and the change in land use. In geological terms, the combustion of fossil fuels (coal, oil and natural gas) can be viewed as a new and relatively rapid flux of large amounts of carbon to the atmosphere. These materials contain carbon that was captured by living organisms over periods of millions of years and has been stored in various places within the Earth's crust (Steffen et al., 2006). Since the onset of

the industrial revolution, these fuels have been mined and combusted at increasing rates and have served as a primary source of the energy that drives modern industrial human civilization. According to the 5th IPCC report (IPCC 2014), the anthropogenic CO_2 emission to the atmosphere has been increasing yearly. In 2004 it was estimated at 10.4 Pg C $year^{-1}$, being remarkably higher (by 80%) than the emission recorded in 1970. At today, fossil fuel combustion produces 6-8 Pg CO_2 $year^{-1}$ (Lord et al., 2016).

With the growth of the human population, a considerable amount of the Earth's land surface has been converted from natural ecosystems to farms and urban areas. Forests and other native ecosystems generally contain more carbon than the cover types they have been replaced with, these changes have therefore resulted in a net flux of ~1.5 Pg CO_2 y^{-1} to the atmosphere (Klein Goldewijk et al., 2011).

CO_2 is a greenhouse gas, its concentration in the atmosphere exceeds 400 ppm (in 2011 it was 390 ppm, Fig. 2), its increase is the most probable cause of the observed rise in global temperatures (Anderson and Peters, 2016) (Fig. 2). Scientists, governments, policymakers, economists and industry leaders are engaged in the process to design a broad international program to understand, predict and manage climate change (IPCC, 2014).

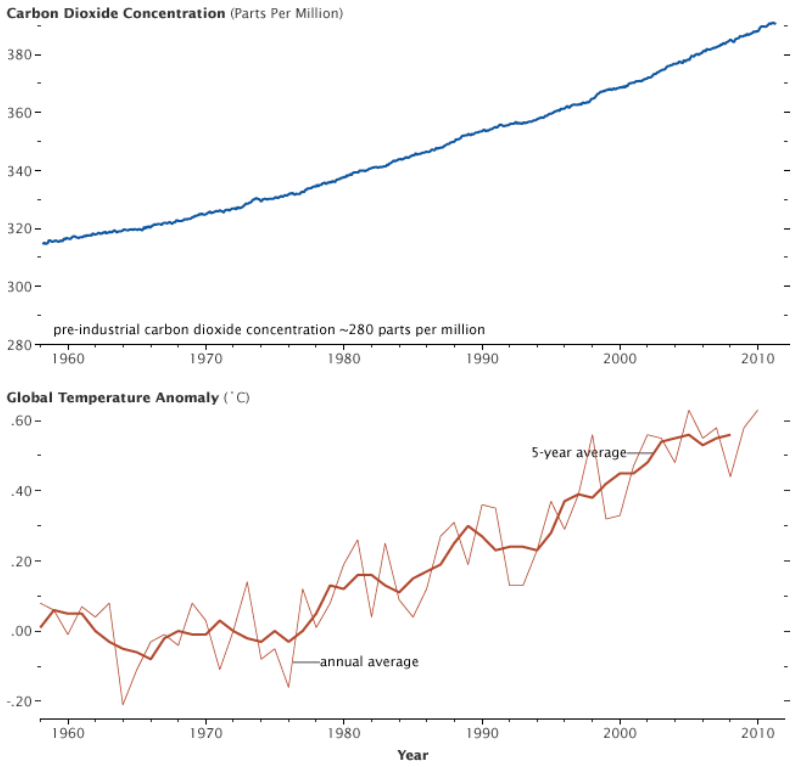

Figure 2. Global annual average temperature and carbon dioxide concentrations (above) (Anderson and Peters, 2016).

2. Global carbon cycle

The global carbon cycle (Fig. 3) is made up of a series of exchanges between its reservoirs; carbon flows through atmospheric inorganic carbon and living and non-living matter present in the ocean and land. Any change in the cycle, that shifts carbon out of one reservoir, puts more carbon in the other reservoirs. Globally, the carbon cycle plays a key role in regulating the Earth's climate by controlling the concentration of CO_2 in the atmosphere.

Most of the Earth's carbon is stored in sedimentary rocks within the planet's crust (100,000,000 PgC), while the rest is in the ocean, atmosphere, plants, soil, and fossil fuels. These are rocks produced either by the hardening of mud (containing organic matter) into shale over geological time, or by the collection of calcium carbonate particles, from the shells and skeletons of marine organisms, into limestone and other carbon containing sedimentary rocks. Fossil fuels (hydrocarbons) are about 4,000 PgC, and it formed over millions of years from ancient living organisms. Terrestrial ecosystems contain carbon in the form of plants, animals, soils and microorganisms (bacteria and fungi). The Earth's plants store approximately 560 PgC, with the wood in trees being the largest fraction, while 1,500 PgC are stored in the global soils.

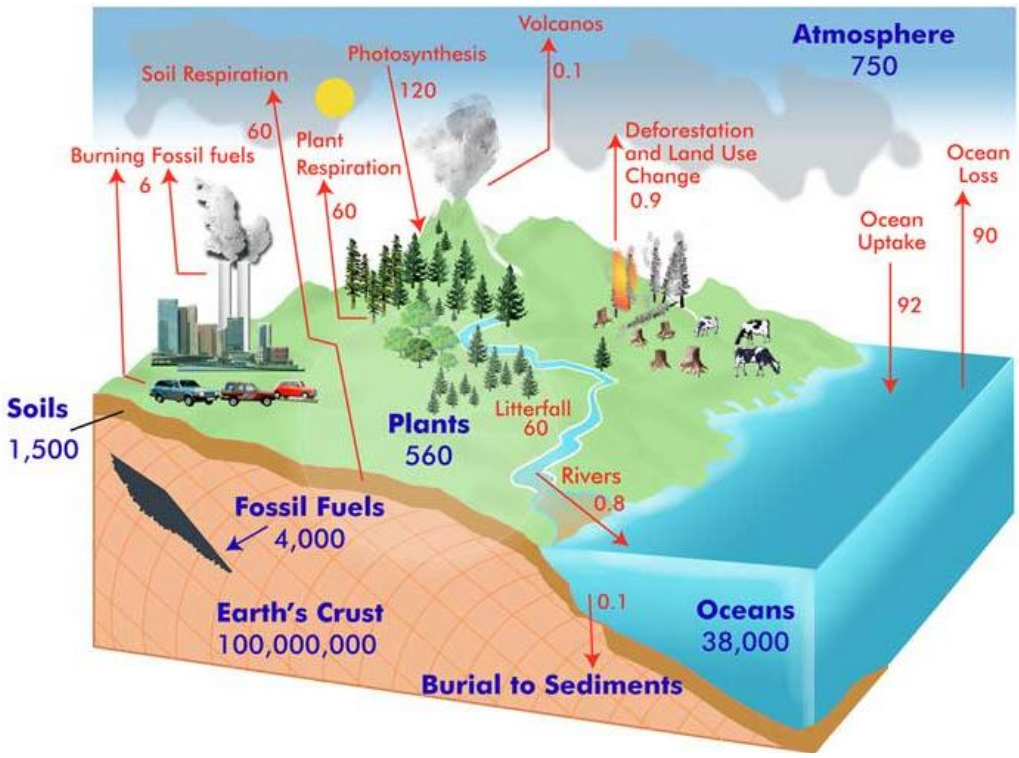

Figure 3. The global carbon cycle. Pool sizes, shown in blue, are given in petagrams (Pg) of carbon. Fluxes, shown in red, are in Pg per year (Source: *www.globe.gov/projects/carbon*).

The atmosphere contains approximately 750 PgC, most of it is in the form of CO_2, with much smaller amounts of methane (CH_4) and various other compounds. Although this amount is considerably less than that contained in the oceans or the Earth's crust, it is of vital importance because of its influence on the climate.

The ocean contains the largest active pool of carbon of the Earth (38,000 PgC), most of which is in the form of dissolved inorganic carbon stored at great depths where it resides for long periods of time. The largest reservoir of organic carbon on the Earth is also contained in the oceans as DOM. The detailed description of the marine carbon cycle is reported in the next paragraphs.

2.1 Marine carbon cycle

Carbon occurs in the marine environment (Fig. 4) mainly in three forms:

(1) the dissolved inorganic carbon (DIC), in the form of carbonate (CO_3^{2-}) and bicarbonate ions (HCO^{3-}). DIC represents the largest resource of carbon globally, estimated at 98% (about 38.000 Pg) of the total carbon that occurs in water (Emerson and Hedges 2008). Atmospheric CO_2 dissolves in the water, following the Henry's law, then it reacts with water to form carbonic acid (H_2CO_3) which dissociates into HCO^{3-} and CO_3^{2-}. The carbonate is found in the sediments as calcium carbonate ($CaCO_3$) in the form of aragonite and, less frequently, of calcite. The CO_2 concentration of surface waters systematically undergoes both seasonal and day-to-day cyclic variations, due to its involvement in photosynthesis. The CO_2-HCO^{3-}-CO_3^{2-} system is the main mechanism for the pH control and the alkalinity of seawater. These components form the so-called carbonate buffer (weak acid and its salts with strong bases). Carbonate buffer balance is described with dissociation and decay constants of H_2CO_3 (Sarmiento and Gruber, 2006). The pH of seawater is generally between 7.0 and 8.5 with an average of 8.2.

(2) the dissolved organic carbon (DOC), which contains about 662 Pg C, a pool equivalent to the atmospheric CO_2 (Fasham et al., 2001; Hansell et al., 2009). Such similarity between these two pools implies that the net oxidation of only 1% of the marine DOM pool within 1 year would be sufficient to generate a CO_2 flux larger than the one produced annually by fossil fuel combustion (Hansell and Carlson, 2001). DOC represents the biggest reservoir of organic

carbon on Earth (Hedges, 2002; Hansell et al., 2009) and plays a crucial role in carbon cycling on a global scale (Zepp et al., 2007; Hansell et al., 2009).

(3) the particulate organic carbon (POC), that represents the smallest reservoir (30 Pg). It is involved in carbon export to depth and sequestration in the sediments (Emerson and Hedges, 2008). Concentrations of POC are determined mainly by the occurrence of phytoplankton and detritus, representing the largest input to the suspended organic matter. Zooplankton and bacteria contribution is much less significant (Stein and Macdonald 2004). POC concentration in sea water is 10–20 times lower than DOC concentration (Hansell, 2002; Gardner et al., 2006), and is subject to a large spatial and seasonal variability.

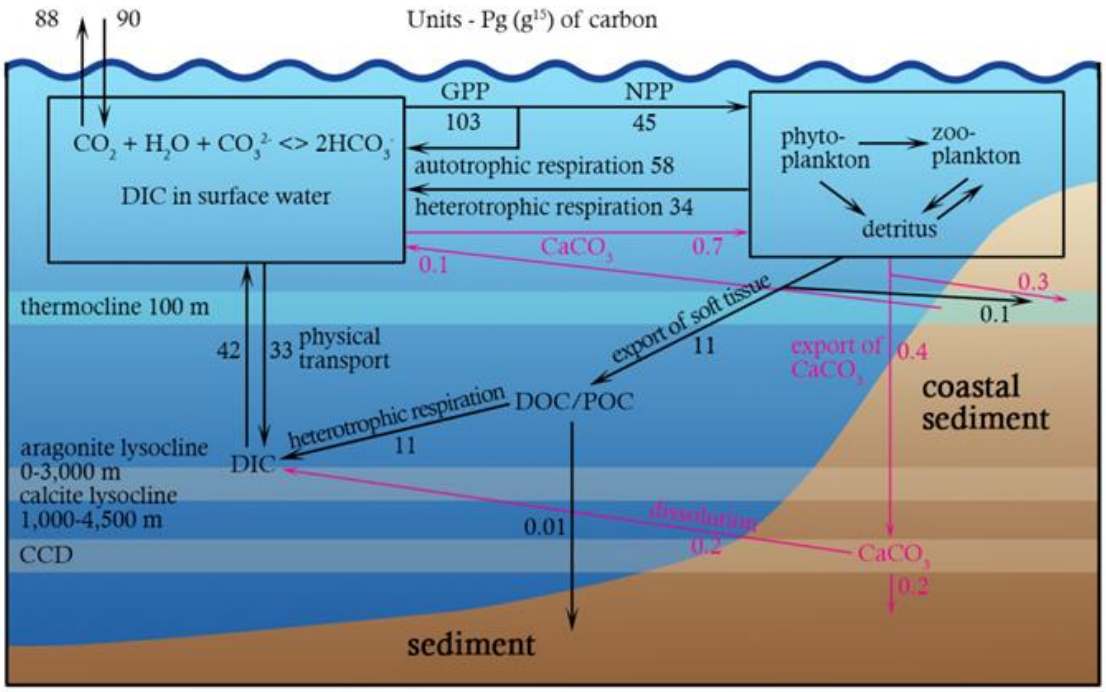

Figure 4. The marine carbon cycle. GPP= gross primary productivity; NPP= net primary productivity; CCD=carbonate compensation depth (Source: *http://www.geochembio.com/ecology/climate-components/carbon-cycle.html*).

The marine carbon cycle is determined by a number of physical, chemical, and biological factors that are cross-related. To a large extent, the cycle is controlled by phytoplankton activity (Dzierzbicka-Głowacka et al., 2010). Absorption and assimilation of dissolved CO_2 by phytoplankton leads to disequilibria in the gas partial pressures between

seawater (lower) and the atmosphere (higher), causing a net flux of CO_2 into the water. The processes that move carbon from the surface to the deep layers are divided into four conceptual components (Sarmiento and Gruber, 2006; Ridgwell and Arndt, 2015): (1) the "solubility" pump, (2) the "organic matter" pump, (3) the "carbonate" (or 'counter') pump, and (4) the "microbial carbon" pump (Jiao et al., 2010).

The **solubility pump** (Fig. 5) is the distribution of DIC between surface and the deep ocean. Since CO_2 is more soluble in cold than warm seawater, the diffusion of CO_2 occurs mainly at high-latitude in cold surface waters, where deep water forms. The rapid sinking of these dense waters and their redistribution in the deep ocean results in an efficient pumping of carbon from the atmosphere to the deep ocean (Ridgwell and Arndt, 2015). The thermohaline circulation allows this redistribution of water mass throughout the dark ocean until the lower latitudes where they warms up and upwells (Raven and Falkowski, 1999).

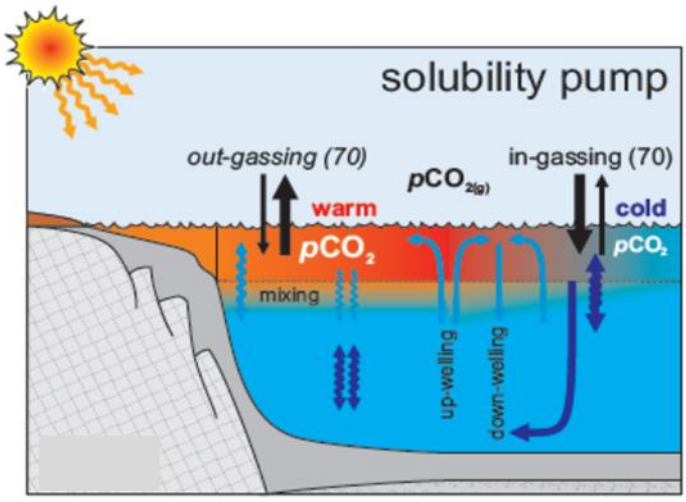

Figure 5. The solubility pump (Ridgwell and Arndt, 2015).

The **organic matter pump** (Fig. 6) refers to CO_2 transformation into organic substances that form biomass and to its sinking and mineralization in the deep waters (Honjo et al. 2008; Goldberg et al., 2009).

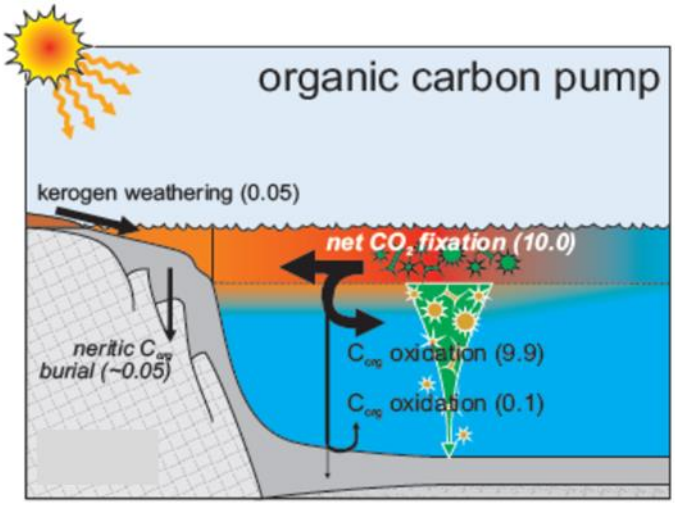

Figure 6. The organic carbon pump (Ridgwell and Arndt, 2015).

This pump, along with physical-chemical constraints on the solubility of CO_2, controls the pattern of CO_2 exchange between the oceans and the atmosphere (Raven and Falkowski, 1999; Raven et al., 2005). Phytoplankton photosynthesis reduces the amount of CO_2 in the surface layer of the ocean, thereby allowing more CO_2 to dissolve from the atmosphere. It is estimated that 50 Pg C y^{-1} is fixed by photosynthesis in the global ocean (Chavez et al., 2010). About 20% of the carbon fixed in the upper layers sinks towards the deeper layers. Most of this carbon is in the form of particulate matter (8 Pg C y^{-1}), and only 2 Pg C y^{-1} comes in the ocean interior as DOM (Hansell et al., 2009). The heterotrophic degradation of POC during sinking is highly efficient, with <1-6% of the POC export production reaching the seafloor, where just 0.3% of this flux, can be buried (Dunne et al., 2007; Ridgwell and Arndt, 2015). The POC deposited in the sediments participates in digenetic processes, conditioned largely by redox potential (Freudenthal et al., 2001; Rullkötter, 2006).

The **carbonate pump** (Fig. 7) concerns the precipitation of calcium carbonate ($CaCO_3$) and magnesium carbonate ($MgCO_3$) produced by calcifying organisms at the ocean surface. In particular, one group of phytoplankton, the coccolithophorids (such as *Emiliania huxleyi*) produces calcium carbonate platelets, and it is estimated that blooms of E. huxleyi cover about 1.4 million km^2 of the ocean every year (Müller et al., 2010). The carbonate pump is an efficient mechanism to sequester particulate inorganic carbon at the short time scale (Elderfield, 2002). It is very likely that around half of all carbonate

dissolves while it sinks (Feely et al., 2004); the rest of $CaCO_3$ reaches the sediment column, where ~20% can be buried (Feely et al., 2004).

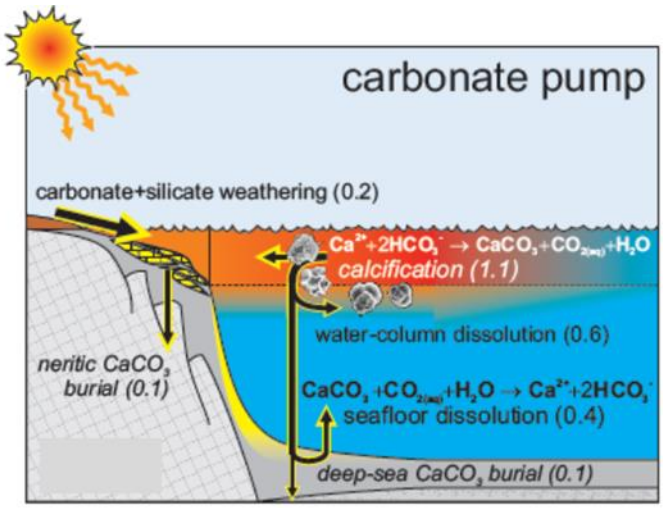

Figure 7. The carbonate pump (Ridgwell and Arndt, 2015).

These three pumps are also important components of the long-term carbon cycle, driving the accumulation, biogeochemical transformation, and burial of carbon in marine sediments (Ridgwell and Arndt, 2015).

Recently, the **microbial carbon pump (MCP)** has been proposed as an important mechanism of carbon sequestration (Fig. 8). It involves the net production of DOC by microbial processing. Indeed, a variable and substantial fraction of primary production (30-50%) is released as DOC (Ducklow et al., 1995; Biddanda and Benner 1997). This pump consists of the conversion of labile DOM into recalcitrant DOM (RDOM), which is not mineralized on the short temporal scale, and thus persists in the water column (Jiao et al., 2011). The biological lability of DOM and the different fractions individuated in DOM pool are discussed in detail in the next section (3. Dissolved organic matter (DOM)).

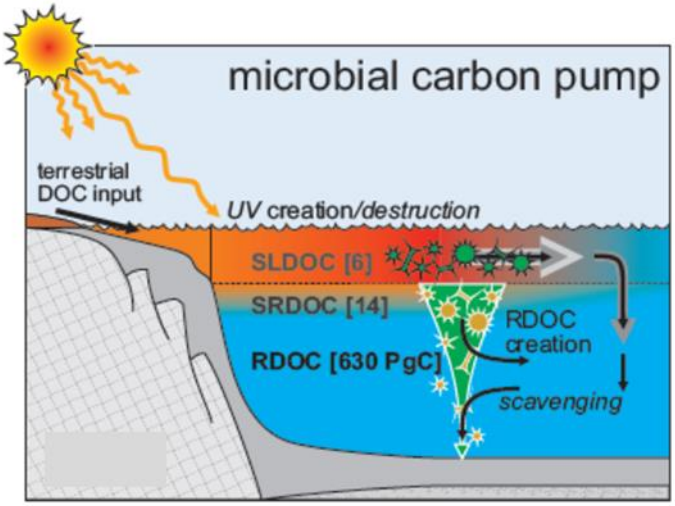

Figure 8. The microbial carbon pump (Ridgwell and Arndt, 2015).

Heterotrophic bacteria process about half of net primary production and thereby play a dominant role in the MCP by altering and transforming labile forms of DOM into recalcitrant forms that persist in the ocean (Jiao et al., 2010). The mechanisms of release of DOM by bacteria have been examined in bioassay experiments using labile substrates as sole carbon sources. Highly abundant lytic viruses may generate RDOM as they lyse most marine organisms and release the cellular material (Weinbauer et al., 2011). It was demonstrated that incomplete hydrolysis of organic matter by bacterial ectohydrolases could lead to RDOM formation as well (Ogawa et al, 2001). The MCP could alter the chemical composition of DOM, resulting in changing ratios of carbon to nitrogen, phosphorus and other elements (Hopkinson and Vallino, 2005). Lechtenfeld et al. (2015) observed that most of the molecules in bacterial DOM included essentially carbon, hydrogen and oxygen (49-52%), while nitrogen only counted for 31-37%.

Any substantial change in the consumption (or mineralization) rate of DOC pool could exert a large effect on atmospheric CO_2 concentration and climate. A variety of environmental factors such as oxygen availability and ecosystem or temperature changes could potentially trigger substantial changes in DOC pool (Ridgwell and Arndt, 2015). Legendre et al. (2015) proposed that the surface-ocean temperature increase or the ocean acidification could favor DOC production and enhance carbon sequestration by the MCP. On the other hand, a negative impact on this sequestration could descend by the consequences of climate change (such as the increase in anthropogenic nutrient supply via continental water and the atmosphere or the slowing down of the thermoaline circulation) (Jiao et al., 2014).

3. Dissolved organic matter (DOM)

Dissolved organic matter (DOM) is operationally defined as a complex mixture of organic molecules that passes through a 0.2 μm filter. DOM is ubiquitous in aquatic environments and represents the largest reservoir of reactive carbon on the Earth (Hansell et al., 2009). DOM plays a crucial role in the functioning of marine ecosystem, in that it is released at all levels of the food web as a byproduct of many trophic interactions and/or metabolic processes, and it represents the main source of energy for heterotrophic prokaryotes (Carlson and Hansell, 2015). The DOM binding activity and photo-reactivity regulates the speciation and bioavailability of trace metals such as iron, and can represent an important mediator in numerous photochemical reactions (Bergquist and Blum, 2007; Carlson and Hansell, 2015). Filtration is the method commonly used to separate the POC and DOC. The filtrate comprises: viruses, colloids, and dissolved substances, whereas zooplankton, phytoplankton, majority of bacteria and detritus remain on the filter (Fig. 9).

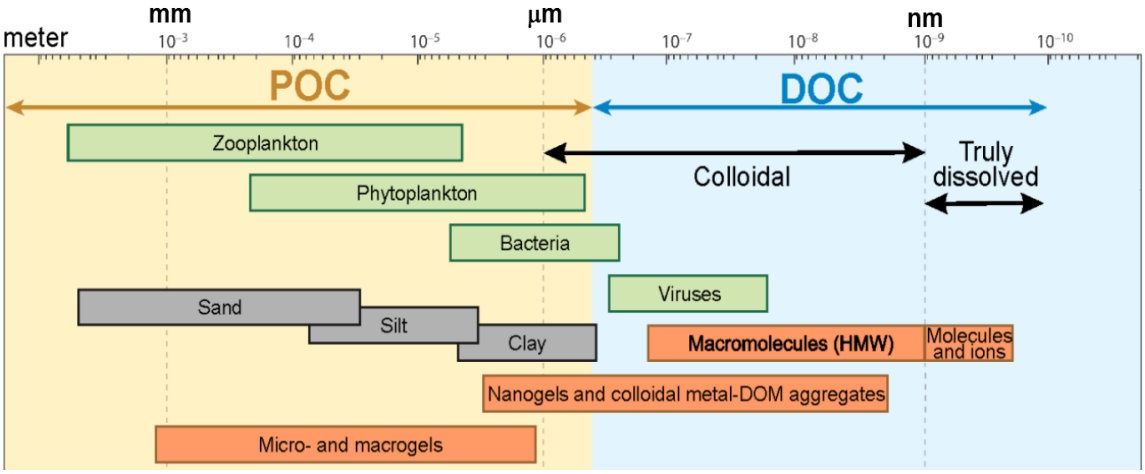

Figure 9.Carbon partitioning in seawater (Emerson and Hedges, 2008).

3.1. Biological lability of DOM

DOM bulk includes a heterogeneous class of organic molecules, with a wide range of bioreactivity (Carlson and Hansell, 2015). Various fractions have been distinguished in its pool depending on their lifetime (Fig. 10).

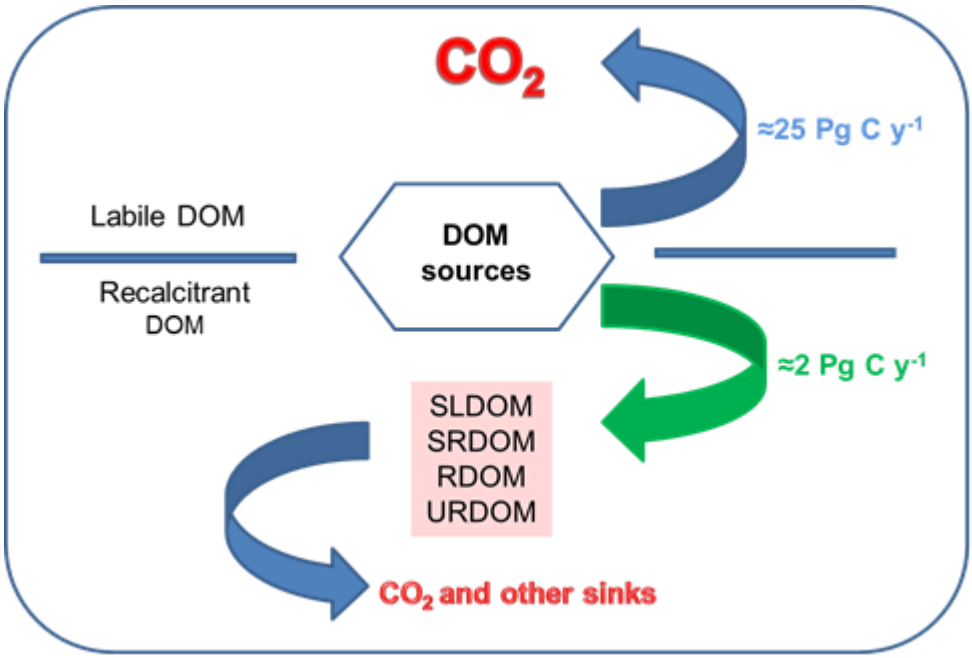

Figure 10. DOM classification (Hansell, 2013).

The Labile DOM (LDOM, lifetime=0.001 years) is rapidly consumed supporting the nutrient demands and the metabolic energy of the heterotrophic prokaryotes (Chavez et al., 2010). It accounts only 1% of the total ocean DOM inventory (Hansell, 2013). RDOM is resistant to rapid mineralization, it can therefore accumulate in the marine environment, creating the ocean stock of DOM (Hansell, 2013). RDOM can be further divided in 4 pools. The Semi-Labile DOM (SLDOM, lifetime=1.5 years) supports the microbial loop in the upper mesopelagic area (>500-1000 m) and is mineralized over months to years (Hansell and Carlson, 2013). The semi-refractory DOM (SRDOM, lifetime=20 years) is localized in the mesopelagic area, particularly in the oceanic regions with a permanent pycnocline. SRDOM is important in carbon sequestration over decades to centuries, since it is mineralized below the pycnocline and the respiratory output returns to the surface layer slowly (Hansell and Carlson, 2013). The refractory DOM (RDOM, lifetime=16000 years) plays the most critical role in long-term C sequestration, with spatial and temporal variations in its production and removal which impacts long-term carbon storage. RDOM accounts for more than 95% of the total DOM in the ocean, and it is involved in the MCP (see paragraph 2.1). RDOM is returned to the surface layer of the oceans over centuries to millennia by water masses circulation. The ultra-refractory DOM (URDOM, lifetime=40000 years) contains black carbon or Pyrogenic carbon (PyC), residue of the incomplete combustion of biomass and vegetation fires, that it is stored in soil and sediments, over decades to thousand years after (Singh et al., 2012). This material is also defined

thermogenic black carbon, and it is formed by the accumulation of polycyclic aromatic hydrocarbons (PAHs) (Dittmar and Paeng, 2009). Thermogenic black carbon could remain in the DOC pool for 2500-13900 ^{14}C-year, so it has radiocarbon ages much greater than ambient bulk deep DOC (Ziolkowski and Druffel, 2010). Black Carbon is not the only component of URDOM, some authors proposed that refractory DOM is predominantly composed by low molecular weight DOM (Amon and Benner, 1996; Benner, 2002; Nebbioso and Piccolo, 2013).

3.2 Sources and sinks of DOM in the oceans

DOM in the oceans can be produced in situ or transported from external sources such as the atmosphere, the rivers and the groundwater (Hansell, 2013; Repeta, 2015). The euphotic zone is the main site of organic matter production in the open sea waters. The processes of production include (i) extracellular release by phytoplankton, (ii) grazer-mediated release and excretion, (iii) release via cell lysis, (iiii) solubilization of detrital and sinking particles, and (v) release from prokaryotes (Carlson and Hansell, 2015).

The main processes of DOM removal are (i) biotic consumption (both prokaryotes and eukaryotes), and (ii) abiotic processes that include (1) phototransformation, (2) sorption of DOM onto particles, (3) condensation of marine microgels, and (4) hydrothermal circulation (Carlson and Hansell, 2015).

3.3. DOM molecular composition

The DOM pool includes compounds such as simple sugars, amino acids, lipids, vitamins and pigments, complex biopolymers (proteins, polysaccharides and lignins), and very complex degradation products of unknown origin (humic substances, black carbon). Most of its molecular composition is poorly known, <10% of DOM has been characterized at a molecular level (Repeta, 2015). Today there is not a technique to isolate the different compounds without losing many of its components; Nuclear Magnetic Resonance (NMR) and chemical analysis of hydrolysis products are the most successful techniques for the characterization of polysaccharides and proteins in the High Molecular Weight DOM (HMW DOM) (Repeta, 2015). ^{13}C NMR analysis showed the occurrence of carbohydrate peaks with almost the same position in samples (collected by ultrafiltration of surface seawater collected from the North Pacific Ocean using a polysulfone membrane with 1-nm pore size) (Repeta, 2015). ^{1}H NMR spectra was complementary to that of ^{13}C NMR analysis. The positions of carbohydrate peaks change little between samples, but changes

in their relative intensities are found (Repeta, 2015). These differences in intensity are observed with depth (Hertkorn et al., 2006), sampling location (Aluwihare et al., 1997) and across salinity gradients (Abdulla et al., 2010a,b) suggesting the presence of at least two major components in HMW-DOM pool. These two different fractions may be due to presence of a polysaccharide fraction consisting of acylated polysaccharide or hetetopolysaccharide (Aluwihare et al., 1997; Abdulla et al., 2010a,b) and a carboxyl acid-alkyl carbon-rich fraction referred to as carboxyl-rich aliphatic matter or carboxyl-rich compounds (Repeta, 2015).

A fast and efficient way to obtain indirect information on DOM molecular properties (aromaticity degree, molecular weight, occurrence of protein-like and humic-like substances) is the study of the optical properties (absorption and fluorescence) of its chromophoric fraction (Stedmon and Nelson, 2015). These properties are widely described in the following paragraphs.

4. Chromophoric dissolved organic matter (CDOM)

CDOM is the fraction of DOM that absorbs light over a broad range of ultraviolet (UV) and visible wavelengths (Fig. 11). CDOM is ubiquitous in natural waters and is the main factor controlling light penetration in open sea waters and in coastal regions with important implications on primary production and biological activity (Del Vecchio and Blough, 2004; Siegel et al., 2005). CDOM can protect marine organisms by ultraviolet radiation, harmful to phytoplankton and other light-sensitive organisms (Arrigo and Brown, 1996; Coble, 2007; Stedmon and Nelson, 2015). The absorption of CDOM increases exponentially with decreasing wavelength (Nelson and Siegel, 2013), UV radiation is consequently more rapidly attenuated than radiation in the PAR range (Tedetti and Sempere, 2006). The absorption of the UV wavelengths can lead to the photochemical degradation of CDOM, with transformation of its molecular properties (Vähätalo and Zepp, 2005; Stedmon et al., 2007). Its photo-reactivity plays a significant role in the biogeochemistry of natural waters through the formation of biologically available compounds that fuel the growth of microbes (Mopper and Kieber, 2002). CDOM absorption can induce the photochemical production of a number of important trace gases such as CO_2 or CO and dimethyl sulfide (Mopper and Kieber, 2002; Siegel et al., 2002). In coastal areas, influenced by rivers, where its concentration is high, CDOM may also have a negative effect on ecosystem productivity, limiting the visible light useful for primary production (Stedmon and Nelson, 2015), in these areas CDOM may also interfere with

satellite remote sensing retrieval of chl-a concentrations that are needed to estimate ocean primary productivity.

The principal sources of CDOM in the oceans are both allochthonous and autochthonous inputs. Allochthonous materials are primarily synthesized by terrestrial and freshwater plants and subsequently transported to the coastal area by rivers and atmosphere (by wet and dry deposition). Autochthonous substances are produced in the oceans by marine plants or phytoplankton and processed within the marine food web (Stedmon and Nelson, 2015).

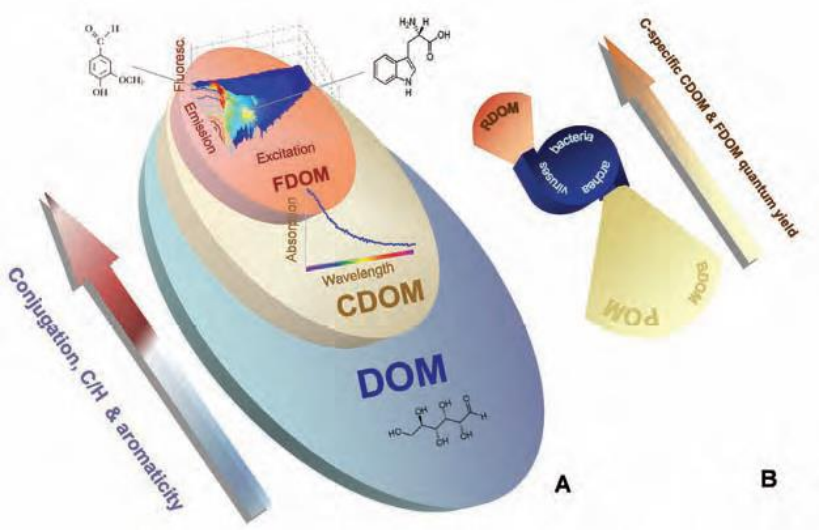

Figure 11. Scheme of the chromophoric (CDOM) and fluorescent (FDOM) fractions of the total DOM pool (Stedmon and Alvares-Salgado, 2011).

Aromatic amino acids (Yamashita and Tanoue, 2003, 2008), lignin, phenols and humic substances (Nelson and Siegel, 2013) represent the main groups of molecules occurring in CDOM pool.

5. Fluorescent dissolved organic matter (FDOM)

Fluorescent dissolved organic matter (FDOM) is the fraction of CDOM that fluoresces when irradiated in the UV or visible range (Fig. 11). The substances able to re-emit part of the absorbed light, are termed fluorophores. Although chromophores can have several absorption bands corresponding to the transition from ground state to several excited states, the fluorescence spectrum of a specific fluorophore normally has only one peak (Stedmon and Nelson, 2015). This is due to the transition of electrons from the

lowest excited state to the ground state. Aromatic compounds often show fluorescence, since they have not many vibrational degrees of freedom, in contrast to the aliphatic compounds, which are not fluorescent (Stedmon and Nelson, 2015).

The emission spectrum (Fig. 12) of FDOM is unstructured, and the fact that the decreasing of emission intensity is linked to the red-shifts of its maximum with increasing excitation wavelength suggests the presence of numerous absorbing and emission centers. The fluorescence properties of FDOM are limited to excitation wavelengths in the range 240-500 nm and emission wavelengths in the range 300-600 nm. At wavelengths <240 nm, the excitation intensity is too low, in standard fluorimeters, and inner filter effect is very high, in standard cuvettes, due to the high absorbance by CDOM (Stedmon and Nelson, 2015).

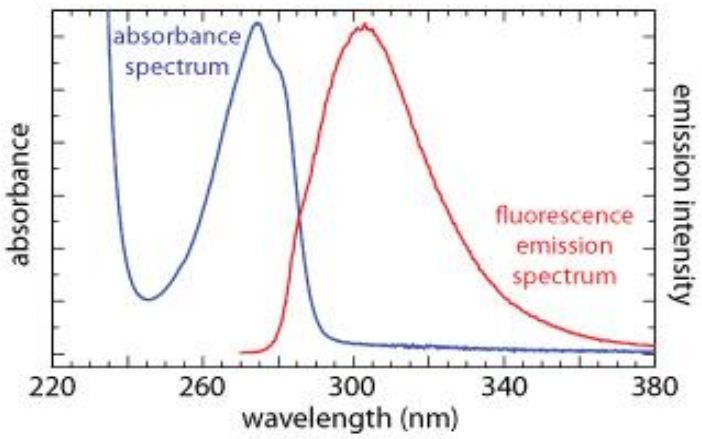

Figure 12. Absorbance and fluorescent emission spectra of tyrosine in a pH 7, 0.1 M phosphate buffer. The emission spectrum uses an excitation wavelength of 260 nm (Source: *http://community.asdlib.org/imageandvideoexchangeforum/2013/07/30/632/; created by David Harley from the original illustration* by Mark Samoza).

5.1 Fluorescence spectroscopy

Fluorescence spectroscopy is a sensitive technique often used for tracing the dynamics of DOM in marine and freshwaters (Stedmon and Bro, 2008). The excitation-emission matrix (EEM) spectroscopy is today commonly used to provide a complete picture of FDOM fluorescence properties. EEM spectroscopy measures emission spectra across a range of excitation wavelengths, then the spectra are combined in one 3D plot, which displays fluorescence emission intensity as a function of the excitation and emission wavelengths (Chen et al., 2003; Gentry-Shields et al., 2013). EEMs provide additional information about the relative fluorescence intensity and the possible sources (soil, fresh

and marine waters) of the various groups of fluorophores occurring in FDOM pool (Mopper and Schultz, 1993; Coble, 1996; Seritti et al., 1998; Stedmon and Markager, 2005a; Kowalczuk et al., 2009; Yamashita et al., 2010b). Changes in FDOM are also a good indicator of biological (Chen and Bada 1992; Nieto-Cid et al. 2006) and photochemical processes (Moran et al. 2000; Nieto-Cid et al. 2006) determining a change in the bulk DOM pool. EEMs allow the visualization of fluorophores in their relative positions in optical space as a 3-dimensional surfaces (Fig. 13).

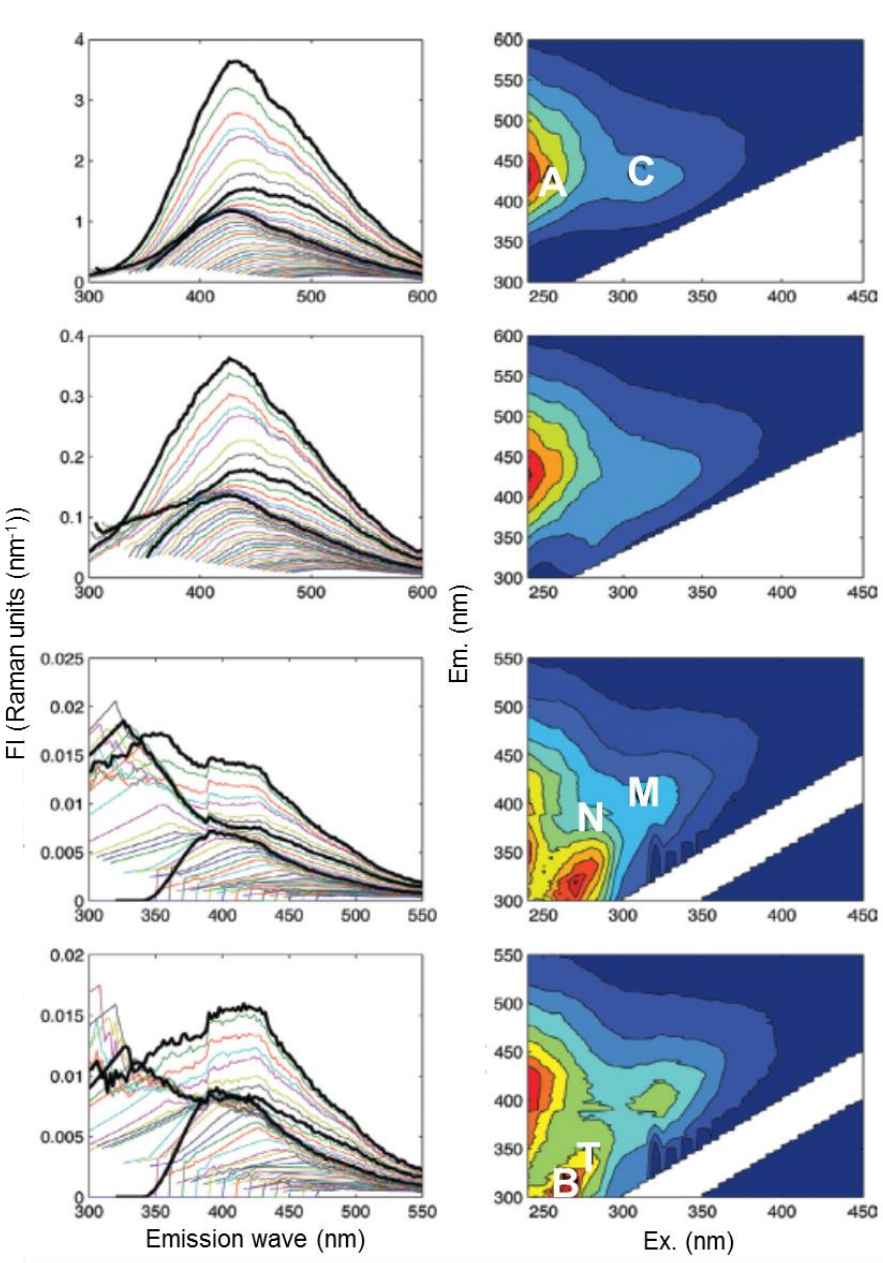

Figure 13. Fluorescence properties of DOM (Excitation: 250-450 nm; Emission: 300-600 nm). Top row: EEM was measured in samples collected from two main streams into a Danish estuary (Stedmon and

Markeger, 2005a); Second row: samples were collected in Horsen estuary (Stedmon and Markeger, 2005b); Third row: samples collected in surface ocean waters (Jorgensen et al., 2011); Fouth row: samples collected in deep ocean waters (Jorgensen et al., 2011). Left panels: emission spectra are plotted on top of each other and the bold black spectra are the emission from 240, 275 and 320 nm ex. Right panels: the contour plot (Source: Stedmon and Nelson, 2015).

Six peaks have been identified in FDOM in aquatic environments, that can be grouped in humic-like and protein-like substances (Coble, 2007; Guéguen and Kowalczuk, 2013) (Table 1). These peaks are clearly visible in the EEMs (Fig.13).

Peak	Ex. Region (nm)	Em. Region (nm)	Constitution
A	230-260	400-460	Terrestrial humic-like
B	270-280	300-310	Tyrosine-like
C	320-360	420-460	Terrestrial humic-like
M	290-320	370-410	Marine humic-like
N	280	370	Amino acid-like
T	270-280	340-360	Tryptophan-like

Table 1. The main fluorescent peaks in marine waters (modified from Stedmon and Carlson, 2015).

Protein-like fluorescence is due to the presence of the aromatic amino acids (tryptophan, tyrosine and phenyalanine) (Coble, 1996; Jorgensen et al., 2011). When bound in proteins, the tryptophan fluorescence can shift to shorter wavelengths, due to shielding from water, while the tyrosine fluorescence is difficult to detect due to the energy transfer to tryptophan and quenching by neighboring groups (Stedmon and Nelson, 2015). The protein-like fluorescent peaks are referred to as B, N and T (Table 1 and Fig. 13).

The humic-like fluorescence is due to the occurrence in the FDOM pool of humic and fulvic acids, tannins, lignin, polyphenols and melanins (Coble, 2007). It shows a wide emission spectra between 400 and 600 nm, the fluorescence in this region is usually referred to as peak A, C and M (Table 1 and Fig. 13). Peaks A and C represent terrestrial humic-like materials, whereas peak M is mainly associated to marine humic-like

substances (Nelson and Siegel, 2013). The excitation and emission maxima of terrestrial humic-like materials are at longer wavelengths than those of marine humic-like substances (Coble, 2007).

It can be very difficult to interpret the underlying variability captured in an EEM, given that the EEMs of FDOM from natural waters are composed of various types of overlapping fluorophores (Coble, 1996; Kowalczuk et al., 2003; Gentry-Shields et al., 2013). Starting in 1997, the parallel factor analysis (PARAFAC) have been widely used to analyze the EEMs (Bro, 1997) and to discriminate among the discrete fluorescent fractions occurring in FDOM pool (Stedmon and Bro, 2008).

5.2 PARAFAC analysis and components

PARAFAC can decompose the fluorescence signal of an EEM into underlying individual fluorescent phenomena (Stedmon and Bro, 2008: Murphy et al., 2013, 2014) (Fig. 14). The PARAFAC model has been widely used to study the variability of FDOM in coastal areas, to observe production and degradation processes of FDOM in marine environments (Stedmon and Markager, 2005a), and to trace anthropogenic pollutants in the oceans (Murphy et al., 2006, 2008).

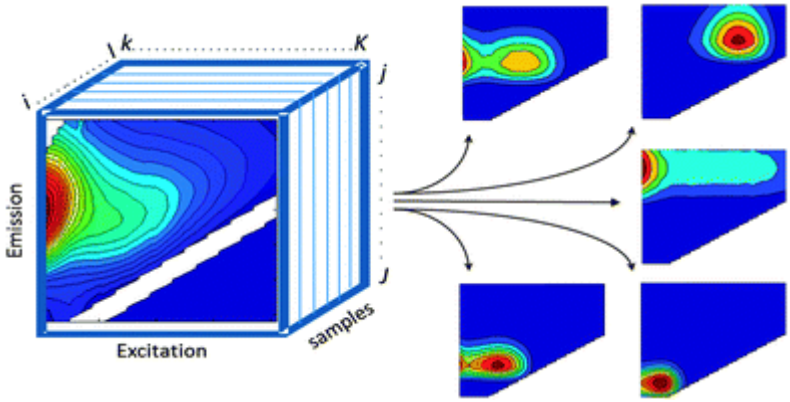

Figure 14. EEM dataset in a 3-D structure, decomposed into five PARAFAC components (Murphy et al., 2013).

PARAFAC model allows for the identification of different components, which represent the groups of fluorophores occurring in FDOM pool (Murphy et al., 2014). PARAFAC provides both a quantitative and qualitative model of the data (Stedmon et al., 2003; Stedmon and Bro, 2008). The specific identification of a single fluorophore is not possible in complex and heterogeneous mixtures such as FDOM, because components likely represent a group of co-varying fluorophores and the relationships between

component spectra, absorptivity, and fluorescence quantum yield are unknown for each group (Gentry-Shields et al., 2013). Therefore, the fluorescence of each component at the respective excitation and emission maximum (F_{max}) and the relative % of components are used to compare groups of fluorophores. F_{max} values provide estimates of the relative fluorescence intensity of each component in a sample (Stedmon an Bro, 2008; Murphy et al., 2014). In addition to the two main groups described in the previous paragraph (protein- and humic-like substances), in recent years some authors identified a third group of fluorescent substances, due to the presence of a mixture of PAHs, pollutants persistent in the environment, with mutagenic and carcinogenic potential (Murphy et al., 2006, 2008; Gonnelli et al., 2016).

6. Air-sea interactions

The atmosphere and the ocean form one system and, if either is to be understood properly, must be considered together. What occurs in one affects the other, and the two are linked by complex feedback loops. Ocean-atmosphere fluxes play a critical role in the regulation of climate. It is therefore crucial to understand the physical, chemical and biological processes affecting exchange of gases, mass, and energy across the air-sea interface from nanometer to global scales (Fig. 15).

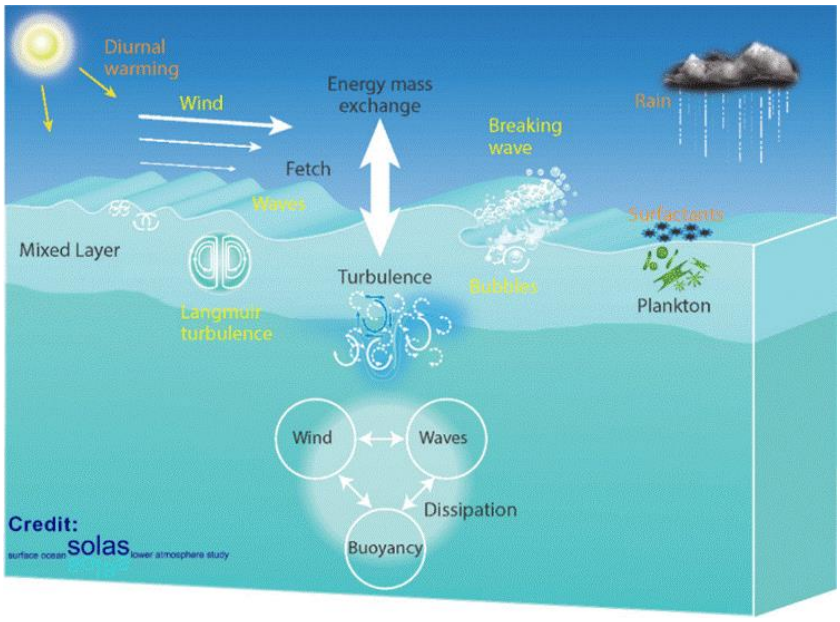

Figure 15. Dominant processes controlling air-sea fluxes of mass and energy in the open ocean (Source: *http://www.solas-int.org/Theme_2.html*).

The atmosphere receives heat from the ocean, influencing the atmospheric circulation and surface winds, which in turn generate oceanic currents and the large scale ocean circulation. The air-sea interface is dominated by several physical, biological and chemical processes in both the atmosphere and ocean that regulate the efficiency of transfer of gases and particles (Garbe et al., 2014) (Fig. 15). Studying and quantifying ocean–atmosphere exchanges of CO_2 and methane (CH_4) is important for the understanding of the global biogeochemical cycle of carbon in the context of ongoing global climate change (Bakker et al., 2014). In addition, the interactions between the ocean and the atmosphere are considerable regulators of atmospheric composition (Bigg et al., 2003). As fully described in paragraph 2.1, the absorption of CO_2 by the ocean, the carbon transport from the surface to the deep sea and the carbon sequestration in the deep oceans is governed by physical, chemical and biological processes.

The main source of several key particles and compounds (nutrients and trace metals) for the marine ecosystem is the atmosphere. Atmospheric inputs, will vary according to the intensity and type of the deposition (wet or/and dry) and to the mixing between different types of aerosols. Many studies have shown that the atmosphere becomes the predominant external source of nutrients to the surface open waters of the Med Sea, in particular during the stratified period affecting primary productivity (Krom et al., 2004; Bonnet and Guieu, 2006; Pulido-Villena et al., 2010). Marine productivity in turn affects air-sea exchange of greenhouse gases and consequently radiative balance and climate (Jickells et al., 2017). The contribution of dust from atmospheric deposition is crucial for marine ecosystem. Sahara desert produces more Aeolian soil dust than any other desert in the world, and Saharan dust has an important impact on climatic processes, nutrient cycles, soil formation and sediment cycles (Romero et al., 2011). Moreover, recent studies have shown that desert dust inputs to the oligotrophic ocean preferentially stimulate heterotrophic processes compared to autotrophic production (Pulido-Villena et al. 2008a, Maranon et al. 2010, Pulido-Villena et al. 2014).In the following paragraphs, a state of the art about atmospheric deposition of nutrients and organic compounds is presented, with a particular focus on the Med Sea.

6.1 Atmospheric aerosols

Aerosols are an important constituent of the atmospheric boundary layer. An aerosol consists of a suspension of particles and its surrounding medium. For atmospheric aerosols the surrounding medium is the air in which the aerosol particles (or droplets) are

suspended (de Leeuw et al., 2014). Atmospheric aerosol particles affect the Earth's radiative balance directly by scattering or absorbing light, and indirectly by acting as cloud condensation nuclei (CCN), thereby influencing the albedo and life-time of clouds (Fig. 16). Atmospheric aerosol is therefore recognized to play an important role in regulating regional and global climate (Kanakidou et al., 2005).

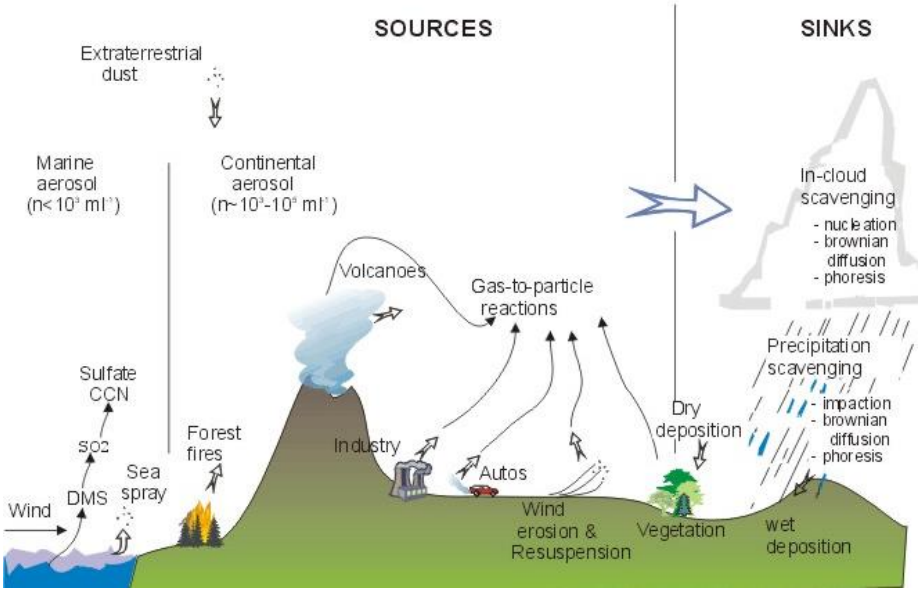

Figure 16. Sources and sink of atmospheric aerosol particles. Credit: National Oceanic and Atmospheric Administration (NOAA) (Source: *https://wattsupwiththat.com/2018/01/26/even-the-tiniest-aerosol-particles-can-kick-up-a-storm/*).

Two different types of aerosols can be distinguished, based on their formation mechanism. The primary aerosol enters the atmosphere directly as particles, while the secondary aerosol forms in the atmosphere from its precursors in the gas phase through physical and chemical reactions (de Leeuw et al., 2014). Once the aerosol is formed, the particles can be transported for thousands of kilometers far from the source. A series of chemical reactions occur between the compounds in the aerosol, the physical processes determine the vertical transport and removal of particles by dry deposition to the surface of the ocean. These processes depend on particle size: very small particles are subject to growth by condensation and coagulation, whereas large particles are subjected to gravitational forces resulting in rapid sedimentation. The concentration of aerosol particles may vary by 10 orders of magnitude depending on the size (de Leeuw et al., 2014). These particles consist of a multitude of small unit structures with diverse chemical composition and origin (soluble acid substances, sodium chloride crystals of marine origin, ammonium

sulfates, insoluble carbonaceous matter, insoluble mineral dust, and insoluble organic substances). All these particles are held together by inter-particle adhesive forces in order to create a single unit in suspension (Tomasi and Lupi, 2017) (Fig.17).

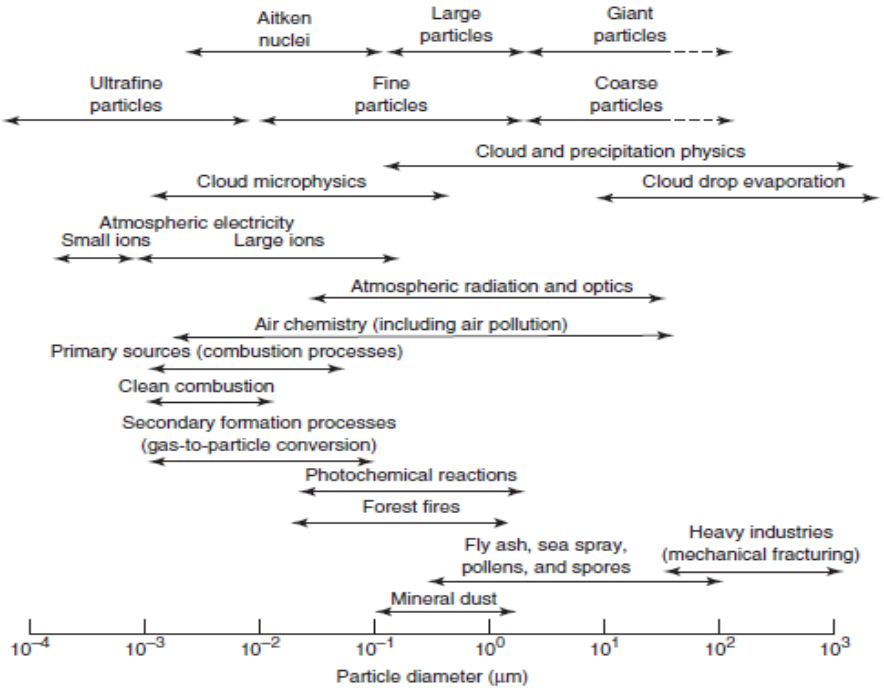

Figure 17. Size range of aerosol particles in the atmosphere (Tomasi and Lupi, 2017).

Aerosol sources are numerous and can be natural and/or anthropogenic.

6.1.1. *Natural sources of aerosol*

The natural ones include sea spray, wind-borne dust, volcanic debris and biogenic aerosol. Estimates of the mass concentration show that the largest aerosol contributions on a global scale are from sea spray and desert dust (Jickells et al., 2005; Andreae and Rosenfeld, 2008). Sea spray aerosol is produced directly at the sea surface from the interaction between wind and waves. Total production is estimated to be 5,900 Tg $year^{-1}$ (Bigg et al., 2003). Although, most of the particles present in the marine atmosphere are deposited to the ocean, where they may affect biological processes; some of them may affect regional air quality (visibility and corrosion) and climate (de Leeuw et al., 2014). It is necessary to highlight that the marine atmosphere aerosol is also significantly influenced by the emission of particles from ship emissions and volcanoes (both part of the primary aerosol) and by secondary aerosol formation from gases released from the sea surface.

Desert and semi-arid areas are a the major source of particles in the global atmosphere (Prospero et al., 2002) and large oceanic areas are regularly under the direct

influence of turbid air masses transported from deserts or semi-arid areas (Tomasi and Lupi, 2017) (Fig. 18).

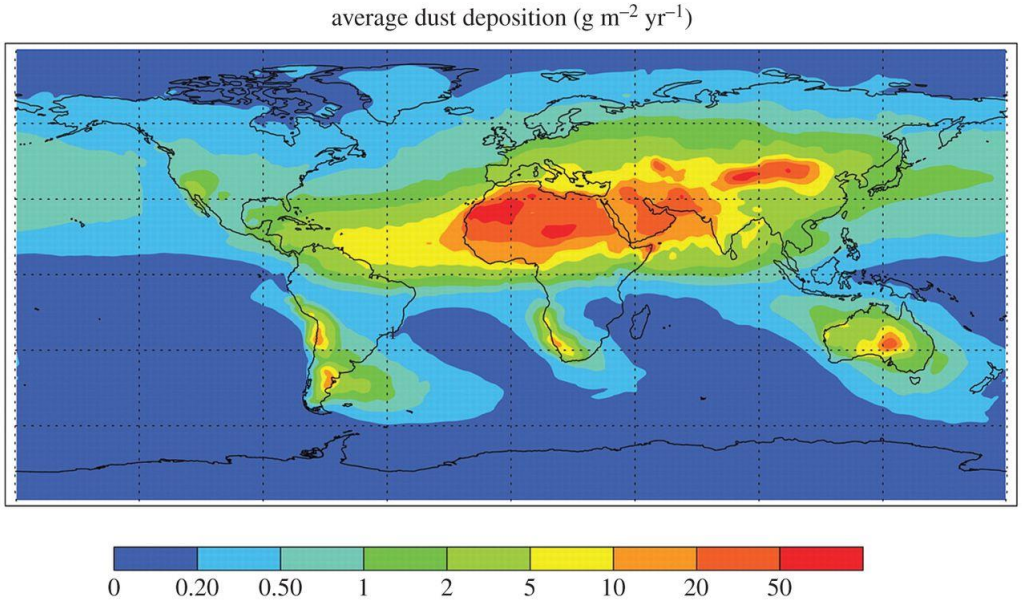

Figure 18. The global transport of dust (Jickells et al., 2016).

The dust transport events cause long-range transfer of huge amounts of matter from continent to the remote surface ocean. The mineral dust deposition to the remote surface ocean significantly influences trace element biogeochemistry. Dust particles also affect the optical properties of surface waters (Sanchez-Perez et al., 2016). Due to the trade wind regimes, dust from the Sahara and Sahel desert is encountered all year long over the tropical Atlantic (Moulin et al., 1997). Other regions of the world ocean are strongly affected by dust deposition from seasonal or episodic dust transport events (e.g. Mediterranean basin and the regions of the North tropical Indian and Pacific Oceans) (de Leeuw et al., 2014). The current estimates for desert dust deposition worldwide range from 0.5 to 5.0 billion tons a year (Perkins, 2001; Mahowald et al., 2014). During its transport, the mineral dust can substantially change the composition of the original aerosol, due to chemical reactions and internal mixing. In some cases, Saharan minerals mixed with sea-salt components (Trochkine et al., 2003), in other cases, the dust can be associated with sulfur and organic matter transported from both urban and agricultural polluted areas (Falkovich et al., 2001) and with organic molecules from combustion smokes and other anthropogenic particulate matter (Guo et al., 2007), suggesting that mineral dust is a potential cleaning agent for organic pollutants (Pósfai and Buseck, 2010).

6.1.2. *Anthropogenic sources of aerosol*

A significant fraction of aerosol particles is anthropogenic. It consists of both primary particles, which originate from diesel exhaust and vehicular traffic dust, and secondary particles formed from the gases emitted by urban and industrial activities. Anthropogenic aerosols certainly contribute to the total aerosol mass loading by more than 10% (Tomasi and Lupi, 2017). The main sources are associated to the sulfates and nitrates industrial emissions, the wind-forced mineral dust mobilized in areas exploited for agricultural activities, the fossil fuel combustion and the biomass burning (Tomasi and Lupi, 2017). Anthropogenic activities are currently modifying the concentration and chemical composition of aerosols, influencing the climate and the ecosystem biogeochemistry upon deposition (Mahowald, 2011).

6.2 Atmospheric deposition of nutrients and metals to the oceans

The atmosphere is the most important pathway for the long-range transport of particulate material to open sea waters (Chester, 2009). Atmospheric deposition is an important source of nutrients for marine ecosystem, with consequences on local, regional, and global biogeochemical cycles, as well as on the climate system. The transport and deposition of atmospheric aerosol is a significant source of iron, nitrogen and phosphorus (and many other elements) to the surface ocean, affecting ocean productivity, in particular in oligotrophic areas (Duce, 1986; Martin et al. 1991; Falkowski et al. 1998; Jickells et al., 2005; Krishnamurthy et al., 2010; Law, 2013; Nyaga et al., 2013; Ussher et al., 2013, Chance et al., 2015). On the other hand, some substances, deposited from the atmosphere, could be toxic for organisms, such as Cu (Paytan et al., 2009). The fundamental processes driving aerosol emission, transport, chemical reactions, and deposition may change atmospheric fluxes to the surface ocean (Fig. 19). In turn, microbial communities respond to changing atmospheric inputs with effects on the marine carbon and nitrogen cycle, as well as on atmospheric carbon dioxide uptake.

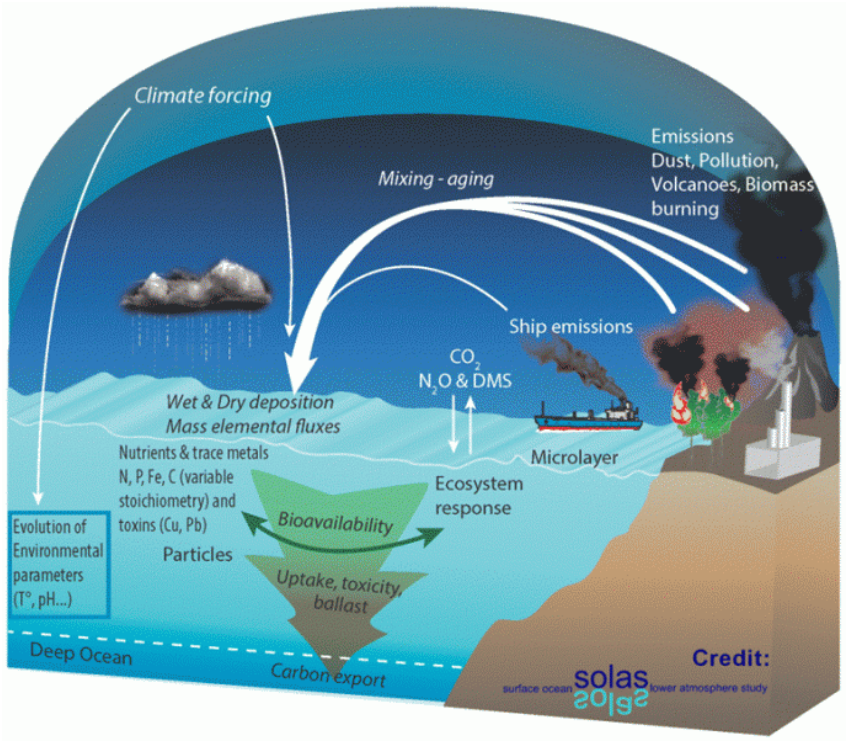

Figure 19. The main processes that control atmospheric fluxes (Source: *http://www.solas-int.org/theme-3.html).*

6.2.1 *Atmospheric deposition of iron*

The main external source of iron to the open ocean is wind-blown desert dust (Jickells et al., 2005; Nickovic et al, 2013), despite the relatively low solubility as compared to that of anthropogenic aerosols (Bonnet and Guieu, 2004). Atmospheric loadings of Fe and other trace metals show high variability over the oceans, reflecting the variety of source regions and the episodic nature of sources such as dust mobilization (Fig. 20). Phytoplankton is limited by Iron availability in as much as 30% of the oceans (Falkowski et al., 1998; Boyd and Doney, 2003). In some areas, such as the Southern Ocean, called ‘‘high-nutrient low-chlorophyll’’ (HNLC) regions (Jickells et al., 2005)Fe limitation results in the incomplete use of macronutrients (N, P, and Si) and relatively low algal abundance. Atmospheric iron deposition increases primary productivity and is estimated to support 30-50% of global export productivity (Jickells and Moore, 2015). Atmospheric iron deposition also increases nitrogen fixation rates, that in turn increase the primary productivity (Berman-Frank et al., 2001; Bigg et al., 2003).

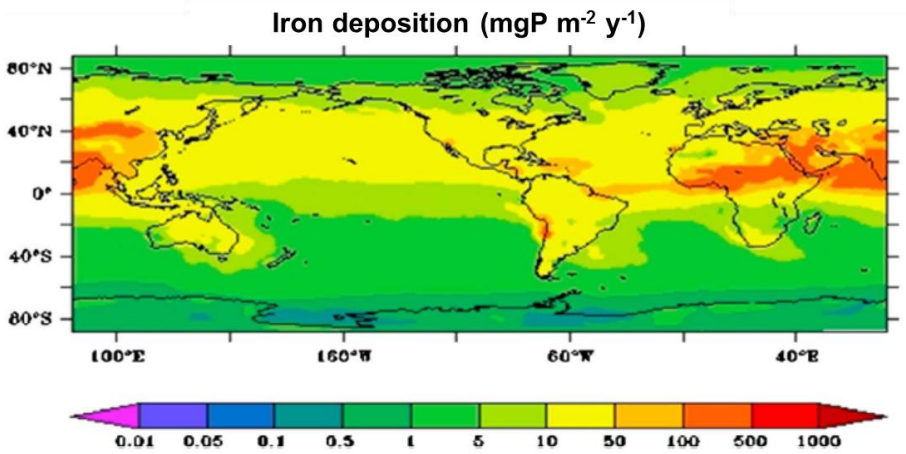

Figure 20. Global atmospheric dissolved iron fluxes derived (Lamarque et al., 2010).

In the last few years some research focused on the role of aerosol organics and humic-like substances in the complexation and dissolution of iron minerals over a wide pH range (Ussher et al., 2013). The global iron cycle is changing rapidly due to accelerating acidification, stratification, warming and deoxygenation (Hutchins and Boyd, 2016), these changes will have an impact on phytoplankton growth across much of the ocean.

6.2.2 *Atmospheric deposition of nitrogen*

Atmospheric deposition is the primary way to transfer terrestrial N to the open ocean. Currently this mechanism is comparable in magnitude to the other external N sources (fluvial inputs and direct waste discharges) (Fig. 21). Anthropogenic perturbations have an enormous impact on the total atmospheric input of N to the ocean (Jickells et al., 2017). NO_x are emitted from the combustion in the atmosphere, where they are converted to nitric acid nitrate in a few days. Nitric acid reacts with gaseous ammonia to form particulate or aerosol nitrate. Ammonia is mainly released by agricultural emissions (Duce et al., 2008), and shipping emissions (Eyring et al., 2005). Atmospheric inputs of N to the ocean may support 3-5% of ocean export productivity (Duce et al., 2008; Krishnamurhy et al., 2010) enhancing the uptake of CO_2 (Bigg et al., 2003; Jickells et al., 2017).. In addition, in the short-term high nitrate and ammonia deposition can perturb the species composition in coastal systems (Bigg et al., 2003).

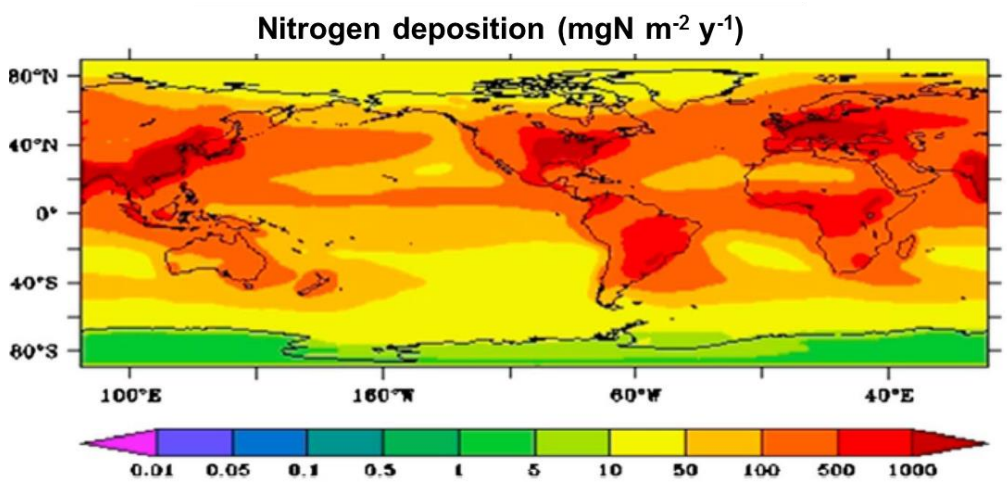

Figure 21. Global atmospheric dissolved nitrogen fluxes derived (Lamarque et al., 2010).

6.2.3 *Atmospheric deposition of phosphorous*

Atmospheric deposition of phosphorous is small compared to the magnitude of that of Fe and N, taking into consideration the phytoplankton requirements for these three elements (Moore et al., 2013) (Fig. 22). Biomass burning, the combustion of oil and coal and the emissions from phosphate manufacture are significant source of P to the atmosphere. The most important non-anthropogenic source of P is the dust from soils and deserts, as well as marine aerosols and primary biological aerosol particles (Mahowald et al., 2008; Tipping et al., 2013). N deposition rates larger than those of P can cause shifts from N to P limitation in many regions of the globe (Moore et al., 2013).

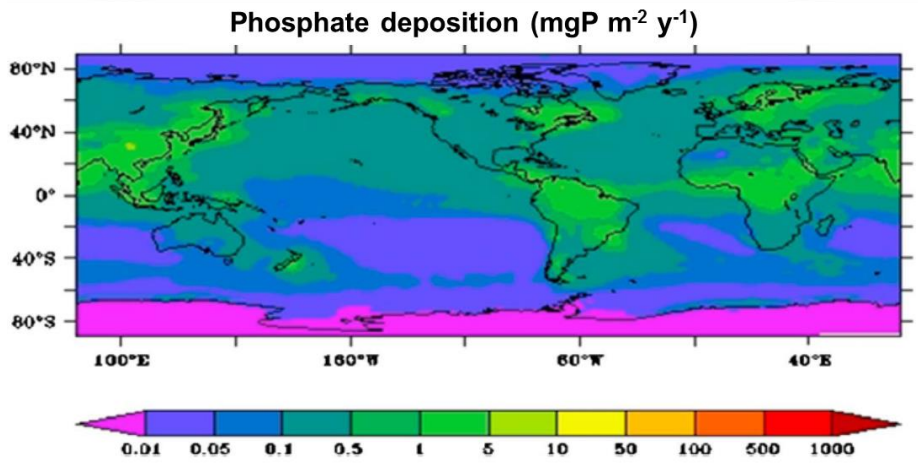

Figure 22. Global atmospheric dissolved phosphate fluxes (Lamarque et al., 2010).

6.3 Atmospheric deposition of DOC and other organic compounds to the oceans

Organic carbon is ubiquitous in the atmosphere and it can be present as particulate airborne and as gaseous volatile organic compounds (VOCs). Organic compounds that are emitted directly in particulate form are referred to as Primary Organic Aerosol (POA). Such compounds are often referred to as semi- or non- volatile, and when residing in the aerosol phase, as Secondary Organic Aerosol (SOA) (Kanakidou et al., 2005).

Organic species are removed from atmosphere via both wet (precipitation) and dry (settling of gaseous and particles) deposition (Fig. 23). Wet deposition (rain, snow, hail and fog) represents the principal pathway of removing the organic C from the atmosphere (Kanakidou et al., 2005). Wet atmospheric deposition of organic C transfers about 306-580 Tg of DOC to the surface of the Earth per year (Willey et al., 2000; Kanakidou et al., 2012). This range is almost equivalent to the half of the C delivered to the oceans by river annually (IPCC, 2014). Wet deposition of OC to the global ocean surface is between 90 and 246 Tg C y^{-1} (Willey et al., 2000; Kanakidou et al., 2012), and this range is close to the amount of terrestrial POC exported by the rivers to the ocean (200±135 Tg C y^{-1}) (Galy et al., 2015).

Sources of atmospheric organic carbon are emissions from plants and forest fires (biogenic), but also fossil fuel combustion (anthropogenic) (Decina et al., 2018). In particular, ~90% of organic carbon is emitted from terrestrial ecosystems, and ~30-50% of it is deposited into the oceans (Jurado et al., 2008; Kanakidou et al., 2012). Wet deposition is a relevant sink for atmospheric OC emitted from fossil fuel combustion, around 4-46 Tg C y^{-1} of fossil OC are removed per year (Yan and Kim, 2012; Iavorivska et al., 2016), and this range is close to the emissions from fossil fuel of primary OC (3.2-33.9 Tg C y^{-1}) (Hallquist et al., 2009). Estimates of the organic fraction associated with dust vary widely, but long-term monitoring studies of atmospheric deposition close to dust sources agree that at least 8% to 14% of the particulate matter is organic carbon (Koulouri et al., 2008; Mladenov et al., 2011). The deposition flux of carbon can affect regional C cycling, radiative forcing and human health, in particular through the vehicle of toxic and carcinogenic compounds such as PAHs (Yan and Kim, 2012; Decina et al., 2018).

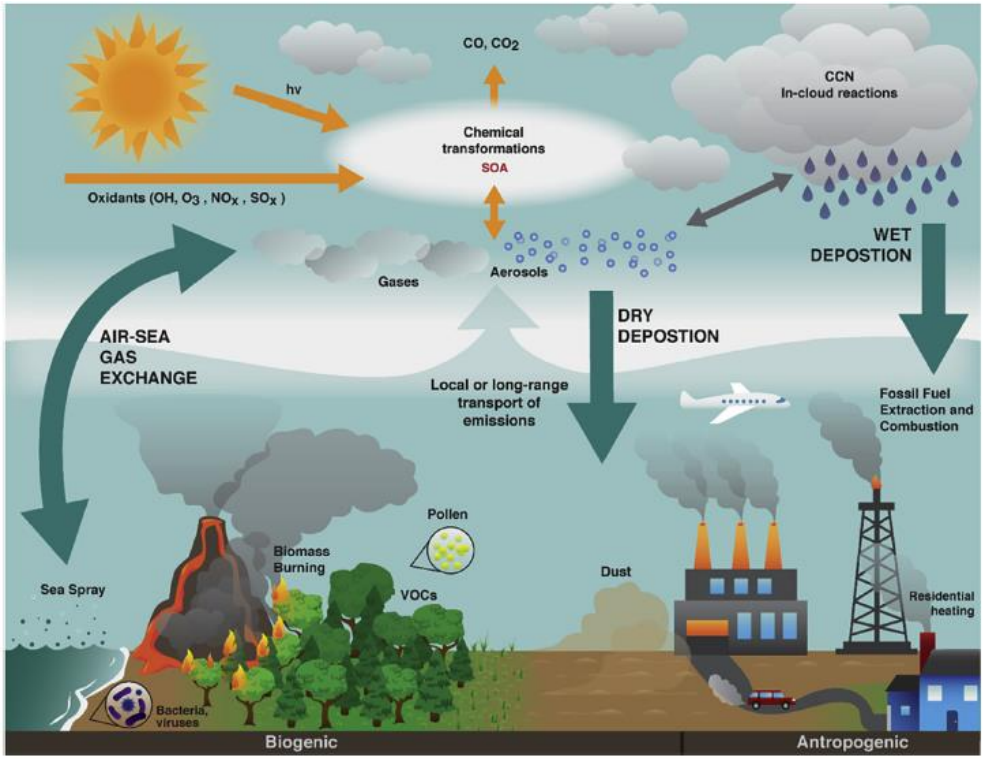

Figure 23. Sources and processes affecting the organic carbon in atmosphere (Iavorivska et al., 2016).

Previous investigations on organic components of land-derived aerosols found lipids of higher plant waxes, primary saccharides such as arabitol, mannitol, sucrose from fungal spores, plants, animals (Simoneit et al., 2004; Bauer et al., 2008) and biomass burning tracers such as levoglucosan, mannosan, and galactosan (Simoneit and Elias, 2000; Simoneit, 2002). Aeolian particles also contain fragments of weathering rocks, soils, biogenic detritus, and other anthropogenic organic compounds (Simoneit, 2006). Other compounds recorded in atmospheric aerosols include phthalate esters, secondary organic aerosols tracers (isoprene, terpenes and sesquiterpenes), low molecular weight dicarboxylic acids and keto acids, pesticides, and PAHs (Sempéré and Kawamura, 2003; Manodori et al., 2006; Guitart et al., 2010; Fu et al., 2013).

6.4 Atmospheric deposition of airbone microbes and their interactions with dust

The oceans cover over 70% of the Earth's surface and are the probably source and, at the same time, the final destination of a large fraction of airborne microbes. Transport of airborne microbes may play a central role in microbial dispersal, in the sustenance of diversity in marine systems as well as in meteorological processes such as cloud formation (Mayol et al., 2017). Airborne microorganisms are found in remote marine and freshwater environments, reaching concentrations of ~10^4 bacteria, ~10^3 fungi and ~10^7

virus m^{-3} of air (Pósfai et al., 2003; Leck and Bigg 2008). A considerable fraction (typically 1-20% but can be up to 25%) of these airborne microbes may remain viable during transport (Womack et al., 2010) and affect phytoplankton community composition, activity, growth rates and may even cause algal bloom decline (Gachon et al. 2006). These microorganisms can be associated with dust and be easily transported for thousands of kilometers away from their place of origin within a few days. The biogeochemical effects of atmospheric deposition on marine waters have been extensively examined using aerosols/dust addition bioassays (in-situ, microcosms, mesocosms). A recent study from the southeastern Med Sea showed that aerosols contained a unique bacterial consortia which can become viable upon deposition in seawater, interacting with the surface microbial populations (Rahav et al, 2016a, 2016b). Pitta et al. (2017) studied Saharan dust effects on the microbial food web in Eastern Med. These authors found that auto- and hetero-trophic components of the food web were enhanced by the dust addition during mesocosm experiment. Pulido-Villena et al. (2014) carried out a dust-addition mesocosm in the northwestern Med Sea, and they found that heterotrophic metabolic rates increased. However, after dust addition experiments the results are variable, and depend on numerous processes that may have contrasting effects. These can includes: (a) differences in the mineralogical and chemical composition of aerosols (Herut et al., 2002; Mills et al., 2004; Bonnet and Guieu, 2006; Astrahan et al., 2016), (b) the release of toxic elements and other pollutants (Paytan et al., 2009; Després et al., 2012; Jordi et al., 2012; Krom et al., 2016), (c) the transport and deposition dynamics of dust due to storms (Giovagnetti et al., 2013; Guieu et al., 2014), (d) the degree of oligotrophy of the system where deposition occurs (Maranon et al., 2010; Tsiola et al., 2017). However, other processes, that have been little studied, such as supply of DOM with different biological lability, may play a key role in the processes driven by dust addition. Indeed, no information are available about the biological lability of atmospheric DOM and its role in contributing to the viability of airborne microorganisms as well as its impact on marine ecosystem.

In the following paragraphs, a focus on the Med Sea is presented, with particular attention to the state of the art about atmospheric inputs of DOM (DOC, DON and DOP), CDOM and FDOM.

7. The Mediterranean Sea

The Med Sea is the largest semi-enclosed basin in the world, and one of the most oligotrophic area in the world. It continuously receives anthropogenic aerosols from industrial and domestic activities from all around the basin and other parts of Europe (Sciare et al., 2003), as well as Saharan dust from the south, with some 'extreme events' of dust deposition (Guerzoni et al. 1999; Bonnet and Guieu, 2006). Although the organic aerosol fraction plays a crucial role in the C, N, and P cycles, very limited information on its biogeochemical role in the Med Sea is available (Markaki et al., 2010; Djaoudi et al., 2018). Its small inertia compared to other oceans makes this basin more sensitive to natural variations in the atmosphere-ocean exchanges.

D'Ortenzio and Ribera d'Alcalà, (2009) analyzed ten years of SeaWiFS satellite surface chlorophyll concentrations and observed different seasonal cycle of the surface biomass of phytoplankton in the different areas of the basin (Fig. 24). Med Sea is characterized by ''non-blooming'' areas (e.g. the Tyrrhenian Sea), exhibiting a sub-tropical regime, as well as by areas where, under particular conditions (both atmospheric and hydrographic), North Atlantic bloom-like events take place (e.g. the Gulf of Lions).

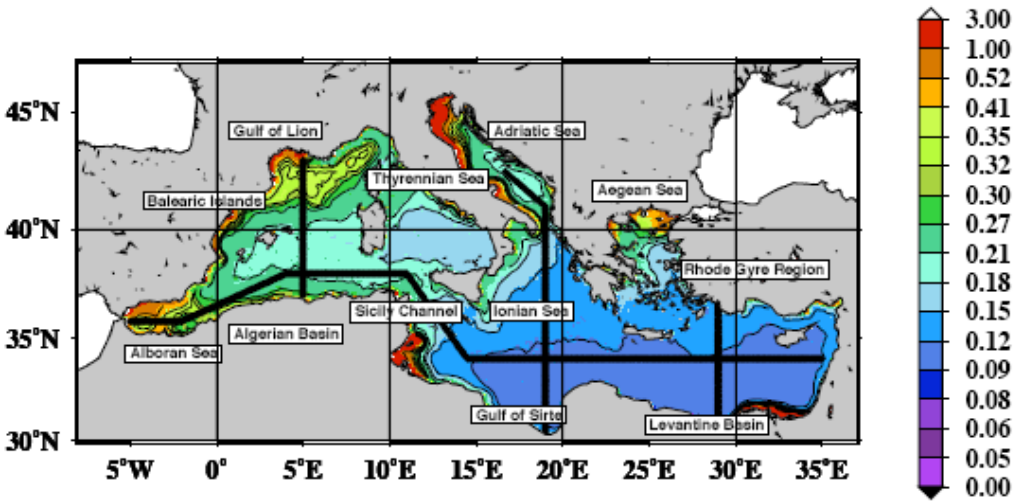

Figure 24. Distinct trophic and ecological regimes of the Med Sea by analyzing ten years of SeaWiFS satellite surface chlorophyll concentrations (D'Ortenzio e Ribera d'Alcalà, 2009).

Med Sea is a natural laboratory to gain information about the impact of atmospheric deposition on DOM dynamics. It shows DOC concentrations and distribution similar to those observed in the oceans (Santinelli, 2015), enhanced DOC mineralization (Santinelli et al., 2010) and respiration rates (Christensen et al., 1989) in the deep waters. Santinelli et al. (2013) observed a different functioning of the microbial loop, in the West Med it

represents a link of C to the food web, while in the East Med it is a sink of C and is not able to use the DOC, that therefore accumulates. This west to east pattern could be explained by atmospheric deposition.

One of the most intriguing aspect of DOC dynamics in the Med Sea is that it shows concentrations and distribution very similar to that observed in the global oceans, even if the Med Sea water are at least 10-times younger (Santinelli et al., 2015). These authors show that DOC in the Med Sea deep water is more depleted in both ^{14}C and ^{13}C than in the deep Atlantic Ocean, with an estimated age of 4500-5100 years, suggesting that at least 10% and up to 45% of the Atlantic RDOC entering the Med Sea is removed and replaced by allocthonous DOC. They proposed that atmosphere can be the main source of allocthonous DOC to this basin.

7.1 Atmospheric DOM input to the Med Sea

The large data set available for the Med Sea allowed for a re-assessment of DOC stocks in the different depth-layers of the two sub-basins, its fluxes at the straits and its external inputs (Santinelli, 2015). The rough estimate of DOC fluxes due to river run-off and atmospheric depositions suggests that atmospheric input of DOC could play a crucial role in DOC cycling in the Med Sea. Although the effects of atmospheric inputs on biological and biogeochemical cycles of P and N in the marine Mediterranean ecosystem are known (Migon et al., 1989; Bergametti et al., 1992; Herut et al., 2002; Ridame and Guieu, 2002; Markaki et al., 2003, 2010), very few data are available, in particular on atmospheric organic substances input. Atmospheric DOC flux was studied in the southern France during 2006 (0.04-1.20 mmol C m^{-2} day^{-1}) (Pulido-Villena et al., 2008a) and in 2015 (0.16 mmol C m^{-2} d^{-1}) (Djaoudi et al., 2018). In the first study, the highest DOC flux was observed in correspondence with a Saharan storm, suggesting a combination of heterogeneous reactions between organic matter and mineral dust in the troposphere (Usher et al., 2003), whereas in the second study the Saharan rain event coincided with a minimum of DOC input, suggesting the presence of an aerosol poorly enriched in organic matter (Djaoudi et al., 2018). A similar range was observed in the Southern Spain (0.18-0.42 mmol C m^{-2} d^{-1}), within an area exposed to intense dust events (De Vicente et al., 2012). Direct measurements of total OC (TOC) in rainwater, at the Crete Island (Eastern Mediterranean), indicate that wet deposition can account for an input of 0.14 mmol C m^{-2} d^{-1} (Economou and Mihalopoulos, 2002). The lack of sufficient information about DOC input from the atmosphere to the Med Sea, together with its relevance to marine

biogeochemical cycle highlighted the need for a better and robust estimation of atmospheric DOC input.

7.2 Atmospheric CDOM and FDOM input to the Med Sea

Few information are present about impact of atmospheric deposition on *in situ* CDOM. De Vicente et al. (2012) studied the contribution of dust inputs to DOC and CDOM in three Mediterranean reservoirs in Southern Spain. The main result was that the CDOM associated with the dust inputs affected significantly the water transparency to ultraviolet radiation with a residence time of CDOM in terms of days. More recently, EEMs elaborated with PARAFAC allowed for the identification of protein-like and humic-substances in a study carried out in alpine lakes (Mladenov et al., 2011). Tryptophan-like and tyrosine-like represented the predominant components of FDOM in both atmospheric and lake water samples (Mladenov et al., 2011). Dust was the main source of FDOM, even if it occurred only in some periods of the year (Mladenov et al., 2011).

7.3 DOM stoichiometry

Many papers report anomalous nutrient ratios in the Med Sea with respect to other oceanic areas (Herut et al., 1999; Kress and Herut, 2001; Ribera d'Alcalà et al., 2003; Krom et al., 2005). In recently ventiled deep waters, DON/TDN (Total Dissolved Nitrogen) and DOP/TDP (Total Dissolved Phosphorous) percentages is higher than in deep oceans, suggesting that a large fraction of both N and P is organic (Santinelli, 2015). However this nutrient ratios anomaly is still an intriguing point for the understanding of the functioning of the Med Sea (Mermex group, 2011).

An interesting aspect of the Med Sea is related to DOM stoichiometry. Measurements of C:N:P ratios and anomalies relative to Redfiled values (105:16:1) are useful to describe the processes controlling marine biogeochemistry (Pujo-Pay et al., 2011). Mediterranean DOC and DON concentrations and their ratios are similar to those reported for the ocean (Pujo-Pay et al., 2011; Santinelli, 2015), despite in the surface waters (0-100 m), C:N:P ratios show that Mediterranean DOM is depleted in DOP with respect to DOC and DON.

It is important the study of C:N:P ratios of DOM in atmospheric deposition, in order to estimate the relative contribution of atmospheric DOM input to the inventory of the surface DOM pool. C:N ratios recently obtained (Djaoudi et al., 2018) are in agreement with C:N ratios of water soluble fraction of aerosols reported in both northern and southern

Pacific (Sempéré and Kawamura, 2003). The N:P ratios obtained by Djaoudi et al. (2018) are of the same order of magnitude of those reported in other studies (Krom et al., 2004; Markaki et al., 2010).

8. The Northern Red Sea

Northern Red Sea (NRS) is an oligotrophic system, with similar characteristics to that of the western and central Mediterranean basin, and it is routinely exposed to high amounts of atmospheric depositions. During the summer the water column is thermally stratified, with mixed layer depths of about 20 m (Chase et al., 2006), and low surface concentrations of major nutrients (NO_3<200 nM, PO_4<60 nM) (Genin et al., 1995). Winter cooling breaks down stratification and deep overturning occurs between November and April. Winter mixing usually reaches depths of 300-400 m, and during expectionally cold winters, may even reach depths as great as 860 m during exceptionally cold winters (Genin et al., 1995). DOC concentrations range from 70 to 90 μM (Yahel et al. 2003). Currently, no information is available about CDOM/FDOM concentration in this semi-enclosed basin.

Goals of this PhD thesis

With this project I aimed to test 3 main hypothesis:

1. In the Med Sea, DOM pool is constituted by a relevant fraction of allocthonous molecules.
2. In the Med Sea, atmospheric DOM input is the predominant source of allocthonous DOM.
3. Atmospheric deposition impacts the DOM dynamics in the surface ocean affecting the function of marine ecosystem.

In order to test these hypothesis the following work was carried out:

1. New data on optical properties (absorption and fluorescence) of CDOM were collected in a large open sea area of the Med Sea.
2. The annual flux of DOC, DON and DOP from the atmosphere was quantified at the island of Lampedusa. The atmospheric C:N:P molar ratio was measured. The optical properties of atmospheric CDOM were investigated and compared with those of marine CDOM.
3. A mesocosm experiment with the addition of 2 types of dust was carried out in the Northern Red Sea in July 2017.

METHODS

“Research is creating new knowledge.”

Neil Armstrong

Methods

1. Sampling of total atmospheric deposition

In march 2015, the first Italian total atmospheric deposition sampler (Fig. M1) for DOM was deployed on the roof of the ENEA station (45 m a.s.l.). The total deposition (wet and dry) sampler, used successfully in previous studies (Pulido-Villena et al., 2008a; De Vicente et al., 2012; Djaoudi et al., 2018), is composed by a 10-L Polycarbonate bottle, with a polyethylene funnel attached on the top and a 20 μM mesh that covers the funnel stem in order to prevent a possible contamination by insects or organic debris. In case of dry deposition, 250 ml of ultrapure Milli-Q water were used to carefully wash the funnel and the carboy and were collected in 250 ml polycarbonate bottle and immediately frozen. In case of wet depositions, rain was collected in two 250 ml polycarbonate Nalgene bottles and immediately frozen. Depositions were collected twice a month, or immediately after strong rain or dust storm events. Unfortunately, due to logistic problems the sampling period was longer than 20 days for 7 deposition (Table 2.1). In this work, I will present and discuss data collected between March 19th 2015 and November 3rd, 2016 for a total of 33 samples.

Samples for DOC and CDOM analysis were thawed and immediately filtered in the laboratory at the Island of Lampedusa through a sterile 0.2 μm Nylon filter, pre-washed with 300 ml of Milli-Q water to avoid any contamination. Samples rich in suspended material or dust, were prefiltered through a 1.2 μM pre-filter Nylon filter, pre-washed with 300 ml of Milli-Q waterd (Fig. M2). Filtered samples were frozen again until the analysis carried out in the laboratory of IBF-CNR in Pisa.

Figure M1. Total deposition collector.

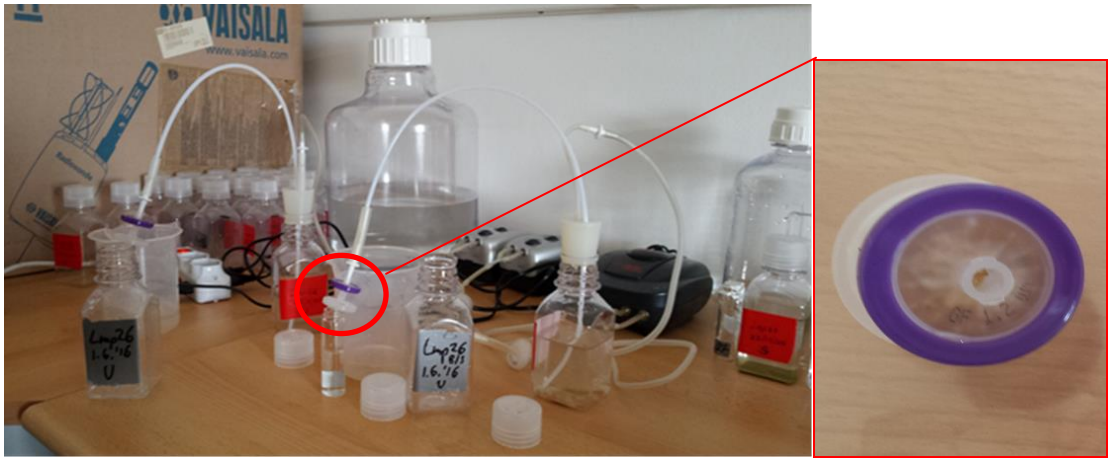

Figure M2. The filtration of sample and the 1.2 μM filter.

1.1 Sampling of seawater

1.1.1 *Open sea waters of the Mediterranean Sea*

Samples for DOC and CDOM analysis were collected in open sea waters of the Med Sea during 3 oceanographic cruises carried out in March/April 2008 (S-IT4 cruise), August 2010 (Venus 1 cruise) and November 2011 (SICSIA cruise) on board the R/V Urania of the Italian National Research Council (CNR). Samples were collected in 200 ml dark glass bottles, preconditioned with filtered deep seawater and rinsed 3 times with the sample before its collection. Samples were immediately filtered on board via sterile 0.2 μm nylon filters (Sartorius, 17845-ACK). Filtered samples were stored at 4 °C in the dark until the analysis. More details are provided in the Chapter 1.

1.1.2 *Mesocosm experiment in the Northern Red Sea*

Samples for DOC and CDOM analysis (200 ml) were collected daily from the center of each mesocosm and immediately filtered through a 0.2 μm Nylon filter, pre-washed with 500 ml of Milli-Q water to avoid any contamination. Filtered samples were stored at 4 °C in the dark until the analysis. More details are provided in the Chapter 3.

2. DOC analysis

DOC measurements were carried out with a Shimadzu TOC-V_{CSN}, equipped with a quartz combustion column filled with 1.2% Pt on alumina pillows of ~2 mm diameter. Samples were first acidified with 2N HCl and bubbled for 3 min with CO_2-free ultra-high purity air in order to remove the inorganic carbon. Replicate injections were performed until the analytical precision was lower than 1% (±1 μM). A five-point linear calibration curve was

done with standard solutions of potassium hydrogen phthalate in the same concentration range as the samples (40-400 μM). If DOC concentration was higher than 400 μM samples were diluted with low-carbon Milli-Q water. The system blank was measured every day at the beginning and the end of analyses using low-carbon Milli-Q water (<3 μM C). The detection limit of the instrument was 4.1 μM, while the coefficient of variation (CV) was 1.5% max (measurement accuracy).

The instrument functioning was assessed every day by comparison of data with DOC Consensus Reference Material (CRM), kindly provided by Prof. D. Hansell. For atmospheric deposition samples, DOC nominal value was 41-44 μM (batch 15 Lot #07-15), DOC measured value was 42.78±1.20 μM (n=15) (Hansell, 2005). For open sea waters of the Med Sea, all information are reported in Chapter 1 (paragraph 2.3). For mesocosm sample (Red Sea), DOC nominal value was 41-44 μM (batch 15 Lot #07-15) and measured concentrations was 43.4 ± 1.0 μM, n = 11. DOC analyses were carried out at the laboratory of the Biophysics Institute of the CNR in Pisa.

3. DOP and DON analysis

Twenty-six samples out of the total 33 were used for the DON and DOP analyzes, the volume of samples Lmp02, Lmp03 and Lmp05 to Lmp09 was not enough for nutrient analysis.

DON was estimated by subtracting the dissolved inorganic nitrogen (DIN) from the total dissolved N (TDN) (DON=TDN-DIN). DIN and TDN were analyzed by continuous flow according to Aminot and Kerouel (2007) using a Technicon autoanalyser with an estimated limit of detection of 20 nM. TDN was analyzed after persulfate wet-oxidation (Pujo-Pay et al., 1997).

DOP concentrations were calculated indirectly by subtracting the inorganic form, the soluble reactive phosphorus (SRP) from the total P (DOP=TDP-SRP). SRP was measured spectrophotometrically following the formation of phosphomolybdic acid, and TDP was obtained after UV digestion (Armstrong et al., 1966). SRP analysis involved an acidified solution of ammonium molybdate, ascorbic acid and antimony-tartrate. The blue posphomolybdenum complex formed was read colorimetrically at 880 nm (Murphy and Riley, 1962). TDP consisted of an UV digestion of the sample followed by autoanalysis of the digestion product. The modified photoxidation technique included a 2 hours UV treatment. Organic phosphorus standard (β-glycerol-phosphate) was used in order to check the efficiency of digestion. A calibration curve was performed from a potassium

phosphate monobasic (KH_2PO_4) standard solution (1 mM). Working standard was prepared by volumetric dilutions of the stock using glass pipettes and a plastic volumetric flask.

These analysis were carried out at the laboratory of the Mediterranean Institute of Oceanography (MIO) under the supervision of Dr. Elvira Pulido Villena.

4. CDOM and FDOM analysis

CDOM and FDOM analysis were carried out at the laboratory of the Biophysics Institute of the CNR in Pisa.

4.1 Absorption of CDOM

Absorbance spectra were registered between 230 and 700 nm every 0.5 nm, using a Jasco Mod-7850 spectrophotometer with a 10 cm quartz cuvette. Absorption coefficients (a) were calculated by the Eq. (1):

$$a_{(\lambda)}=2.303*(A_{(\lambda)}/l) \qquad \text{(Eq. 1)}$$

where A_λ is the absorbance at the wavelength λ, L is the path length expressed in meters and 2.303 is the conversion factor between base 10 logarithm and natural logarithm. The absorption spectrum provides both quantitative and qualitative information on CDOM. The values were calculated at the following wavelengths: 254, 280, 325, 355 and 443 nm. 280 and 355 nm were chosen because of the maximum in protein-like and humic-like absorption, 254, 325 and 443 were selected in order to facilitate the comparison with the literature. The intensity of a_λ at 254 nm (a_{254}) is usually used as an indicator of the concentration of CDOM, since at this wavelength most of the compounds occurring in CDOM pool absorb (Del Vecchio and Blough, 2004). The shape of the absorption spectrum indicates changes in CDOM composition.

The dependence of a_λ on λ is typically described by the following exponential function:

$$a_{(\lambda)}=a_{(\lambda 0)}*e^{-S(\lambda-\lambda 0)} \qquad \text{(Eq. 2)}$$

where a_λ and $a_{\lambda 0}$ are the absorption coefficients at wavelength λ and reference wavelength λ_0. S is the spectral slope coefficient in the λ-λ_0 nm spectral range. S defines how rapidly

the absorption decreases with increasing wavelength. S can be used as a proxy for average molecular weight of CDOM (Floge and Wells, 2007; Guéguen and Cuss, 2011).

Another approach for characterization of CDOM absorption spectra is to use a linear fit of the log-linearized a_λ spectrum over the 275-295 nm spectral range ($S_{275-295}$), because this range is characterized by the greatest variations (Helms et al., 2008) and can be related to the percentage of terrestrial DOC (Fichot and Benner, 2012). The $S_{275-295}$ and also the ratio of S values from UVB and UVA (350-400 nm), named the slope ratio (S_r), are correlated with molecular weight and exposure to photochemical degradation (Helms et al., 2008; Guéguen and Cuss, 2011). The S_r values are normally <1 for terrestrial CDOM, and >1.5 for oceanic and extensively photodegrated terrestrial CDOM (Stedmon and Carlson, 2015).

Additional qualitative information have been obtained normalizing the a_{254} by DOC concentration (Stedmon and Nelson, 2015). This parameters is termed SUVA, and is a valuable indicator of DOM quality (Weishaar et al., 2003; Stedmon and Nelson, 2015).

4.2 Fluorescence of CDOM

Excitation-emission matrices (EEMs) were measured using the Aqualog Spectrofluorometer (Horiba Jobin Ivon), with a 10x10 mm^2 quartz cuvette. This instrument has been specifically developed to measure EEMs of FDOM. It is equipped with a TE-cooled CCD fluorescence emission detector allowing for data acquisition up to100 times faster than any other benchtop fluorimeter. The fast acquisition also maintains photobleaching at its minimum. The emission spectra were measured in the range of 212-619 nm at 3 nm increment over an excitation wavelength between 250 and 450 nm at 5 nm increment. The integration time was adjusted on the basis of fluorescence intensity of the samples and it was 5 seconds for atmospheric samples and 10 seconds for seawater samples. Fluorescence signal were corrected for the inner-filter effect. EEMs were corrected for instrumental bias in excitation and emission and subtracted by the spectrum of Milli-Q water (blank) measured in the same conditions as the sample. Rayleigh and Raman scatter peaks were removed by using the monotone cubic interpolation (shape-preserving) (Gonnelli et al., 2016), since blank subtraction do not completely remove their signals. Spectra were normalized to the water Raman signal, dividing the fluorescence by the integrated Raman band of Milli-Q water (λ_{ex}=350 nm, λ_{em}=371-428 nm), measured the same day of the analysis. The fluorescence intensity is reported as equivalent water Raman Units (R.U.) (Lawaetz and Stedmon, 2009).

4.2.1 *PARAFAC modeling*

The parallel factorial analysis (PARAFAC) (drEEM Toolbox, Murphy et al., 2014) was applied to the EEMs after the normalization to their maximum, in order to avoid the removal of the high intensity EEMs as outliers. The analysis was conducted with Matlab R2015a (MathWorks, USA). A 5-component model was validated in the FDOM pool of open sea waters of the Mediterranean Sea, starting from 103 EEMs. A 7-component model was validated in the FDOM pool of atmospheric deposition collected at the island of Lampedusa, starting from 84 EEMs. A 5-component model was validated in the FDOM pool of surface waters of the Northern Red Sea (mesocosm experiment), starting from 88 EEMs. More detailed are provided in the Chapter 1, 2 and 3, respectively. Model validation was performed by split-half diagnostics and random initialization. To this end, the set of input data is split into two halves and PARAFAC is carried out for both halves independently. The model is considered to be applicable if the results gained from both halves are similar.

Murphy et al. (2014) developed an on-line database (https://openfluor.lablicate.com) of published fluorescent spectra in which it is possible to search for matches with any set of unknown spectra, coming from different environments, such as rivers, lakes, coastal area, polluted waters, open sea, wastewaters.

5. Nutrients and metals soluble fraction

The concentration of soluble metals was measured on the samples filtered on 47 mm pre-fired, 2 μm-nominal porosity quartz filters. These filters have low blanks level for metals and ions respect to the determined concentration both in the soluble and particulate fraction (the latter data set was not included in this paper). After filtration ~10 mL of sample were collected in vials and spiked by 0.1 mL of sub-boiled distilled (s.b.) HNO_3 to preserve the metals in their soluble form.

Metals were determined by means of an Inductively Coupled Plasma Atomic Emission Spectrometer (ICP-AES, Varian 720-ES) equipped with an ultrasonic nebulizer (U5000 ATC, Cetac Technologies Inc.). Daily calibration standards (internal standard: 1 ppm Ge) were used for quantification. Chemical analyses were carried out at Department of Chemistry "Ugo Schiff", University of Florence by Dr.ssa Silvia Becagli.

6. Atmospheric fluxes

Atmospheric fluxes of the different parameters (DOC, DON, DOP, CDOM, FDOM and metals) were calculated using the following formula:

$$X_{Flux} = X \cdot V/A \cdot days \qquad \text{(Eq. 3)}$$

where X is the concentration measured in the sample: μM for DOC, DON and DOP, μg/L for metals, m^{-1} for CDOM, and Raman Unit (R.U.) for FDOM; V is the volume (L) of rain collected by the sampler or the volume of Milli-Q water used to wash the funnel walls in case of dry deposition (250 ml) and A is the area of the funnel (0.1018 m^2).

7. PM_{10} analysis

PM_{10} is routinely sampled on a daily basis at the island of Lampedusa (Becagli et al., 2013; Marconi et al., 2014; Calzolai et al., 2015) by using a low-volume dual-channel sequential sampler (HYDRA FAI Instruments) equipped with two PM_{10} sampling heads, operating in accord with UNI EN12341. The PM_{10} mass was determined by weighting the filters before and after sampling with an analytical balance in controlled conditions of temperature (20±1 °C) and relative humidity (50±5%). The estimated error on PM10 mass is around 1% at 30 μg m^{-3} in the applied sampling conditions. PM_{10} analyses were carried out at Department of Chemistry "Ugo Schiff", University of Florence by Dr.ssa Silvia Becagli.

8. Air mass trajectories

Air masses trajectories computed by the Hybrid Single-Particle Lagrangian Integrated Trajectories (HYSPLIT) model (Draxler and Rolph, 2003; NOAA Air Resources Laboratory, Silver Spring, Maryland, available at *http://www.arl.noaa.gov/ready/hysplit4.html*) were used to assess the African provenance of the air masses reaching the study area. The study of the air masses trajectories allows to associate their origin with the transport of dust (Meloni et al., 2008; Escudero et al. 2006, 2011) and atmospheric pollutants (Pongkiatkul and Oanh, 2007). To this end, 5-day back trajectories at three different altitudes (500, 1500 and 3000 m above sea level) were obtained daily, starting at 12:00 UTC. The choice of the altitudes was done in agreement with the literature and the recent studies carried out in Lampedusa (Vincent et al., 2016).

9. Bacterial production (BP)

BP was measured during the dust addition experiment (Chapter 3). Rates of bacterial production were estimated using the [4,5-3H]-leucine incorporation method (Simon et al., 1990). Three aliquots (1.7 mL) from each mesocosm were incubated with 10 nmol of leucine L-1 (Perkin Elmer, specific activity 156 Ci mmol-1) for 4-6 h, at ambient temperature in the dark. Samples treated with trichloroacetic acid (TCA) at T0 were used as a control. The incubations were terminated with 100 µL of TCA (100%), followed by micro-centrifugation. After adding 1 mL of scintillation cocktail (Ultima-Gold) to each vial, the samples were counted using a TRI-CARB 2100 TR (Packard) liquid scintillation counter. A conversion factor of 1.5 kg C per mole leucine incorporated was used (Simon et al., 1989).

10. Bacterial abundance (BA)

BA was measured during the dust addition experiment (Chapter 3). Seawater samples (1 mL) were fixed with 50% glutaraldehyde (Sigma G7651), stained with 0.5 nM SYTO9 (Applied-Biosystems) and analyzed with an Attune acoustic focusing flow-cytometer (Applied-Biosystems) as described in Rahav and Bar-Zeev (2017).

CHAPTER 1

This chapter reports the paper titled “DOM dynamics in open sea waters of the Mediterranean Sea: New insights from optical properties” under second revision in Deep Sea Research, I.

“You must not lose faith in humanity. Humanity is an ocean; if a few drops of the ocean are dirty, the ocean does not become dirty.”

Mahatma Gandhi

DOM dynamics in open sea waters of the Mediterranean Sea: New insights from optical properties

Galletti Y.[1], Gonnelli M.[1], Retelletti Brogi S.[1,2], Vestri S.[1], Santinelli C.[1*]

[1] Biophysics Institute, Italian National Research Council. Via G. Moruzzi 1, Pisa 56124, Italy
[2] Department of Environment & Energy, Sejong University, Seoul 05006, South Korea

*** Corresponding author**

Chiara Santinelli

E-mail: chiara.santinelli@pi.ibf.cnr.it

Tel. +39 050 3152755

ABSTRACT

In the Mediterranean Sea (Med Sea), Dissolved Organic Matter (DOM) dynamics shows some peculiarities that can be investigated by using its optical properties. Despite being a marginal sea, it behaves as a miniature ocean for DOM concentrations and distribution, but its surface waters are “greener” than it would normally result from their generally low phytoplankton content and DOC in the deep water is ~1000 years older and more degraded than in the Atlantic Ocean, suggesting a greater contribution of allochthonous substances to the DOM pool in this basin. With this work we aim at presenting new data on optical properties (absorption, CDOM and fluorescence, FDOM) of DOM in open sea waters of the Med Sea, in order to investigate the main drivers of CDOM and FDOM dynamics in both surface and deep waters and to get insights into CDOM and FDOM origin in the offshore waters of the Med Sea.

Our data support the different DOM composition with respect to the oceans and suggest some differences with respect to the other marginal basins, opening intriguing questions about the source and cycle of allochthonous molecules in the open sea waters of the Med Sea. CDOM absorption in the western Med Sea and Ionian Sea is generally lower than that observed in the other marginal seas, but higher than in the oceans. The parallel factor analysis unveiled the presence of a PAH-like and terrestrial humic-like component found in the other marginal basins but not in the open oceans. In contrast with the oceans and most of the marginal seas, only one protein-like component was found. Interestingly, no production of humic-like DOM as function of mineralization rates was observed in the intermediate and deep waters of the Med Sea, supporting that in this basin, humic-like DOM mainly has an allochthonous origin. Our data confirm that in the surface layer photobleaching plays a relevant role in the removal of humic-like fluorescence, and that the release of both protein-like and humic-like substances occur in proximity of the deep chlorophyll maximum.

KEYWORDS

CDOM
DOC
Carbon cycling
Mediterranean Sea
Fluorescence excitation-emission matrixes
Terrestrial humic-like substances
PARAFAC

1. Introduction

Dissolved organic matter (DOM) in the oceans contains one of the largest reservoirs of reduced carbon on the Earth, the Dissolved Organic Carbon (DOC) (Hansell et al., 2009). DOC is a key player in the global carbon cycle and in the functioning of marine ecosystem. Various fractions have been distinguished in its pool depending on their lifetime, going from hours-days (labile, LDOC), to months (semi-labile, SLDOC), years (semi-refractory, SRDOC) up to thousands of years (16,000 years, refractory, RDOC; ~40,000 years, ultra-refractory, URDOC) (Hansell, 2013). Most of the labile DOC is produced in the ocean epipelagic layer (0-150 m) and this fraction supports the metabolic energy and nutrient demands of heterotrophic prokaryotes (Carlson and Hansell, 2015). In the oceans, DOC shows concentrations ranging between 80 μM in surface waters and mid ocean gyres and 48-34 μM in the deep Atlantic and Pacific (Hansell et al., 2009). A highly variable fraction of DOM is chromophoric (CDOM), it absorbs light at the UV and visible wavelengths and can emit part of the absorbed light as fluorescence (FDOM). CDOM is ubiquitous in marine environment and influences the optical properties of the water column, it has been also reported as a tracer of deep biogeochemical processes and circulation (Nelson and Siegel, 2013). Optical properties (absorption and fluorescence) of CDOM can give indirect information about qualitative changes in DOM pool and its main sources. The parallel factor analysis (PARAFAC) applied to the fluorescence excitation emission matrixes (EEMs) is today one of the most used tools to gain information on CDOM composition and origin (Stedmon and Bro, 2008; Stedmon and Markager, 2005; Stedmon et al., 2003; Yamashita et al., 2013; Jørgensen et al., 2011; Catalá et al., 2015; 2016; Margolin et al., 2018; Gonnelli et al., 2016).

DOM dynamics shows some peculiarities in the Mediterranean Sea (Med Sea) that can be investigated by using its optical properties. Despite being a marginal sea, it shows DOC concentrations and distributions very similar to those observed in the global oceans (Santinelli et al., 2015), but its surface waters (0-20 m) are “greener” than it would normally result from their generally low phytoplankton content, making the algorithms commonly in use in Space Agencies for the retrieval of Chlorophyll overestimating the field values (Antoine et al., 2008). This feature can be explained by the enhanced absorption in the blue and enhanced backscattering in the green parts of the visible spectrum likely resulting from the presence of submicron Saharan dust in suspension within the upper layer (Claustre et al., 2002), as well as by the unusually high yellow substances content of the surface Med Sea water (Morel et al., 2007). Morel and Gentili (2009), using simultaneous

consideration of marine reflectance at 4 spectral bands (412, 443, 490 and 550 nm), supported that CDOM (quantified as the absorption coefficient at 443 nm) is about twice in the Med Sea than in the Atlantic Ocean at the same latitude. In the offshore waters of the western Med Sea (Boussole site) CDOM dominates light absorption at 440 nm (>50%) all over the year with the exception of March and April, when the absorption is dominated by the photosynthetic pigments of phytoplankton, and it was the only dominant light-absorbing substance below the deep chlorophyll maximum (DCM) (Organelli et al., 2014). In coastal areas CDOM mainly has a terrestrial origin, (Gonnelli et al. 2013,: Retelletti Brogi et al. 2015; Para et al., 2010; Vignudelli et al., 2004; Seritti et al., 1998), whereas in the surface offshore waters of the Med Sea, it shows a clear seasonal dynamics related to phytoplankton and microbial activity, supporting that it is mainly autochthonous (Pérez et al., 2016; Organelli et al., 2014; 2017; Xing et al., 2014). A recent extended study about CDOM dynamics showed that in the epipelagic layer community respiration drives DOC and a_{254} dynamics, whereas water column stability and photobleaching are the main drivers of a_{325} and spectral slope (Catalá et al., 2018). These studies are limited to CDOM absorption, no fluorescence data are reported.

Moving to deep waters, isotope data unveil that DOC is depleted in both $\Delta^{14}C$ and $\delta^{13}C$ with respect to the deep Atlantic Ocean, suggesting that its pool is ~1000 years older than in the Atlantic Ocean (Santinelli et al., 2015). This finding was explained by the replacement of 10% and up to 45% of the Atlantic RDOC entering the basin by allocthonous (isotopically lighter and older) DOC (Santinelli et al., 2015). The different chemical composition of DOC in the Med Sea with respect to the oceans is also supported by the Fourier Transform Ion Cyclotron Resonance mass spectroscopy (FT-ICR-MS) data (Martínez-Pérez et al., 2017a). These authors showed that DOC in the Med Sea outflow is more degraded than in the Atlantic inflow. Few information are reported about CDOM and/or FDOM dynamics in intermediate and deep waters (Bracchini et al., 2010; Catalá et al., 2018; Martìnez-Pérez et al. 2017) to support these observation and only one paper reports basin-wide patterns of a_{254} and $S_{275-295}$, showing that below the euphotic zone, CDOM dynamics is mainly shaped by water masses mixing and basin-scale mineralization (Catalá et al., 2018).

Despite CDOM is a relevant player in the biogeochemistry and bio-optical properties of the Med Sea, many aspects need to be clarified in particular about CDOM and FDOM dynamics in open sea waters. With this work we aim at presenting new data on DOC and optical properties (both absorption and fluorescence) of CDOM in open sea waters of the

Med Sea, in order to: (i) investigate the main drivers of CDOM and FDOM dynamics in both surface and deep waters of the Med Sea; (ii) get insights into CDOM and FDOM origin in the offshore waters of the Med Sea. These data will also contribute to test the hypothesis that in the Med Sea DOM pool is constituted by a larger fraction of allocthonous (humic-like, yellow substances) material than in the oceans, despite the DOC concentration and distribution is exactly the same as in the open ocean.

2. Materials and methods

2.1 *Study sites and sample collection*

Samples for DOC, CDOM and FDOM analysis were collected in open sea waters of the Med Sea during 3 oceanographic cruises carried out in March/April 2008, August 2010 and November 2011 on board the R/V *Urania* of the Italian National Research Council (CNR) (Fig. 1.1 and Table 1.1).

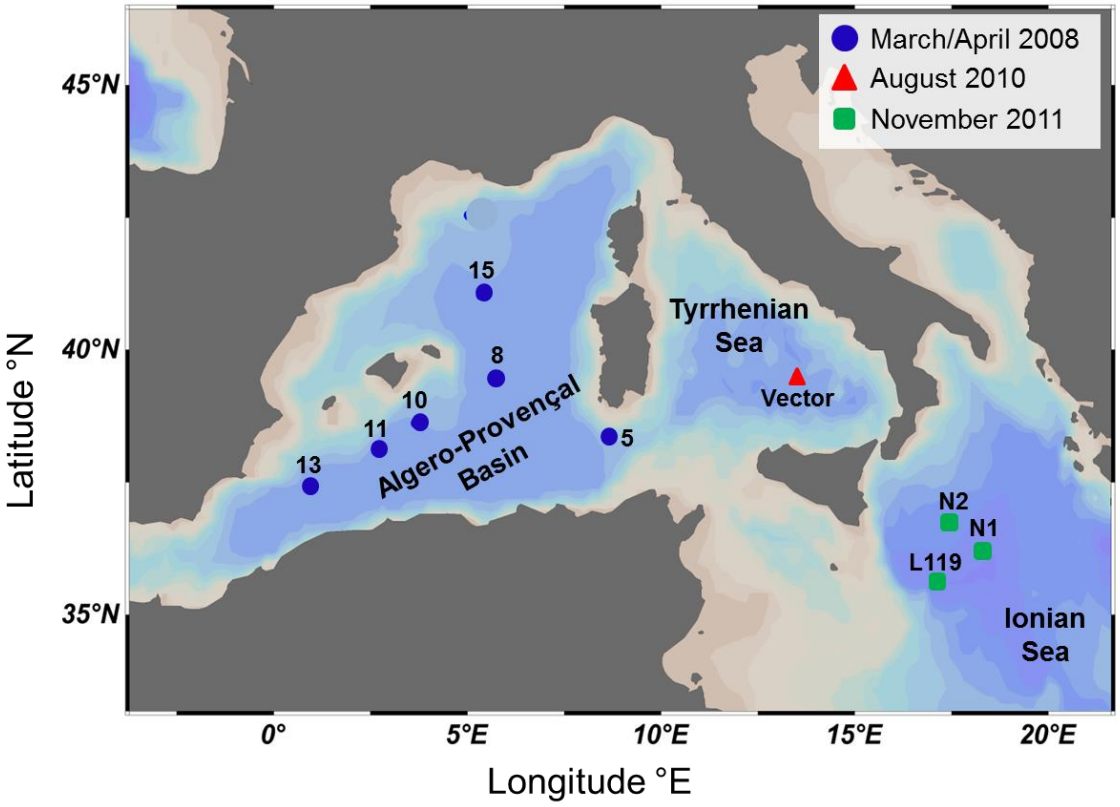

Figure 1.1. Study areas and sampling stations.

At all stations pressure, salinity, temperature and oxygen were measured through a SBE 911 plus CTD, equipped with a rosette sampler with 24 x 10-L Niskin bottles. The

CTD-rosette system was lowered at a speed of 1 m·s-1. The data were processed in real time, viewed and corrected to eliminate errors. CTD-oxygen was calibrated by Winkler titration (Williams and Jenkinson, 1982) of selected discrete samples. Oxygen saturation was calculated using calibrated CTD data and the solubility equations of Garcia and Gordon (1992) and coefficients of Benson and Krause (1984). Apparent oxygen utilization (AOU) was calculated as difference between oxygen saturation and oxygen.

Chlorophyll-a fluorescence (Chl-a) was measured by means of a SEA-TECH fluorometer mounted on the rosette sampler. Data are reported as Fluorescence Units (Fl.U.). Assuming that no drift in the instrument response occurred within each cruise, fluorescence profiles are used to highlight differences in autotrophic biomass among stations and to determine the depth interval of the DCM (Santinelli et al., 2008).

The index of stratification ($Index_{str}$) was calculated as the difference between density at 5 m and at 200 m, according to Santinelli et al. (2013).

Mixed layer depths (MLD) were estimated from CTD temperature profiles, and defined by a ≥ 0.1 °C deviation with respect to the temperature at 5 m depth, in agreement with Pérez et al., (2016).

Study Area	**Cruise**	**Date**	**Time h**	**Station**	**Lat °N**	**Long °E**	**$Index_{str}$ $kg \cdot m^{-3}$**	**MLD m**
Algero-Provençal Basin	Sesame S-IT4	03-29-2008	13:13	5	38.32	08.65	0.56	>250
		03-30-2008	10:46	8	39.50	05.65	0.93	29(139)
		04-02-2008	14:01	10	38.62	03.65	1.12	70
		04-02-2008	7:50	11	38.18	02.65	1.23	38(86)
		04-01-2008	12:26	13	37.43	01.00	1.27	38
		04-05-2008	11:31	15	41.03	05.33	0.30	56
Tyrrhenian Sea	Venus-1	08-18-2010	2:13	Vector	39.30	13.30	3.86	19
Ionian Sea	SICSIA 2011	11-26-2011	19:51	N1	36.14	18.33	1.39	57
		11-27-2011	2:49	N2	36.74	17.43	1.22	58
		11-25-2011	7:48	L119	35.61	17.08	1.88	39

Table 1.1. Details of the sampling stations. $Index_{str}$ is the stratification index, MLD is the Mixed Layer Depth.

2.2 *Sample treatment*

Samples for DOC, CDOM and FDOM measurements were collected along the water column at the following depths: 2, 20, 50, 75, 100, 150, 200, 400, 500, and every 250 m until the bottom. Samples were collected in 200 ml dark glass bottles, preconditioned with filtered deep seawater and rinsed 3 times with the sample before its collection. Samples were immediately filtered on board via sterile 0.2 µm nylon filters (Sartorius, 17845-ACK) under pressure of high-purity air (Santinelli et al., 2010). Filtered samples were stored at 4 °C in the dark until the analysis, carried out within 1 month from the sampling. No change in DOC concentration and optical properties of CDOM was observed within this period (Santinelli et al., 2010).

2.3 *DOC analysis*

DOC measurements were carried out with a Shimadzu TOC-VCSN, by high-temperature catalytic oxidation. Samples were acidified with HCl 2N and sparged for 3 min with CO_2-free pure air in order to remove inorganic carbon. From 3 to 5 replicate injections were performed until the analytical precision was lower than 1% (±1 µM). A 5-point calibration curve was done by injecting standard solutions of potassium hydrogen phthalate between 20 and 130 µM. At the beginning and at the end of each analytical day, the system blank was measured using Milli-Q water and the functioning of the instrument was checked by comparison of data with DOC Consensus Reference Material (CRM) (Hansell, 2005) (batch#7-2007, batch#10-2010/Lot#5-10, batch#11-2011/Lot#03-11, Consensus values: 41 - 44 µM, measured concentration: 41.9 ± 1.3 µM, standard error = 0.23 µM, n = 39). For further analytical details see Santinelli et al. (2010).

2.4 *CDOM optical properties*

2.4.1 Absorbance measurements

CDOM absorbance was measured throughout the UV and visible spectral domains (230-700 nm) with a resolution of 0.5 nm, by using a JASCO Spectrophotometer V-550 and a 10 cm quartz cuvette. The photometric reproducibility of the instrument is ± 0.001 Abs. The spectrum of Milli-Q water, measured in the same conditions, was subtracted from

each sample. Initial, intermediate and final blanks were measured to check for the instrument functioning. The absorbance (A) was converted into absorption coefficients (a) by using equation (1):

$$a_\lambda = 2.303 \cdot \frac{A_\lambda}{L} + k \quad (1)$$

where A_λ is the absorbance at the wavelength λ and L is the cuvette pathlength expressed in m and k is an offset calculated as the mean absorbance between wavelengths 650 nm and 700 nm (approximately zero) (Green and Blough 1994). The absorption coefficient (a_λ) was calculated at different wavelengths (254, 280, 325 nm), in order to facilitate the comparison with data reported in the literature. a_{254} is considered representative of the CDOM pool, since it is a proxy for the abundance of conjugated carbon double bounds (Lakowicz, 2006), it is therefore used to gain quantitative information on the whole CDOM pool.

The CDOM absorption spectrum is typically described using equation (2), according with Green and Blough, (1994):

$$a_\lambda = a_{\lambda_0} \cdot e^{-S(\lambda-\lambda_0)} \quad (2)$$

where S is the spectral slope coefficient in the λ-λ_0 nm spectral range. S was estimated over the 275-295 nm spectral range ($S_{275\text{-}295}$), because this range is characterized by the greatest variations and it has been demonstrated to be a reliable proxy of CDOM average molecular weight (Helms et al., 2008) and a potential indicator of photobleaching and DOM source in marine environment (Helms et al., 2008; Fichot and Benner, 2012).

The specific ultraviolet absorbance at 254 nm (SUVA254) was calculated by dividing the A_{254} by DOC concentration in units mg C L^{-1} (Weishaar et al. 2003). SUVA254 has been reported to be strongly correlated with percent aromaticity, it is therefore considered a useful parameter for estimating the dissolved aromatic carbon content in aquatic systems (Weishaar et al. 2003).

Five measurements (including all handling steps), carried out within the period of the analysis on the same seawater sample, showed that the reproducibility of measurements was approximately ± 0.01 m^{-1} for a_{254} and a_{280}, ± 0.003 m^{-1} for a_{325} and ± $4 \cdot 10^{-4}$ nm^{-1} for $S_{275\text{-}295}$, that is ~1% for all the parameters.

2.4.2 Fluorescence Excitation Emission Matrixes (EEMs)

Fluorescence Excitation Emission Matrixes (EEMs) were recorded by using the Fluoromax4 spectrofluorometer (model FP770 Horiba) with a 1 x 1 cm quartz cuvette in the range 250-450 nm for the excitation and 300-600 nm for the emission. The EEMs were corrected for instrumental bias and subtracted by the EEM of Milli-Q water measured in the same conditions (blank). The Rayleigh and Raman scatter peaks were removed by using the monotone cubic interpolation (shape-preserving) (Carlson and Fritsch, 1989), since water subtraction did not completely remove their signals (Gonnelli et al., 2016; Margolin et al., 2018). EEMs were normalized to the water Raman signal, dividing the fluorescence by the integrated Raman band of Milli-Q water (λ_{ex}=350 nm, λ_{em}=371-428 nm), measured the same day of the analysis (Lawaetz and Stedmon, 2009). The fluorescence intensity is therefore reported as equivalent water Raman Units (R.U.). This standardized method was chosen because it is rapid, simple and suitable for routine measurements. No significant variation was observed in the integral of the Raman peak from repeated measurements during the period of the analysis (< 2%). In order to check the repeatability of our measurements the same sample was analyzed 5 times during a period of 3 months, the results showed that the variation was less than 2% for all the components.

The 103 EEMs were elaborated with the parallel factor analysis (PARAFAC) by using the DOMFluor toolbox (Stedmon and Bro, 2008). The validation of the model was done by visual inspection of the residuals, split half analysis and percentage of explained variance (99.5%). PARAFAC components were compared with the spectra of commercial compounds: Suwannee River (Suwriver) fulvic acids (FA) and Pahokee Peat humic acids (HA) from the International Humic Substances Society (IHSS) and tryptophan (Trp) from Sigma–Aldrich. Solutions of each individual compound were prepared by dissolving them in deep-sea water, with a low fluorescent signal, to a final concentration of: 0.5 $mg \cdot ml^{-1}$ for HA and FA, and 1 $\mu g \cdot ml^{-1}$ for Trp. Single fluorescence emission spectrum of these solutions was measured with the Fluoromax4, with 1x1 cm quartz cuvettes. Each spectrum was subtracted by the spectrum of the deep-sea water used for the dilution, measured in the same conditions.

2.5. Statistics

Differences were tested by using one-way ANOVA and the Tukey test and were considered significant when $p<0.05$ (Origin 8.5.1 software).
The correlation were investigated by using Origin 8.5.1 software and were considered robust when $p<0.0001$ for the whole dataset and $p<0.05$ for the single areas.

3. Results

3.1 *PARAFAC components*

The PARAFAC analysis, applied to the 103 EEMs measured in this study, allowed for the identification of 5 groups of fluorophores (components) in the FDOM pool. In order to identify these components, their spectra were compared with (i) spectra of commercial Trp, HA and FA dissolved in seawater, (dotted lines in Fig. 1.2), (ii) similar components reported in the literature and (iii) matching spectra obtained from the OpenFluor database database (plugin for OpenChrom, version 1.3.0; Murphy et al., 2014). These spectra were considered similar when the Tucker's congruence coefficient (TCC) exceed 0.95 (Table 1.2).

Component 1 ($C1_{PAH}$) shows spectral characteristics similar to those of anthracene (245/382 nm) and pyrene (240-270/374-392) dissolved in water (Ferretto et al., 2014). The excitation maximum at 250 nm implies low conjugation degree and low molecular weight material, typical of phenols and/or quinones of terrestrial origin. A similar component was found in the China and Okhotsk Seas, in ballast waters and in harbors (Table 1.2). $C1_{PAH}$ can be attributed to PAH contaminants and it was identified as terrestrial with an anthropogenic origin.

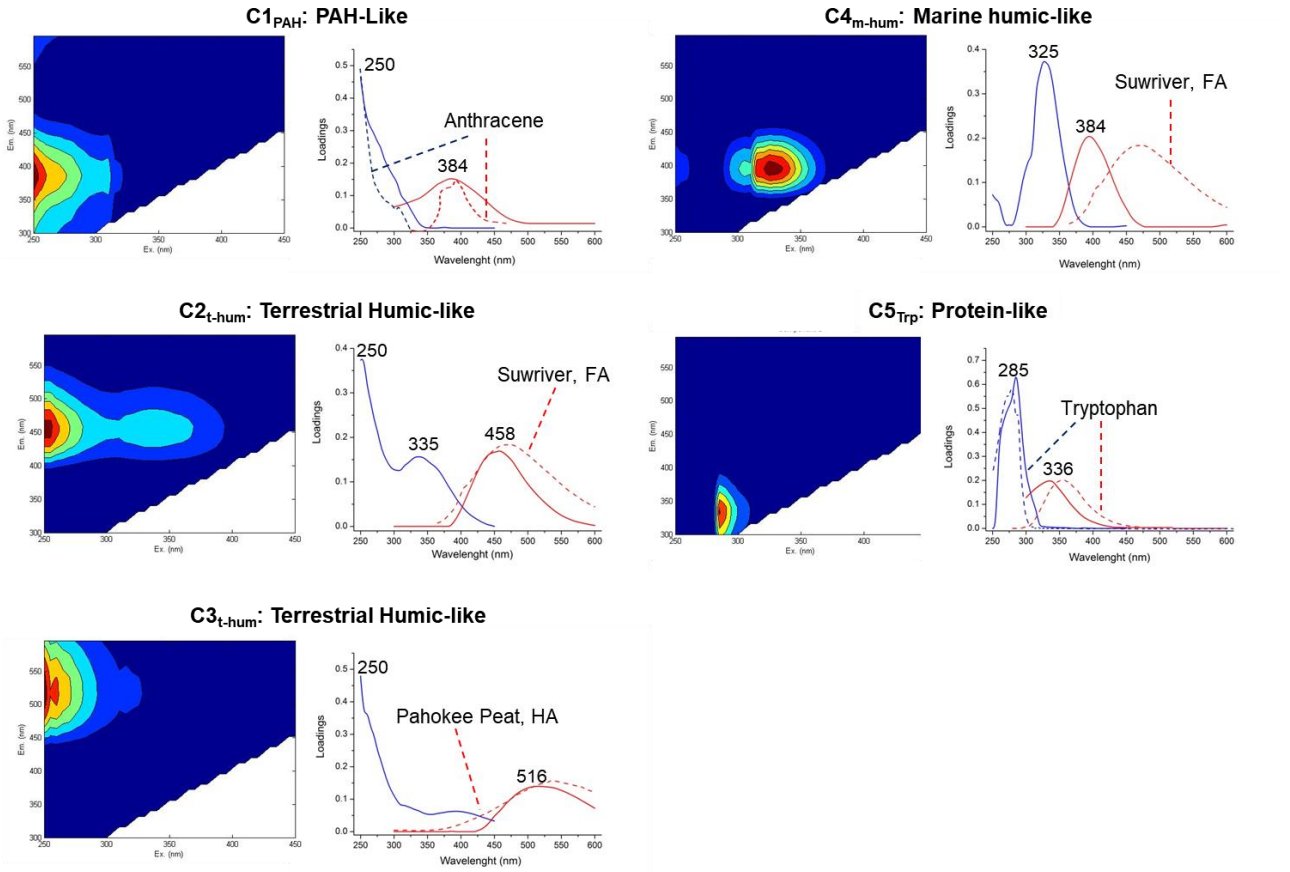

Figure 1.2. Fluorescence characteristics of the five components, dataset = 103 EEMs. Excitation (blue) and Emission (red) spectra of the five components. The spectra are overlapped to those of commercial substances (dotted lines).

Components 2 ($C2_{t\text{-}hum}$) and 3 ($C3_{t\text{-}hum}$) show spectral characteristics typical of terrestrial humic-like compounds (Table 1.2). The emission spectrum of $C2_{t\text{-}hum}$ is very similar to that of Suwannee River FA (Fig. 1.2). The Suwannee River rises in the Okefenokee Swamp in south Georgia and the decomposing vegetation is the main source of DOC to its waters. In the literature, $C2_{t\text{-}hum}$ was attributed to humic-like fluorophores derived by terrestrial input exported from natural or agricultural catchments (Stedmon and Markager, 2005a). Fluorescence spectra similar to those of $C2_{t\text{-}hum}$ were found to correlate with lignin (Walker et al., 2009), a biomarker of terrestrial plant material, further supporting its terrestrial origin. $C2_{t\text{-}hum}$ matched with 21 models in the OpenFluor, of which only 2 relative to samples collected in offshore and deep ocean waters (Jørgensen et al., 2011; Yamashita et al., 2010b) (Table 1.2).

The emission spectrum of $C3_{t\text{-}hum}$ overlaps the emission spectrum of the Pahokee peat humic acids (Fig. 1.2), that is a typical agricultural peat soil of the Florida Everglades, formed in organic deposits of freshwater marshes. A similar component was found in

estuaries and marginal sea (Baltic and North Sea, Black Sea and South Atlantic Bight) (Table 1.2). No similar component was found in offshore and deep ocean waters.

1 **$C1_{PAH}$**	250(310) /384	*PAH-like of terrestrial origin*	Pacific and Atlantic (C4) China Sea(C2) Okhotsk Sea (C1) Ballast water (C4)	NA NA NA NA	Murphy et al., 2008 Wang et al., 2017 Granskog et al., 2015 Murphy et al., 2006
2 **$C2_{t\text{-}hum}$**	250(335) /458	*Terrestrial humic-like substances (Fulvic Acids)*	Peaks “A” and “C” Epipelagic oceans (C1) Dark oceans (C1) Black Sea (C2) China Sea(C1) China Sea(C1) Okhotsk Sea (C2) Aegean Sea (C1) Horsens Estuary, Denmark (C4) Florida Keys (C2) Ballast water (C8) Wetland (C1) Patagonia lakes (C2) Baltic Sea (C1) Wastewater (C2) Wastewater (C1) South Atlantic Bight (C1) Ocean off-shore (C1) Ocean off-shore (C1)	NA NA NA NA NA NA NA NA NA NA NA 0.987 0.985 0.984 0.981 0.978 0.972 0.970 0.955	Coble, 1996 Catalá et al., 2016 Catalá et al., 2015 Margolin et al., 2018 Wang et al., 2017 Zhu et al., 2018 Granskog et al., 2015 Pitta et al., 2017 Stedmon and Markager, 2005a Yamashita et al., 2013 Murphy et al., 2006 Yamashita et al., 2010a Cárdenas et al., 2017 Stedmon et al., 2007 Murphy et al., 2011 Murphy et al., 2011 Kowalczuk et al., 2009 Jørgensen et al., 2011 Yamashita et al., 2010b
3 **$C3_{t\text{-}hum}$**	250(395) /516	*Terrestrial humic-like substances (Humic Acids)*	Peaks “A” and “C” Ballast water (C3) South Atlantic Bight (C4) Florida Keys (C4) Baltic Sea (C3) Horsens Estuary, Denmark (C2) Shark Bay Estuary (C2) Baltic and North Sea (C2) Black Sea (C4)	NA NA NA 0.959 NA NA 0.958 0.952 NA	Coble, 1996 Murphy et al., 2006 Kowalczuk et al., 2009 Yamashita et al., 2013 Stedmon et al., 2007 Stedmon and Markager, 2005a Cawley et al., 2012 Osburn and Stedmon, 2011 Margolin et al., 2018
4 **$C4_{m\text{-}hum}$**	325/394	*Marine humic-like substances*	Marine humic peak “M” Aegean Sea (C2) Baltic Sea (C2) Ocean off-shore (C4) Epipelagic oceans (C2) Dark oceans (C2) Ballast water (C2) Horsens Estuary, Denmark (C5)	NA NA NA NA NA NA NA NA	Coble, 1996 Pitta et al., 2017 Stedmon et al., 2007 Jørgensen et al., 2011 Catalá et al., 2016 Catalá et al., 2015 Murphy et al., 2006 Stedmon and Markager, 2005a

			South Atlantic Bight (C3)	NA	Kowalczuk et al., 2009
			Florida Keys (C1)	NA	Yamashita et al., 2013
5 **$C5_{Trp}$**	285/336	*Protein-like (Tryptophan)*	Peak "T"	NA	Coble, 1996
			Horsens Estuary, Denmark (C7)	NA	Stedmon and Markager, 2005a Stedmon et al., 2007
			Baltic Sea (C5)	NA	Murphy et al., 2006
			Ballast water (C6)	NA	Jørgensen et al., 2011
			Ocean off-shore (C5)	NA	Yamashita et al., 2013
			Florida Keys (C5)	NA	Stedmon and Markager, 2005b
			Mesocosm, Baltic Sea (C6)	NA	Kowalczuk et al., 2009
			South Atlantic Bight (C6)	NA	Pitta et al., 2017
			Aegean Sea (C4)	NA	Osburn and Stedmon, 2011
			Baltic and North Sea (C6)	NA	Catalá et al., 2016
			Epipelagic oceans (C3)	NA	Catalá et al., 2015
			Dark oceans (C3)	NA	Margolin et al., 2018
			Black Sea (C5)	NA	Wang et al., 2017
			China Sea(C4)	NA	Zhu et al., 2018
			China Sea(C3)	NA	Granskog et al., 2015
			Okhotsk Sea (C3)		

Table 1.2. Identification of the 5 components through the comparison with literature data. Tucker's congruence coefficient (TCC) is reported for matching spectra obtained from the OpenFluor database. In bold are indicated components refering to the marginal seas.

Component 4 ($C4_{m\text{-}hum}$) shows spectral characteristics similar to those of marine humic-like substances (peak M; Coble, 1996), and is attributed to humic-like substances produced in-situ by phytoplankton and microbial activity (Zhao et al., 2017; Stedmon and Markager, 2005b; Murphy et al., 2006; 2008). However, the small shoulders at 250 nm and 310 nm could imply that the there is an overlap with C1 and that the two components were not very well resolved.

Component 5 ($C5_{Trp}$) shows features typical of tryptophan-like fluorescence as supported by the very good overlapping with the spectra of commercial Trp (Fig. 1.2). A similar component was observed in both open ocean waters and in marginal seas (Table 1.2).

Taking into consideration all the samples collected along the water column in the 3 areas, $C1_{PAH}$ shows a robust linear correlation with $C2_{t\text{-}hum}$, this correlation improves when only the samples collected in the upper 200 m of the water column are taken into consideration, whereas it is weaker in the intermediate and deep waters (200 m to the bottom) (Table 1.3). $C2_{t\text{-}hum}$ shows a good linear correlation with both $C3_{t\text{-}hum}$ and $C4_{m\text{-}hum}$, that strongly improves for $C3_{t\text{-}hum}$ in the upper 200 m. $C3_{t\text{-}hum}$ and $C4_{m\text{-}hum}$ show a good linear correlation in the upper 200 m, that is completely lost below 200 m. Finally, $C4_{m\text{-}hum}$ and

$C5_{Trp}$ shows a good linear correlation in the intermediate and deep waters that is lost in the upper 200 m.

	$C1_{PAH}$			$C2_{t\text{-}hum}$			$C3_{t\text{-}hum}$			$C4_{m\text{-}hum}$		
	0-btm	0-200	200-btm	0-btm	0-200	200-Btm	0-Btm	0-200	200-Btm	0-Btm	0-200	200-Btm
$C1_{PAH}$												
$C2_{t\text{-}hum}$	**0.50****	**0.58****	0.35**									
$C3_{t\text{-}hum}$	0.21**	0.40**	0.11*	**0.57****	**0.75****	0.36**						
$C4_{m\text{-}hum}$	0.29**	0.25**	0.40**	**0.56****	**0.56****	**0.56****	0.33**	**0.51****	0.11*			
$C5_{Trp}$	0.36**	0.20*	**0.53****	0.11*	-	0.27**	-	-	-	-	-	**0.53****

Table 1.3. Values of r^2 and *p* for the linear correlations among the 5 components, taking into consideration all the data collected in this study. All the correlations are direct. Btm= Bottom. Values of $r^2 < 0.1$ are not reported; values of $r^2 > 0.5$ are in bold. *p<0.005; **p<0.0001.

3.2 *Physical characteristics of the study area*

In order to simplify the representation of the results, the stations were assembled in 3 groups based on their thermohaline properties, that correspond to the 3 sampled areas: APB=Algero-Provençal Basin, TS=Tyrrhenian Sea and IS=Ionian Sea. Intermediate and deep waters at station 5, located in the Sardinian Channel (Fig. 1.1), show thermohaline properties more similar to those at the Vector station, than at the other stations sampled in the APB (Fig. A1), this station was therefore included in the TS group. The vertical profiles of mean DOC, AOU, CDOM and FDOM components were calculated taking into consideration the 3 groups of stations.

3.3 *Vertical profiles of DOC and AOU*

DOC showed the highest and most variable concentrations (50-84 μM) in the surface layer (0-100 m) (Fig. 1.3). Average values in the upper 100 m were significantly lower ($p < 0.05$) in the APB (57±4 μM) than in the IS and TS (64±5 μM). In the intermediate layer, DOC gradually decreased with depth (Fig. 1.3) to reach the lowest average concentration (40±1 μM in the WM, 42±3 μM in the TS and 39±2 μM in the IS) between 750 and 2000 m. Below 2000 m, the mean values were almost constant (42-43 μM) in the 3 areas, with a slight increase in the samples close to the bottom, in particular in the APB (40-49 μM, 2500-bottom). Vertical profiles of AOU were opposite to those of DOC. The lowest values were observed in the surface layer, followed by a maximum between 200 and 500 m in the APB and TS (81±3 and 73±2 μM, respectively), and in

correspondence with the DOC minimum (1000-1500 m) in the IS (66±4 µM). In the deep waters, AOU was almost constant with depth in the TS (69-72 µM, 2500-bottom), while in the APB and IS it slightly decreased below 500-1000 m, in correspondence with the DOC increase (Fig. 1.3).

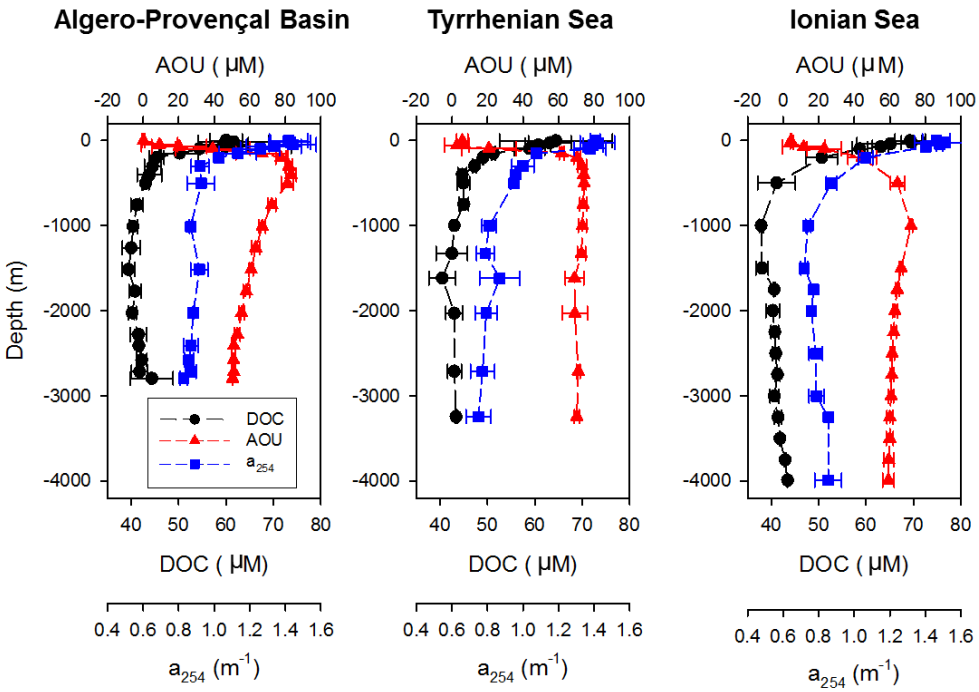

Figure 1.3. Vertical profiles of mean DOC, AOU and CDOM (a_{254}) for the 3 areas. Error bars refer to the standard deviation among stations.

3.4 Vertical profiles of CDOM

Taking into consideration all the data collected in this study, a_{254}, a_{280}, and a_{325} ranged between 0.69-1.54 m^{-1}, 0.07-0.33 m^{-1}, 0.09-0.28 m^{-1} respectively. $S_{275-295}$ ranged between 0.02 and 0.04 nm^{-1} with the highest values in the surface layer of the TS and IS. The lowest values of a_{254} were observed between 750 and 2000 m in the IS (0.36±0.02 m^{-1}), in correspondence with $S_{275-295}$ values of 0.030 nm^{-1}.

The vertical profiles of mean a_{254} showed the highest values in the surface layer (0-100 m) (0.8±0.09 m^{-1}), a sharp decrease below the pycnocline and values almost constant (0.36-0.49 m^{-1}) between 500-1000 m and the bottom (Fig. 1.3). Vertical profiles of a_{254} were very similar to those of DOC, with a highly significant correlation between the 2 variables (DOC = 15 (±2) + 32 (±1) a_{254}; r^2=0.80, p < 0.0001; n=119) (Fig. 1.4, Table 1.5). The linear correlation between DOC and a_{254} is maintained, even if it is less robust, when only the samples collected in the upper 200 m are taken into consideration (DOC = 22 (±6)

+ 27 (±5) a_{254}; r^2=0.40, p < 0.0001; n=51); whereas it is completely lost when only the data collected in the upper 200 m are excluded.

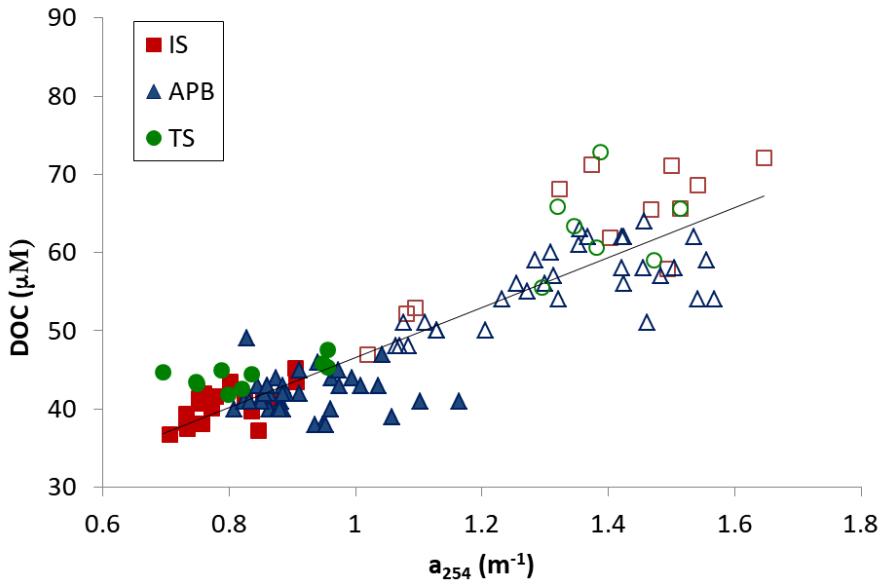

Figure 1.4: Correlation between DOC and a_{254} taking into consideration all samples. Empty symbols refer to samples collected in the upper 200 m, filled symbols to samples collected between 200 m and the bottom.

3.5 Vertical profiles of FDOM

The average vertical profiles of $C1_{PAH}$ and the 3 humic-like components were similar in the 3 areas, with the lowest intensities in the surface layer and an increase to reach a subsurface maximum, well visible in the TS and IS (Fig. 1.5). Below 150 m, a decrease was observed with intermediate and constant fluorescence values until the bottom. Along the water column, $C2_{t\text{-}hum}$ and $C3_{t\text{-}hum}$ fluorescence was significantly higher ($p<0.05$) in the APB than in the IS and TS.

The average vertical profiles of the protein-like fluorescence ($C5_{Trp}$) showed the highest intensity in the surface layer (0-20 m) and a gradual decrease with depth in the 3 areas to reach below 1000 m values 2-fold lower than in the surface waters ($p<0.05$) (Fig. 1.5). $C5_{Trp}$ fluorescence in the upper 200 m was 1.6-fold higher ($p<0.05$) in the APB than in the IS and TS.

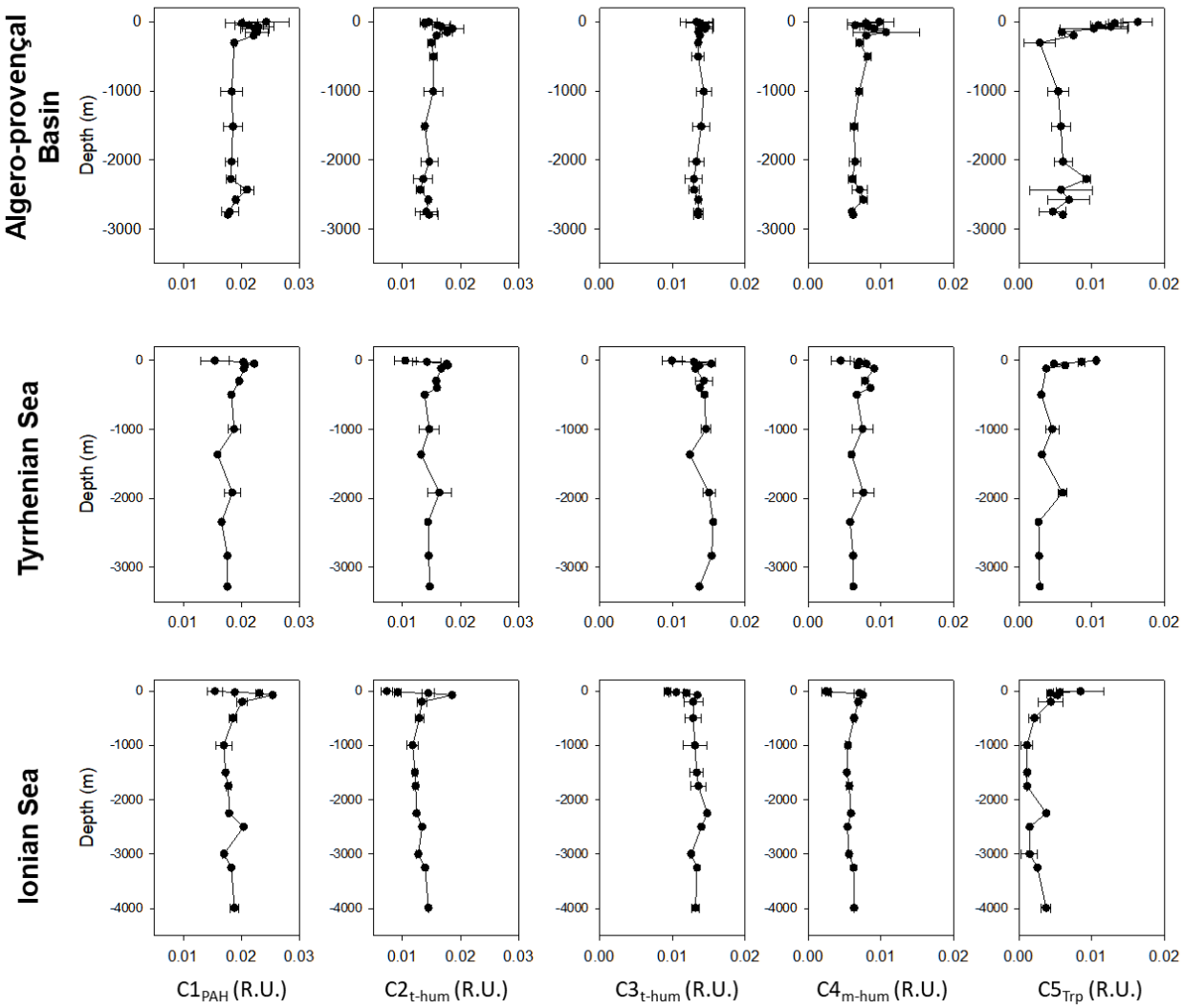

Figure 1.5. Vertical profiles of mean values for the 5 components in the 3 areas. Error bars refer to the standard deviation among stations. The x-axes scale is different, in order to better represent the vertical profiles.

3.6 Surface layer

Due to the high variability of the surface layer and to the different period of the cruises (Table 1.1), a zoom (0-250 m) of the vertical profiles of chlorophyll, temperature, density and salinity, DOC, a_{254}, $S_{275-295}$, $C3_{t\text{-}hum}$, $C4_{m\text{-}hum}$ and $C5_{Trp}$ is reported for each station separately (Fig. 1.6, 1.7 and 1.8). $C3_{t\text{-}hum}$ is reported as representative of the terrestrial humic-like FDOM, given the good linear correlation with $C2_{t\text{-}hum}$, in the upper 200 m (Table 1.3). The mixed layer was well visible in the Tyrrhenian and Ionian Seas, whereas in the Algero-Provençal Basin each station showed a different structure of the water column clearly affecting the vertical distribution of DOM, CDOM and FDOM. A well-defined mixed layer was visible only at station 13; stations 5 and 15 were almost

completely mixed, at stations 11 a weak two-stair stratification can be observed (Fig. 1.6-1.8). The highest stratification degree (stratification index > 1, Table 1.1) was observed at stations 10, 11 and 13 and it progressively decreased moving toward the Gulf of Lions (station 15) and the Sardinian Channel (station 5).

Station 13, located in the westernmost part of the study area, was characterized by a MLD of 38 m and a DCM at 50 m (Fig. 1.6); in correspondence with the DCM, a decrease in $S_{275-295}$ (0.027 nm^{-1}) as well as a peak in both $C4_{m\text{-}hum}$ and $C5_{Trp}$ (Fig. 1.7) is visible. $C3_{t\text{-}hum}$ showed a minimum in the upper 30 m, where the highest DOC values were observed and an increase in correspondence with the thermocline (Fig. 1.8).

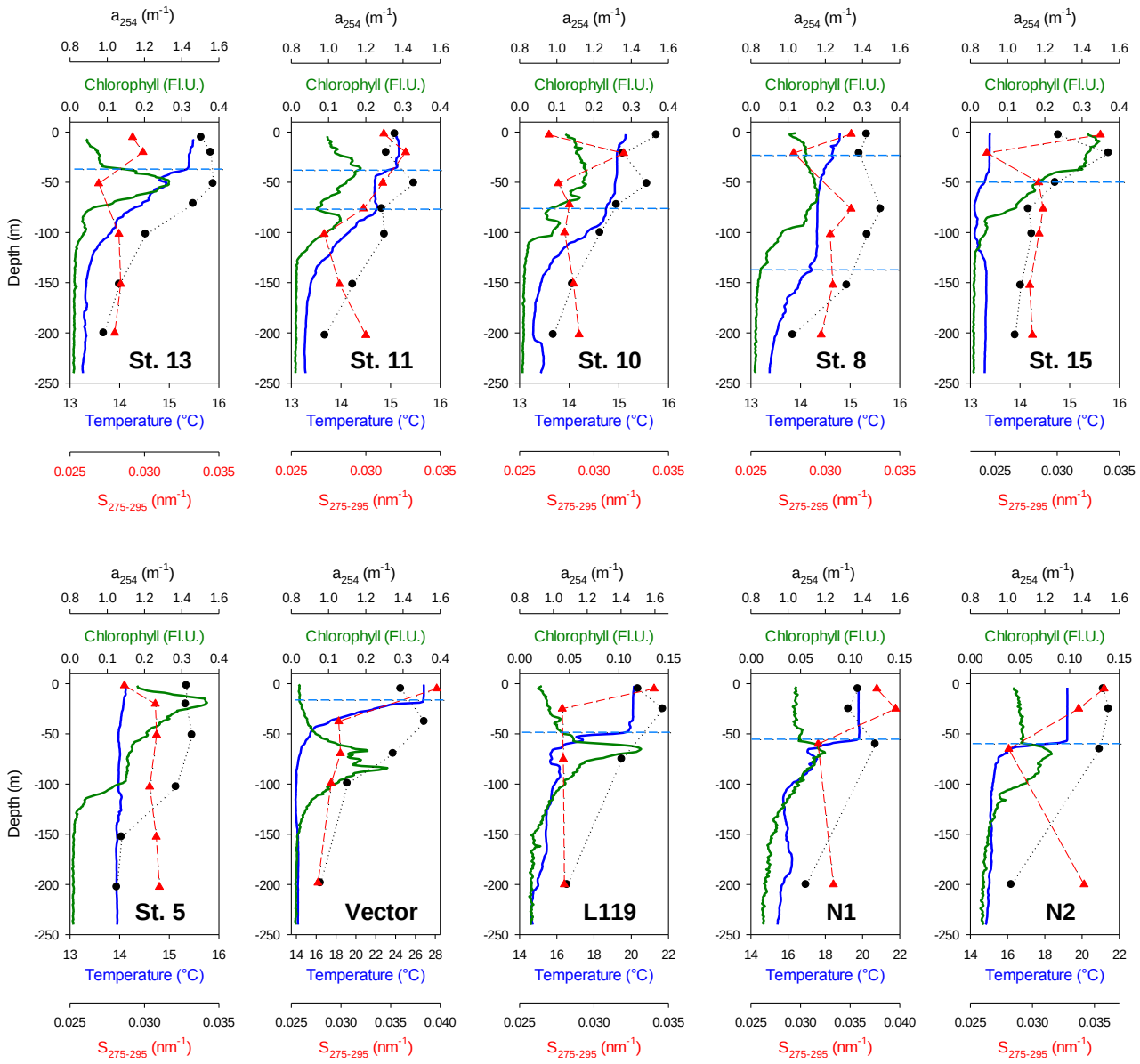

Figure 1.6. Vertical profiles in the upper 250 m of temperature, chlorophyll, a_{254} and $S_{275-295}$ for each station.

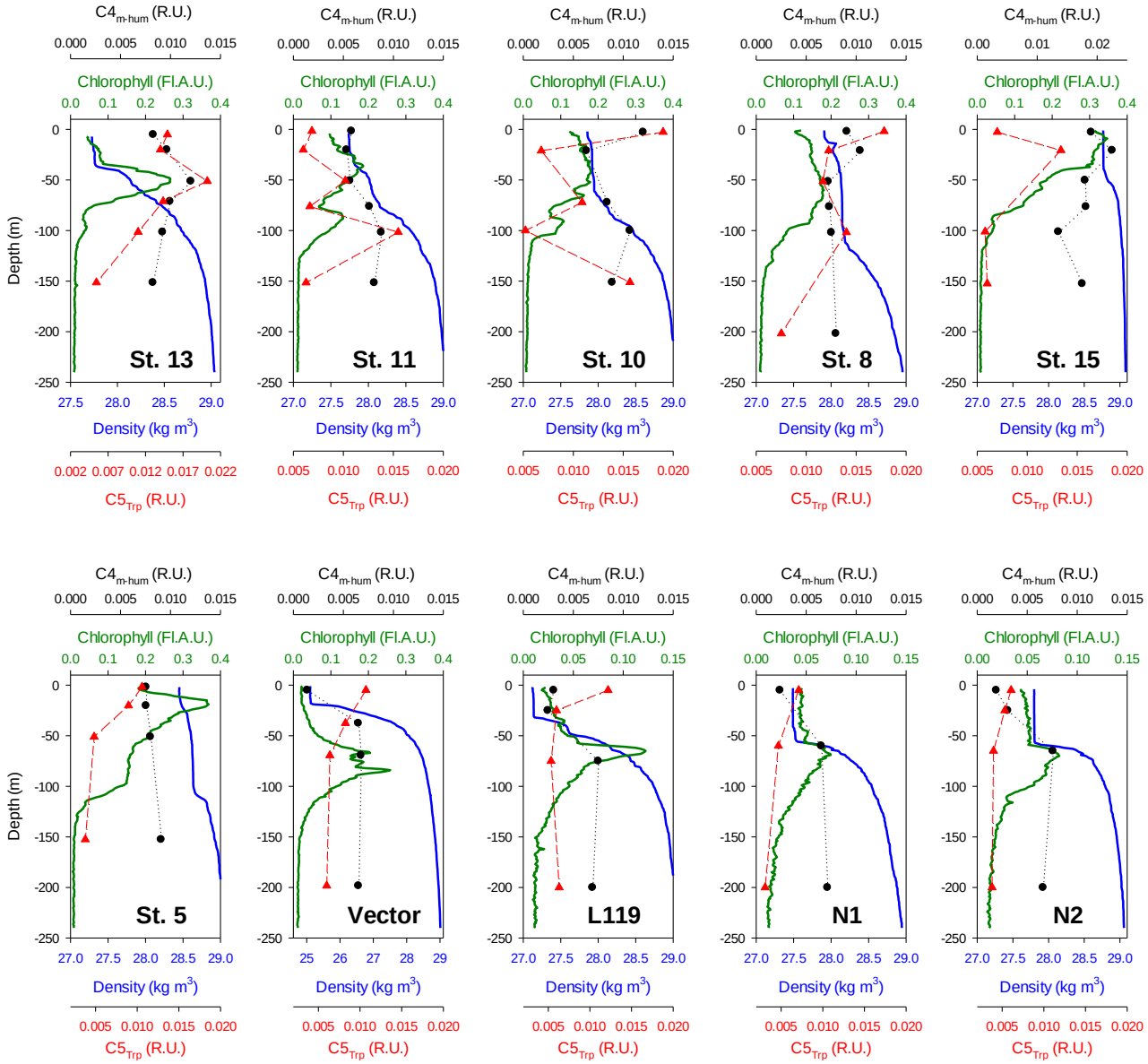

Figure 1.7. Vertical profiles of density, chlorophyll, $C4_{m\text{-}hum}$ and $C5_{Trp}$ for each station.

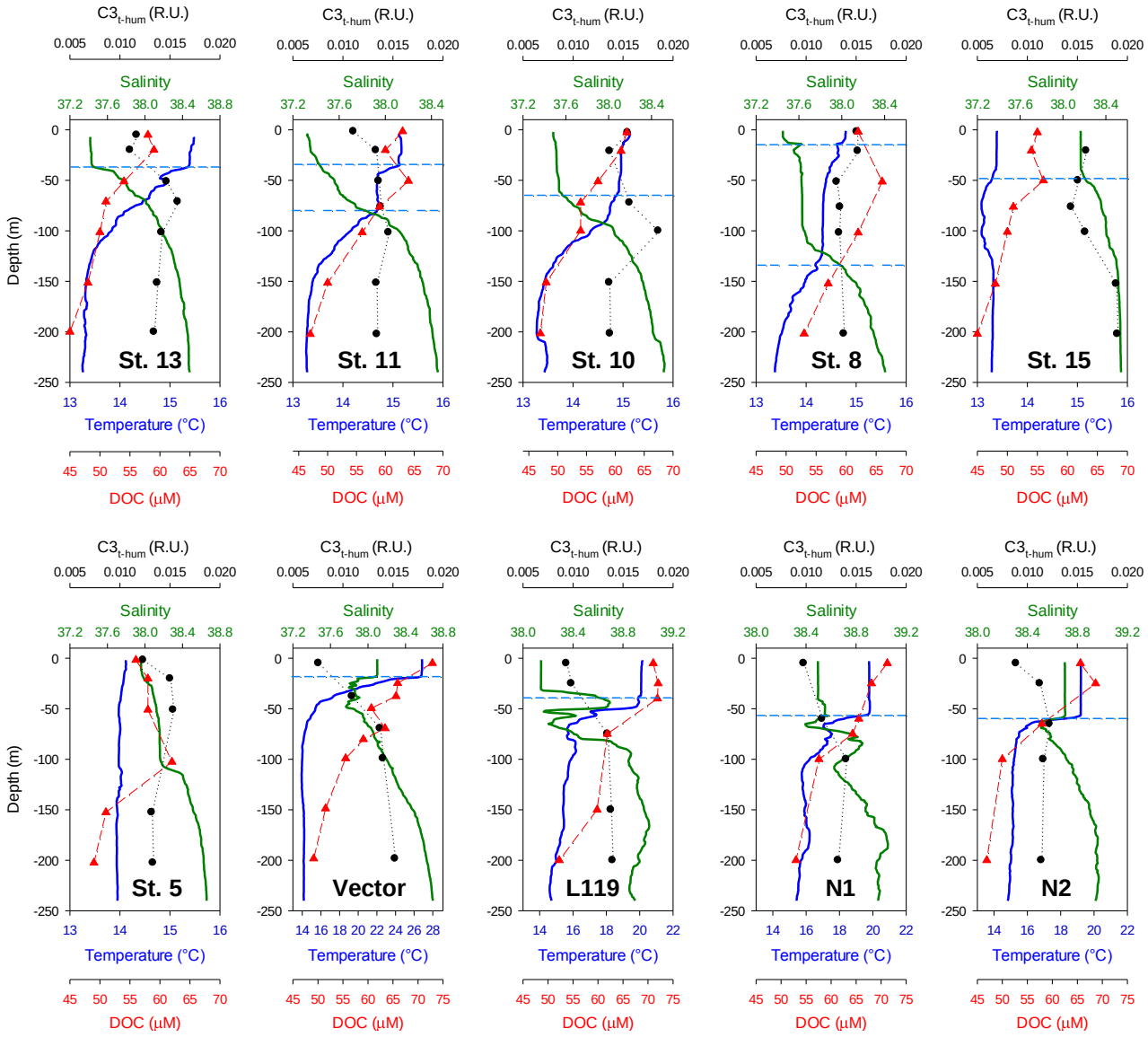

Figure 1.8. Vertical profiles of Temperature, Salinity, DOC and $C3_{t\text{-}hum}$, for each station.

Station 11 showed a 2-stairs thermocline leading to a deep mixed layer (100 m) (Fig. 1.6). Two peaks in chlorophyll are visible at 36 and 87 m, but they are less marked than at station 13. A slight increase in DOC and a_{254} can be observed at about 50 m, whereas $C5_{Trp}$ showed a peak at both 50 and 100 m. A slight decrease in $S_{275\text{-}295}$ was observed at 100 m, in correspondence with the thermocline (Fig. 1.6).

Moving toward station 10, stratification index decreased (Table 1.1) with a MLD of 75 m. A general increase in chlorophyll fluorescence was observed in the upper 50 m, without the formation of the DCM (Fig. 1.6). The surface sample was characterized by high values of a_{254}, $C4_{m\text{-}hum}$ and $C5_{Trp}$ and a low value of $S_{275\text{-}295}$ (0.027 nm^{-1}). DOC showed the highest value in the surface sample and a progressive decrease in the mixed layer, to

reach the lowest value (47 µM) at 150 m. It is noteworthy the increase in both $C3_{t\text{-}hum}$ and $C4_{m\text{-}hum}$ below the mixed layer.

Station 8 was characterized by low stratification index (0.93 $kg \cdot m^{-3}$) and a MLD of 110 m (Table 1.1). A slight increase in chlorophyll fluorescence was observed in the mixed layer, without a DCM. The high vertical mixing of the water column caused an almost uniform distribution of DOC, CDOM and FDOM in the mixed layer, excluding the peak in $C5_{Trp}$ observed at the surface.

The upper 250 m of Station 15 were completely mixed, as indicated by the stratification index that is the lowest one observed in this study (0.30 $kg \cdot m^{-3}$) and the vertical profile of density that is almost vertical (Fig. 1.7). The high extent of vertical mixing can explain the low and almost homogenous values of DOC, $C3_{t\text{-}hum}$ and $C4_{m\text{-}hum}$; interestingly $S_{275\text{-}295}$ showed the lowest values observed in the APB (0.024 nm^{-1}) at ~20 m in correspondence with a peak in a254 and $C5_{Trp}$. In the upper 50 m, chlorophyll showed the highest fluorescence. In the upper 75 m of this station, the values of $C3_{t\text{-}hum}$ (0.014-0.019 R.U.) and $C4_{m\text{-}hum}$ (0.018-0.022 R.U.) are the highest ones observed in this study (Fig. 1.7 and 1.8).

Station 5 was characterized by a low stratification index (0.56 $kg \cdot m^{-3}$), a MLD deeper than 250 m and a DCM at 20 m (Fig. 1.6). DOC, CDOM and FDOM showed an almost uniform distribution with slight higher values of DOC and a_{254} in the upper 100 m and no clear pattern in correspondence with DCM.

Due to the sampling period (August 2010), the Tyrrhenian Sea station was characterized by the highest stratification index that resulted in DOC and CDOM accumulation above the thermocline, a surface minimum of $C3_{t\text{-}hum}$ and $C4_{m\text{-}hum}$ and the highest $S_{275\text{-}295}$ value (0.040 nm^{-1}). A similar DOM dynamics was observed at the 3 stations located in the Ionian Sea and sampled in November 2011, when the water column was well stratified with a MLD of 35 m at station L119 and 50 m at both stations N1 and N2 (Table 1.1). DOC, CDOM and $C5_{Trp}$ accumulated in the mixed layer, whereas $C3_{t\text{-}hum}$ and $C4_{m\text{-}hum}$ showed their minimum and $S_{275\text{-}295}$ the highest values.

4. DISCUSSION

4.1 CDOM in the Med Sea, a comparison with the oceans and the marginal seas

The data reported in this study are limited to the western Med Sea and the Ionian Sea, with a gap in both the Westernmost (e.g. Alboran Sea and Strait of Gibraltar) and

Easternmost areas. The range of values of a_{254} well compare with data reported by Catalá et al. (2018) for the entire basin. The linear correlation between DOC and a_{254} is very similar to that reported by Catalá et al. (2018) (DOC=9 (±1)+46 (±1)·a_{254}; r^2 =0.87, $p < 0.001$, n=273), supporting that a_{254} can be considered representative of the CDOM dynamics on the basin scale. In contrast, a_{325} showed a marked decrease associated with an increase in $S_{275-295}$ in the ultra-oligotrophic Levantine Basin, where they show values lower than those observed in our study (a_{325} = 0.05-0.15 m^{-1} and $S_{275-295}$ = 0.030-0.045 nm^{-1}) the same applies for data collected in the deep Ionian Sea (Figure 4 in Catalá et al., 2018). These data support that CDOM optical properties in the western and eastern Med Sea are different, the following discussion will therefore focuses only on the western Med and Ionian Sea.

The comparison with studies focused in coastal areas, or in marginal seas, shows that the CDOM absorption in open water of the Med Sea is generally lower than those observed in coastal areas impacted by river input (Seritti et al., 1998, a_{280}=0.95-2.3 m^{-1}; Vignudelli et al., 2004) and in the other marginal seas (Table 1.4). The values reported in our study are in the range of those reported for the oceans (Table 1.4), however, if we focus in the upper layer (0-100 m), values are 0.18-0.33 m^{-1}, whereas oceanic values range between 0.02 and 0.15 m^{-1} (Nelson and Siegel, 2013). Moving to dark open ocean, if only the data with AOU = 50-100 µM are taken into consideration, a_{325} ranged between 0.11 and 0.2 m^{-1} in the North Atlantic, with most of the samples with values of 0.12-0.14 m^{-1} and between 0.040 and 0.12 m^{-1} in the Pacific and Indian Oceans, respectively (Nelson et al., 2010, their Figure 4). The comparison with our data (a_{325} = 0.07-0.24 m^{-1}) suggests that CDOM absorption in open water of the Western Med Sea and Ionian Sea is generally higher than in Pacific and Indian Oceans (Nelson et al., 2010; Nelson and Siegel, 2013; Catalá et al., 2015), whereas it is similar to values observed in the North Atlantic, that receives considerable amount of terrestrial organic matter from the Arctic Ocean and the continents.

In the APB, TS and IS, $S_{275-295}$ is lower than in the open ocean (~0.04 nm^{-1}) (Aurin and Mannino, 2012) and in oligotrophic waters of the northern Gulf of Mexico (0.048 nm^{-1}) (Fichot and Benner, 2012), but in the range of values reported for the other marginal Seas (Table 1.4). In contrast, SUVA254 is 2-4 times lower than those observed in the other marginal Seas (Table 1.4). The S_R values reported by Catalá et al. (2018) are significantly lower than in the global ocean for the same range of AOU. These results indicate that in the Med Sea, CDOM is characterized by molecules with an average molecular weight and

aromaticity degree lower than in coastal areas or marginal seas affected by terrestrial input but higher than in the open oceans, supporting the occurrence of an higher percentage of molecules with a terrestrial signature in this basin than in the open oceans.

Basin	**Salinity**	**DOC (µM)**	**CDOM (m^{-1})**	**$SUVA_{254}$ ($m^2 \cdot g^{-1}C$)**	**$S_{275-295}$ (nm^{-1})**	**Reference**
Med Sea	37-39* 36.5-39.5[a]	37-84* 35-75[a]	0.07-0.33 (a_{325})* 0.69-1.65 (a_{254})* 0.32-0.92 (a_{280})* 0.05-3.22 (a_{355})* 0.5-1.3 (a_{254})[a] 0.05-0.27 (a_{325})[a]	0.6-1.1*	0.020-0.035* 0.025-0.045[a] **S_R=1.75-3.25**[a]	*This study [a]Catalá et al., 2018
Baltic Sea	6.8±0.1[b] 10-20[d]	708 ±58[b] 300[d]	3.0-5.8 (a_{350})[c] 4-5 (a_{300})[d]	2[b]	0.025[b]	[b]Rowe et al., 2018 [c]Stedmon et al., 2007 [d]Osburn and Stedmon, 2011
North Sea	20-35[d] 32-35.5[e]	62-185 (109 ± 16)[e] 100-250[d]	1-3 (a_{300})[d] 0.09-2.74 (a_{375})[e]	0.55-4.42[e]	0.021±0.007[e] **S_R=1.5-12.9**[e]	[e]Painter et al., 2018
Black Sea	18-22.3[f]	113-205[f]	3.58-8.66 (a_{254})[g] 0.46-1.31 (a_{325})[g]	0.9-2.61[g]	0.026-0.034[g]	[f]Margolin et al. 2016. [g]Margolin et al. 2018
South China Sea	26-35[h,l]	57-117[l]	1.1-1.5 (a_{280})[h] 0.26-4.57 (a_{280})[i] 0.07 to 0.20 (a_{350})[m]		0.027-0.031[h] 0.031±0.009[i] 0.02-0.05[m]	[h]Lin et al., 2012 [i]Zhou et al. 2018 [l]Meng et al., 2017 [m]Wang et al. 2017
Okhotsk Sea	15-34[m]	60-400[m]	0.24-0.31 (a_{350})[n]			[m]Nakatsuka et al., 2004 [n]Granskog et al. 2015
Oceans	34-37[r]	34-80[r]	0.05-0.25 (a_{325})[o] 0.05-0.50 (a_{325})[p] 0.04-0.25 (a_{325})[q]		0.04-0.05[p]	[o]Nelson et al., 2010 [p]Catalá et al., 2015 [q]Nelson and Glauglitz, 2016 [r]Hansell et al., 2009

Table 1.4. Comparison of Salinity, DOC concentrations and CDOM data among the Med Sea, the other marginal seas and the oceans.

4.2 FDOM characteristics in the Med Sea

The fluorescence PARAFAC components observed in this study well compare with the global ocean fluorescence inventories reported by Jørgensen et al. (2011) and Catalá et al. (2015; 2016) as well as with components found in the other marginal seas (Table

1.2), even if some differences can be highlighted. $C1_{PAH}$ from this study was not found in the open oceans, it matches with a component associated to ballast water (Murphy et al., 2006) and a component (C4) dominating in harbors, the English Channel and in the Atlantic shelf approaching Delaware and Chesapeake Bay outflows and identified as PAHs substances (Murphy et al. 2008). The occurrence of a PAH-like component in the Med Sea is in agreement with the observation by Castro-Jiménez et al. (2012), that indicates an important net atmospheric input of PAHs to open sea waters of the WM and the IS. The robust linear correlation with $C2_{t\text{-}hum}$ (Table 1.3), supports that they have a common origin, probably allocthonous. A similar component was found in the China and Okhotsk Seas (Table 1.2), but it was attributed to terrestrial humic-like FDOM. Comparative data and additional analysis are needed to confirm that component $C1_{PAH}$ is exclusively a tracer of PAH pollutants.

A component with a such long wavelength emission maximum (516 nm) as $C3_{t\text{-}hum}$ has never been found in the open oceans. It is noteworthy that the wavelength of this emission maximum (516 nm) is typical of terrestrial humic acids characterized by either highly substituted aromatic nuclei or conjugated unsaturated systems capable of high degree of resonance, these characteristics suggest the presence of terrestrial molecules with a small degree of degradation (Senesi et al., 1989). A similar component was found in the Baltic, North and Black Seas (Table 1.2), supporting its strong terrestrial signature. The other terrestrial humic-like component ($C2_{t\text{-}hum}$), being similar to the terrestrial humic-like component found in the Black, China and Okhotsk Seas (Table 1.2), shows excitation and emission maxima shifted towards shorter wavelengths with respect to the terrestrial humic-like component reported by Catalá et al. (2015, 2016) (C2: Ex/Em=370/470 nm) for the oceans. Suggesting that the Med Sea is characterized by a very complex, not degraded, terrestrial humic-like component ($C3_{t\text{-}hum}$) not observed in the open oceans and another one ($C2_{t\text{-}hum}$) more degraded than the terrestrial humic-like component found in oceanic waters.

In contrast with the oceans and the Baltic, China and Okhotsk Seas where between 2 and 4 protein-like components were observed, in the Med Sea our model found only 1 protein-like component ($C5_{Trp}$). The same applies for the Black Sea. There are evidences that protein-like substances are produced in-situ by phytoplankton and microbes (Stedmon and Markager, 2005b, Zhao et al., 2017; Romera-Castillo et al., 2010). In our study, the phenylalanine-like and tyrosine-like components were not found, in contrast with oceanic studies, that observed that the tyrosine-like fluorophores dominated in the open ocean waters (Jørgensen et al. 2011; Mopper and Schultz 1993; Yamashita et al. 2010b). Our

data suggest the predominance of proteins containing Trp with respect to those containing only Tyr in the Med Sea. The different protein composition could be explained by a different microbial community in the Med Sea, in agreement with the first data on marine microbe diversity, which indicate that prokaryotic assemblages are highly diverse, with the presence of bacterial and archaeal ecotypes, adapted to the unique hydrological, geological and geomorphological features of this basin (Luna, 2015).

The 5 components showed a different distribution within and below the mixed layer (Fig. 1.7-1.8), indicating that each component is affected by different processes leading a change in the relative percentage of each component in FDOM pool. Vertical profiles of both humic-like and protein-like components well compare with those observed in the Atlantic, Pacific and Indian Oceans (Yamashita et al. 2010b; Jørgensen et al. 2011; Catalá et al., 2016). FDOM in the Med sea was dominated by humic-like components representing 70-95% and 65-100% of the total fluorescence in the upper 200 m and between 200 m and the bottom, respectively.

In the upper 200 m, DOC showed a significant ($p<0.0001$) inverse relationship with $C2_{t\text{-}hum}$, $C3_{t\text{-}hum}$, and $C4_{m\text{-}hum}$, whereas no correlation was found with $C1_{PAH}$ and $C5_{Trp}$ (Table 1.5). In contrast with oceanic observations (Yamashita and Tanoue, 2009) a_{254} and a_{325} did not correlate with the 5 components (if we exclude the weak correlation between a_{325} and $C1_{PAH}$) nor taking into consideration all the data, nor focusing in the surface either the deep waters (Table 1.5), indicating that in the Med Sea, CDOM and FDOM dynamics are decoupled and that absorption and fluorescence give information on different fraction of DOM. Interestingly, the robust correlation between $C4_{m\text{-}hum}$ and $C5_{Trp}$ (Table 1.3) below 200 m, indicates that the 2 components are coupled in the intermediate and deep waters, suggesting that both are produced in situ, but in the surface layer the removal processes are different, with photobleaching affecting $C4_{m\text{-}hum}$ more than $C5_{Trp}$ as supported by the correlations with temperature (Table 1.5).

All samples																				
	Temp			**AOU**			**Chl**	**DOC**			**a_{254}**			**a_{325}**			**$S_{275-295}$**			
	0-Btm	0-200	200-Btm	0-Btm	0-200	200-Btm	0-100	0-Btm	0-200	200-Btm	0-Btm	0-200	200-Btm	0-Btm	0-200	200-Btm	0-Btm	0-200	200-Btm	
Temp																				
AOU	*0.40***	*0.25***	0.12**																	
Chl		-			-															
DOC	**0.68****	**0.60****	-	***0.65****	***0.70****	-	*0.19*													
a_{254}	0.43**	0.11	-	***0.67****	***0.56****	-	-	**0.80****	0.40**	-										
a_{325}	0.12**	-	-	*0.30***	-	-	0.13	0.41**	-	-	**0.75****	0.35**	**0.62****							
$S_{275-295}$	-	**0.50****	-	-	*0.17*	-	*0.14*	-	0.48**	-	-	-	*0.15*	*0.18***	***0.53****	***0.48****				
$C1_{PAH}$	-	*0.34***	-	-	011	-	0.19	-	*0.22*	-	-	-	0.12	0.21**	0.35**	-	-	***0.62****	-	
$C2_{t\text{-}hum}$	*0.16***	***0.68****	-	-	0.20	-	0.32	-	***0.55****	-	-	-	0.20	0.18**	0.25	-	*0.22***	***0.80****	-	
$C3_{t\text{-}hum}$	*0.29***	***0.57****	-	-	0.18	-	0.27	*0.11*	*0.49***	-	-	-	-	-	-	-	*0.12*	***0.52****	-	
$C4_{m\text{-}hum}$	-	*0.40***	-	-	0.13	-	0.35**	-	*0.41***	-	-	-	0.23**	0.16**	0.11	-	*0.13*	***0.49****	-	
$C5_{Trp}$	-	-	-	-	-	-	-	-	-	-	-	0.15	-	-	*0.20*	-	-	-	-	

Table 1.5. Values of r^2 and p for the linear correlations among the 5 components, taking into consideration all the data collected in this study. Values of $r^2 < 0.1$ are not reported; values of $r^2 > 0.5$ are in bold. **p<0.0001. Negative correlations are indicated in italic. Btm= Bottom.

Algero-Provencal Basin																			
	Temp			**AOU**			**Chl**	**DOC**			**a_{254}**			**a_{325}**			**$S_{275-295}$**		
	0-Btm	0-200	200-Btm	0-Btm	0-200	200-Btm	0-100	0-Btm	0-200	200-Btm	0-Btm	0-200	200-Btm	0-Btm	0-200	200-Btm	0-Btm	0-200	200-Btm
Temp																			
AOU	*0.23***	*0.38**	**0.79****																
Chl		*0.33**																	
DOC	**0.78****	**0.52****	0.26**	*0.34***	***0.68****	-	-												
a_{254}	**0.76****	**0.51****	-	*0.45***	*0.45**	-	-	**0.78****	0.41*	-									
a_{325}	**0.60****	0.46**	-	*0.27***	*0.20**	-	-	**0.55****	0.12*	-	**0.88****	**0.71****	**0.60****						
$S_{275-295}$	-	**-**	-	-	-	-	-	-	0.23*	0.20*	-	-	*0.23**	*0.27***	*0.17**	***0.58****			
$C1_{PAH}$	-	-	-	-	-	-	0.14	-	-	-	0.12*	-	-	0.14*	0.15*	-	-	*0.41**	-
$C2_{t\text{-}hum}$	-	*0.15**	-	-	0.11	-	0.33*	-	*0.30**	-	0.18*	-	-	0.30**	-	-	*0.18**	***0.70****	-
$C3_{t\text{-}hum}$	-	*0.12**	-	-	-	-	0.19*	-	*0.16**	-	-	-	-	-	-	-	-	*0.23**	-
$C4_{m\text{-}hum}$	-	*0.28**	-	-	-	-	0.30*	-	*0.15**	-	-	-	-	0.12*	-	-	-	*0.36**	-
$C5_{Trp}$	-	0.13*	-	-	-	-	-	-	-	-	-	0.41	-	-	0.43*	*0.12**	-	-	-

Table 1.6. Values of r^2 and p for the linear correlations among the 5 components, taking into consideration the data collected in the Algero-Provencal Basin. Values of $r^2 < 0.1$ are not reported; values of $r^2 > 0.5$ are in bold. *p<0.05; **p<0.0001. Negative correlations are indicated in italic. Btm= Bottom.

Tyrrhenian Sea (TS)																			
	Temp			**AOU**			**Chl**	**DOC**			**a_{254}**			**a_{325}**			**$S_{275-295}$**		
	0-Btm	0-200	200-Btm	0-Btm	0-200	200-Btm	0-100	0-Btm	0-200	200-Btm	0-Btm	0-200	200-Btm	0-Btm	0-200	200-Btm	0-Btm	0-200	200-Btm
Temp							-												
AOU	*0.22**	-	0.33*				*0.15*												
Chl		*0.32**			*0.15*														
DOC	0.45**	**0.54***	0.42*	***0.72****	***0.85****	**0.63****	*0.34**												
a_{254}	0.16*	-	0.16	***0.83****	***0.69****	-	-	**0.72****	-	-									
a_{325}	-	*0.38**	0.23*	***0.70****	*0.49**	-	-	0.37*	-	-	**0.77****	0.23	**0.66****						
$S_{275-295}$	0.34	**0.78***	-	-	-	-	-	0.19*	0.42*	-	-	-	*0.13*	-	***0.67****	***0.60****			
$C1_{PAH}$	*0.39*	***0.93****	0.21	***0.50****	-	-	0.15	0.42*	*0.48*	*0.12*	**-**	-	**0.62***	0.34*	**0.58***	0.18	*0.23**	***0.89****	-
$C2_{t\text{-}hum}$	***0.67****	***0.95****	-	*0.28**	-	***0.63****	0.28	-	***0.57****	*0.13*	-	-	0.46*	-	0.35	0.12	*0.32**	***0.73****	-
$C3_{t\text{-}hum}$	***0.70****	***0.78****	-	-	-	-	**0.60***	*0.17**	*0.44*	-	*0.17**	-	-	-	0.22	-	0.14	*0.44*	-
$C4_{m\text{-}hum}$	***0.57***	***0.92****	-	-	*?*	*0.26*	0.29	*0.41**	***0.81****	-	-	**-**	**0.75***	-	0.21	0.35*	*0.37**	***0.74****	-
$C5_{Trp}$	-	0.14	-	-	-	-	-	*0.18**	0.16	-	-	0.17	0.26*	-	-	-	-	-	-

Table 1.7. Values of r^2 and p for the linear correlations among the 5 components, taking into consideration the data collected in the Tyrrhenian Sea. Values of $r^2 < 0.1$ are not reported; values of $r^2 > 0.5$ are in bold. *p<0.05; **p<0.0001. Negative correlations are indicated in italic. Btm= Bottom.

Ionian Sea (IS)																				
	Temp			**AOU**			**Chl**	**DOC**			**a_{254}**			**a_{325}**			**$S_{275-295}$**		
	0-Btm	0-200	200-Btm	0-Btm	0-200	200-Btm	0-100	0-Btm	0-200	200-Btm	0-Btm	0-200	200-Btm	0-Btm	0-200	200-Btm	0-Btm	0-200	200-Btm
Temp																			
AOU	***0.91*** **	***0.75*** **	-																
Chl		***0.83*** **			0.30														
DOC	**0.93** **	**0.86** **	0.13*	***0.96*** **	***0.85*** **	***0.57*** **	***0.75*** *												
a_{254}	**0.85** **	0.48*	0.14	***0.93*** **	***0.77*** *	*0.17**	-	**0.93** **	**0.67***	0.33*									
a_{325}	0.24*	-	-	*0.32**	-	-	-	0.39*	-	0.13	**0.60** **	0.17	**0.67***						
$S_{275-295}$	0.21*	0.16	-	*0.18**	-	-	-	0.11*	-	-	-	-	*0.13*	-	***0.75*** *	***0.50*** *			
$C1_{PAH}$	-	*0.34**	-	-	0.13	*0.14**	**0.54***	-	-	0.28*	-	-	0.19	0.35*	0.35*	-	-	***0.58*** *	-
$C2_{t\text{-}hum}$	*0.33**	***0.63*** *	-	0.25*	0.32	*0.39**	**0.70***	*0.14**	*0.27*	0.23*	-	-	0.21*	-	0.11	-	*0.20**	*0.40**	-
$C3_{t\text{-}hum}$	***0.63*** **	***0.71*** *	-	**0.52** **	0.47*	-	**0.72***	*0.48***	*0.41**	-	*0.43**	*0.26*	-	-	-	-	*0.13**	*0.27*	-
$C4_{m\text{-}hum}$	*0.41**	***0.79*** *	0.11	0.43*	**0.67***	-	**0.68***	***0.24*** **	***0.55*** *	0.28*	*0.15**	*0.26*	**0.52***	-	-	0.19	*0.14**	*0.21*	-
$C5_{Trp}$	**0.65** **	0.24	-	***0.66*** **	*0.19*	*0.14*	*0.43*	**0.69** **	0.32	0.23*	**0.60**	-	0.23*	0.26*	-	-	-	-	-

Table 1.8. Values of r^2 and p for the linear correlations among the 5 components, taking into consideration the data collected in the Ionian Sea. Values of $r^2 < 0.1$ are not reported; values of $r^2 > 0.5$ are in bold. *p<0.05; **p<0.0001. Negative correlations are indicated in *italic*. For chlorophyll, only the values collected in the upper 100 m were taken into consideration. Btm= Bottom.

4.3 The main drivers of CDOM distribution in the surface layer (0-200 m)

Our data are in good agreement with the other Med Sea studies reporting a decoupling of CDOM dynamics between the surface layer, where CDOM dynamics is mainly explained by physical processes (sea surface temperature and photobleaching) and subsurface layer, where CDOM is mainly driven by biological processes (phytoplankton release and/or microbial transformation) (Bracchini et al., 2010; Organelli et al., 2014; Xing et al., 2014; Pérez et al 2016). However, in these papers no FDOM data is reported. Our study unveils that this decoupling is even more clear when the FDOM components are taken into consideration and highlights that the PARAFAC components are differently affected by physical and biological processes. In the APB, samples were collected at the beginning of spring, this season is characterized by the initial phase of the phytoplankton bloom, as supported by the high chlorophyll fluorescence (Fig. 1.6) and a high extent of vertical mixing, as supported by the low stratification index (Table 1.1) and the vertical profiles of both temperature and density (Fig. 1.6 and 1.7). In contrast, in the Tyrrhenian and Ionian Seas samples were collected in August and November, respectively, when the water column is highly stratified (Table 1.1, Fig. 1.6). We therefore expect that different processes are the main drivers of DOC, CDOM an FDOM dynamics in the 3 areas/periods.

4.3.1 CDOM and FDOM release by phytoplankton and/or bacterioplankton

In most of the APB stations a decrease in $S_{275-295}$ to reach a minimum of 0.024-0.027 nm^{-1} and an increase in $C5_{Trp}$ and $C4_{m-hum}$ was observed in correspondence with the DCM (high chlorophyll values) (Fig. 1.6 and 1.7), whereas no clear pattern was observed for a_{254} (excluding station 15) nor for DOC (Fig. 1.6 and 1.8). At some stations (e.g. Station 10) a minimum in $S_{275-295}$ in correspondence with high values of a_{254}, $C5_{Trp}$ and $C4_{m-hum}$ was observed in the surface sample. The low values of $S_{275-295}$ in correspondence with high values of $C5_{Trp}$ and $C4_{m-hum}$ can be a clear indication of FDOM in-situ production, since microbial activity counteracts the photobleaching effect increasing the molecular weight and aromaticity (Helms et al., 2008; Catalá et al., 2015; Maqbool et al., 2017). A peak in protein-like FDOM in correspondence with DCM was observed in the oceans (Catalá et al., 2016), whereas a peak in CDOM together with a decrease in S was observed few meters above the DCM in the Sargasso Sea

(Nelson et al., 2004), at the Boussole site in spring and summer (a_{442}, Organelli et al., 2014), in the northwestern Med Sea in September 2011 and May 2012 (a_{320}, Pérez et al., 2016) and in the Ionian Sea in November 2004 (a_{300}, Bracchini et al. 2010). Xing et al. (2014), investigating absorption data at 412 nm (a_{412}), estimated from fluorometric and radiometric measurements of "Bio-Argo" floats in both the northwestern and eastern sub-basin, found a sub-surface maximum of a_{412} in correspondence with the DCM in fall, whereas in winter and early spring it deepened following the MLD. The low sampling frequency in the upper 200 m hinders to know the exact position of the CDOM/FDOM peak in our data, we cannot therefore exclude that it is few meters above the DCM. The peak in $C5_{Trp}$ and $C4_{m\text{-}hum}$ in proximity of the DCM supports that phytoplankton and/or bacterioplankton actively growing release both humic-like and protein-like substances as widely documented (Romera-Castillo et al., 2010, 2011; Lønborg et al., 2015; Zhao et al., 2017) and that these components are not immediately removed and accumulate. The direct production of recalcitrant DOM with a chromophoric signature and of recalcitrant humic-like FDOM by bacterioplankton has been observed in the oceans (Nelson et al., 2004; Yamashita and Tanoue, 2008; Jørgensen et al., 2014; Lønborg et al., 2015; Romera-Castillo et al., 2011). The peak in FDOM can be explained not only through the direct release of recalcitrant FDOM but also through bacterial transformation of the labile DOM into recalcitrant FDOM in agreement with the model of the microbial carbon pump (Jiao et al., 2010).

No correlation was observed between chlorophyll and DOC, CDOM nor FDOM (Table 1.5), even when only samples collected in the APB are taken into consideration (Table 1.6), in agreement with results from open ocean waters (Jørgensen et al., 2011). The time shift between chlorophyll maximum and CDOM accumulation (Xing et al., 2014; Organelli et al., 2014; Nelson et al., 2004) may hinder to find a direct relationship in our data. Time-series of CDOM, FDOM, chlorophyll and prokaryotic heterotrophs abundance are therefore mandatory to investigate the direct release of them by phytoplankton or their transformation by microbes. When only the data collected in the upper 100 m of the Ionian Sea (November) are taken into consideration, a very good inverse correlation is observed between chlorophyll and both temperature and DOC, in addition chlorophyll directly correlates with all the humic-like components (Table 1.8). This correlation suggests a direct production of FDOM by phytoplankton as a function

of their chlorophyll cellular, even if a negative effect of temperature on both FDOM (photobleaching) and phytoplankton (photo-acclimation of intracellular chlorophyll concentration together with nutrient limitation) cannot be excluded.

It is noteworthy that in the Gulf of Lions (WM, station 15, Fig. 1.1), the most productive area of the Med Sea due to the upwelling, surface fluorescence intensities of $C4_{m\text{-}hum}$ (marine humic-like) are significantly higher (2.6-fold, $p<0.05$) than in all the other stations. The net production of humic-like fluorescence in upwelling regions has been observed in the oceans (Nieto-Cid et al., 2005) and can be explained by the upwelling, determining the input of nutrients that induced the phytoplankton bloom and microbial productivity and the uplifting of water with higher values of humic-like FDOM from deeper layers (Siegel et al., 2002; Catalá et al., 2016).

In the surface layer, the robust linear inverse correlation between AOU, used as a proxy for microbial mineralization, and both DOC ($r^2=0.70$) and a_{254} ($r^2=0.56$) (Table 5; Fig. 1.9) indicates that microbial removal is the main processes affecting DOC and CDOM dynamics and it can explain up to 70% of DOC and 55% of CDOM decrease observed in the upper 200 m, in agreement with the results by Catalá et al. (2018). No significant correlation was observed between FDOM and AOU (Table 1.5), suggesting that in the Med Sea photobleaching is the main processes affecting FDOM dynamics in the surface layer.

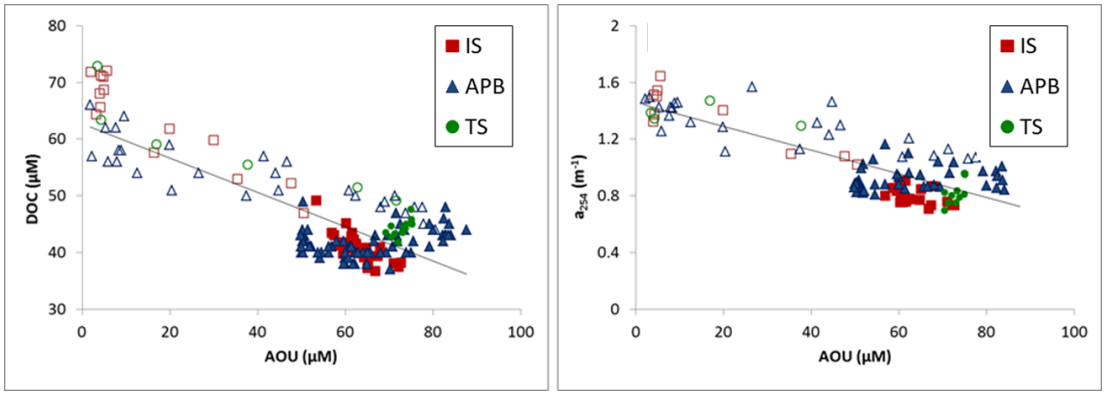

Figure 1.9: Correlation between DOC and AOU (on the left) and between a_{254} and AOU (on the right). Empty symbols refer to samples collected in the upper 200 m, filled symbols to samples collected between 200 m and the bottom.

4.3.2 Photobleaching

In both the TS and IS, the high extent of vertical stratification favors the accumulation of DOM in the mixed layer making photobleaching the main process

affecting CDOM and in particular FDOM dynamics. A robust power law correlation was observed between temperature $C2_{t\text{-}hum}$, $C3_{t\text{-}hum}$ and $C4_{m\text{-}hum}$ (inverse) (Fig. 1.10); a good linear correlation was also observed between temperature and DOC (Fig. 1.10), whereas no correlation was observed between temperature and CDOM nor $C5_{Trp}$ (Table 1.5).

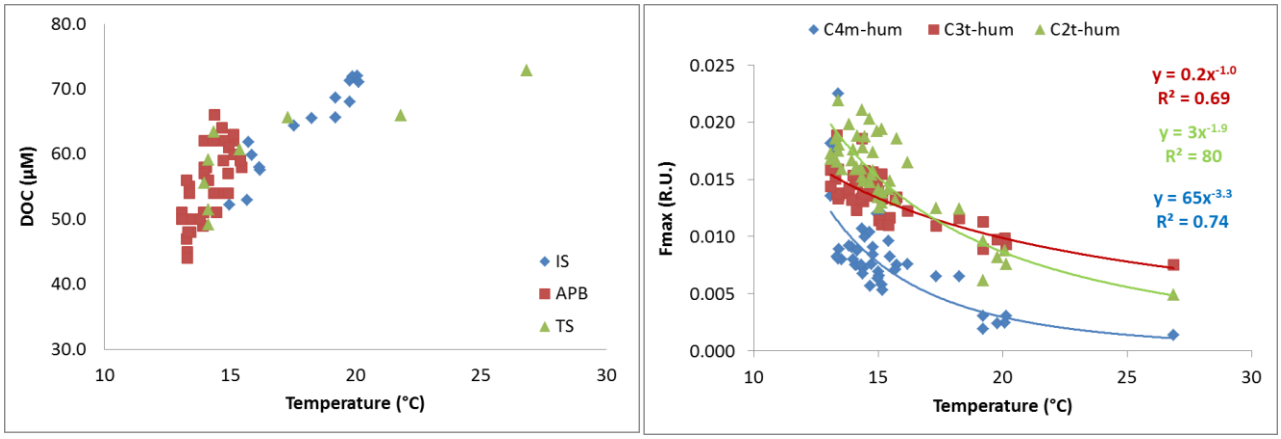

Figure 1.10: Correlation between temperature and DOC (On the left) and between temperature and the 3 humic-like components.

Temperature does not affect directly DOM dynamics, but it can be considered as a tracer of different processes that can impact DOM dynamics. Higher temperatures are indicators of a higher degree of stratification and therefore of a more prolonged exposure to solar radiation, leading to photodegradation. No correlation was found between temperature and Chlorophyll supporting that temperature is mainly an indicator of photobleaching and stratification. The robust direct correlation between temperature and DOC (r^2=0.60, Table 1.5) supports that DOC accumulates in warm waters, in agreement with observations previously reported for the Med Sea (Santinelli et al., 2013), whereas the inverse correlation with FDOM (Table 1.5) indicates that photobleaching affects both terrestrial and marine humic-like components, as observed by Xing et al. (2014) and Catalá et al. (2018). As expected this correlation was not found in the APB (Table 1.6), and strongly improves in the TS (Table 1.7) and IS (Table 1.8). A robust direct linear correlation was also observed between temperature and $S_{275\text{-}295}$ (Table 1.5), supporting the occurrence of the smallest molecules produced by photodegradation in the warmest water (Helms et al., 2008). These data support that photodegradation represents the main removal mechanism for humic-like substances and controls CDOM abundance in the surface ocean, whereas its impact on protein-like substances is lower (Bracchini et

al., 2010; Nelson et al., 2010; Nelson and Siegel, 2013; Stedmon and Markager, 2005b; Nelson et al., 2007; Vodacek et al. 1997; Yamashita et al., 2010b). The microbial degradation of humic-like FDOM cannot be excluded, even if it is not considered a major sink (Stedmon and Markager, 2005b) as suggested by the weak correlation between AOU and FDOM (Table 1.5). Photobleaching and degradation processes by zooplankton and bacteria represent an important sink for PAHs, especially for the low molecular weight (LMW) ones (Castro-Jiménez et al., 2012), explaining the minimum in $C1_{PAH}$ observed in the photic zone.

4.4 The main drivers of DOM distribution in the deep waters

In the deep open ocean and marginal seas, the fluorescence intensity of humic-like substances correlates positively with AOU (Hayase and Shinozuka, 1995; Yamashita et al., 2007, 2008; Yamashita and Tanoue, 2008, 2009; Jørgensen et al., 2011; Nelson et al., 2010; Nelson and Siegel, 2013; Catalá et al., 2015) or with Apparent Carbon Mineralization (ACM) (Margolin et al., 2018), suggesting that when organic matter, mainly coming from sinking particles, is oxidized a fluorescent by-product is formed. In the Med Sea, a_{254}, and DOC showed a robust inverse linear correlation with AOU (a_{254} = 1.45 (±0.03) - 0.008 (±0.0006)·AOU; r^2 = 0.67, $p < 0.0001$, n = 109; DOC = 63(±1) - 0.3 (±0.02) · AOU; r^2 = 0.65, $p < 0.0001$; n = 172); a weaker but significant correlation was also observed with a_{325} (Table 1.5). However, the correlation is lost when the data collected in the upper 200 m are excluded from the regression, with the exception of the TS (r^2=0.63) and IS (r^2=0.57) where an inverse linear correlation between AOU and DOC was found even between 200 m and the bottom (Table 1.7 and 1.8). This finding is in contrast with what reported in the oceans, where the correlation was positive. This apparent inconsistency can be solved looking at the value of AOU. In our study the maximum value of AOU is 88 µM, whereas in the oceans AOU is up to 300 µM. Looking at the relationship observed by Nelson et al. (2010) it is clear that if only the data with AOU<100 µM were taken into consideration none relationship would have been found, even in the oceans. This observation suggests that the production of FDOM in deep waters occurs only when AOU is > 100 µM, that is in deep waters older than those found in the Med Sea or in waters where oxidation processes removed all the oxygen, leading to anoxia as in the Black Sea (Margolin et al., 2018). The low sinking POC fluxes

characteristics of the Med Sea (Speicher et al., 2006), can help to explain the absence of the correlation.

These data indicate that in the Med Sea, the main source of humic-like FDOM is not in situ mineralization, suggesting a greater contribution from external sources and a significant role for mixing and general circulation in determining the CDOM distribution in the deep waters (Catalá et al., 2015; Jørgensen et al., 2011; Nelson et al. 2007, 2010; Nelson and Siegel, 2013).

4.5 The Med Sea: a marginal basin with biogeochemical characteristics similar to the oceans

The Med Sea is the largest marginal basin in the world. It has a high coastline to surface ratio and it is connected with the oceans through the Gibraltar Strait (286 m deep and 14 km large). It does have a high value of drainage area to surface area compared to the open ocean. Despite being a marginal basin it has less “terrestrial” characteristics than the other marginal basins (Table 1.4), since it has a large volume ($3.75 \cdot 10^6$ Km^3), its continental shelves are narrow and it is a negative basin, meaning that evaporation is higher than the precipitations and run off. It is therefore the only marginal basin characterized by salinity higher than the oceans (Table 1.4) and stock of nutrients much lower than the other marginal basins and even lower than the oceans (Ribera d’Alcalà et al., 2003). It also features an anti-estuarine circulation, meaning that all the waters entering in the surface layer recirculate in the intermediate and deep layer before exiting the basin, with residence time of waters much longer than the other marginal basins, where the circulation is estuarine and all the water entering the surface layer exits from the surface layer. These peculiarities reflect in DOC concentrations almost identical to those reported for oceanic waters (Hansell, 2002; Hansell et al., 2009; Carlson et al., 2010; Hansell and Carlson, 2013) but much lower than those observed in the other marginal Seas (Table 1.4). DOM dynamics in the Med Sea well compare with the oceanic one, despite terrestrial inputs are expected to affect DOM dynamics to a larger extent than in the open ocean. If the Med Sea behaves as a miniature ocean for DOC concentrations and distribution, its composition shows some intriguing differences, supported by radiocarbon (Santinelli et al., 2015) and Fourier Transform Ion Cyclotron Resonance mass spectroscopy (FT-ICR-MS) data (Martinez-Pérez et al., 2017a). These papers suggest that DOM in

the Med Sea is older, lighter and with an higher degradation index than the DOM coming from the Atlantic Ocean.

Optical properties support the different DOM composition with respect to the oceans and suggest some differences with respect to the other marginal basins, opening intriguing questions about the source and cycle of allocthonous molecules in the open sea waters of the Med Sea. The data reported in this paper support the hypothesis that a larger fraction of DOM is chromophoric and characterized by a larger percentage of humic-like substances than in the open oceans. The external sources of DOM to the Med Sea are the rivers, the atmosphere and the groundwaters. Unfortunately, a direct comparison of CDOM input from external sources between the Med Sea, the oceans and the other marginal seas is very difficult to make due to the lack of CDOM data. In the following paragraph we therefore report a comparison of DOC fluxes from rivers and the atmosphere between the Med Sea and the oceans assuming that a similar fraction of DOC coming from these sources is composed by chromophoric molecules. While these assumptions can be valid for the riverine DOM, we expect that an higher fraction of atmospheric DOM is composed by chromophoric molecules in the Med Sea than in the ocean, due to the smaller size, higher urbanization degree of this basin and the higher impact of Saharan dust deposition events.

The most recent estimate of river input of DOC to the Med Sea indicates a total flux of 0.644-0.712 × 10^{12} g DOC y^{-1} (Santinelli et al., 2015). The total DOC input from the rivers, divided by the entire volume of the basin (3.75·10^6 km^3), suggests a contribution of 0.17-0.19·10^6 g DOC y^{-1} Km^{-3}, assuming that terrestrial DOC is not removed. This value is comparable to that estimated for the global ocean (0.14-0.18·10^6 g DOC y^{-1} Km^{-3}), suggesting that even if river can be an important source of terrestrial DOM, they are not enough to explain the richness in humic-like molecules observed in the Med Sea.

Data on wet and dry DOC depositions from the atmosphere are scarce for the Med Sea and limited to specific areas (De Vicente et al., 2012; Djaoudi et al., 2018; Economou and Mihalopoulos, 2002; Pulido-Villena et al., 2008). In order to have a regional estimate of the total (wet + dry) atmospheric input of DOC, the annual average DOC flux (0.14 to 0.42 mmol m^{-2} d^{-1}) was multiplied by the Med Sea area (2.5·10^6 km^2) (for further details refer to Santinelli, 2015). This calculation indicates a flux of 1.5-4.6·10^{12} g DOC y^{-1} suggesting that atmospheric input can be 2 to 6 fold larger than river input. The global estimation for wet

atmospheric DOC deposition to the global ocean is 90-246 10^{12} g DOC y^{-1} (Kanakidou et al., 2012; Willey et al., 2000) and 1.5 10^{12} g DOC y^{-1} to the Med Sea (Economou and Mihalopoulos, 2002). If these fluxes are normalized by the volume of the water, we obtain that atmospheric input accounts for $4 \cdot 10^5$ g DOC y^{-1} Km^{-3} in the Med Sea and 0.7-1.8 10^5 g DOC y^{-1} Km^{-3} in the oceans. These values are 2-5 times larger in the Med Sea than in the oceans, suggesting that atmosphere can be the main source of allocthonous DOM to the Med Sea, thus explaining its richness in humic-like substances. In contrast with results from the North Atlantic (Jørgensen et al., 2011), no correlation was found between salinity and terrestrial humic-like FDOM below 200 m, further supporting that rivers are not the main source of terrestrial humic-like FDOM to the Med Sea. It cannot be excluded that terrestrial FDOM is transformed, mixed and transported by water masses circulation, masking the correlation.

The idea that atmosphere can be the major source of allocthonous DOM to the Med Sea is also in agreement with the observations by Sánchez-Pérez et al. (2016), who collected a 2-year time series data on FDOM deposition in the Northwestern Med Sea and showed that aerosol deposition induced an increase in the proportion of FDOM in DOM pool.

5. Conclusions

The data on DOC and optical properties (both absorption and fluorescence) of CDOM reported in this study support that the Med Sea behaves as a miniature ocean for DOC concentrations and distribution, whereas its chromophoric pool shows peculiar characteristics. CDOM absorption in the western Med Sea and Ionian Sea is generally lower than those observed in the other marginal seas, but higher than in the oceans. The fluorescence PARAFAC components observed in this study show some differences with both the oceans and the marginal seas. The PAH-like ($C1_{PAH}$) and terrestrial humic-like ($C3_{t\text{-}hum}$) component were found in other marginal basins but not in the open oceans. In contrast with the oceans and most of the marginal Seas, only one protein-like component was found, opening intriguing questions about the role of microbial communities in its production and removal in the Med Sea. Interestingly, no production of humic-like FDOM as function of mineralization rates was observed in the intermediate and deep waters of the Med Sea, supporting that in this basin humic-like FDOM mainly has an

allocthonous origin. The observation that DOM pool in the Med Sea is dominated by humic-like substances with an allocthonous origin opens intriguing questions about the impact of external sources of DOM to the basin.

Our data confirm that a_{254} can be a good proxy for DOC in the Med Sea and that in the surface layer photobleaching plays a relevant role in the removal of humic-like fluorescence and that the release of both protein-like and humic-like substances occur in proximity of the DCM. Additional data on microbial communities and DOM molecular composition as well as additional studies combining different approaches (in-situ data, incubation experiments, modelling effort) are mandatory to unveil the fascinating DOM dynamics in the Med Sea. The few information available on CDOM and FDOM input from external sources hinders an estimate of their relative importance and require further research.

Acknowledgments

This research was supported by PERSEUS project, Funded by the EU under FP7 Theme “Oceans of Tomorrow” OCEAN.2011-3 and by the Italian Flagship project RITMARE funded by the Italian Ministry of Research and University. Most of the samples were collected in March/April 2008 during the cruise S-IT4, carried out in the framework of the European IP Project SESAME (Southern European Seas Assessing and Modelling Ecosystem changes). CTD and oxygen data were kindly provided by K. Schroeder and M. Borghini (CNR-ISMAR), by M. Sprovieri (CNR-IAMC), F. Conversano (SZN) and by E. Zambianchi (Università Parthenope). We also thank the 3 anonymous reviewers for their helpful suggestions and comments.

CHAPTER 2

Part of this chapter corresponds to a manuscript under final revision of the co-authors. In addition the results of this chapter have been presented during two international conferences: (1) Galletti Y., di Sarra A., Becagli S., Gonnelli M., Sferlazzo D.,Vestri S., Santinelli C. Atmospheric deposition of DOC at the island of Lampedusa: a preliminary study. 41st CIESM Congress, September 12th-16th 2016, Kiel, Germany; (2) Galletti Y., di Sarra A., Becagli S., Gonnelli M., Pulido-Villena E., Sferlazzo D.,Vestri S., Santinelli C. Total atmospheric DOM at the island of Lampedusa. EGU General Assembly 2018. April 8th-13th 2018. Vienna, Austria.

"Without atmosphere a painting is nothing".
Rembrandt

Atmospheric deposition of DOM at the island of Lampedusa

The following chapter reports and discusses data about the total atmospheric deposition collected at the island of Lampedusa between March 19th 2015 and November 3rd 2016. A detailed description of sampling periods and deposition types is reported in Table 2.1.

Sample name	Sampling period			Deposition type	Volume collected (L)
	Start date	End date	Total days		
Lmp01	18/03/2015	28/03/2015	10	wet and dry	6
Lmp02	28/03/2015	17/04/2015	20	dry	0.26
Lmp03	17/04/2015	02/05/2015	16	dry	0.27
Lmp04	02/05/2015	21/05/2015	19	wet and dry	1.8
Lmp05	21/05/2015	05/06/2015	15	dry	0.28
Lmp06	05/06/2015	19/06/2015	15	dry	0.29
Lmp07	19/06/2015	04/07/2015	16	dry	0.26
Lmp08	04/07/2015	17/07/2015	14	dry	0.26
Lmp09	17/07/2015	31/07/2015	14	dry	0.27
Lmp10	31/07/2015	21/08/2015	20	wet and dry	9
Lmp11	21/08/2015	11/09/2015	22	wet and dry	2
Lmp12	11/09/2015	01/10/2015	20	wet and dry	5
Lmp13	01/10/2015	30/10/2015	29	wet and dry	0.5
Lmp14	30/10/2015	09/11/2015	11	wet and dry	2
Lmp15	09/11/2015	23/11/2015	14	wet and dry	0.6
Lmp16	23/11/2015	02/12/2015	9	wet and dry	1.2
Lmp17	02/12/2015	21/12/2015	19	wet and dry	1.9
Lmp18	21/12/2015	08/01/2016	18	wet and dry	1.8
Lmp19	08/01/2016	28/01/2016	20	wet and dry	6.1
Lmp20	28/01/2016	16/02/2016	19	wet and dry	2.7
Lmp21	16/02/2016	11/03/2016	26	wet and dry	2.1
Lmp22	11/03/2016	09/04/2016	28	wet and dry	7.1
Lmp23	09/04/2016	04/05/2016	26	wet and dry	0.3
Lmp24	04/05/2016	10/05/2016	6	wet and dry	2.3
Lmp25	10/05/2016	13/05/2016	3	wet and dry	1.9
Lmp26	13/05/2016	01/06/2016	19	wet and dry	0.7
Lmp27	01/06/2016	22/07/2016	50	dry	0.26
Lmp28	22/07/2016	10/08/2016	19	dry	0.24
Lmp29	10/08/2016	26/08/2016	16	dry	0.24
Lmp30	26/08/2016	12/09/2016	17	wet and dry	0.8
Lmp31	12/09/2016	08/10/2016	26	wet and dry	12
Lmp32	08/10/2016	24/10/2016	16	wet and dry	0.5
Lmp33	24/10/2016	03/11/2016	10	wet and dry	11

Table 2.1. Sampling period and type of deposition for the 33 samples collected at the Island of Lampedusa. The thick black line separates samples collected in 2015 and 2016.

1. Study area

Total atmospheric depositions were collected at the Station for Climate Observations “Roberto Sarao”, maintained by ENEA (the Italian National Agency for New Technologies, Energy and Sustainable Economic Development) since 1997. This station is located in Capo Grecale, along the northeastern coast of the Lampedusa Island (35.52°N, 12.63°E), Italy (Fig. 2.1). ENEA climatic station is part of the regional World Meteorological Organization/Global Atmospheric Watch network. At this site, continuous observations of the following parameters are carried out: greenhouse gases concentration (Artuso et al., 2007, 2009), aerosol properties (di Sarra et al., 2011, 2015; Becagli et al., 2013; Marconi et al., 2014; Calzolai et al., 2015), total ozone, ultraviolet irradiance (Meloni et al., 2005), solar and infrared radiation (di Sarra et al., 2011; Meloni et al., 2012, 2015), and other climatic parameters. In 2015, an oceanographic buoy was also deployed in order to study the air-sea interactions.

Figure 2.1. Position of the Island of Lampedusa and of the station for Climate Observations “Roberto Sarao”, maintained by ENEA.

The Island of Lampedusa (Fig. 2.1) is representative of the remote marine environment of the central Med Sea and is located in a strategic position for the study of the relevance of atmospheric DOC fluxes to the open Med Sea and climate because: (1) it is far from large islands or continental areas and from relevant pollutant sources, excluding ship traffic (Becagli et al., 2012, 2017); (2) It is small, rocky, and has very poor vegetation; (3) it is relatively close to Africa, and one of the southernmost locations in Europe, and therefore strongly affected by Saharan dust deposition (Vincent et al., 2016). Indeed, the input of Saharan dust has important effects on the chemistry of the Mediterranean aerosols and its deposition can enrich the Med Sea with many elements (such as Co, Ni, trace metals), but little is known about the interaction between dust aerosol and organic compounds (Aymoz et al., 2004). Wet deposition controls the flux of Saharan dust to the Med Sea, but dry deposition can also be important (Guerzoni et al., 1997) and it depends strongly on meteorological conditions and local emissions (Inomata et al., 2009). In addition the annual dust flux can be controlled by few episodes of Saharan outbreaks, indeed a single outbreak can account for 40-80% of the flux (Guerzoni et al., 1997).

The importance of this study area is that previous work reported DOC atmospheric deposition in coastal areas, less representative of what is actually arriving to the open Med Sea.

2. DOC atmospheric fluxes

DOC atmospheric fluxes ranged between 0.06 and 1.78 mmol C m^{-2} day^{-1} in 2015, and between 0.08 and 0.98 mmol C m^{-2} day^{-1} in 2016 (Table 2.2). In most of the sampling periods (60%), deposition was lower than 0.2 mmol C m^{-2} d^{-1}.

In 2015, the lowest deposition rates (<0.1 mmol C m^{-2} d^{-1}) were measured in July (Lmp09), in October (Lmp13) and in November (Lmp15). The highest deposition rates (>1.2 mmol C m^{-2} d^{-1}) were observed between March and April (Lmp02), and in June (Lmp06), both periods characterized by dry depositions (Fig. 2.2). High DOC fluxes (0.6-1.2 mmol C m^{-2} d^{-1}) were also observed in March (Lmp01), May (Lmp04) and at the end of July (Lmp10), in correspondence with periods dominated by wet deposition (total precipitation in the three periods = 120 mm). The year 2015 was rather rainy, with a total rain intensity of 360 mm, slightly higher than the average annual rainfall at the Island of Lampedusa (325 mm with

42 days of rain), (data from: *http://www.arpa.sicilia.it/ and http://www.eurometeo.com/italian/climate*).

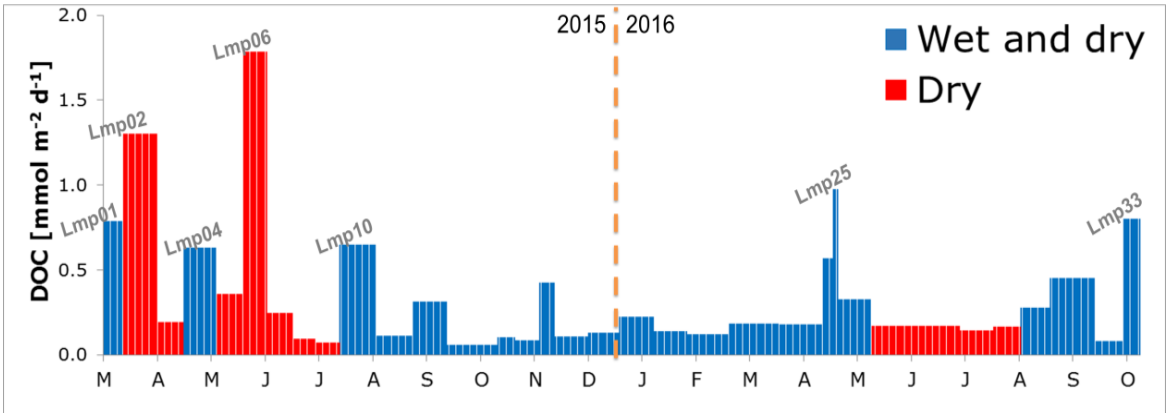

Figure 2.2. Atmospheric DOC fluxes.

In 2016, DOC deposition rates were rather low compared to the previous year, with a smaller variability. DOC fluxes ranged between 0.1 and 0.3 mmol C m^{-2} d^{-1} for most of the year (January to August; Lmp18 to Lmp23 and Lmp27 to Lmp30). Between May 4th and 13th (Lmp24 to Lmp26) the highest DOC flux (>0.8 mmol C m^{-2} d^{-1}) was observed (Lmp25) in correspondence with a period characterized by strong rain. High DOC fluxes were also observed between October and November (Lmp31 and Lmp33) (Fig. 2.2 and Table 2.2).

Atmospheric fluxes of DOC were significantly correlated with precipitation rates (r^2=0.56, p<0.0001, n=23). This relationship confirms the high efficiency in DOM atmospheric deposition of DOC via rain events in the Med Sea, as recently reported by Djaoudi et al. (2018) and in previous studies (Kanakidou et al., 2012).

Sample name	DOC fluxes [mmol m^{-2} d^{-1}]	DON fluxes [mmol m^{-2} d^{-1}]	TSN fluxes [mmol m^{-2} d^{-1}]	DOP fluxes [mmol m^{-2} d^{-1}]	TDP fluxes [mmol m^{-2} d^{-1}]
Lmp01	0.80	0.10	0.17	0	$7 \cdot 10^{-4}$
Lmp02	1.30	n.a.	n.a.	n.a.	n.a.
Lmp03	0.19	n.a.	n.a.	n.a.	n.a.
Lmp04	0.63	0.01	0.05	$9 \cdot 10^{-4}$	$3 \cdot 10^{-3}$
Lmp05	0.36	n.a.	n.a.	n.a.	n.a.
Lmp06	1.78	n.a.	n.a.	n.a.	n.a.
Lmp07	0.25	n.a.	n.a.	n.a.	n.a.
Lmp08	0.10	n.a.	n.a.	n.a.	n.a.
Lmp09	0.07	n.a.	n.a.	n.a.	n.a.
Lmp10	0.65	0.02	0.11	$3 \cdot 10^{-3}$	$5 \cdot 10^{-3}$
Lmp11	0.11	0.01	0.09	$1 \cdot 10^{-4}$	$6 \cdot 10^{-4}$
Lmp12	0.31	0.03	0.10	$3 \cdot 10^{-4}$	$1 \cdot 10^{-3}$
Lmp13	0.06	$1.5 \cdot 10^{-3}$	$3 \cdot 10^{-2}$	$7 \cdot 10^{-5}$	$1 \cdot 10^{-4}$
Lmp14	0.10	0.01	0.03	$2 \cdot 10^{-4}$	$4 \cdot 10^{-4}$
Lmp15	0.09	$8 \cdot 10^{-3}$	0.06	$2 \cdot 10^{-5}$	$6 \cdot 10^{-4}$
Lmp16	0.43	0.05	0.14	$2 \cdot 10^{-4}$	$5 \cdot 10^{-4}$
Lmp17	0.11	0.03	0.11	$7 \cdot 10^{-5}$	$1 \cdot 10^{-4}$
Lmp18	0.13	0.04	0.25	$9 \cdot 10^{-5}$	$4 \cdot 10^{-4}$
Lmp19	0.23	0.04	0.20	$3 \cdot 10^{-4}$	$9 \cdot 10^{-4}$
Lmp20	0.14	0.03	0.12	$2 \cdot 10^{-4}$	$2 \cdot 10^{-4}$
Lmp21	0.12	0.02	0.10	$2 \cdot 10^{-4}$	$3 \cdot 10^{-4}$
Lmp22	0.18	0.02	0.05	$3 \cdot 10^{-4}$	$4 \cdot 10^{-4}$
Lmp23	0.18	$6 \cdot 10^{-3}$	0.10	$1 \cdot 10^{-4}$	$2 \cdot 10^{-4}$
Lmp24	0.57	0.25	0.47	$3 \cdot 10^{-4}$	$2 \cdot 10^{-3}$
Lmp25	0.98	0.12	0.32	$9 \cdot 10^{-5}$	$3 \cdot 10^{-3}$
Lmp26	0.33	n.a.	n.a.	n.a.	n.a.
Lmp27	0.17	0.02	0.08	$2 \cdot 10^{-5}$	$1 \cdot 10^{-4}$
Lmp28	0.14	0.05	0.19	$9 \cdot 10^{-5}$	$5 \cdot 10^{-4}$
Lmp29	0.17	0.01	0.12	$2 \cdot 10^{-4}$	$1 \cdot 10^{-3}$
Lmp30	0.28	0.04	0.18	$2 \cdot 10^{-4}$	$9 \cdot 10^{-4}$
Lmp31	0.45	0.07	0.22	$1 \cdot 10^{-3}$	$3 \cdot 10^{-3}$
Lmp32	0.08	0.02	0.10	$4 \cdot 10^{-5}$	$2 \cdot 10^{-4}$
Lmp33	0.80	0.10	0.34	$2 \cdot 10^{-3}$	$2 \cdot 10^{-3}$

Table 2.2. Fluxes of DOC, DON, TSN, DOP and TDP. The thick black line separates samples collected in 2015 and 2016.

In both years, the highest deposition rates were observed between spring and autumn, periods characterized by the most intense dust deposition events in agreement with previous observations (Bergametti et al., 1989; Loye-Pilot and Martin, 1996; Avila et al., 1997; Ternon et al., 2010; Vincent et al., 2016). These results suggest that dust events can contribute significantly to the DOC fluxes from the atmosphere observed in spring and autumn.

Taking into consideration the entire sampling period, a mean daily rate of 0.32 mmol C m^{-2} d^{-1} was calculated, resulting in an annual DOC flux of 117.7 mmol C m^{-2} $year^{-1}$. It is noteworthy that the two highest peaks observed in 2015 (Lmp02 and Lmp06, dry deposition) together accounted for the input of 52 mmol C m^{-2} y^{-1}, that is 44% of the annual DOC flux. This observation highlights the importance of single deposition events that, depending on the origin and trajectories of the air masses, can carry significant amounts of DOC.

The annual input of DOC from the atmosphere, observed in this study, is in the range of the values measured at Cap Ferrat peninsula (Southern France) in 2006 (129 mmol C m^{-2} y^{-1}) (Pulido-Villena et al., 2008a) and in 3 lakes in the Southern Spain in 2005 (65.7 mmol C m^{-2} y^{-1} in 2004 and 153.3 mmol C m^{-2} y^{-1}) (De Vicente et al., 2012). Our values are higher than those reported for the north-western Med Sea from February 2015 to July 2016, at Frioul island, Marseille Bay (59 mmol C m^{-2} y^{-1}) (Djaoudi et al., 2017). If the same sampling period is taken into consideration (from March 2015, the beginning of sampling in Lampedusa, to July 2016, the end of sampling at Frioul island), DOC input is 2-times higher at Lampedusa than at Frioul Island. This variability is probably due to the different temporal and seasonal cycles of dry and wet deposition. The difference between these 2 sites could be also due to the presence of a south-north decreasing gradient in the intensity of the mineral dust deposition (Vincent et al, 2016), combined with the different trajectories of air masses affecting the amount and quality of organic carbon present in the aerosol.

Assuming that the annual DOC flux from this study (117.7 mmol C m^{-2} y^{-1}) is valid for the whole Med Sea (area=$2.5 \cdot 10^{12}$ m^2), we can estimate a total input to the basin of 3.55 Tg DOC y^{-1}. The global estimation for wet atmospheric DOC deposition is 306-580 Tg C y^{-1} and the input to the global ocean ranges between 90 and 246 Tg C y^{-1} (Willey et al., 2000; Kanakidou et al., 2012). The global dry deposition of OC has been estimated to be 11 Tg C y^{-1}, (Jurado et al., 2008) leading to a total OC deposition to the oceans of 101-247 Tg C y^{-1}. The comparison of these estimates indicates that the Med Sea receives from 1.44 to 4% of the global atmospheric input of DOC, despite it covers only 0.7% of the global oceans area. In addition, these values are up to 6 times larger than the estimate of the total river input to the Med Sea (0.6-0.7 Tg DOC y^{-1}; Santinelli, 2015).

In addition to the fluxes estimation, it is crucial to know the main sources of DOC to the atmosphere, in order to understand the role of atmospheric DOC in local and global C budgets. Raymond (2005) studied the $\delta^{13}C$ and $\Delta^{14}C$ signatures of organic carbon (OC) rainfall (collected in the Northeastern Unided States) and found that multiple sources were involved, even if most OC in rainwater deposited over the ocean was from the ocean and fossil fuel burning.

3. DON and TSN, DOP and TDP atmospheric fluxes

DON and Total Soluble Nitrogen (TSN) fluxes ranged between $1.5 \cdot 10^{-3}$ and 0.25 mmol DON m^{-2} d^{-1} and between $3 \cdot 10^{-2}$ and 0.47 mmol TSN m^{-2} d^{-1}, respectively (Fig. 2.3 and Table 2.2). In most of the sampling period (93%), DON deposition was lower than 0.1 mmol m^{-2} d^{-1}. The main peaks were observed in March 2015 (Lmp01), in May (Lmp24 and Lmp25) and October 2016 (Lmp33) in correspondence with high DOC deposition (Fig. 2.2, Fig. 2.3 and Table 2.2).

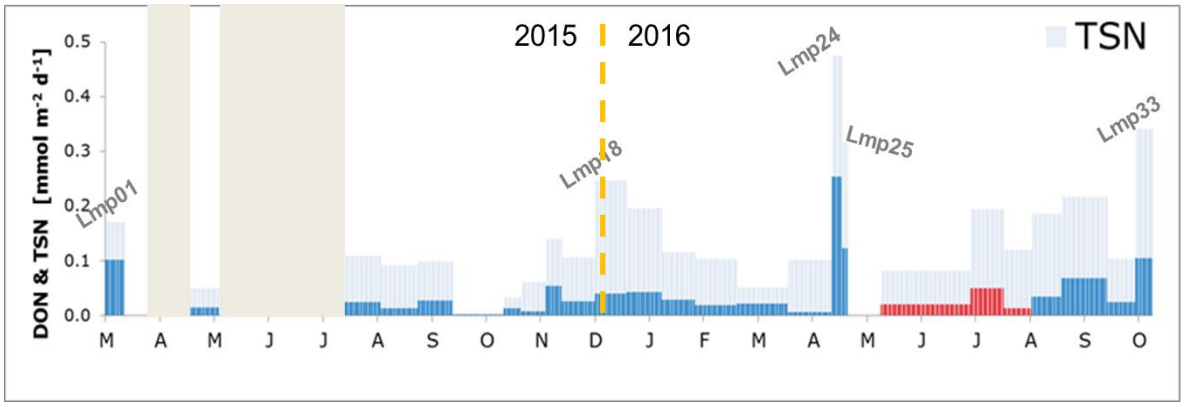

Figure 2.3. The atmospheric DON in blue (wet deposition) and red (dry deposition), and Total Soluble Nitrogen (TSN) in cyan. No data are available in the grey areas.

DOP and Total dissolved phosphorous (TDP) fluxes ranged between 0 and $2.7 \cdot 10^{-3}$ mmol DOP m^{-2} d^{-1} and $1 \cdot 10^{-4}$ and $4.9 \cdot 10^{-3}$ mmol TDP m^{-2} d^{-1}, respectively (Fig. 2.4 and Table 2.2). Between August 2015 and September 2016 (Lmp10-Lmp30) both DOP and TDP showed low fluxes. In 2015 atmospheric DOP and TDP showed the highest fluxes in May (Lmp04) and August (Lmp10). In 2016, the main peaks in DOP and TDP deposition were observed in October (Lmp31) and November (Lmp33).The four peaks in atmospheric DOP and TDP (Lmp04, Lmp10, Lmp31 and Lmp33) were responsible for 16% of total depositions and were in correspondence with high DOC fluxes, excluding Lmp31 (Fig. 2.2). It noteworthy that in May 2016 (Lmp25), in correspondence with high fluxes of both DOC, DON

and TDP ($3 \cdot 10^{-3}$ mmol m^{-2} d^{-1}), DOP was very low ($9 \cdot 10^{-5}$ mmol m^{-2} d^{-1}) (Fig. 2.4 and Table 2.2).

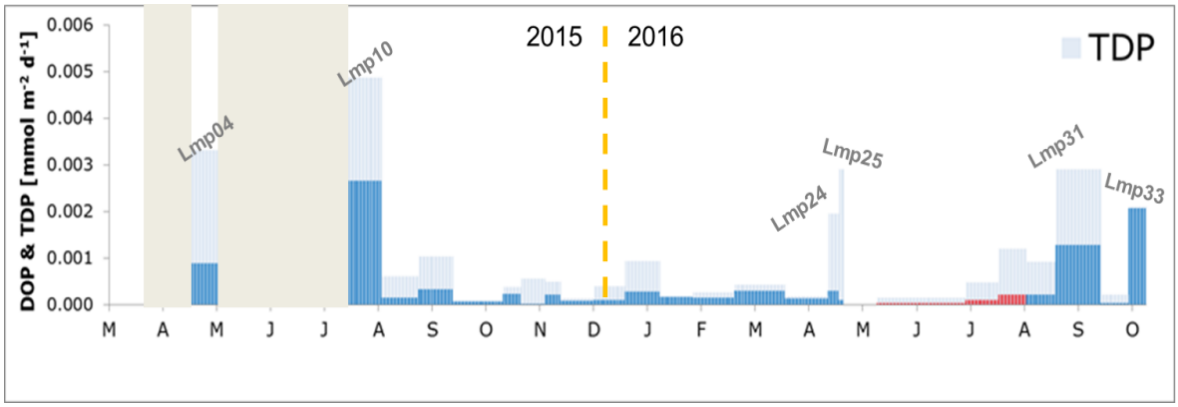

Figure 2.4. Atmospheric fluxes of DOP in blue (wet deposition) and red (dry deposition), and Total Dissolved Phosphorous (TDP) in cyan. No data are available in the grey areas.

Taking into consideration the entire sampling period, a mean DON and DOP daily deposition rate of 0.032 mmol DON m^{-2} d^{-1} and $3.8 \cdot 10^{-4}$ mmol DOP m^{-2} d^{-1} was calculated, resulting in annual fluxes of 11.6 mmol DON m^{-2} y^{-1} and 0.14 mmol DOP m^{-2} y^{-1}. The comparison among these values and the few data reported in the literature for DOP shows that the fluxes at Lampedusa are markedly higher than the annual DOP flux reported in literature for the western Med Sea (0.07 mmol P m^{-2} y^{-1}, Djaoudi et al., 2018; 0.03 mmol P m^{-2} y^{-1}, Migon and Sandroni, 1999), whereas they are lower than those obtained by Violaki et al. (2017) for both the West Med Sea (1.16 mmol P m^{-2} y^{-1}) and the East Med Sea (0.90 mmol P m^{-2} y^{-1}). Our values are instead very similar to those reported for the eastern Med Sea in 2001 and 2002 (0.15 mmol P m^{-2} y^{-1}) (Markaki et al., 2010). About DON, the annual flux observed at Lampedusa was lower than that measured at Frioul island (north-western Med Sea), western basin (17.80 mmol DON m^{-2} y^{-1}, Djaoudi et al., 2018). Only one paper reports data on atmospheric DON fluxes for the eastern basin (Markaki et al., 2010), these authors reported an annual flux (18.49 mmol DON m^{-2} y^{-1}) higher than that observed at Lampedusa.

Annual TDP flux at the Island of Lampedusa was 0.36 mmol TDP m^{-2} y^{-1}, this value is similar to that observed at Frioul in 2015-2016 (0.39 mmol TDP m^{-2} y^{-1}) (Djaoudi et al., 2018), whereas it is lower than that observed in dry depositions at the Finokalia station, in the eastern Med Sea (1.60 mmol TDPm^{-2} y^{-1} in 2012 and 1.41 mmol TDP m^{-2} y^{-1} in 2013) (Violaki et al., 2017), and at Cap Béar

(western Med Sea), between 2005 and 2011 (2.16 mmol TDP m^{-2} y^{-1}) (Violaki et al., 2017).

Annual TSN flux at the Island of Lampedusa was 44.75 mmol TSN m^{-2} y^{-1}, this value is higher than that observed at Frioul Island in 2015-2016 (39.28 mmol TSN m^{-2} y^{-1}) (Djaoudi et al., 2018).

It should be noted that the missing data in 2015 could determine an underestimate of the annual flux for DON, TSN, DOP and TDP.

These data indicate that a significant percentage of the dissolved P and N in the atmospheric depositions was in the organic form. Over the entire time-series, the average contribution of DOP and DON to the TDP and TSN was 40% and 26%, respectively (Fig. 2.3 and 2.4). These values are similar to those observed in previous studies at the Frioul Island (DOP 40%, DON 25%) (Djaoudi et al., 2018), and in both western and eastern Med Sea (DOP 38%; DON 32%) (Markaki et al., 2010).

The similarity among the depositions collected at the two sites suggests that the remote site of Lampedusa is representative of what the Mediterranean area receives, especially the western basin. However, once again, the importance of investigating the sources should be emphasized, since they could equally impact both on coastal sites and on remote sites.

4. Elemental ratios in atmospheric DOM

DOC:DON:DOP ratios showed a marked variability in the different periods (Fig. 2.5 and Table 2.3). DOC:DON molar ratios ranged between 2.9 (Lmp28) and 45.9 (Lmp04) (Fig. 2.5a), with an average value of 11.6±11.4. DOC:DOP molar ratios ranged between 244 (Lmp10) and 11008 (Lmp25) (Fig. 2.5b), with an average of 1909±2513.- DON:DOP ratio ranged between 9.2 (Lmp10) and 1371 (Lmp25) (Fig. 2.5c), with an average value of 292±350. No clear seasonal trend was observed, even if in autumn (November 2015 and October 2016) and late spring (May 2016) depositions were very poor in P, compared to the other two elements. This trend could be explained by the origin of the aerosol and the trajectories of the air masses. These data show that each deposition is characterized by a specific molecular ratio, suggesting a high variability in DOM composition and the presence of multiple sources. In some cases the values are surprisingly high, while in others they are in good agreement with data reported in literature (Djaoudi et al., 2018). These authors observed DOC:DON:DOP molar

ratios of 1228:308:1 in atmospheric DOM, collected in the north-western Med Sea. It is important to stress the high variability found in our samples. Lmp25 for example shows extremely high values and this makes the average values rather high. In the surface Med Sea, DOC:DON:DOP ratios ranges between 1050:84:1 in the western basin to 1560:120:1 in the eastern basin (Pujo-Pay et al., 2011). The average values observed in atmospheric deposition (1909:292:1) indicate that atmospheric DOM is enriched in DOC and DON with respect to marine DOM. This observation is also valid when we compare our values with those recently measured on marine samples collected at the MOOSE ANTARES offshore station (north-western Med Sea) (1227:100:1, Djaoudi et al., 2018). The contribution of atmospheric deposition to the marine DOM stoichiometry in the Med Sea may be relevant, in particular during the stratification period, but further data are needed to establish a direct link between atmospheric deposition and marine biogeochemistry.

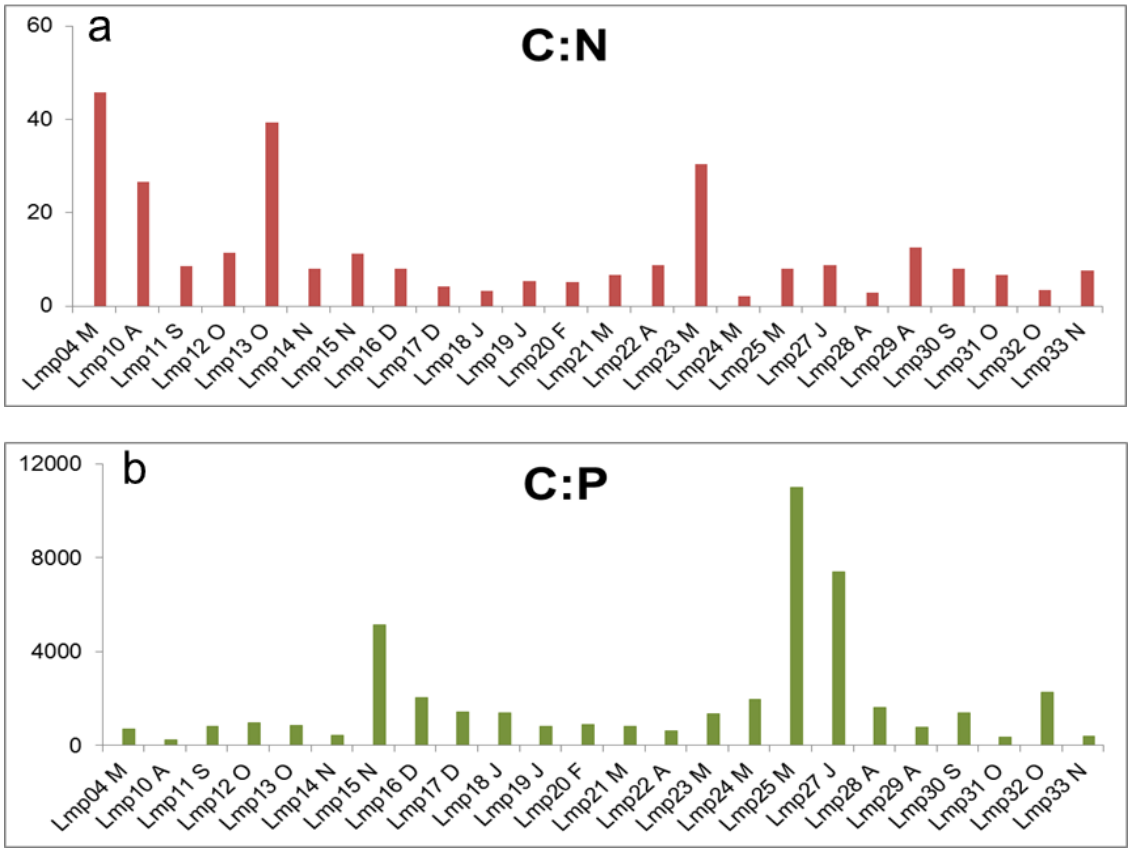

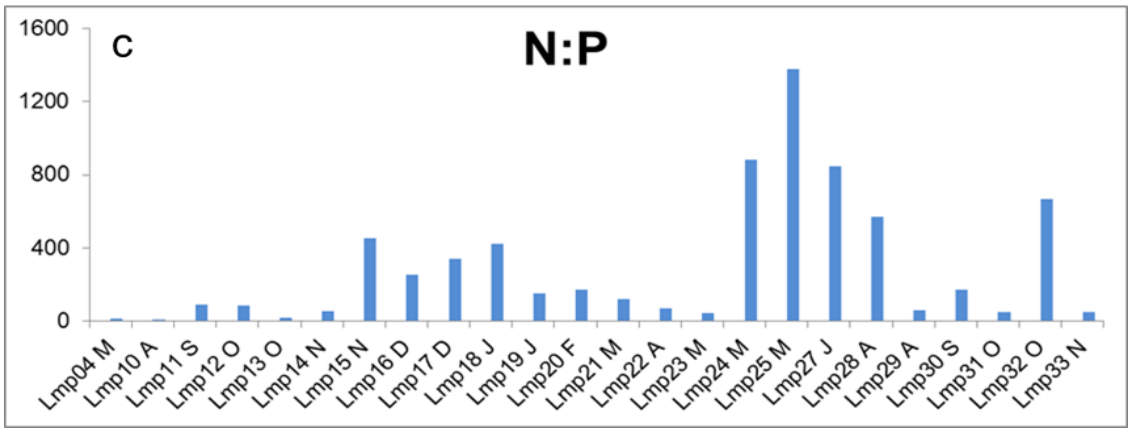

Figure 2.5. Temporal evolution of C:N (a), C:P (b) and N:P (c) ratios.

Sample	Sampling date	C:N	C:P	N:P
Lmp01	28/03/2015	7.78	n.a.	n.a.
Lmp04	21/05/2015	45.87	715.08	15.59
Lmp10	21/08/2015	26.57	244.38	9.20
Lmp11	11/09/2015	8.67	807.94	93.15
Lmp12	01/10/2015	11.37	977.79	85.98
Lmp13	30/10/2015	39.44	864.07	21.91
Lmp14	09/11/2015	8.02	449.04	56.00
Lmp15	23/11/2015	11.26	5131.65	455.83
Lmp16	02/12/2015	7.97	2036.66	255.42
Lmp17	21/12/2015	4.24	1448.37	341.90
Lmp18	08/01/2016	3.34	1406.60	420.55
Lmp19	28/01/2016	5.38	832.69	154.79
Lmp20	16/02/2016	5.09	882.80	173.40
Lmp21	11/03/2016	6.63	812.40	122.55
Lmp22	09/04/2016	8.78	645.65	73.53
Lmp23	04/05/2016	30.48	1353.57	44.41
Lmp24	10/05/2016	2.24	1976.03	882.33
Lmp25	13/05/2016	7.99	11008.94	1377.41
Lmp27	22/07/2016	8.73	7405.29	848.62
Lmp28	10/08/2016	2.89	1641.49	568.76
Lmp29	26/08/2016	12.66	796.68	62.95
Lmp30	12/09/2016	8.06	1376.27	170.77
Lmp31	08/10/2016	6.74	356.03	52.84
Lmp32	24/10/2016	3.41	2275.72	666.53
Lmp33	03/11/2016	7.68	389.57	50.73

Table 2.3. C:N:P molar ratios in atmospheric DOM.

5. DOC and DOP fluxes: a comparison between different sampling stations

In this section, the data collected at the Island of Lampedusa are compared with those collected at the island of Frioul (north-west Med Sea) in the same period and with the same sampling method, frequency and analysis (more details in Djaoudi et al., 2018), in order to highlights similitude and differences between 2 areas of the Med Sea differently affected by Saharan dust deposition and anthropic activities. The monthly average fluxes were calculated from the daily fluxes, and the data of the two sampling areas were compared. Atmospheric DOM in Lampedusa is richer in DOC (>30%) and in DOP (>50%) than in Frioul. In Lampedusa, it is very important the input of organic matter due to Saharan dust deposition events, whereas the Frioul Island is more influenced by anthropogenic aerosols, coming from the northern Europe (Chester et al., 1996; Sciare et al., 2003). A good correlation was found between the two sites, for DOC and DOP (r^2=0.90) (Fig. 2.6 and 2.7), no correlation was observed for DON. About DOC (Fig. 2.6), taking into consideration only the blue points (n=6: July and October 2015; February, March, June and July 2016), a slope of 1 was obtained, with r^2=0.93. All the outliers (red squares) have a much higher concentration of DOC in Lampedusa than in Frioul.

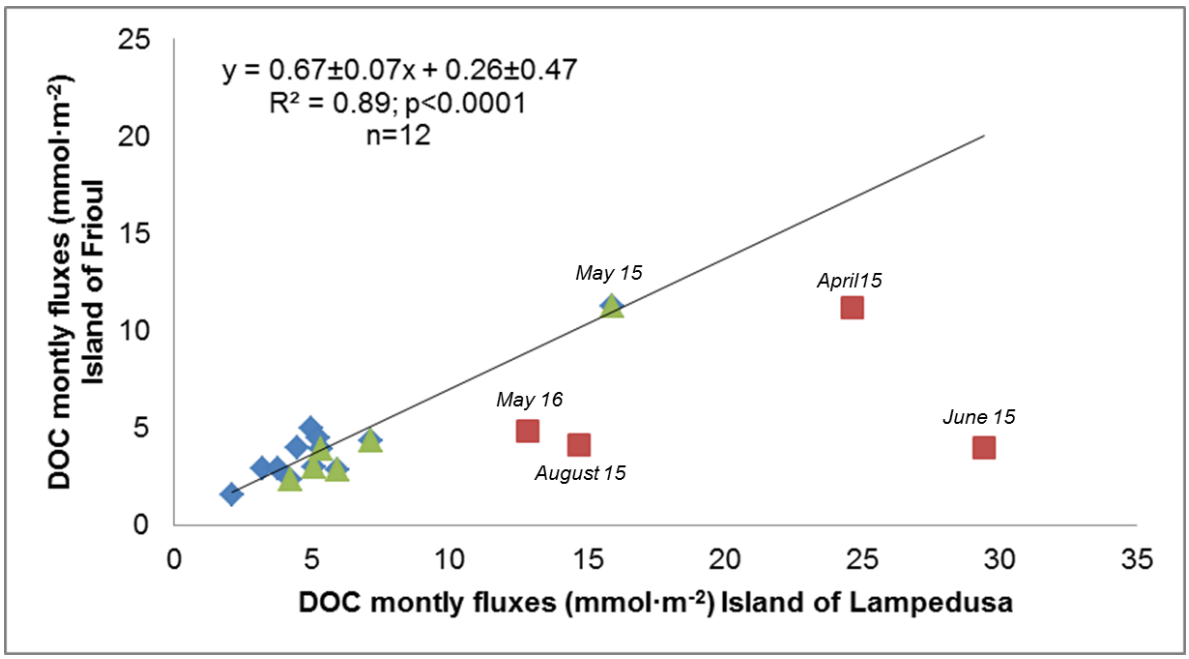

Figure 2.6. Comparison between DOC montly fluxes of the two different islands.

About DOP (Fig. 2.7), taking into consideration only the blue points (n=5: September, October and December 2015; February and April 2016), a slope of 1

was observed, with r^2=0.97. All the outliers (except 1, July 2016) had a much higher concentration of DOP in Lampedusa than in Frioul. In June and August 2015, the enrichment of P was probably relative to Saharan dust events. In July 2016, there was very probably an underestimation of DOP in Lampedusa due to the long sampling period (50 days). Definitely, good relationship can support the possibility to estimate DOC and DOP inputs on a basin scale.

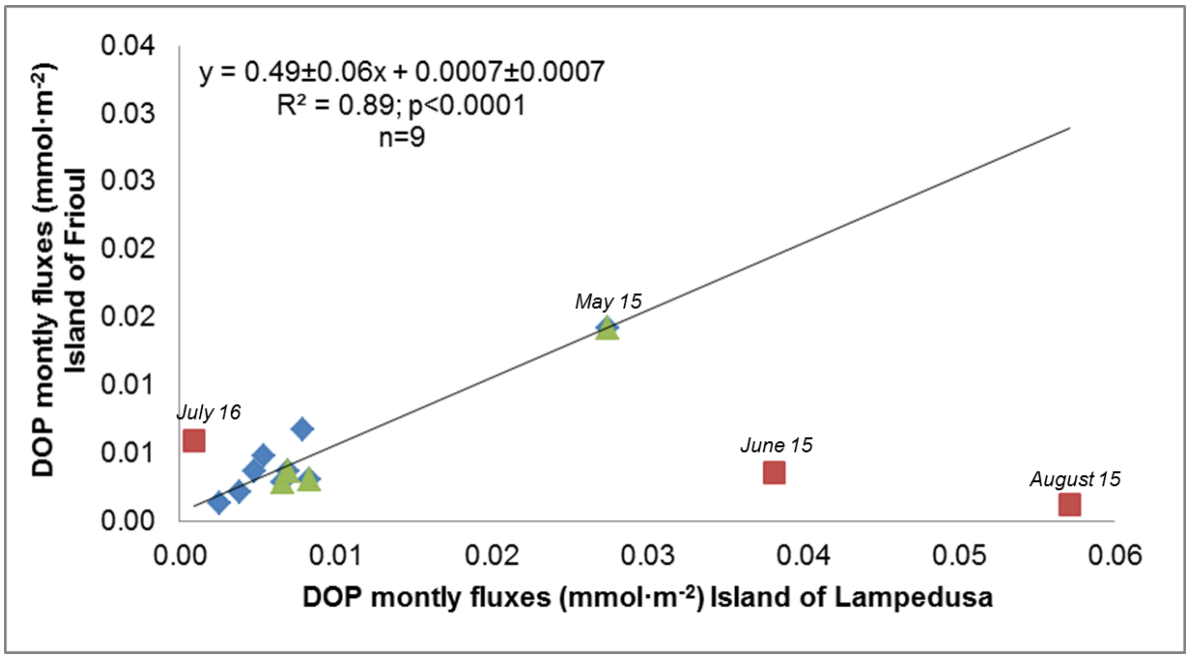

Figure 2.7. Comparison between DOC montly fluxes of the two different islands.

6. Atmospheric iron, vanadium and lead fluxes

6.1 *Fe atmospheric fluxes*

Fe fluxes ranged between $3.6 \cdot 10^{-7}$ and $2.4 \cdot 10^{-3}$ mmol m^{-2} d^{-1} with a marked variability (up to 4 order of magnitude) (Fig. 2.8). During most of the sampling period (87%), fluxes were lower than $1 \cdot 10^{-5}$ mmol m^{-2} d^{-1}. Only in March 2015 (Lmp01) and May 2016 (Lmp25), the deposition was greater than 0.0018 mmol m^{-2} d^{-1}. In June 2015 (Lmp06), a high Fe flux (>0.0008 mmol m^{-2} d^{-1}) was observed in dry depositions. The annual flux of Fe was 0.038 mmol m^{-2} y^{-1}. This value is similar to the flux estimated by Bonnet and Guieu in 2006 for the western Med Sea (0.042 mmol m^{-2} y^{-1}). It is interesting to stress the marked variability that occurs in the depositions, the two highest fluxes in 2015 (Lmp01, Lmp6), accounted for the input of 0.032 mmol m^{-2} d^{-1} (total sampling periods: 25 days), that is 71% of the annul flux in 2015. In 2016, the big deposition event, observed in May (Lmp25), was responsible for ~30% of the annual flux in just 3 days.

The 3 peaks (Lmp01, Lmp06 and Lmp25) occurred in correspondence with DOC peaks (Fig. 2.2). Considering the main sources of Fe, known in literature, a clearer picture of the possible DOC sources could be described. Fe in aerosol mainly come from mineral sources (95%) even if industry, biofuels and biomass burning can contribute for a small percentage (Luo et al., 2008). In the recent past, the atmospheric input of Fe in Corsica was studied and the results showed that the atmospheric Fe was mainly connected to dust deposition from the Sahara, with only 4% of samples not having a Saharan origin (Guieu et al., 2002). In the absence of Saharan dust transport, the Fe concentration in the surface layer was almost zero (Sarthou and Jeandel, 2001; Guieu et al., 2002). It is therefore reasonable to think that the three depositions, enriched in DOC and Fe, originated from natural sources, showing an important Saharan dust signature.

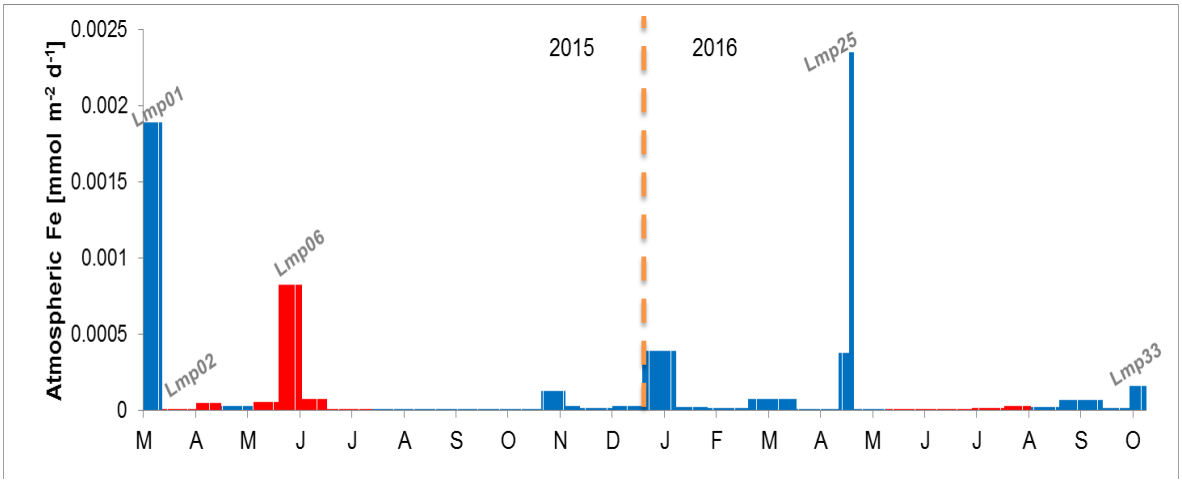

Figure 2.8. Temporal evolution of soluble iron.

6.2 *V atmospheric fluxes*

The atmospheric fluxes of vanadium ranged between $2.75 \cdot 10^{-6}$ and $1.2 \cdot 10^{-4}$ mmol m^{-2} d^{-1} and showed a lower variability with respect to the other elements (Fig. 2.9). In 2015, V was lower than $3 \cdot 10^{-5}$ mmol m^{-2} d^{-1} in 89% of deposition, with 2 peaks (>$6.5 \cdot 10^{-5}$ mmol m^{-2} d^{-1}) in March (Lmp01) and August (Lmp10). Another smaller peak was observed in May ($2.94 \cdot 10^{-5}$ mmol m^{-2} d^{-1}) (Lmp04). In contrast, in 2016, V was lower than $3 \cdot 10^{-5}$ mmol m^{-2} d^{-1} in 69% of deposition, with 3 peaks (>$6.4 \cdot 10^{-5}$ mmol m^{-2} d^{-1}), two in May (Lmp24 and Lmp25) and one in November (Lmp33). The total annual flux of V was 0.007 mmol m^{-2} y^{-1}.

It should be noted that 2 peaks in V input (Lmp01 and Lmp25) were observed in correspondence with high depositions of both Fe (Fig. 2.8) and DOC

(Fig. 2.2); while the other 3 peaks in V (Lmp04, Lmp10 and Lmp33) were observed in correspondence with high depositions of DOC but not of Fe. As done for iron, knowing the main sources of V, some considerations on the origin of atmospheric DOC can be made. The major source of V in the sea are ships (39%), petroleum refineries (35%) and industry (19%) (Visschedijk et al, 2013). Becagli et al. (2012) observed the presence of high values of metals, including V, in daily aerosol samples collected at the Lampedusa Island from 2004 to 2008. These authors observed the highest concentrations of V in spring-summer and attributed these high values to the ship emissions. In agreement with Becagli at el. (2012, 2017), our data show an enrichment in V in samples collected in March, May and between August and September 2015. In 2016, the peak in V deposition was observed in May, whereas V flux was at its minimum between June and September.

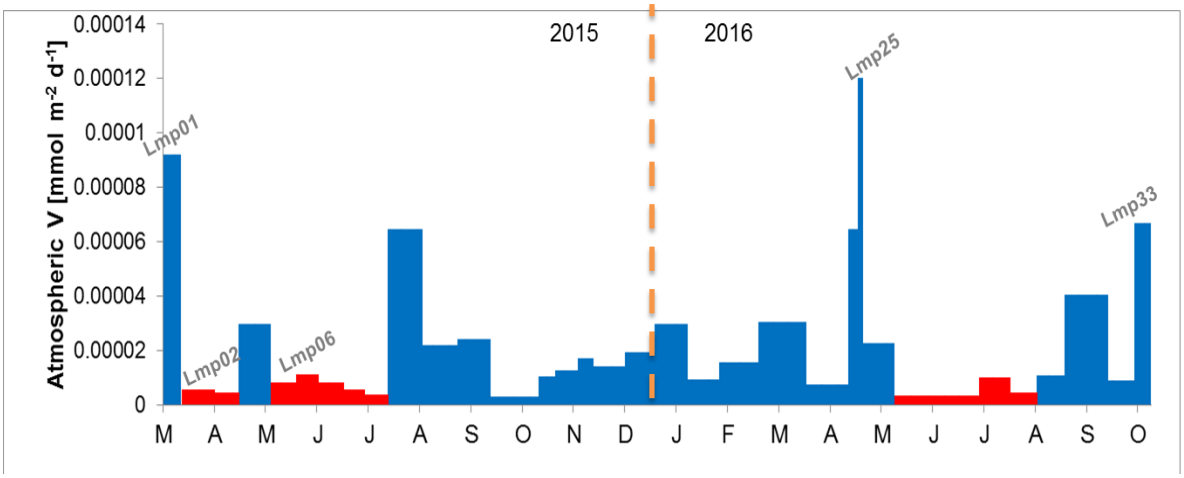

Figure 2.9. Temporal evolution of soluble vanadium.

6.3 *Pb atmospheric fluxes*

Pb fluxes ranged between $7.2 \cdot 10^{-7}$ and $4 \cdot 10^{-5}$ mmol m^{-2} d^{-1} and, as observed for V, showed a lower variability with respect to the other elements (Fig. 2.10). No link between the kind of deposition (wet or dry) and the input of Pb was observed. The highest values were found in 2015, with 5 main peaks (>$1.2 \cdot 10^{-5}$ mmol m^{-2} d^{-1}) representing 32% of deposition. In 2016, 6 peaks were observed, representing 27% of depositions. The highest peak was observed in January (Lmp19, $1.76 \cdot 10^{-5}$ mmol m^{-2} d^{-1}), the others showed values between 1.2 and 1.5 mmol m^{-2} d^{-1} and were in February (Lmp20), in May (Lmp24 and Lmp25), in October (Lmp31) and in November (Lmp33). The average annual flux was 0.0029

mmol m^{-2} y^{-1}. Despite its notorious dangerousness, there are few studies in literature on the atmospheric input of Pb to the Med Sea. In the past, an in-depth study was conducted on the atmospheric lead fluxes in the northwestern Mediterranean area, and the authors found an annual flux ($3.8 \cdot 10^{-9}$ mmol m^{-2} y^{-1}, Remoudaki et al., 1991) much lower than that obtained at Lampedusa. One of the possible explanations is that Pb, in the study of Remoudaki et al., was not shown to be efficiently transported during rainy periods, while in our case the highest depositions occur in correspondence with wet deposition. Moreover, it is reasonable to hypothesize that this element is subject to spatial and temporal patterns and/or that the Pb depositions have increased after almost 30 years. Pb is a heavy metal that occurs naturally in the Earth's crust, but once transformed into man-made products dispersed throughout the environment, becomes highly toxic to humans (Loh et al., 2016). The residence time of the particles containing Pb in the atmosphere varies according to the height of the emission source, their size, the intensity of the winds and the annual mean precipitation amount.

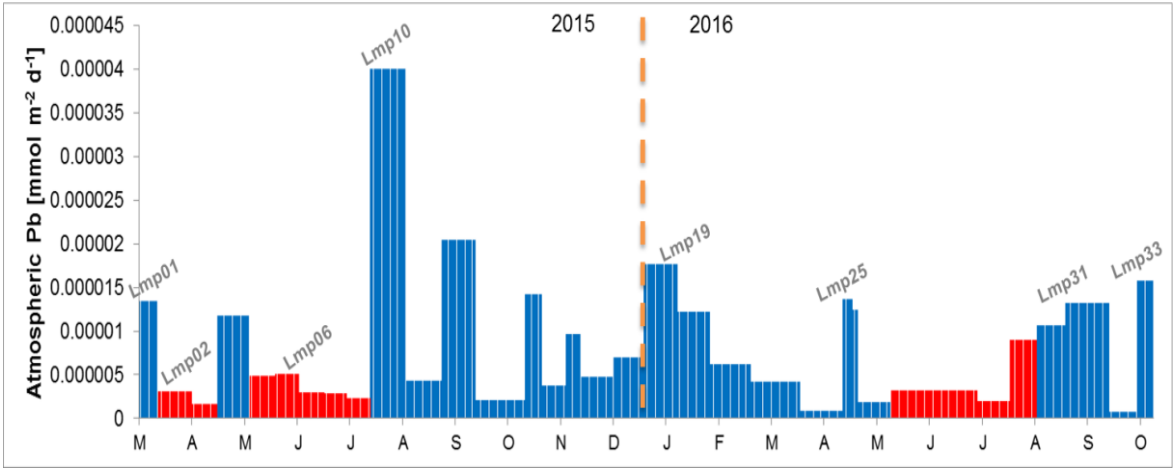

Figure 2.10. Temporal evolution of soluble lead.

7. The main peaks of DOC

The highest fluxes in atmospheric DOC deposition (≥0.8 mmol C m^{-2} d^{-1}) were Lmp01, Lmp02, Lmp06, Lmp25 and Lmp33 (Fig. 2.2 and Table 2.2). In order to gain information about their most probable sources, the air mass back trajectories were studied (Fig. 2.12 and Fig. 2.13), PM_{10} data were analyzed (Table 2.4), and the Fe/Al ratios were determined (Table 2.4). The latter ratio is a good indicator of the crustal origin in the aerosol composition, and it eliminates the variability owing to different mineralogical compositions, due to the variations in

the concentrations of quartz and carbonates (Guieu et al., 2002). The calculation of Fe/Al ratio was made taking into account the total concentrations (soluble plus particulate).

In general, iron and aluminum are significantly correlated (r^2=0.99, p<0.0001, n=33; Fig. 2.11) and the value of the slope (0.60) indicates a clear Saharan signature in all the depositions. A value ranging between 0.60 and 0.63 has been widely reported in the literature as typical of Saharan dust end-member (Chester et al., 1984; Bergametti et al., 1989; Krom et al., 1999; Guieu et al., 2002).

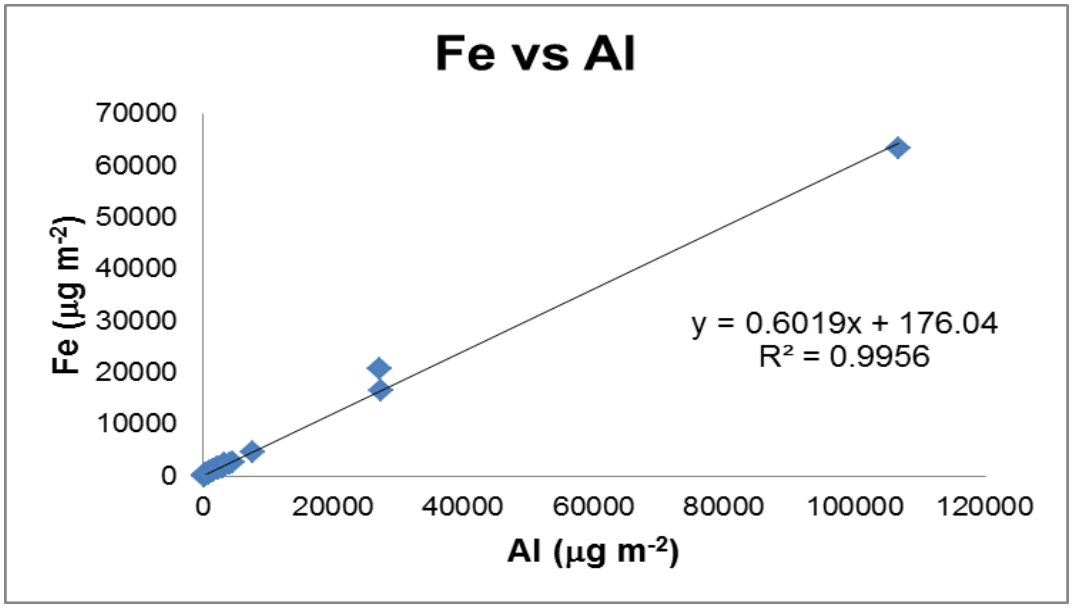

Fig. 2.11. Correlations between iron and alluminium in total atmospheric deposition.

7.1 *Lmp01*

This deposition was collected between 18th and 28th March 2015, the trajectories of the air masses clearly indicates that the aerosol mainly come from the Saharan region. In the first sampling period, the air masses crossed the North-Western Africa (Fig. 2.12 a) and the eastern Atlantic ocean, close to Gibraltar. In the second half of the sampling period (Fig. 2.12 b), part of the air flux originated from Sahara and the air masses swept across the Adriatic coast of Balkan Peninsula, crossing the Italian peninsula before arriving to Lampedusa.

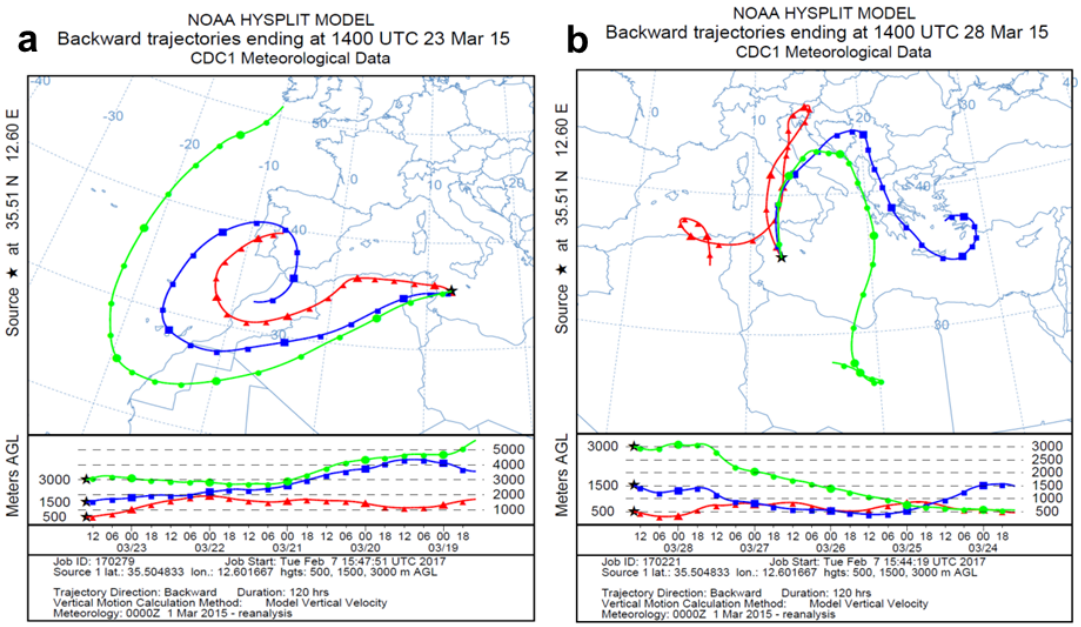

Figure 2.12. Five-days air back-trajectories arriving to the Lampedusa island in the 10 days preceding the collection of Lmp01, March 2015.

The mean concentration of PM_{10} in the 10 days of sampling was 50.1 μg m^{-3}, it was strongly influenced by dust deposition between March 23rd (55.8 μg m^{-3}) and 25th (102.8 μg m^{-3}). The peak in Fe further supports the Saharan origin of this aereosol, however the Fe/Al ratio was 0.76 (Table 2.4), slightly higher than the values reported in the literature for Saharan dust end-member, suggesting that aerosol was enrinched in Fe during its route to Lampedusa. This period was also characterized by a peak of Vanadium, whose emission mainly comes from human activities (39% sea going ships, 35% petroleum refineries, 19% industry, Visschedijk et al, 2013), in particular from the area of Western Europe.

These results indicate that this peak in DOC deposition is associated to a Saharan dust deposition event and that the aerosol, during its route to Lampedusa, was probably enriched with organic substances and iron coming from anthropic sources. We hypothesize that the dust present in the aerosol worked as condensation nuclei for organic molecules facilitating their accumulation and transport. Indeed, in previous studies organic material was found linked with dust particles (Buseck and Pòsfai, 1999; Zappoli et al., 1999) and the adsorption of organics to the surface of minerals may be the significant process (Goss and Schwarzenbach, 1999).

Sample name	Fe/Al	Mean PM_{10} [$\mu g/m^3$]
Lmp01	**0.76**	**50.1**
Lmp02	**0.72**	**29**
Lmp03	0.70	28.1
Lmp04	0.72	26.4
Lmp05	0.78	16.7
Lmp06	**0.70**	**23.1**
Lmp07	0.71	22.2
Lmp08	0.76	26.5
Lmp09	0.72	28.3
Lmp10	0.72	29.1
Lmp11	0.76	N.A.
Lmp12	0.83	N.A.
Lmp13	0.70	N.A.
Lmp14	0.71	N.A.
Lmp15	0.69	N.A.
Lmp16	0.61	N.A.
Lmp17	0.73	N.A.
Lmp18	0.63	N.A.
Lmp19	0.67	N.A.
Lmp20	0.37	N.A.
Lmp21	0.62	N.A.
Lmp22	0.61	N.A.
Lmp23	0.59	39.5
Lmp24	0.60	30.7
Lmp25	**0.59**	**133.7**
Lmp26	0.57	25.9
Lmp27	0.62	26.2
Lmp28	0.62	24.7
Lmp29	0.61	25
Lmp30	0.68	22.4
Lmp31	0.68	24.5
Lmp32	0.57	32.9
Lmp33	**0.63**	**31.8**

Table 2.4. The total Fe/Al ratio and the mean PM_{10} values of the atmospheric DOC deposition. In bold the ratios related to the five highest atmospheric DOC fluxes.

7.2 *Lmp02*

This atmospheric deposition was collected between March 28th and April 17th 2015, the trajectories of the air masses clearly indicates that the aerosol mainly come from the North-Western U.S. and Greenland (Fig. 2.13 a), the Northern Europe and Atlantic Ocean (Fig. 2.13 b), Scandinavia and Northern Italy

(2.13 c), Atlantic Ocean and Eastern Europe (Fig. 2.13 d). PM_{10} mean concentration was 29 μg m^{-3} (Table 2.4). Fe, V and Pb showed very low values, but the Fe/Al ratio was 0.72, suggesting that this aerosol is enriched in Fe with respect to Saharan aerosol. It is difficult to explain the high DOC deposition in this period, since the trajectories of the air masses moved over densely populated urban areas and Atlantic Ocean, this deposition could be enriched with DOC with anthropogenic and natural (sea spray) origin. The dust may have contributed to the transport of these organic compounds following some heterogeneous reactions on the surface of the mineral dust particles.

The most interesting aspect concerns the fact that Lmp02 is a dry deposition, highlighting the importance of dry deposition on local and regional scale, with significant consequences on the marine environment, as suggested by Jurado et al. (2008).

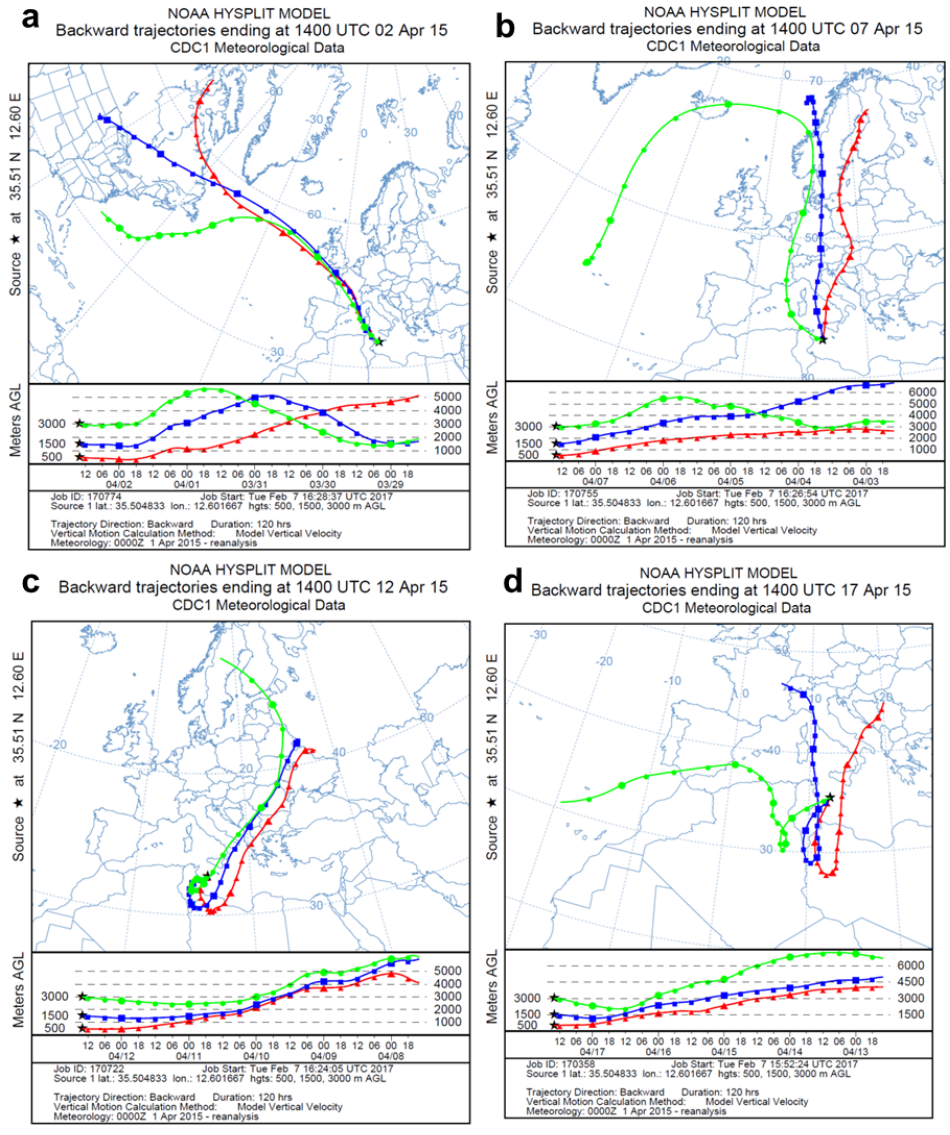

Figure 2.13. Five-days air back-trajectories arriving to the Lampedusa island in the 20 days preceding the collection of Lmp02, April 2015.

7.3 *Lmp06*

This atmospheric deposition was collected between 5th and 19th June 2015, it was characterized by air masses originated from the Northern African Coast (Morocco to Libya) and the Western Mediterranean Sea (Fig. 2.14 a) in the first period (5th-9th June), whereas air masses originated from Atlantic Ocean and Ionian Sea in the second period (10th-14th June) (Fig. 2.14 b), and in the last one they originated again from the Atlantic Ocean and partially from the Northern Europe (Fig. 2.14 c). The mean PM_{10} concentration was 23.1 μg m^{-3}, Fe showed a relevant peak (Fig. 2.8), and the Fe/Al ratio (0.70) was higher than the values reported in the literature for Saharan end-member (Guieu et al., 2002).

Although the PM_{10} did not show high concentration, taking into consideration the trajectories of the air masses, and also considering the value of the Fe/Al ratio, atmospheric DOC seems to have both an anthropogenic (from European countries) and natural (marine spray) origin, and it is associated with mineral dust.

The exceptional fact is that, as for Lmp02, it was a dry deposition, emphatizing once again the importance of these depositions, with probable positive or negative effects on the Mediterranean marine ecosystem.

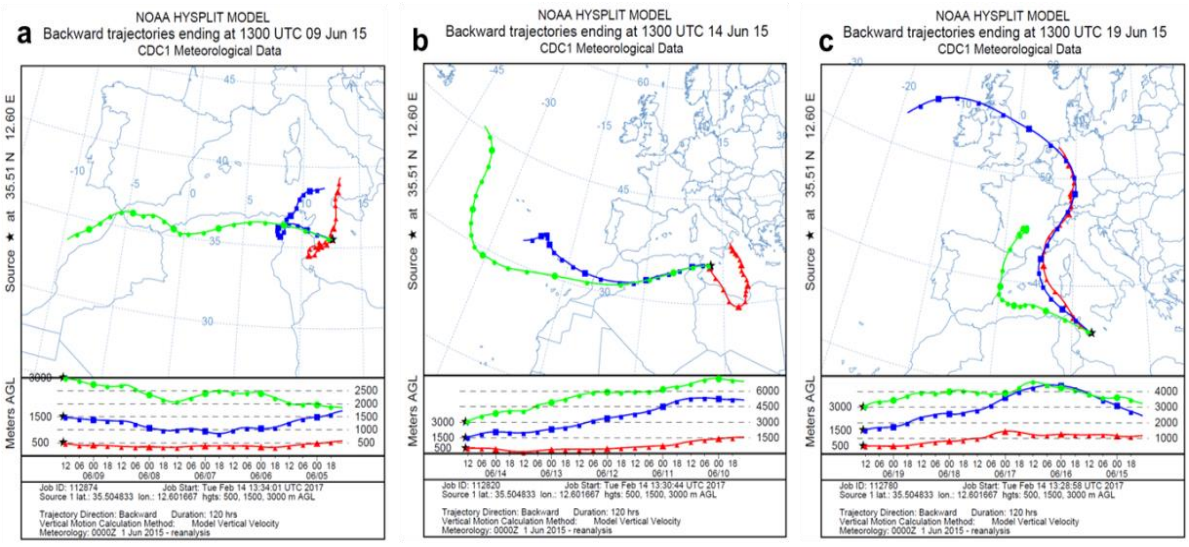

Figure 2.14. Five-days air back-trajectories arriving to the Lampedusa island in the 15 days preceding the collection of Lmp06, June 2015.

7.4 *Lmp25*

Atmospheric deposition was collected between 10th and 13th May 2016. In this period the air masses originated from the Atlantic Ocean, and then swept across the northwestern African countries, partly inland and partly on the coast (Fig. 2.15). The mean PM_{10} concentration was 133.7 μg m^{-3} with a peak of 267.4 μg m^{-3} on May 11th. This is the highest value observed in the entire sampling period and indicates the occurrence of a Saharan dust deposition event. The high Fe input and the ratio of Fe/Al (0.59), very similar to typical for Saharan dust (Guieu et al., 2002), confirm that the aerosol mainly has a Saharan dust component. The intense intrusion of Saharan was favored by one synoptic situation in which the role of a cyclonic circulation with a minimum depression was significant (http://www.meteogiornale.it/). This deposition was also characterized by high concentrations of DON, TSN (Fig. 2.3) and TDP (Fig. 2.4), as well as by a peak in V and pretty high values in Pb, suggesting that the Saharan dust during its transfer could be enriched with anthropogenic material. This data suggests that Saharan dust during its transport to Lampedusa was enriched with DOM and nutrients, looking at air masses trajectories we can hypothesis that the main source of DOM is natural, since air travelled above the Atlantic Ocean. However the high values of both V and Pb hindered to exclude a possible contribution from anthropic activities (probably from southern Iberian coast).

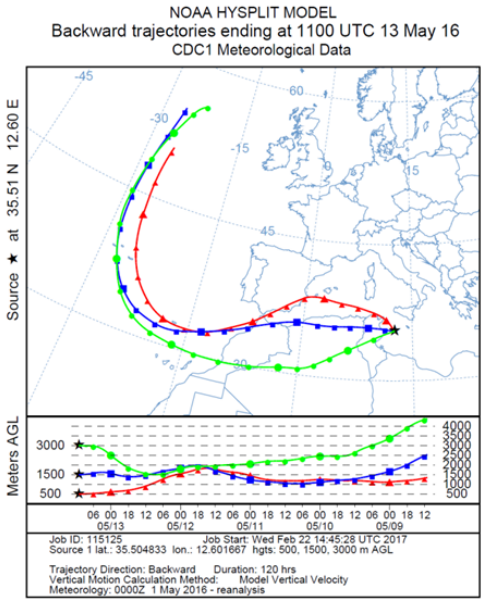

Figure 2.15. Five-days air back-trajectories arriving to the Lampedusa island in the 3 days preceding the collection of Lmp25, May 2016.

7.5 *Lmp33*

This atmospheric deposition was collected between October 24th and November 3rd 2016. Air masses back trajectories show that in the first period, air masses originated from north eastern Europe and Greece (Fig. 2.16 a), in the second period they mainly formed in the northwestern part of the Mediterranean Sea, the Gulf of Naples (Italy) and Northern Europe, crossing many eastern European states (Fig. 2.16 b). The mean concentration of PM_{10} was 38.1 μg m^{-3} and with Fe/Al ratio (0.63) typical for Saharan dust (Guieu et al., 2002). This deposition was characterized by high deposition values of TSN, DON (Fig. 2.3), TDP and DOP (Fig. 2.4) as well as high values of V (Fig. 2.9) and Pb (Fig. 2.10). These data together suggest that the main origin of the aerosol is anthropic, and organic matter and nutrients absorbed to the particles are brought from the north Europe toward the south. The significant amount of particulate matter (high values of PM_{10}) suggests that atmospheric deposition can also represent an important sink for organic carbon emitted to atmosphere from human activities, in agreement with the observation that between 4 and 52% of DOC in precipitation is fossil carbon, deriving from the fossil fuel combustion (Avery et al., 2006; Raymond, 2005; Wang et al., 2015). The transport of organic substance seems to be linked to the saharan dust also in this case, and the trajectories of the air masses show that this could happen in the last 5 days of deposition.

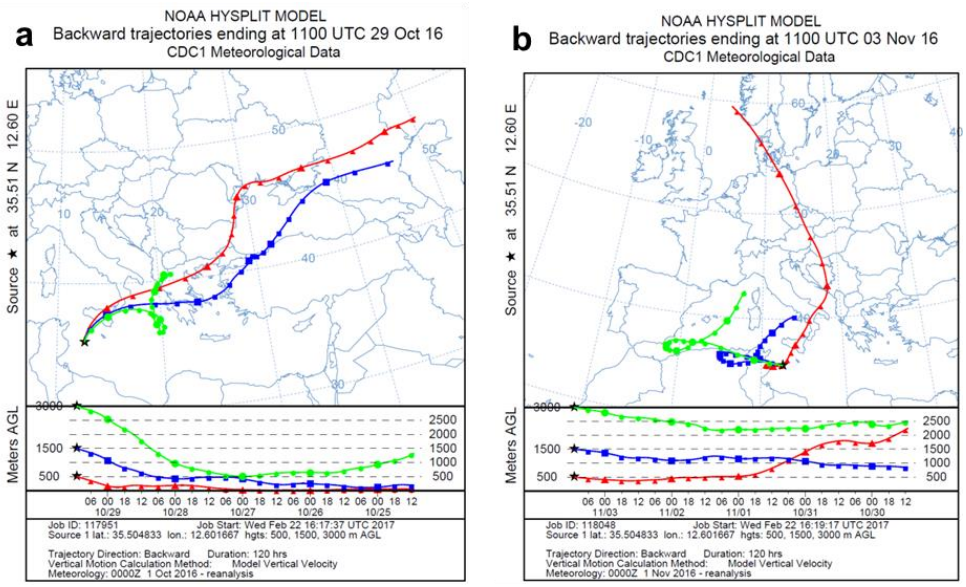

Figure 2.16. Five-days air back-trajectories arriving to the Lampedusa island in the 10 days preceding the collection of Lmp33, November 2016.

8. CDOM atmospheric dynamics

The fluxes of CDOM, reported as absorption coefficient at 254 nm (a_{254}), showed a marked variability during the entire sampling period, with values ranging from 1.06 to 38.98 m^{-1} m^{-2} d^{-1} (Fig. 2.17 and Table 2.5). The peaks of a_{254} corresponded to those of DOC (Fig. 2.2) with the highest one (38.98 m^{-1} m^{-2} d^{-1}) in May 2016 (Lmp25) in correspondence with a Saharan deposition event. The trend similar to that of DOC suggests that CDOM dynamics in the atmosphere is driven by the same processes as DOC, it can have the same sources and attach to the mineral dust in the aerosol, faciliting its transport. This work reports the first information about the total atmospheric fluxes of CDOM to the Med Sea, no comparison with literature data is therefore possible.

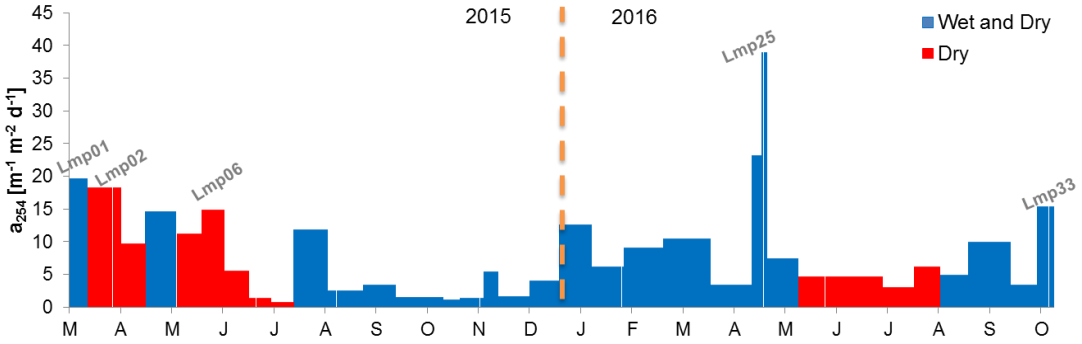

Figure 2.17. The atmospheric a_{254} fluxes.

Sample name	a_{254} fluxes [m^{-1} m^{-2} d^{-1}]	$S_{275-295}$ [nm^{-1}]
Lmp01	19.68	0.019
Lmp02	18.22	0.014
Lmp03	9.67	0.012
Lmp04	14.61	0.024
Lmp05	11.22	0.016
Lmp06	14.87	0.021
Lmp07	5.49	0.020
Lmp08	1.33	0.014
Lmp09	0.78	0.022
Lmp10	11.86	0.023
Lmp11	2.45	0.024
Lmp12	3.34	0.024
Lmp13	1.42	0.023
Lmp14	1.06	0.025
Lmp15	1.30	0.017
Lmp16	5.38	0.022

Lmp17	1.62	0.021
Lmp18	3.95	0.016
Lmp19	12.57	0.017
Lmp20	6.11	0.017
Lmp21	9.04	0.018
Lmp22	10.41	0.020
Lmp23	3.37	0.022
Lmp24	23.10	0.017
Lmp25	38.98	0.017
Lmp26	7.40	0.020
Lmp27	4.61	0.025
Lmp28	3.05	0.022
Lmp29	6.11	0.022
Lmp30	4.93	0.021
Lmp31	9.92	0.020
Lmp32	3.40	0.020
Lmp33	15.39	0.021
Average	8.69	0.020

Table 2.5. Information about sampling period and atmospheric CDOM parameters.

The spectral slope (S) calculated between 275 and 295 nm ($S_{275-295}$) gives indirect information on molecular weight and aromaticity degree of CDOM (Helms et al., 2008) and is independent on CDOM concentration. $S_{275-295}$ values ranged between 0.012 and 0.025 nm^{-1} in 2015 and between 0.016 and 0.025 nm^{-1} in 2016 (Fig. 2.18 and Table 2.5), suggesting that in 2016 CDOM pool was characterized by a higher fraction of molecules with lower molecular weight and lower aromaticity degree than in 2015. The $S_{275-295}$ values are in the range of values observed in the Arno River (0.012-0.016 nm^{-1}), and in coastal waters and at river's mouth (0.025 nm^{-1}) (the maximum value, 0.025 nm^{-1}, is typical of coastal waters and influenced by the mixing in river's mouth between sweet and salty waters), but they are lower than the values observed in in the open ocean (0.048 nm^{-1}) (Aurin and Mannino, 2012; Fichot and Benner, 2012). These values are also lower than those observed in open waters of the Med Sea (0.020-0.035 nm^{-1}) (Chapter 1), suggesting that the atmosphere is a source of DOM with higher molecular weight and higher aromaticity degree than marine DOM. This observation supports the hypothesize that atmosphere can be a major source of terrestrial DOM to the Med Sea (Chapter 1). Focusing on the depositions with the highest DOC concentrations $S_{275-295}$ values ranged between 0.014 and 0.019 nm^{-1} in correspondence with 3 of them and a value of 0.021 nm^{-1} in the other 2 (Lmp6

and Lmp33) was found (Table 2.5), highlighting an important signature of terrigenous material. Lmp01 (0.19 nm^{-1}), Lmp25 (0.17 nm^{-1}) and Lmp02 (0.14 nm^{-1}) were in the range of minimum values found in the Mediterranean Sea, emphasizing the presence of molecules with molecular weight higher than the two other depositions but still terrigenous, and likely linked with Saharan dust transport.

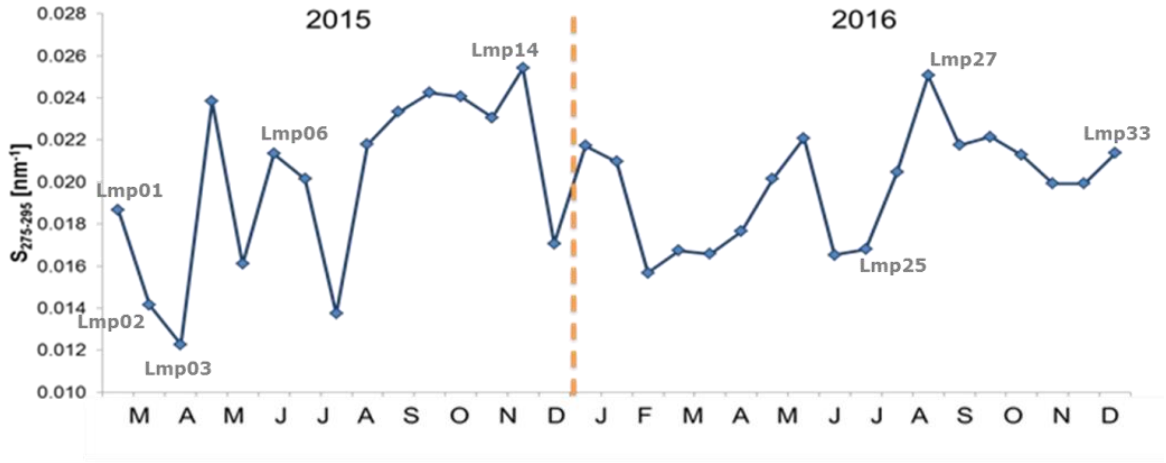

Figure 2.18. Temporal changes in Spectral slope ($S_{275-295}$).

9. Identification of FDOM atmospheric components by PARAFAC

The Parallel Factorial Analysis (PARAFAC) applied to the fluorescence excitation emission matrixes (EEMs) measured in total deposition, allowed for the validation of a 7-component model (Fig. 2.19). The 7 groups of fluorophores were identified by comparison with the literature and matching spectra obtained from the OpenFluor database (Murphy et al., 2014). Similar components were observed in the open ocean (Jorgensen et al., 2011), in a previous study on dust inputs on alpine lakes (Mladenov et al., 2011) and more recently in aerosol particles collected in the polar region (Fu et al., 2015).

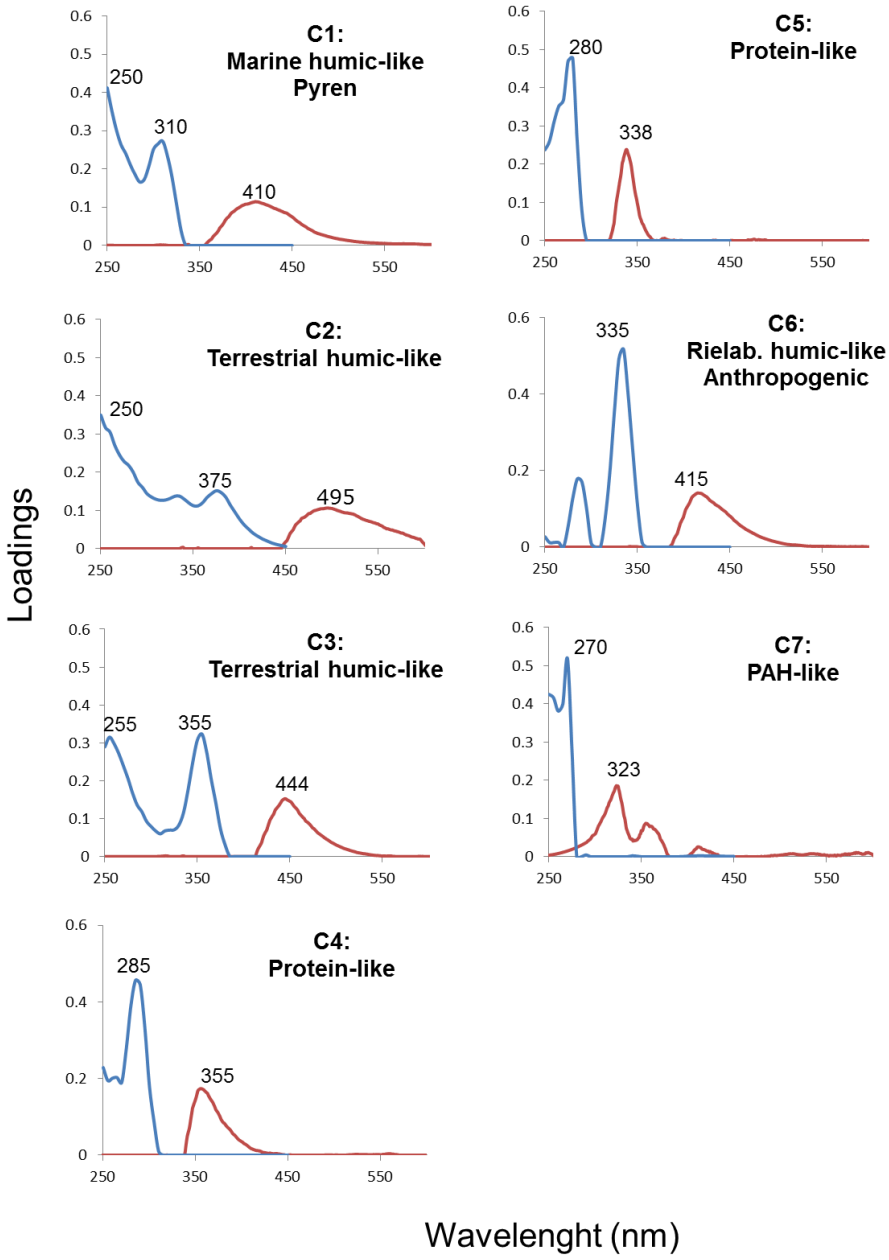

Figure 2.19. Excitation (blue) and emission (red) spectra of the seven components.

The component 1 (C1) showed the excitation peak at 250 (310) nm and the emission maximum at 410 nm. This peak was attributed to marine humic-like substances. It was identified by Coble (1996) (peak M) and observed in many studies on marine DOM (Stedmon and Markager, 2005a; Kowalczuk et al., 2009; Tedetti et al., 2012; Gonnelli et al., 2016). These humic fluorophores have been observed to be released by phytoplankton cells in exponential growth (Romera-Castillo et al., 2011). On the other hand, the spectroscopic characteristics of the C1 are similar to those of Pyrene, a PAH. Using the OpenFluor database, C1 matched with just 1 model. It was similar (TCC>0.95) to marine humic-like component identified in Baltic Coastal Sea Ice (Stedmon et al., 2007) (Table 2.6).

The first atmospheric component is thus classified in the same way, and many previous studies confirm the ubiquitous presence of PAHs and humic substances in the atmospheric compartment. In particular humic-like compounds, such as polycarboxylic acids, are been observed in rainwater (Facchini et al., 2000; Kieber et al., 2007). PAHs, due to chemical/microbiological stability, low water solubility, lipophilic properties, and vapor pressure, are globally allocated in the atmosphere (Duce et al., 1991) and may accumulate in both aquatic and terrestrial systems (Park et al., 2001). In addition, C1 was also observed in Open Sea FDOM pool (C1, Chapter 1) as a mixture of marine humic-like and PAHs substances.

The component 2 (C2) showed the excitation peak at 250 nm and the emission maximum at 495 nm, while the component 3 (C3) showed the excitation peak at 355 nm and the emission maximum at 444 nm. These components were identified as terrestrial humic-like. In previous studies they were identified as peak C by Coble (1996) and in many others studies (Kowalczuk et al., 2009; Yamashita et al, 2013) as terrestrial humic-like substances. They are considered representative of marine coastal DOM, impacted by terrestrial input, in particular they are linked to materials exported from natural or agricultural catchments (Stedmon and Markeger, 2005a; Zeri et al, 2014). Using the OpenFluor database C2 matched with 8 terrestrial humic-like components (TCC between 0.954 and 0.973). It was similar to terrestrial humic-like components identified in Central European mixed forests (Graeber et al., 2012), in tropical rivers (Yamashita et al., 2010a; Lambert et al., 2016), in the Baltic Sea and surrounding seas and estuaries (Stedmon and Markager, 2005a; Stedmon et al., 2007; Osburn and Stedmon, 2017) and in the Shark Bay, Australia (Cawley et al., 2012) (Table 2.6). Terrestrial FDOM was also observed by Kieber et al. (2006) in rain samples collected in North Carolina (U.S.), and it is interesting issue because these substances behave as cloud condensation nuclei (Facchini et al., 2000). In addition, C2 and C3 were observed in Open Sea FDOM pool (C3 and C2, respectively, Chapter 1) as terrestrial humic-like components.

The component 4 (C4) showed the excitation peak at 285 nm and the emission maximum at 355 nm, while the component 5 (C5) showed the excitation peak at 280 nm and the emission maximum at 338 nm. Their spectroscopic characteristics are similar to those of protein-like substances. In previous studies, these components have been observed in open ocean waters (Murphy et al., 2008; Jorgensen et al. 2011) and recently aromatic amino acids have been

identified in an area exposed to oil spill pollution (Gonnelli et al., 2016). Protein-like materials were also found in the water soluble organic carbon (WSOC) from dry deposition (Mladenov et al., 2011). Alpine lakes samples are dominated by the presence of tryptophan-like and tyrosine-like, instead protein-like is less represented in the WSOC samples collected in the Arctic (Fu et al., 2015). Saharan dust may influence the FDOM composition in the area of the alpine lakes, binding and transporting fluorescent material. Indeed, peaks in the short excitation/emission wavelength range represent groups of fluorophores contained in both alpine lakes and atmospheric samples, suggesting that the Sahara is an important source of fluorescent protein-like material. Less recently, protein-like was also observed in rain samples (Kieber et al., 2006). In addition, C5 was also observed in Open Sea FDOM pool (C5, Chapter 1) as a protein-like component.

The component 6 (C6) showed the excitation peak at 335 nm and the emission maximum at 415 nm. C6 was identified as transformed/microbial humic-like. It showed spectroscopic characteristics similar to peak C observed in the literature. It was often found in coastal area and associated to humic-like materials, with terrestrial origin (Coble 1996; Murphy et al., 2008; Kowalczuk et al., 2009). A similar group of fluorophores was also found in open sea waters sample (Jorgensen et al., 2011).

Component 7 (C7) showed the excitation peak at 270 nm and the emission maximum at 323 nm. This component can be due to the occurrence of a mixture of different PAHs, in particular its spectroscopic characteristics are very similar to those of naphthalene (Ferretto et al., 2014; D'Sa et al., 2016; Gonnelli et al., 2016). Total deposition of atmospheric organic compounds is a relevant pathway for PAHs to the coastal environments (Liu et al., 2013). Atmosphere can be an important source of PAHs, that are present as a big mixture with particles and other organic material. There are over a hundred of PAHs, but the most dangerous to the health of humans and animals, due to their carcinogenic and mutagenic properties, are: Anthracene, Pyrene, Phenanthrene, Fluorene and Fluoranthene (Kim et al., 2013).

Comp.	Ex/Em	Probable composition and source	TCC
1	250(310)/	*Marine humic-like+Pyren*	
	410	Baltic Coastal Sea Ice (C3) (Stedmon et al., 2007)	0.954
		Peak M (Coble, 1996)	N.A.
		Horsens Estuary, (DK) (C5) (Stedmon and Markager, 2005a)	N.A.
		Bay of Marseilles, France (Tedetti et al., 2012)	N.A.
		Eastern Ligurian Sea (C1) (Gonnelli et al., 2016)	N.A.
2	250(375)/	*Terrestrial humic-like*	
	495	Horsens Estuary, (DK) (C2) (Stedmon and Markager, 2005a)	0.963
		Baltic Coastal Sea Ice (C2) (Stedmon et al., 2007)	0.958
		Tropical rivers, Venezuela (C2) (Yamashita et al., 2010)	0.967
		Arctic Ocean (C2) (Stedmon et al., 2011)	0.956
		Shark Bay, Australian Shelf (C2) (Cawley et al., 2012)	0.954
		Mixed forests, Germany (C2) (Graeber et al., 2012)	0.962
		Tropical rivers, Africa (C2) (Lambert et al., 2016)	0.973
		Baltic and Kattegat Sea (C2) (Osburn and Stedmon, 2011)	0.972
3	(255)355/	*Terrestrial humic-like*	
	444	Peak C (Coble, 1996)	N.A.
		South Atlantic Bight (C2) (Kowalczuk et al., 2009)	N.A.
		Florida Keys (C2) (Yamashita et al., 2013)	N.A.
		Marmara–North Aegean Seas (C1) (Zeri et al., 2014)	N.A.
4	285/355	*Protein-like*	
		Pacific and Atlantic (P7) (Murphy et al., 2008)	N.A.
		Ocean off-shore (C2) (Jorgensen et al., 2011)	N.A.
		Alpine lakes and atmosph. samples (Mladenov et al., 2011)	N.A.
5	280/338	*Protein-like*	
		Florida Keys (C5) (Yamashita et al., 2013)	N.A.
		Mesocosm, Baltic Sea (C6) (Stedmon and Markager, 2005b)	N.A.
		South Atlantic Bight (C6) (Kowalczuk et al., 2009)	N.A.
		Aegean Sea (C4) (Pitta et al., 2017)	N.A.
6	335/415	*Rielaborated humic-like/Anthropogenic substances*	
		Peaks A and C (Coble, 1996)	N.A.
		Pacific and Atlantic (C8) (Murphy et al., 2008)	N.A.
		South Atlantic Bight (C3) (Kowalczuk et al., 2009)	N.A.
		Ocean off-shore (C4) (Jorgensen et al., 2011)	N.A.
7	270/323	*PAH-like*	
		Deepwater Horizon oil spill, Gulf of Mexico (C6) (Zhou et al., 2013)	N.A.
		Mobile Bay, Alabama, U.S. (C1, dwh12) (D'Sa et al., 2016)	N.A.
		Eastern Ligurian Sea (Gonnelli et al., 2016)	N.A.

Table 2.6. Spectral characteristics of the seven components compared to previously identified sources.

9.1 *FDOM atmospheric dynamics and seasonal evolution*

The temporal evolution of C2 (humic-like) and C4 (protein-like) is reported as representative of the 2 main groups of fluorophores occurring in the atmospheric FDOM pool.

The humic-like component (C2) showed a marked variability during the entire sampling period, the values ranged from 0.019 to 1.022 R.U. m^{-2} d^{-1} (Fig. 2.20), with an average value of 0.132 R.U. m^{-2} d^{-1}. It is noteworthy that FDOM trend is very similar to that of DOC (Fig. 2.2), the highest flux in both 2015 and 2016 (0.687 R.U. m^{-2} d^{-1}, Lmp06, in 2015 and 1.022 R.U. m^{-2} d^{-1}, Lmp25, in 2016) was observed in correspondence with the highest DOC deposition. These data suggest a similar dynamics of DOC and humic-like substances in the atmosphere (e.g. similar sources and removal mechanisms).

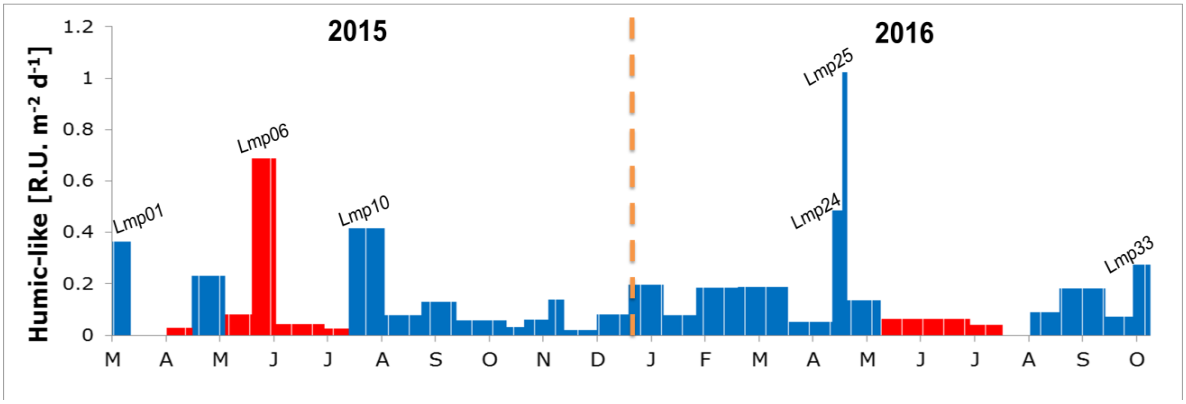

Figure 2.20. The atmospheric humic-like (C2) fluxes.

The protein-like (C4) FDOM fluxes showed a similar temporal evolution to that of humic-like (Fig. 2.21) and DOC (Fig. 2.2). However C4 showed two high deposition in addition to those observed for the humic-like fraction (Lmp11 and Lmp26). The values of protein-like ranged from 0.021 to 0.709 R.U. m^{-2} d^{-1}. The highest fluxes were 0.709 R.U. m^{-2} d^{-1} in 2015 (Lmp06), and 0.709 m^{-1} m^{-2} d^{-1} in 2016 (Lmp26). The average of the sampling period was 0.556 R.U. m^{-2} d^{-1}.

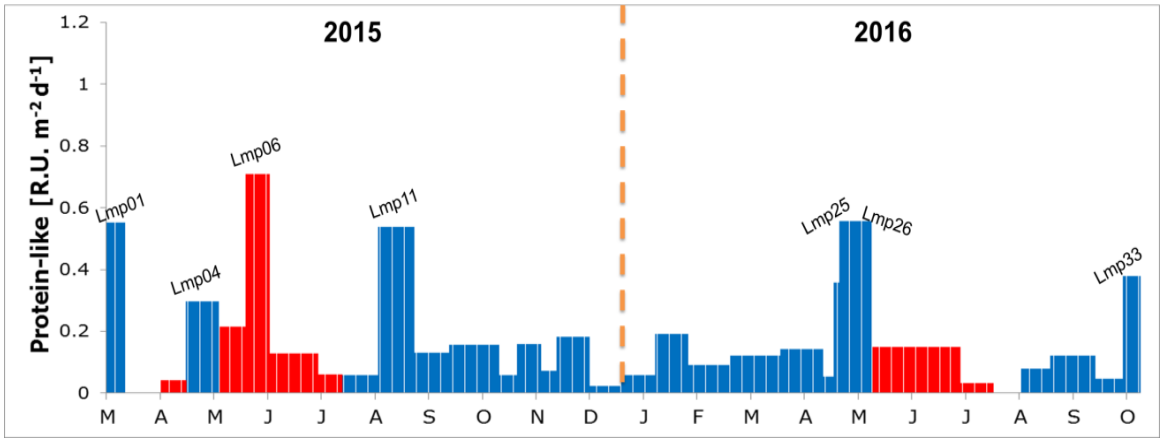

Figure 2.21. The atmospheric protein-like (C4) fluxes.

The atmospheric FDOM (humic-like, protein-like and PAH-like) was normalized to DOC (C2*, C4*, C7*) in order to obtain information about changes in the composition of FDOM pool as an intrinsic metric (Korak et al., 2014) (Fig. 2.22 and Table 2.7). Seasonal trend of normalized protein-like and humic-like FDOM showed the highest values in summer-autumn 2015 and winter 2016 (Fig. 2.22 a and 2.22 b). Normalized PAH-like FDOM showed the lowest values between spring and summer 2016 (Fig. 2.22 c).

Although the largest Saharan dust transport events over the Med Sea are commonly concentrated in spring and summer (Volpe et al., 2009), they were characterized by high deposition values of both CDOM and FDOM also during the other seasons, in agreement with recent observations by Sánchez-Pérez et al. (2016). Indeed, these authors collected a 2-year time series data on FDOM deposition in the Northwestern Med Sea and showed that aerosol deposition induced an increase in the proportion of FDOM in marine DOM pool and they observed that the highest FDOM deposition values coincided with the Saharan dust events.

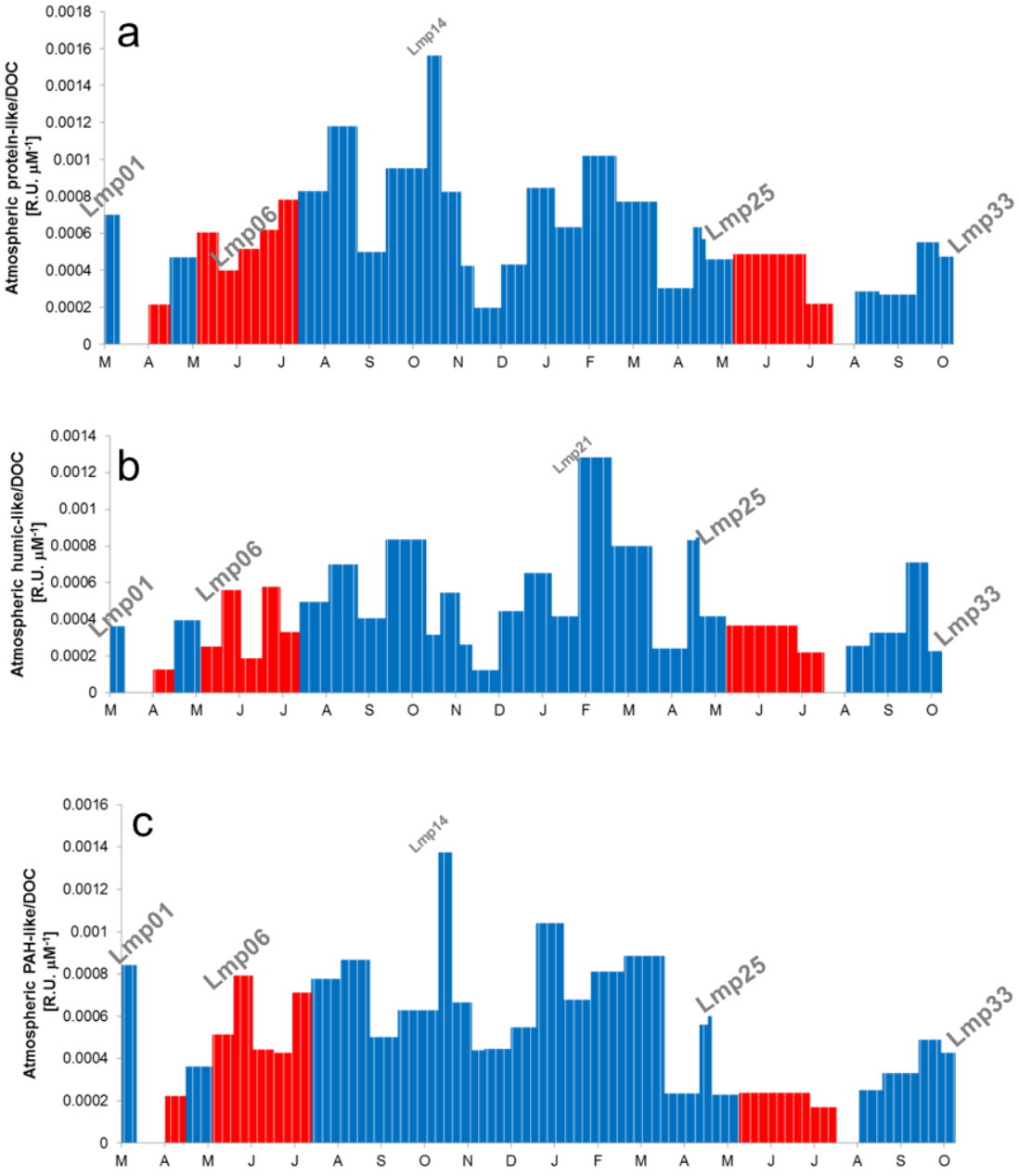

Figure 2.22. Temporal evolution of protein-like (a), humic-like (b) and PAH-like (c) materials.

Sample name	DOC [μM]	C2 [R.U.] Humic-like	C4 [R.U.] Protein-like	C7 [R.U.] PAH-like	Humic-like/DOC	Protein-like/DOC	PAH-like/DOC
Lmp01	133.8	0.05	0.09	0.11	0.0004	0.0007	0.0008
Lmp02	10190.8	Sample not available					
Lmp03	1170.0	0.15	0.25	0.26	0.0001	0.0002	0.0002
Lmp04	679.3	0.27	0.32	0.24	0.0004	0.0005	0.0004
Lmp05	1932.9	0.48	1.16	0.99	0.0002	0.0006	0.0005
Lmp06	9382.1	5.23	3.73	7.41	0.0006	0.0004	0.0008
Lmp07	1542.1	0.29	0.80	0.68	0.0002	0.0005	0.0004
Lmp08	515.4	0.30	0.32	0.22	0.0006	0.0006	0.0004
Lmp09	381.2	0.13	0.30	0.27	0.0003	0.0008	0.0007
Lmp10	146.6	0.07	0.12	0.11	0.0005	0.0008	0.0008
Lmp11	123.6	0.09	0.15	0.11	0.0007	0.0012	0.0009
Lmp12	127.1	0.05	0.06	0.06	0.0004	0.0005	0.0005
Lmp13	349.9	0.29	0.33	0.22	0.0008	0.0009	0.0006
Lmp14	56.6	0.02	0.09	0.08	0.0003	0.0016	0.0014
Lmp15	205.3	0.11	0.17	0.14	0.0005	0.0008	0.0007
Lmp16	325.9	0.09	0.14	0.14	0.0003	0.0004	0.0004
Lmp17	110.1	0.01	0.02	0.05	0.0001	0.0002	0.0004
Lmp18	133.6	0.06	0.06	0.07	0.0004	0.0004	0.0005
Lmp19	75.2	0.05	0.06	0.08	0.0007	0.0008	0.0010
Lmp20	100.7	0.04	0.06	0.07	0.0004	0.0006	0.0007
Lmp21	150.5	0.19	0.15	0.12	0.0013	0.0010	0.0008
Lmp22	73.6	0.06	0.06	0.07	0.0008	0.0008	0.0009
Lmp23	1562.6	0.38	0.47	0.37	0.0002	0.0003	0.0002
Lmp24	150.2	0.13	0.10	0.08	0.0008	0.0006	0.0006
Lmp25	156.9	0.13	0.09	0.09	0.0008	0.0006	0.0006
Lmp26	896.5	0.37	0.41	0.21	0.0004	0.0005	0.0002
Lmp27	3342.1	1.22	1.62	0.80	0.0004	0.0005	0.0002
Lmp28	1161.9	0.25	0.25	0.20	0.0002	0.0002	0.0002
Lmp29	1135.4	Sample not available					
Lmp30	601.5	0.15	0.17	0.15	0.0003	0.0003	0.0002
Lmp31	99.8	0.03	0.03	0.03	0.0003	0.0003	0.0003
Lmp32	270.3	0.19	0.15	0.13	0.0007	0.0006	0.0005
Lmp33	74.0	0.02	0.04	0.03	0.0002	0.0005	0.0004

Table 2.7. Information about DOC concentrations and atmospheric FDOM parameters.

Conclusions

This study highlights a marked variability in DOM deposition and a remarkable contribution of Saharan dust events to DOC deposition over the Mediterranean Sea. The organic substances transported by Saharan dust can have both a natural (e.g. marine spray) and an anthropogenic origin. Even if CDOM and FDOM data also suggest a terrestrial origin for a fraction of DOM (vegetation, soils, desiccated lake sediments). Interestingly, dry depositions plays a crucial role in the Mediterranean Sea, whereas in the oceans some models have estimated that wet deposition represent up to 75-95% of total deposition.

Our study supports that dust is an excellent vehicles for the chromophoric and fluorescent components, opening interesting scenarios regarding the impact on the marine optical properties of DOM, and their distribution.

Our study supports also that atmosphere can represent a relevant external source of DOM for Med Sea.It is mandatory to understand the lability of this organic compounds, their potential toxicity, and their fate once atmospheric DOM enters into the marine ecosystem, in order to obtain information about their impact on the biogeochemistry of the surface ocean and carbon export.

CHAPTER 3

Part of this chapter is included in the paper *Airborne microbes contribute to N_2 fixation in surface seawater* by Rahav E., Paytan A., Mescioglu E., Galletti Y., Rosenfeld S., Raveh O., Santinelli C., Ho T.-Y., Herut B. It was submitted in Geophysical Research Letters , abstract is present in the appendix.

"My dear, my dearest dust; I come, I come."

Diane Zahler, *The Thirteenth Princess*

Impact of desert dust on dissolved organic matter, a mesocosm approach in the Northern Red Sea

Considering the important role of dust in transferring organic compounds to the marine ecosystem, a mesocosm experiment has been carried out to get insights into the impact of desert dust on DOM dynamics in the surface ocean. This was a first experiment, with the interest and intention to replicate it in the Lampedusa area. The collaboration with Rahav E. and Herut B. was fundamental to undertake an international collaboration and to understand how to organize this type of experiment.

1. Study area

The Gulf of Aqaba is the northeastern extension of the Red Sea, bordered by Israel, Jordan, Egypt and Saudi Arabia.. Eilat is Israel's southernmost city, and is located on the Gulf of Aqaba at the edge of a long narrow estuary separating the Arabian Peninsula and the Sinai desert. (Fig. 3.1).

Figure 3.1. The geographical area of the experiment, the Gulf of Aqaba in the Northern Red Sea.

The Gulf of Aqaba is a deep, narrow, semi-enclosed basin surrounded by desert. Precipitation and runoff are close to zero (Chase et al., 2006). The surface waters of the Gulf are considered oligotrophic throughout nost months, with maximum chlorophyll-a concentrations of 0.75 mg m^{-3} in spring at the onset of stratification and minimum concentrations of 0.25 mg m^{-3} in midsummer (Labiosa et al., 2003). Exchange of seawater between the Gulf of Aqaba and the Red Sea

occurs only across a 250 m sill at the southern end (the Strait of Tiran). The phytoplankton community is dominated by relatively small species (<8 μm) where the cyanobacteria, *Synechococcus* spp. and *Prochlorococcus* spp., dominate in the spring and summer respectively, while picoeukaryotic species are more abundant during winter mixing events (Lindell & Post 1995; Lis and Shaked, 2009).

2.The main goals of the experiment

The Gulf of Aqaba receives large dust inputs from the Sahara and adjacent deserts. Recent studies show that airborne microbes inputs may cause a decline in populations of coral, sea-fans, sea-urchins and may alter pelagic heterotrophic and autotrophic bacteria and phytoplankton (both abundance and function) (Gachon et al. 2006; Haas et al., 2010; Astrahan et al., 2016; Herut et al., 2016; Rahav et al., 2016b; Tsagaraki et al., 2017). Atmospheric DOM bioavailability can be one of the main factor that affects the viability and activity of airborne microbes The main hypothesis we wanted to test with this experiment is that dust input affects DOM dynamics in the surface layer of the Gulf of Aqaba by the input of airborne microorganisms and nutrients.

3. Experimental setup

Aerosol samples were collected at the Interuniversity Institute (IUI) in Eilat, Israel (29 °28′N, 34°55′E) during two storm events: dust 1 was collected in February 28th 2017 and dust 2 was collected in May 18th 2017, using pre-cleaned glass plates (Rahav et al., 2018).Dust samples were placed in sterile Eppendorf tubes, and were kept frozen until the experiment. Before the experiment, the samples were homogenized by vortex and transferred to new sterile and clean Eppendorf tubes.Triplicate dust-subsamples were exposed to UV-irradiation for 48 h ('UV-killed dust') in a biological hood (SLEE, London), in order to kill the airborne microbes.

The incubations were carried out in 15 polycarbonate mesocosm bags (r=0.3 m, h=1.5 m) pre-cleaned with 10% HCl and filled with 300 L of seawater collected in the mixed layer (~10 m depth) in the NRS on July 9th 2017. The bags were completely immersed in a pool and tied to the edges of the pool (Fig. 3.2).

Figure 3.2. The pool of the experiment with 15 mesocosms bags and the shedding net.

Seawater temperature ranged between 25 and 28°C and no stratification was developed in the water inside the mesocosms. A shedding net was placed above the mesocosms in order to maintain ambient surface light (80-100 µmol quanta m^{-2} s^{-1} during midday, LI-COR PAR sensor). The mesocosms were mixed manually every 6-8 h to assure uniform distribution of the dust particles. Five treatments were conducted (all in triplicates): (1) control (no dust was added); (2) untreated 'live-dust' collected in February 2017 (live dust1), (3) 'UV-killed dust' collected in February 2017 (UV-killed dust1), (4) untreated 'live-dust' collected in May 2017 (live dust2), and (5) 'UV-killed dust' collected in May 2017 (UV-killed dust2) (Table 3.1). The 'live-dust' contains nutrients, DOM, trace-metals and viable airborne microorganisms that may be release from particles upon deposition in the surface seawater. The 'UV-killed dust' is expected to release to the water only nutrients, DOM and trace-metals, since the airborne microbes were not active due to the damaging effects of UV exposure.

The amount of aerosol added to each mesocosm was ~0.8 mg L^{-1}, in agreement with the amount of natural deposition to the upper mixed layer of the NRS (~15 m) that usually set down when dust storm events occur (Chen et al., 2008; Jish-Prakash et al., 2015; Torfstein et al., 2017). Sampling was carried out using acid-clean Tygon tubing from ~0.5 m depth. Water was extracted via suction and gravity flow as described in Herut et al. (2016), after shaking for homogenization. The collected seawater was transferred to the 250 ml polycarbonate Nalgene bottles and taken to the lab within a few minutes for samples treatment.

Mesocosm	Mesocosm volume (L)	Treatment	Amount of dust added (mg)	Dust conc. (mg/L)
A1	300	Control	0	0.00
A2	300	Control	0	0.00
A3	300	Control	0	0.00
B1	300	Live dust1	279.4	0.93
B2	300	Live dust1	278.6	0.93
B3	300	Live dust1	275.5	0.92
C1	300	UV-killed dust1	279.9	0.93
C2	300	UV-killed dust1	274.8	0.92
C3	300	UV-killed dust1	278.6	0.93
D1	300	Live dust2	273.1	0.91
D2	300	Live dust2	275.0	0.92
D3	300	Live dust2	284.0	0.95
E1	300	UV-killed dust2	283.6	0.95
E2	300	UV-killed dust2	278.2	0.93
E3	300	UV-killed dust2	283.5	0.95

Table 3.1. Summary of the mesocosm experimental design and addition undertaken.

The experiment started July 9th 2017 and ended in July 13th 2017. The first sampling was performed at 8.30 AM (t_{0-1}). The dust was added at 1 PM on the same day (t_0) and after 4 hours (5 PM) the second sampling was carried out (t_1). The mesocosms were sampled 20 h, 44 h, 68 h and 91 h after the dust addition. DOC, CDOM, FDOM, as well as some additional parameters (bacterial abundance (BA), bacterial production (BP), primary production, chlorophyll-a) were monitored. Other parameters followed with time, but not reported in this chapter are: nutrients and trace-metals, picophytoplankton abundance, microphytoplankton abundance, N_2 fixation, microbial diversity, and exo-enzymatic activity (alkaline phosphatase activity, aminopeptidase and beta-glucosidase).

The significance of mean differences among the treatments and the sampling times in the dust addition experiment were compared using a one-way ANOVA and the Tukey test ($\alpha = 0.05$).

4. Results and discussion

Air-mass back trajectory shows that the two dusts have a different origin; the sample collected in February 2017 was more local and originated from south (a 'Middle East' source) (Fig. 3.3a), whereas the sample collected in May 2017 arrived from the northern Europe (Fig. 3.3b).

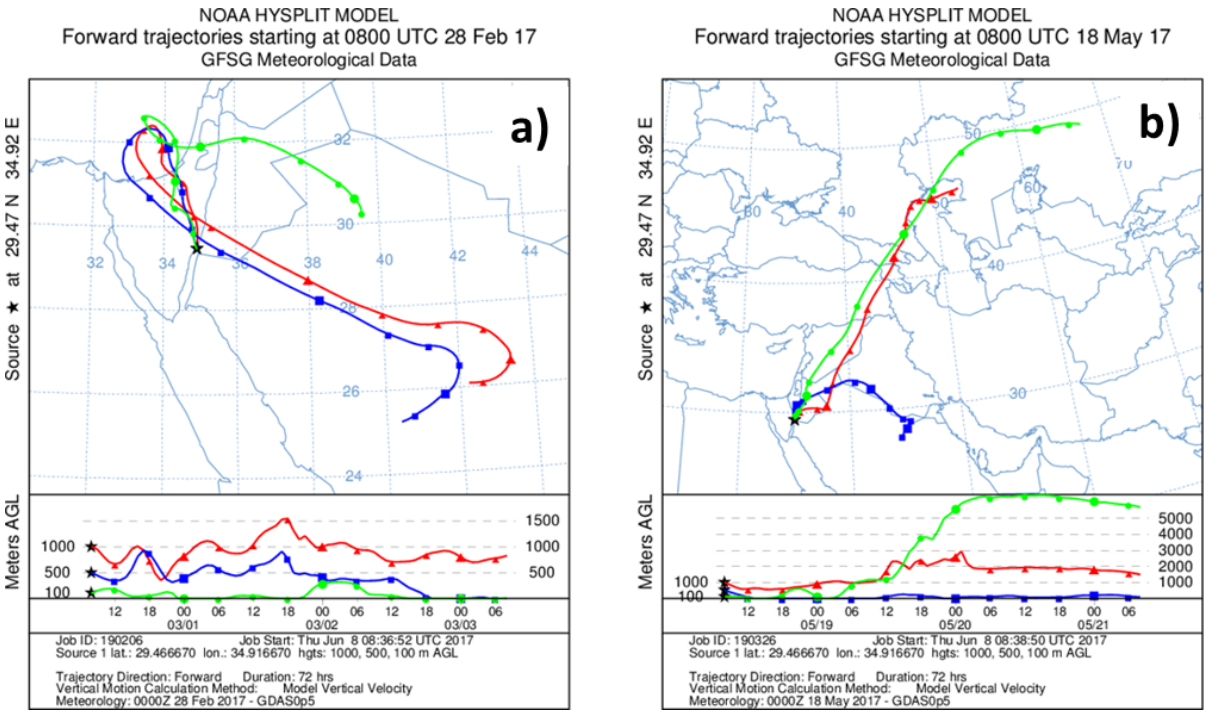

Figure 3.3. A three-day back trajectories arriving at 100, 500 and 1000 m altitude levels showing the origin of the aerosols that were used in the mesocosm experiment. Aerosols were collected in the NRS in 28/2/2017 (a) and 18/5/2017 (b).

Accordingly with the different origin, the two dusts contained different amount of nutrients and DOC (Table 3.2). Leaching experiments demonstrated that each mg of dust1 (collected in February 2017) released 20 nmol NO_3+NO_2,~2 nmol PO_4, 55 nmol DOC to seawater. Higher nutrient and DOC concentrations were released from dust2 (collected in May 2017), 60 nmol NO_3+NO_2, 3 nmol PO_4, and 206 nmol DOC per mg of dust. Thus, the addition of 0.8 mg L^{-1} of dust1 and dust2 resulted in the addition of ~50 nM NO_3+NO_2, ~2.5 nM PO_4, 44 nM DOC, and ~20 nM NO_3+NO_2, <2 nM PO_4 and 165 nM DOC, respectively (Table 3.2). These additions resulted in 30-70% increase of NO_3+NO_2 and ~10% increase of PO_4 relative to the ambient concentration (Table 3.3). Dust1 and dust2 addition increased DOC concentration of just 0.06% and 0.22%, respectively; this increase in concentration is within analytical error of the method. During the leaching experiment organic carbon concentration was measured in both filtered and unfiltered samples, thus enabling to quantify the total amount of organic carbon (TOC=DOC+POC) contained in the dust independently from its capability to dissolve in water. Dust1 contained 127 nmol TOC mg^{-1}, dust 2 contained 282 nmol TOC mg^{-1}, these values represent the maximum amount of organic carbon that can be released by dusts assuming that all the carbon adsorbed to dust can dissolved.

Variable	Leached element conc. (nmol mg^{-1} dust)		Concentration increase in the mesocosm due to dust addition (nM)	
	February 2017	May 2017	February 2017	May 2017
NO_3+NO_2	20±3	60±4	16±2	48±2
PO_4	2±1	3±1	<2	2.4±1
DOC	55±4	206±7	44±3	165±2

Table 3.2. Leached nutrients and DOC from the aerosols collected in February and May 2017 and calculated net increase of ambient concentration in the mesocosms following ~0.8 mg L^{-1} of dust addition. Data shown are average ± standard deviation from 3 independent replicates.

Parameter	Unit	Average ± SD (n=3)
NO_3+NO_2	nM	140
PO_4	nM	8
Dissolved Organic Carbon	µM	74±1
Bacterial abundance	Cells x10^4 mL^{-1}	350±15
Bacterial production	µg C L^{-1} d^{-1}	1.41±0.08

Table 3.3. The initial chemical and biological properties of the NRS surface water during July 2017 before amendments were performed.

4.1 *DOC concentrations*

Taking into consideration all the mesocosms, DOC concentration was 74.2±2.4 µM before the addition of dusts (Table 3.4). Four hours after the dust addition (t1), DOC concentration decreased to 70.9±1.5 µM, with no significant differences (ANOVA, $p>0.05$) among the treatments (Fig. 3.4). The same decrease in DOC concentration was also observed in the unamended control mesocosms, suggesting that it is independent from the dust addition. Bacterial abundance (BA) showed an opposite trend, it was $3.6\pm0.4\cdot10^5$ cells·ml^{-1} at the beginning of the experiment and showed a significant increase reaching an average value of $5.4\pm1.0\cdot10^5$ cells·ml^{-1} 4 hours after the dust addition (t1) in the 4 treatments, whereas in the control BA remained unchanged from T_0 (the differences are not statistically significant). Indicating a fertilization effect of

aerosols on bacteria. Bacterial production (BP) showed a trend very similar to that observed for bacterial abundance; it increased from 1.4±0.08 μg $C \cdot L^{-1} \cdot h^{-1}$ to 1.7 ± 0.2 μg $C \cdot L^{-1} \cdot h^{-1}$ after the addition of the 2 'live' dusts and in the treatment with the UV-killed dust2, whereas the control and the treatment with the UV-killed dust 1 BP did not show significant differences. The increase in BP in the treatment with the UV-killed dust2 can be explained by the input of substances associated with dust2 that stimulate the growth of marine bacteria or by the incomplete killing of airborne mcirobes associated with dust2. Assuming a conversion factor of 20 fg C per cell and a Bacterial Growth Efficiency (BGE) of 10-30%, the removal of 1-3 μM of DOC at t_1 would be sufficient to explain the observed increase in biomass and this is consistent with the DOC decrease. In agreement with this observation, the removal of 1 μM of DOC would be enough to sustain the observed increase in BP. What is difficult to explain is the decrease of DOC observed in the control where no increase in biomass was observed. These data suggest that dust addition did not affect directly DOC concentrations, in agreement with the data from the leaching experiment, but it could promote the net removal of DOC to sustain the bacterial growth of marine microbes stimulated by nutrient and metals addition by dust.

The addition of dust1 did not affect DOC dynamics in the first part of the experiment, a slight increase in DOC was observed 68 h after the addition of both live and UV-killed dust1. No similar trend was observed in the other parameters.

Focusing on the treatments with dust2, a marked increase in DOC concentration was observed 20 h after the addition (t2) of both the live and UV-killed dust2, followed by a sharp decrease between 20 and 44 h in both treatments (Fig. 3.4), then DOC did not change significantly with the exception of a slight increase at the end of the experiment in the treatment with UV-killed dust2, but the same increase was also observed in the control.

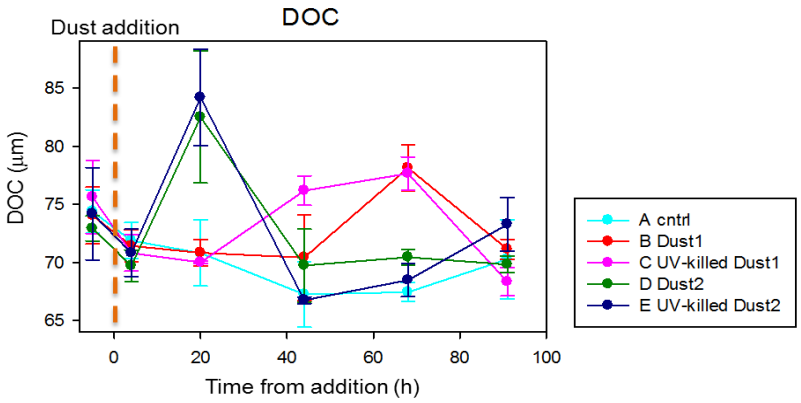

Figure 3.4. Temporal evolution of DOC.

It is noteworthy that accordingly with DOC, BP and BA showed the highest values 20 h later the addition of both live and UV-killed dust2, whereas chlorophyll-a showed a peak only in the treatment with UV-killed dust2 (Fig. 3.5). The temporal evolution of DOC and BP showed a good direct linear correlation (BP=0.082±0.008·DOC-3.98±0.6, $p<0.0001$; $n=15$) in the treatment with UV-killed dust2, suggesting that their dynamics is strictly linked and that are processes other than DOC removal affecting both of them during the incubation. A possible explanation is that the addition of dust2 stimulate the production of both labile DOC, that is immediately used for bacterial growth, and semi-labile DOC, that can accumulate.

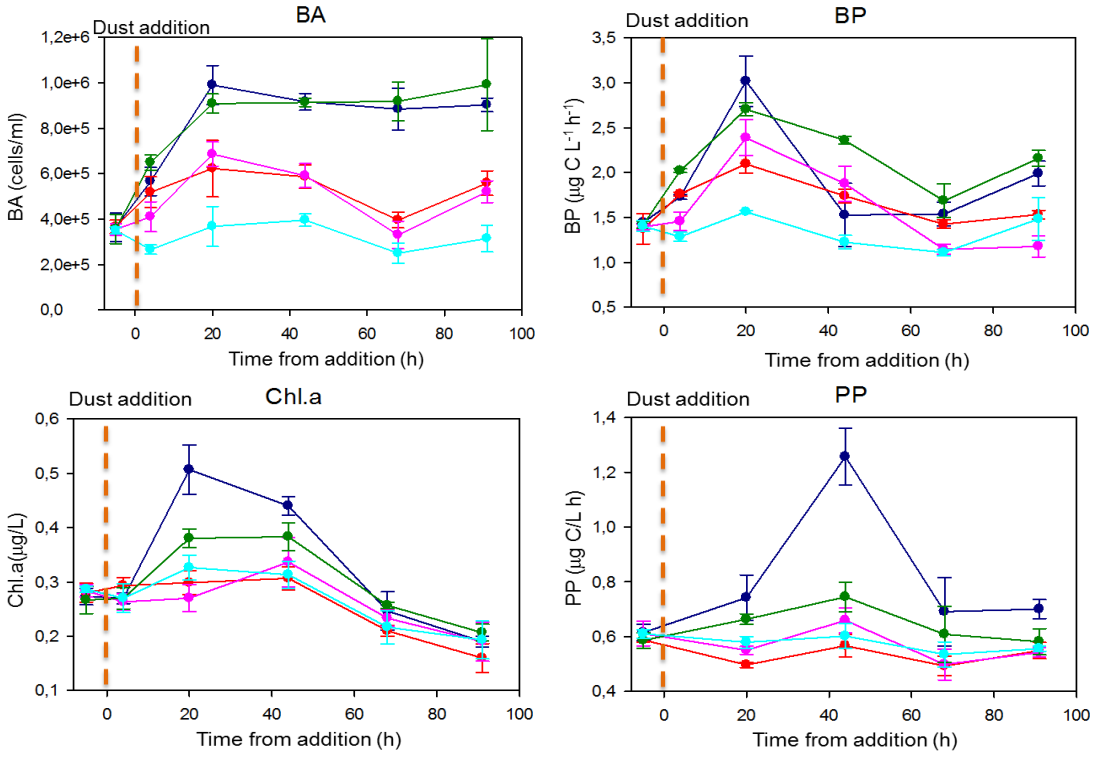

Figure 3.5. Temporal changes of bacterial abundance, bacterial production, chlorophyll-a and primary production.

It is difficult to explain the marked increase in both DOC concentration and bacterial biomass at 20 h. Assuming a conversion factor of 20 fg C per cell and a BGE of 10-30 %, the removal of 2-7 μM of DOC is necessary, in order to sustain a BA increase of $4 \cdot 10^5$ cells·ml^{-1}, whereas DOC increased of 12 μM. The leaching of DOC from dust is excluded, since the leaching experiment showed that the total organic carbon associated to dust2 is 0.2 μM, this is therefore the maximum increase in DOC that can be explained by dust addition. Another explanations could be the DOC release via cell lysis of both marine and airborne microbes. Marine virioplankton is considered the most abundant predatory agents in the sea (Breitbart, 2012; Suttle, 2007). The production of viral progeny through lytic infection causes the death and lysis of the host, resulting in the release of DOM lysate. There are ~10^{30} phage in the ocean, infecting prokaryotic cells at a rate of 10^{23} infections per second and removing 5-40% of prokaryotic standing stock on a daily basis (Suttle, 1994, 2007; Middelboe, 2008). Dust2 could have thus enriched sea water with airborne microbes and/or viruses, determining the release of DOC. However, if this would be the case we should not have observed an increase in bacterial abundance. In addition assuming a conversion factor of 20 fg C per cell the lysis of all the bacteria occurring in the mesocosm would not be enough to explain the observed increase in DOC. Since external source of organic carbon other than the added dust are not present in the experiment, the *in-situ* production by chemosynthesis is therefore necessary to explain the observed trend. Chlorophyll shows a peak at 20 h, but we cannot exclude that it was higher between 4 and 20 h, however primary production showed a peak at 40 h, that is after the peak of DOC. We can therefore exclude that the increase in DOC is due to primary production. The only possible explanation is the chemosynthesis, that was not measured in the experiment. If this is the case, dust2 could contain chemical elements that can stimulate chemosynthesis, even if the surface water conditions in the NRS may not support this reaction. We can exclude an impact of airborne microbes, since a similar increase in DOC was observed in the treatment with UV-killed dust2. However, since dust storms contributed significantly to N_2 fixation in NRS and carried a high diversity of airborne microbes (bacteria, archaea), including diazotrophs (Rahav et al., 2018), this may have stimulated

chemosynthetic bacteria, which use ammonia, and therefore organic substance was produced, starting from inorganic substances. A similar increase in both DOC and bacterial production was observed by Pitta et al. (2017) in a similar mesocosm experiment carried out in the Eastern Med Sea after a single addition of 3 g dust m^{-2} day^{-1}, and less recently, by Pulido-Villena et al. (2008). In the latter study, the authors observed a relation between dust and organic matter, in fact a relevant Saharan dust event delivered the largest flux of DOC. At the same time, dust produced an increase in abudance and respiration rate in all treatments of their experiment, stimulating heterotrophic bacteria growth. BGE is highly dependent on phosphorus availability, but despite dust addition increased soluble reactive phosphorous concentration in experimental bottles, BGE remained very low, with slight differences between treatments (7.7–9.7%). Dust pulses increased C mineralization, reducing the amount of exported bioavailable DOC, thus a shift in the heterotrophic bacterial role on the C cycle from ‘‘sink’’ to ‘‘link’’ did not induce.

An interesting hypothesis to explain the decrease of DOC observed between t_2 and t_3 can be made in relation to the results obtained by Louis et al. (2017). These authors reported the formation of transparent exopolymer particles (TEP) after the introduction of dust, with subsequent POC export. This is an abiotic process that would be a relevant pathway of organic carbon export in particular in that region submitted to dust deposition with low productivity (such as Med Sea or NRS) (Louis et al., 2017).

Time	Time (h)	Treatment	DOC (μM)	BA (10^5 cells/ml)	PP (μg C/L/h)	BP (μg C/L/h)	Ch-.a (μg/L)
t_{0-1}	-5	A	74.4±1.9	3.5±0.1	0.61±0.02	1.40±0.06	0.29±0.01
t_1	4	A	71.9±1.6	2.6±0.2	NA	1.28±0.05	0.27±0.03
t_2	20	A	70.8±2.9	3.7±0.9	0.58±0.02	1.56±0.02	0.33±0.02
t_3	44	A	67.2±2.8	4.0±0.3	0.60±0.04	1.22±0.08	0.31±0.03
t_4	68	A	67.4±0.8	2.5±0.5	0.53±0.05	1.11±0.03	0.22±0.03
t_5	91	A	70.3±3.4	3.1±0.6	0.56±0.01	1.48±0.24	0.19±0.04
t_{0-1}	-5	B	74.0±2.5	3.7±0.3	0.59±0.01	1.37±0.17	0.28±0.02
t_1	4	B	71.4±1.4	5.2±0.7	NA	1.76±0.02	0.29±0.02
t_2	20	B	70.8±1.1	6.2±0.1	0.50±0.01	2.10±0.10	0.30±0.02
t_3	44	B	70.4±3.7	5.9±0.5	0.57±0.04	1.74±0.08	0.31±0.02
t_4	68	B	78.1±2.0	4.0±0.3	0.49±0.04	1.43±0.05	0.21±0.01
t_5	91	B	71.1±0.9	5.6±0.5	0.55±0.03	1.53±0.05	0.16±0.03
t_{0-1}	-5	C	75.6±3.1	3.5±0.2	0.61±0.04	1.39±0.03	0.28±0.01
t_1	4	C	70.8±1.6	4.1±0.7	NA	1.46±0.10	0.26±0.02
t_2	20	C	70.0±0.1	6.9±0.5	0.55±0.01	2.39±0.20	0.27±0.02
t_3	44	C	76.1±1.3	5.9±0.5	0.66±0.04	1.88±0.20	0.34±0.05
t_4	68	C	77.6±1.4	3.3±0.6	0.50±0.06	1.15±0.06	0.23±0.02
t_5	91	C	68.3±1.2	5.2±0.5	0.54±0.02	1.18±0.12	0.19±0.04
t_{0-1}	-5	D	72.90±1.1	3.6±0.6	0.59±0.03	1.42±0.04	0.27±0.03
t_1	4	D	69.71±1.4	6.5±0.3	NA	2.02±0.02	0.27±0.02
t_2	20	D	82.49±5.7	9.1±0.4	0.66±0.02	2.70±0.07	0.38±0.02
t_3	44	D	69.73±3.1	9.1±0.2	0.74±0.05	2.36±0.04	0.38±0.03
t_4	68	D	70.44±0.7	9.2±0.9	0.61±0.10	1.69±0.19	0.26±0.01
t_5	91	D	69.82±0.7	9.9±0.2	0.58±0.05	2.16±0.09	0.21±0.02
t_{0-1}	-5	E	74.18±4.0	3.6±0.6	0.61±0.03	1.45±0.01	0.27±0.02
t_1	4	E	70.82±2.0	5.7±0.6	NA	1.73±0.03	0.27±0.01
t_2	20	E	84.16±4.1	9.9±0.9	0.74±0.08	3.02±0.28	0.51±0.05
t_3	44	E	66.74±0.3	9.2±0.4	1.26±0.10	1.53±0.35	0.44±0.02
t_4	68	E	68.47±1.4	8.8±0.9	0.69±0.13	1.54±0.13	0.25±0.04
t_5	91	E	73.27±2.3	9.0±3.0	0.70±0.03	1.99±0.14	0.19±0.01

Table 3.4. Mean±standard deviations of DOC, BA, PP, BA and Chl-a measured throughout the mesocosms experiment in July 2017. A=Control; B=Dust1; C=UV-killed Dust1; D=Dust2; E=UV-killed Dust2. NA→ Not Available

4.2 *PARAFAC components*

The PARAFAC analysis, applied to the 88 EEMs measured in this study, allowed for the identification of 5 components in the FDOM pool (Fig. 3.6). In order to identify the components, their spectra were compared with similar components reported in the literature and with matching spectra obtained from the OpenFluor database (Murphy et al., 2014) (Table 3.5).

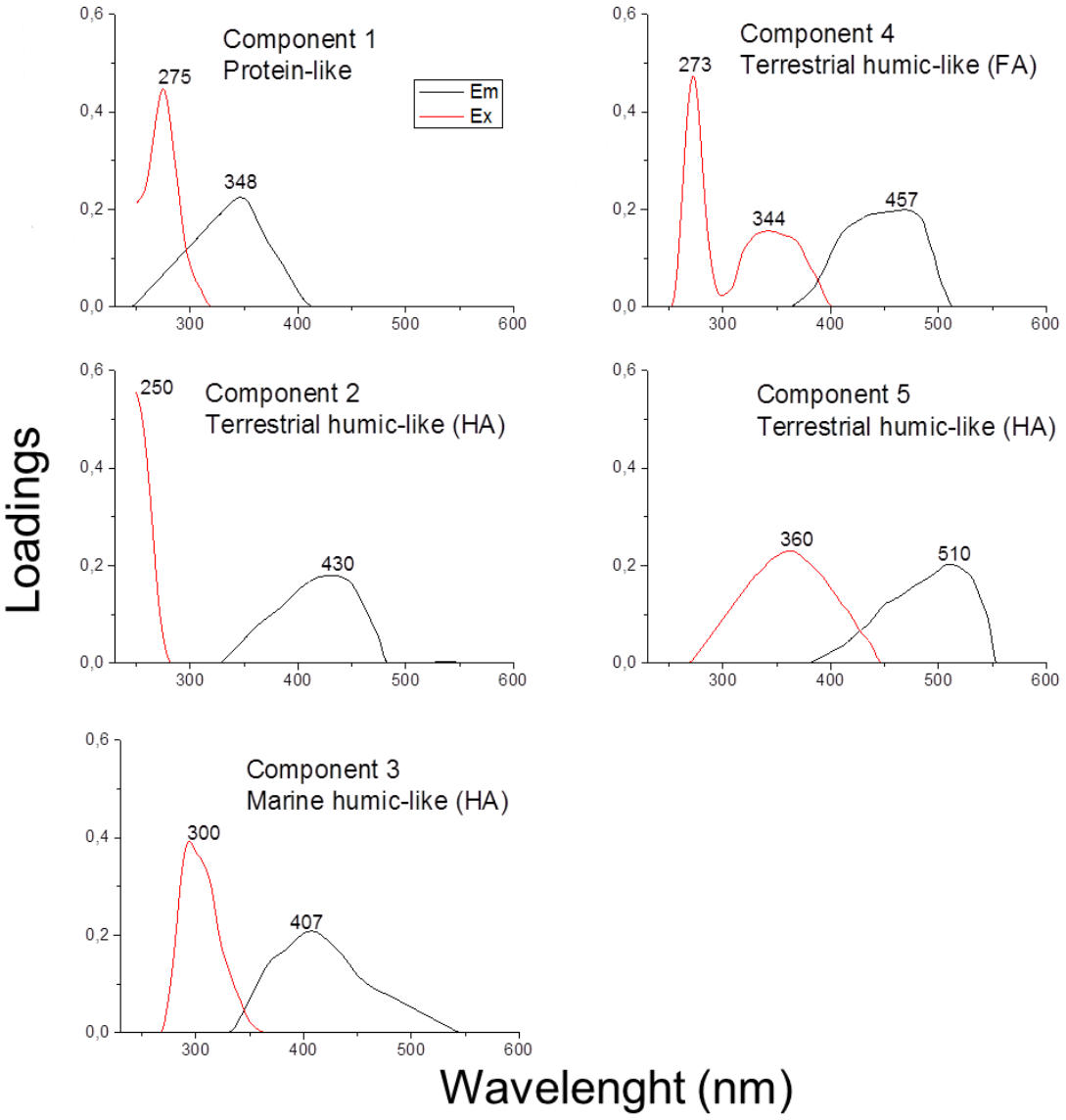

Figure 3.6. Fluorescence characteristics of the five components, with Excitation (red) and Emission (black) spectra.

Comp.	Ex/Em	Probable composition and source	TCC
1	275/348	*Protein-like*	
		Wetlands in the Abitibi region, Canada (C6) (Stubbins et al., 2014)	0.950
		Atlantic surface and deep waters (C3) (Kowalczuk et al., 2013)	0.960
		Neuse River estuary, North Carolina, U.S. (C5) (Osburn et al., 2012)	0.983
		Seawater in mesocosm, Bergen, Norway (C4) (Stedmon and Markager, 2005b)	0.974
		Stormwater and urban ponds, Canada (C7) (Williams et al., 2013)	0.955
		Everglades wetlands, Florida (C7) (Yamashita et al., 2010b)	0.952
		Everglades wetlands, Florida (C5) (Cawley et al., 2012)	0.959
		Estuary from an agro-urban coastal watershed, North Carolina, U.S (C3) (Osburn et al., 2016)	0.964
		Antarctic sea ice brines (C3) (Stedmon et al., 2011)	0.973
		North Patagonian streams (C3) (Nimptsch et al., 2015)	0.951
2	250/430	*Terrestrial humic-like (Humic Acids)*	
		Peaks A and C (Coble, 1996)	NA
		Ballast water from nine research cruises out of Asia, Europe, and the USA (C8) (Murphy et al., 2006)	NA
		Florida Keys (C2) (Yamashita et al., 2013)	NA
		Aegean Sea (C1) (Pitta et al., 2017)	NA
3	300/407	*Marine humic-like (Humic Acids)*	
		Danish freshwaters (C2) (Søndergaard et al., 2003)	0.969
		Peak M (Coble, 1996; Coble et al., 2014)	NA
		Eastern Ligurian Sea (C4) (Gonnelli et al., 2016)	NA
		Aegean Sea (C2) (Pitta et al., 2017)	NA
4	273(344)/ 457	*Terrestrial humic-like (Fulvic Acids)*	
		Peak C (Coble, 1996; Coble et al., 2014)	NA
		Horsens Estuary, Denmark (C1) (Stedmon et al., 2003)	NA
		Pacific and Atlantic waters (P8) (Murphy et al., 2008)	NA
		Eastern Ligurian Sea (C2) (Gonnelli et al., 2016)	NA
5	360/510	*Terrestrial humic-like (Humic Acids)*	
		Peak C (Coble, 1996; Coble et al., 2014)	NA
		Raune Fjord, Denmark (C7) (Stedmon and Markager, 2005a)	NA
		Pacific and Atlantic waters (P3) (Murphy et al., 2008)	NA
		Eastern Ligurian Sea (C3) (Gonnelli et al., 2016)	NA

Table 3.5. Identification of the 5 components through the comparison with literature data. Tucker's congruence coefficient (TCC) is reported for matching spectra obtained from the OpenFluor database.

Component 1 (C1) showed an excitation maximum at 275 nm and an emission maximum at 348 nm. These features are typical of protein-like fluorescence. Using the OpenFluor database C1 matched with 10 protein-like components, with different sources (Table 3.5). A similar component was observed in open oceanic waters (Kowalczuk et al., 2013), in two estuarine rivers in southern Florida (Cawley et al., 2012) and more recently in North Patagonian streams (Nimptsch et al., 2015). Some studies have shown that in seawater without a direct terrestrial input, protein-like components were dominant over the others (Kowalczuk et al., 2013; Murphy et al., 2008), and it can be associated with algal blooms (Para et al., 2010).

Component 2 (C2), 4 (C4) and 5 (C5) showed spectral characteristics typical of terrestrial humic-like compounds. In previous studies they were identified as peaks A and C (Coble, 1996; Stedmon and Markager, 2005a; Murphy et al., 2006; Yamashita et al., 2013; Gonnelli et al., 2016; Pitta et al., 2017) (Table 3.5). In particular, C2 showed excitation/emission maxima in the range of peak A observed by Coble (1996) and has been attributed to high molecular weight humic substances. C4 was attributed to humic-like fluorophores derived by terrestrial input, exported from natural or agricultural catchments (Stedmon and Markager, 2005a). C5 showed a long emission wavelength and it indicates the presence of terrestrial humic-like substance characterized by a higher molecular weight and aromatic degree compared to C2 and C4.

Component 3 (C3) shows an excitation maximum at 300 nm and an emission maximum at 407 nm. These spectral characteristics correspond to those of marine humic-like substances (peak M) identified by Coble (1996), and more recently by Gonnelli et al. (2016) in the Eastern Ligurian Sea and by Pitta et al. (2017) in the Aegean Sea. Using the OpenFluor database, C3 matched with component 2 observed by Søndergaard et al. (2003) in estuarine waters (Table 3.5). The production/release of this humic-like component has been attributed to in-situ microbial activity either release by phytoplankton (Murphy et al., 2006) or transformation of terrestrial humic-like substances by heterotrophs (Stedmon and Markager, 2005b).

The comparison of these components with the PARAFAC model of Mediterranean samples (see chapter 1) shows that the dominant component (C1) that in the Red Sea waters is a protein-like component, highlighting larger

presence of protein material in the Red Sea than in the Med Sea. The occurrence of terrestrial humic-like components are in line with the data reported for the Med sea, suggesting that the NRS is also influenced by external contribution of humic materials, and that atmosphere could play a crucial role in the transfer of compounds with terrestrial origin. In the NRS, no component linked to the presence of PAHs and/or a mixture of these pollutants and humic-like substances was found, indicating a lower presence of these compounds in the waters of the Gulf of Aqaba than the Mediterranean basin. Finally, a marine humic-like component was identified in both models, suggesting the presence of material produced *in-situ* by phytoplankton and/or microbial activity (Murphy et al., 2008; Zhao et al., 2017).

4.3 *Temporal evolution of FDOM*

The 5 components did not show significant differences among the control the 4 treatments (Fig. 3.7). These results suggest that dust addition does not affect significantly FDOM dynamics or that changes in fluorescence signals were too low to be considered.

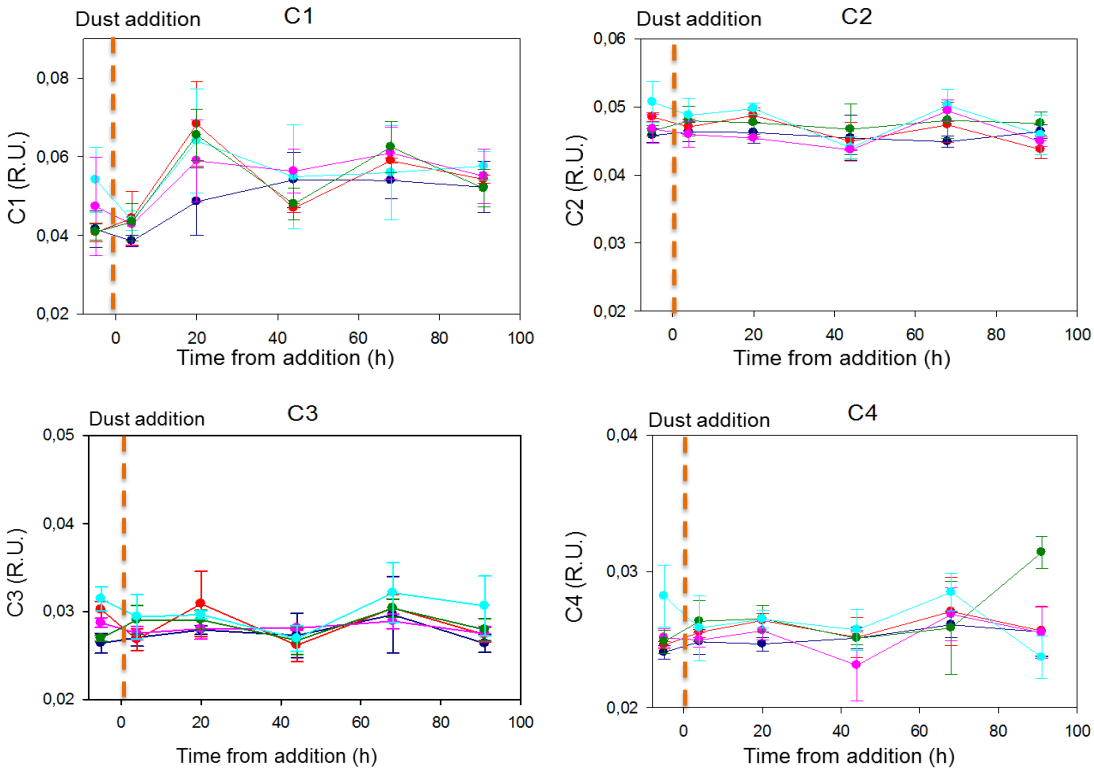

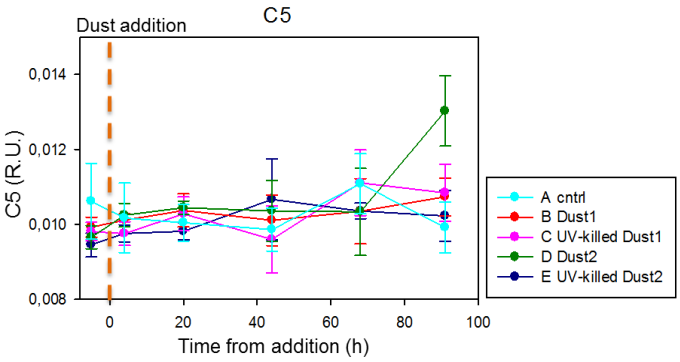

Figure 3.7. Temporal evolution of the five PARAFAC components detailed in Table 3.5.

Conclusions

As expected from the leaching experiments, the addition of dust did not lead to a direct enrichment of DOM or CDOM/FDOM. However, it indirectly affected DOM dynamics through a change in the microbial food web. The increase in DOC concentration observed 20 hours after the addition of the dust collected in May 2017 can be explained by the *in-situ* production of DOC stimulated by dust addition. Primary production, viral lysis of bacteria nor bacterial release alone cannot explain the marked increase in DOC, thus we hypothesized than the addition of dust can have stimulated chemosynthesis. Further data and experiments are mandatory to support this hypothesis.

PARAFAC analysis unveiled the occurrence of 5 components, among them the protein-like showed the highest fluorescence intensities. The other 4 components have been identified as humic-like substance (including three terrestrial and one marine), highlighting the presence in the Northern Red Sea waters of terrigenous material. Saharan dust events could lead to an increase in the FDOM flux in marine surface waters as suggested by other studies and as observed in Lampedusa sampling in the period 2015-2016, however this result was not found in the experiment conducted in the NRS, suggesting the presence of dust poor in chromophoric material or the presence of labile material, rapidly consumed by heterotrophic prokaryotes.

CHAPTER 4:

Discussion

"Limitless and immortal, the waters are the beginning and end of all things on earth."

Heinrich Zimmer

Discussion

The role of atmospheric deposition in the carbon cycle and DOM dynamics

The idea of this project started from the observation that some features of the DOM dynamics in the Med Sea can be explained by atmospheric input and that the data about the atmospheric input of DOM as well as information about its impact on marine ecosystem are really scarce. Atmospheric deposition is a carrier of nutrients, metals and pollutants (e.g. polycyclic aromatic hydrocarbons) to marine ecosystem. In the past years, research devoted a lot of attention to this topic, in order to improve knowledge on the fate of these substances in the atmosphere and the consequences for terrestrial and aquatic ecosystems. Much less attention has been paid to the importance of atmospheric DOM inputs for marine ecosystem.

This dissertation reports new data on the atmospheric input of DOM to the Med Sea and on the impact of dust deposition on marine DOM dynamics. The samples were collected for 20 months at the island of Lampedusa, representative of the remote marine environment of the central Med Sea. This island is close to Africa and therefore it is strategic to study the transport of Saharan dust and its impact on marine ecosystem. Dust represents the most important source of natural aerosols in the atmosphere, and the Sahara accounts for 55% of the total global dust emissions (Ginoux et al, 2012). Although the main message emerging from the literature is that the prominent vehicle of organic carbon is wet deposition (Kanakidou et al., 2005), our study shows that some dry deposition events are important sources of organic matter to both terrestrial and marine environments.

This work represents a step forward in the quantification of organic carbon input to the Med Sea from atmosphere, and in the understanding of the main sources of atmospheric DOM.

1. *Is DOM pool in the Med Sea richer in allocthonous material than in the oceans?*

The presence of terrigenous material in the marine DOM pool is one of the most intriguing question in oceanography (Hedges et al., 1997; Mannino and Harvey, 2000; Stedmon et al., 2007; Medeiros et al., 2015) and the role of atmospheric input in explaining this observation is still unclear. The input of terrestrial and anthropogenic substances from the atmosphere can be relevant in the Med Sea due to its semi-enclosed nature and long coastline. In this basin, DOC shows concentrations and vertical distribution comparable to those observed in the oceans, however isotope data unveil that DOM in the deep waters of the Med Sea is more depleted in both $\Delta^{14}C$ and $\delta^{13}C$ than in the deep Atlantic Ocean (Santinelli et al., 2015). Another peculiarity of the Med Sea is that its surface waters are “greener” than it would be expected from their low phytoplankton content and this observation has been attributed to the occurrence of a larger fraction of humic-like (yellow) substances (Morel and Gentili, 2009). The results reported in chapter 1 confirm that CDOM absorption is 3-times higher in the Med sea than in the ocean and fluorescence data unveiled the presence of 4 humic-like components, 2 of them with a clear terrestrial signature, supporting the hypothesis that in this basin a larger fraction of DOM is chromophoric. This fraction is characterized by a larger percentage of humic-like substances than in the oceans, supporting the occurrence of molecules with a terrestrial signature also in the open sea water of the basin. These data open intriguing questions about the source and cycle of allocthonous molecules in the open sea waters of the Med Sea. The comparison of DOC fluxes from rivers and the atmosphere, normalized by the volume of water, shows that river plays a similar role in the Med Sea and in the oceans, whereas normalized atmospheric fluxes are 2-3 times larger in the Med Sea than in the oceans (Chapter 1), suggesting that the atmosphere can be the main source of allocthonous DOM to the Med Sea.

It is important to keep in mind that organic molecules are ligands for heavy metals, changing their bioavailability and that DOM pool also contains organic pollutants, such as the polycyclic aromatic hydrocarbons (PAHs). Indeed, the component 1, individuated by PARAFAC in marine DOM pool, was identified as a mixture of phenols or quinones of terrestrial originand PAHs (anthracene and pyrene). The occurrence of PAH-like substances is in agreement with the

observation by Castro-Jiménez et al. (2012), that indicates an important net atmospheric input of PAHs to open sea waters of the Western Med Sea. PAHs have two or more single or fused aromatic rings with a pair of carbon atoms shared between rings in their molecules. Light and medium molecular weight PAHs (naphthalene, fluorene, anthracene) are dominant congeners in emission of vehicle engine, waste incinerator, coke plant and steel iron plant (Dat & Chang, 2017). They are carcinogenic, teratogenic and genotoxic compounds, as defined by the International Agency for Research on Cancer. PAHs are currently considered ubiquitous in the atmosphere, and the main mechanism of transfer from the cities and industrial sites to aquatic ecosystems is by atmospheric deposition, but what is the impact of these pollutants on the marine ecosystem is still unclear. Further studies and additional data on chemical composition of DOM are needed to answer this question.

2. *Atmospheric deposition of DOM to the Mediterranean Sea: is atmosphere the main source of allochtonous DOM? What is the role of Saharan dust?*

Only few studies report data on atmospheric DOC fluxes to the Med Sea, and they are focused in the western basin and Creta Island (Fig. 4.1 and Table 4.1).

Figure 4.1. Location of the sampling sites of atmospheric DOC in the Med Sea.

Flux	Collected deposition	Area	Reference
51.1 mmol C m^{-2} y^{-1} (Total organic carbon)	Wet	Crete Island, Eastern Mediterranean Sea	Economou & Mihalopoulos, 2002
129 mmol C m^{-2} y^{-1}	Wet and dry	Southern France (Cap Ferrat), Western Mediterranean Sea	Pulido-Villena et al., 2008a
65.7 mmol C m^{-2} y^{-1}	Wet and dry	Southern Spain (Granada), Western Mediterranean Sea	De Vicente et al., 2012
59 mmol C m^{-2} y^{-1}	Wet and dry	Southern France (Frioul), Western Mediterranean Sea	Djaoudi et al., 2018
15 mmol C m^{-2} y^{-1}	Dry	Crete Island, Eastern Mediterranean Sea	Theodosi et al., 2017
117.7 mmol C m^{-2} y^{-1}	Wet and Dry	Lampedusa Island, Central Mediterranean Sea	*This work*

Table 4.1. Atmospheric DOC fluxes to Mediterranean basin.

The data collected during my PhD allowed to quantify the total atmospheric flux of DOC at the Island of Lampedusa (117.7 mmol C m^{-2} y^{-1}). Assuming this value valid for the whole Med Sea, it would account for a total input of 3.55 Tg DOC y^{-1} that is up to 5-6 times larger than the estimate of the total river input to the Med Sea (0.6-0.7 Tg C y^{-1}) (Santinelli, 2015). These data support that despite the high variability, atmosphere represents an important source of allocthonous DOC to the Med Sea. The annual flux obtained in this study is higher than that obtained in previous studies, it was almost 2-fold the flux measured recently by Djaoudi et al. (2018) at the Frioul island, in the southern France (Table 4.1). Only in one study (129 mmol C m^{-2} y^{-1}, Southern France, Pulido-Villena et al., 2008a), the annual flux is higher than that obtained in Lampedusa. Data reported in Chapter 2 show that 4 of the 5 main peaks in DOC atmospheric deposition (≥0.8

mmol C m^{-2} d^{-1}) are linked to Saharan dust events, suggesting that these events represent a relevant, albeit intermittent, source of DOC to the Med Sea and opening intriguing question about the role of Saharan dust as aggregation center of organic molecules in the atmosphere. The trajectories of the air masses show unequivocally how some of them started from the Saharan region then spread out over European countries. During its route, dust enriched with organic compounds of anthropogenic or natural origin, which then were transported to the sampling site (Usher et al, 2003). The input of Saharan dust has important effects on the chemistry of the Mediterranean aerosols and its deposition can enrich the Med Sea with many elements (such as Co, Ni, trace metals), but little is known about the interaction between dust aerosol and organic compounds (Aymoz et al., 2004). Wet deposition controls the flux of Saharan dust to the Med Sea, but dry deposition can also be important (Guerzoni et al., 1997) and their relative importance strongly depends on meteorological conditions and local emissions (Inomata et al., 2009).

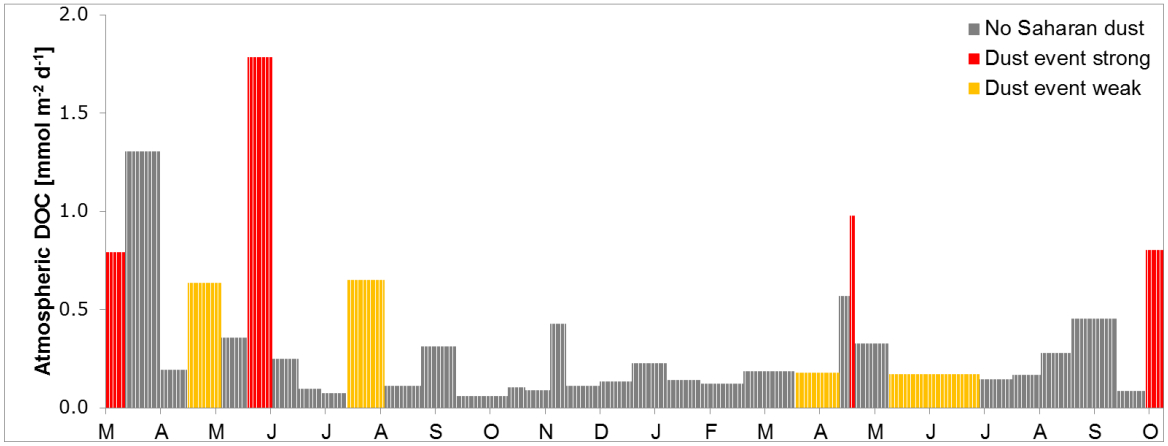

Figure 4.2. Temporal evolution of DOC atmospheric deposition.

Saharan dust contributes to atmospheric deposition of DOC in both years (2015-2016), showing a crucial role in determining its temporal dynamics. On the other hand, high DOC fluxes were also observed in the absence of Saharan dust (Fig. 4.2). In the graph Saharan events are distinguished in strong, that led to a DOC flux ≥0.8 mmol C m^{-2} d^{-1}, and weak, with DOC values that varied between 0.17 and 0.65 mmol C m^{-2} d^{-1}. If all the Saharan dust deposition events (strong and weak) are taken into account, a total input of 83.35 mmol DOC m^{-2} to Lampedusa during the study period can be estimated, this value represents ~71%

of the total flux for the entire sampling period (20 months). Instead, if only the strong dust events are taken into consideration the total flux of 44.57 mmol DOC m^{-2} can be estimated, representing 38% of flux.

3. *Atmospheric deposition of fluorescent DOM: the seven components and the possible sources. How relevant is the terrigenous signature in the atmospheric DOM?*

Data about the input of CDOM and FDOM to the Med Sea due to atmospheric depositions, are really scarce. Fluorescence of DOM provides indirect information about the origin of organic molecules. PARAFAC analysis applied to the EEMs allowed for the identification of 7 components in the atmospheric DOM pool (Chapter 2). Some of these groups of fluorophores show spectroscopic characteristics similar to those observed in open sea CDOM (Chapter 1 and Table 4.2).

Open Sea FDOM Component Ex/Em	Atmospheric FDOM Component Ex/Em	Identification
1 250/384	1 250(310)/410	Mixture of marine humic-like and PAHs substances
2 250(335)/450	3 (255)355/444	Terrestrial humic-like substances
3 250/516	2 250/495	Terrestrial humic-like substances
4 325/384	-	Marine humic-like substances
5 285/336	5 280/338	Protein-like substances
-	4 285/355	Protein-like substances
-	6 335/415	Humic-like substances Anthropogenic material
-	7 270/323	Mixture of PAHs

Table 4.2. Comparison of the two PARAFAC models: (1) open sea FDOM and (2) atmospheric FDOM.

Four components, with similar spectroscopic characteristics, were found in both open sea waters of the Med Sea and atmospheric depositions . The most intriguing result is the presence of 2 components with a clear terrestrial signature in both atmospheric and marine CDOM. The humic-like substances are the majority in both models and it is very likely that the atmospheric deposition is the main vehicle for the transfer of this material to the open sea, impacting the biogeochemistry of the Med Sea. Humic-like substances are heterogeneous, amorphous, organic materials with high molecular weight, which are ubiquitous in the atmosphere (Havers et al., 1998; Duarte et al., 2007; Tan et al., 2016). They play a key role in atmospheric processes due to their water solubility and strong surface activity (Kiss et al., 2005; Dinar et al., 2006; Sun & Ariya, 2006). They can serve as cloud condensation nuclei (Facchini et al., 2000), influencing the growth and nucleation of cloud water droplets (Shulman et al, 1996) and change the hygroscopicity of inorganic particles (Saxena et al., 1995).

The second major group of fluorophores occurring in both pool is the protein-like substances. The comparison between the two models highlights the presence of an additional protein component in the atmospheric DOM (Table 4.2). This observation suggests that one of the two components found in the atmosphere may have an autochthonous origin, it could be produced by the airborne microbial community. Some recent papers report that these protein-like substances may be also associated with fluorescent compounds of anthropogenic origin (Tedetti et al., 2012; Ferretto et al., 2014). Finally, our study suggests that the protein-like FDOM (C4) occurring in the atmosphere could be made up of labile DOM, produced and consumed in the atmospheric compartment before reaching the marine ecosystem. On the other hand, in addition to the transformation of this fluorescent material, a dilution in seawater cannot be excluded. The same hypothesis also apply to components 6 and 7 of the atmospheric PARAFAC model (Table 4.2), but these hypothesis should be tested with incubation experiments.

A mixture of PAH is also widely diffused in both models and, as previously described, this is due to the ubiquity of these pollutants in all the environmental compartments.

Saharan dust can also be enriched in FDOM, the data reported in Chapter 2 clearly show high fluxes of FDOM in correspondence with the major Saharan dust events (Figure 4.2). This finding is in agreement with the observation of a relationship between FDOM and Saharan dust inputs in alpine lakes (Mladenov et al., 2011) and a recent study on aerosol inputs affecting the optical proprierties of DOM in north-western Med Sea (Sánchez-Pérez et al., 2016).

4. *The impact on marine ecosystem: is atmospheric DOM labile or recalcitrant? Which are the main implications for the marine environment?*

The measurements carried out at the Island of Lampedusa clearly show that the atmosphere is the predominant source of allocthonous DOM to the Med Sea. Very few information are available about the biological lability of atmospheric DOM, if it is labile it can be used very quickly by the microbial loop whereas if it is mainly recalcitrant it can accumulate and be transported by water masses circulation. In order to estimate the impact of atmospheric DOC deposition to the biogeochemistry of surface waters we took into consideration DOC samples

collected at 6 stations located in the central Med Sea close to the island of Lampedusa (Fig. 4.3). Samples were collected between May 24th and June 12th 2017 during the oceanographic cruise *Sentinel-3* on board the R/V Minerva Uno of the Italian National Research Council (CNR) (chief scientist Rosalia Santoleri, CNR-ISAC).

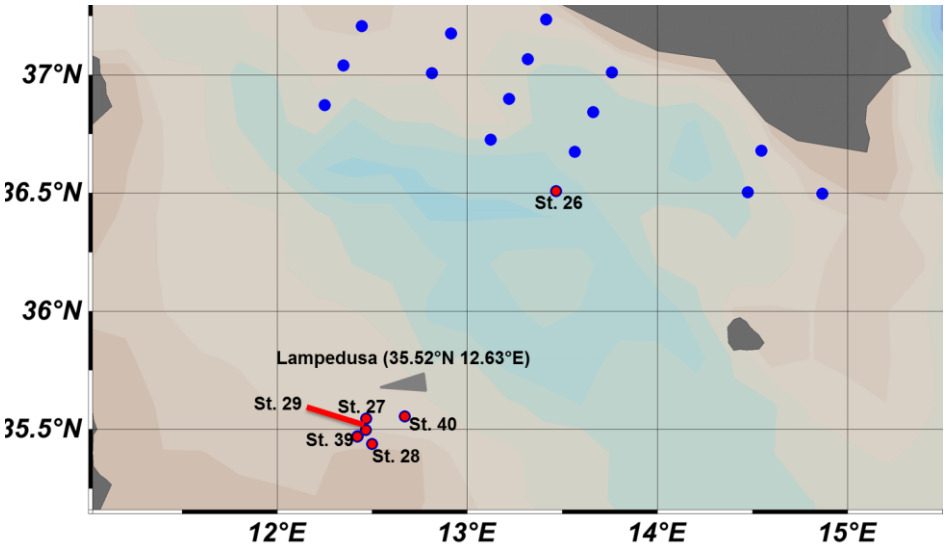

Fig. 4.3. Sampling stations.

The vertical profile of DOC, salinity, density and temperature is reported, the mixed layer depth (MLD) was visually estimated at the six stations and ranged between … and… (Fig. 4.4). DOC values ranged between 43 and 56 μM in the Sicily Channel (station 26), and between 41 and 62 μM at the stations close to the island of Lampedusa. Santinelli et al. (2012) observed an average DOC concentration of 60 μM in the same area in September 1999 (in the mixed layer), and estimated a bacterial carbon demand (BCD) of 0.32 μM C d^{-1} (assuming a BGE of 15%), which represents the total amount of carbon needed to support the observed bacterial production.

If we take into consideration the atmospheric DOC fluxes determined between May and June (the period of *Sentinel-3* cruise) 2015 and 2016 (the period of the measurements of atmospheric samples), atmospheric DOC flux was 1.04 mmol C m^{-2} d^{-1} in 2015, and 0.27 C m^{-2} d^{-1} in 2016. The average MLD (Fig. 4.4) was 12 m for the stations close to Lampedusa. Dividing the atmospheric fluxes by the MLD (12 m), we estimated that the DOC input from the atmosphere is expected to increase DOC concentration in the mixed layer of 0.02-0.09 μM C d^{-1}.

Assuming the values of BCD observed in September (0.32 μM C d^{-1}) valid also for summer and that the DOC coming from the atmosphere is labile it could satisfy 6-28% of the daily BCD. These results highlight the key role of atmosphere input of DOC in sustaining the bacterial productivity in the surface layer, particularly when the column is strongly stratified.

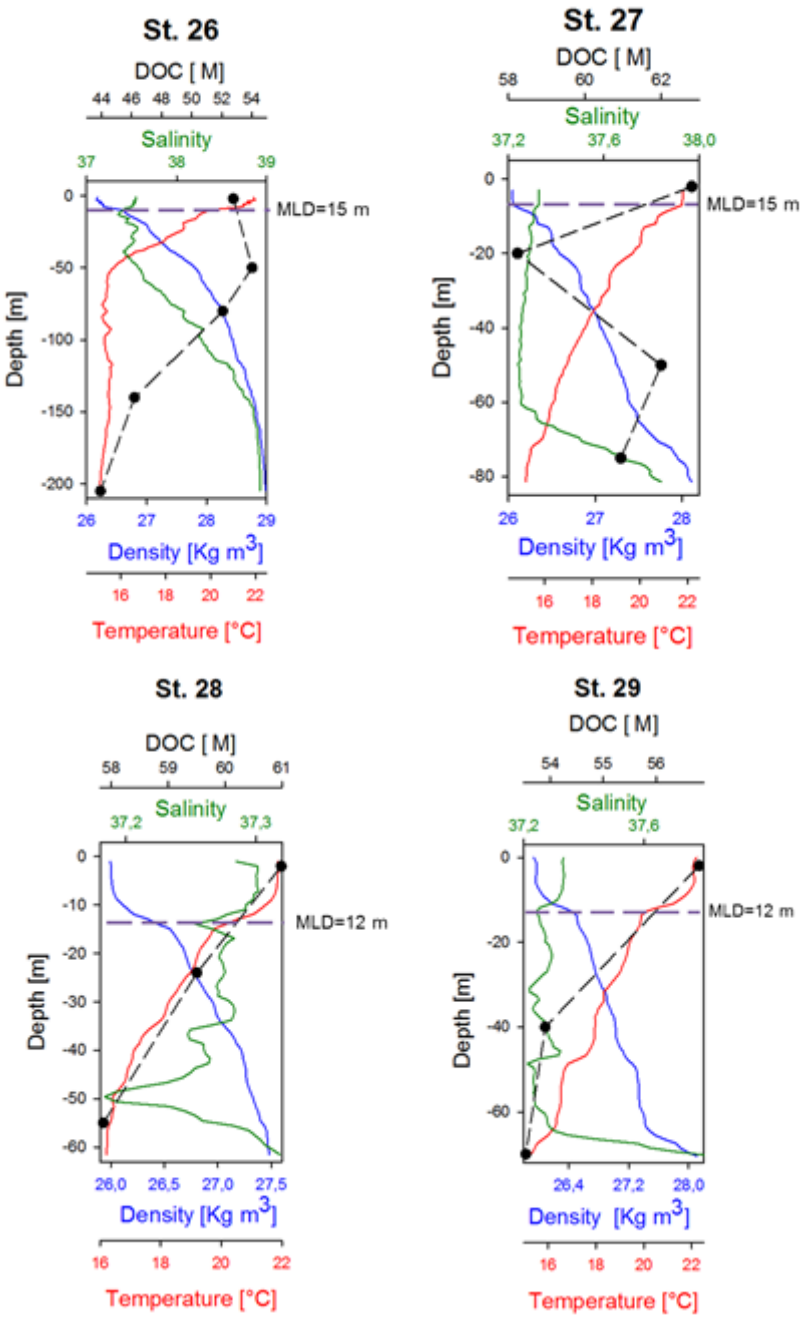

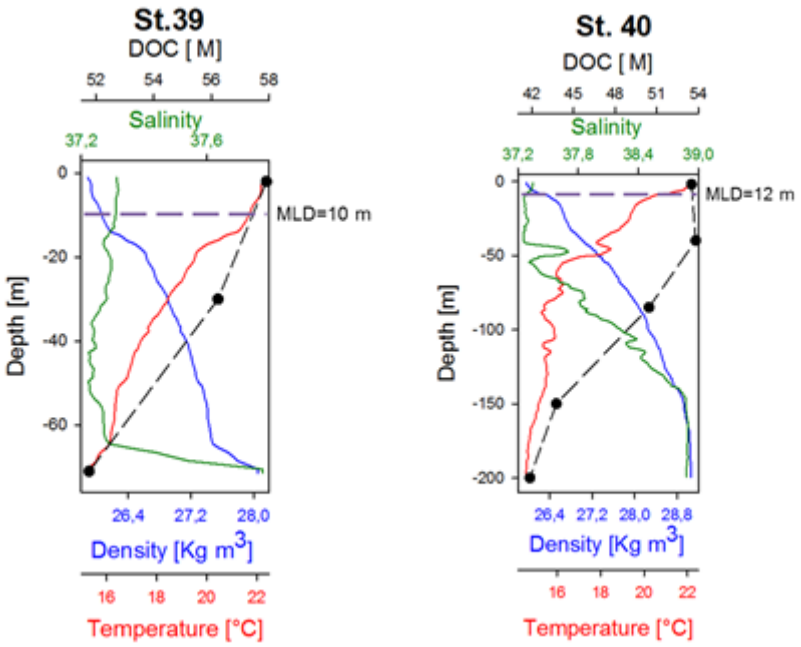

Figure 4.4. Vertical profiles of Temperature, Density, Salinity and DOC, for the six stations of *Sentinel-3* cruise.

The Mediterranean MLD seasonal variability is characterized by a basin scale deepening from November to February-March and an abrupt restratification in April, which is maintained throughout the summer and early autumn. Even if these data stress the potential role of atmospheric DOC in sustaining bacterial productivity in the surface ocean, a time series of BCD, MLD and DOC concentrations in the surface layer could be crucial in order to have an accurate estimates of the impact of atmospheric input of DOC to the functioning of microbial loop. It should be also noted that a fraction of atmospheric DOC could be recalcitrant and therefore be transported to depth, playing a key role in carbon sequestration to depth. The refractory nature of a part of atmospheric DOC is hypothesised bySanchez-Perez et al. (2016), who collected a 2-year time series data on FDOM deposition in the North-western Med Sea and studied the changes in the quality and quantity of marine DOM in the Barcelona coastal area (Spain). Their results showed that atmospheric inputs induced changes in the quality of organic matter, increasing the proportion of FDOM substances in DOM pool. They also found a negligible utilization of the chromophoric compounds over the experimental period, suggesting that the FDOM associated with aerosols have a recalcitrant nature.

DOC and CDOM dynamics in response to dust input studied during a mesocosm experiment, carried out in Eilat (Northern Red Sea, Israel), in July 2017 (Chapter 3) showed that the addition of dust did not lead to an enrichment of DOM nor CDOM, however it indirectly affected DOM dynamics through a change in the microbial food web.

General conclusions

&

Future perspectives

"Everyday, you leave a footprint!"

Ernest Agyemang Yeboah

General conclusions

The data reported in this study were able to support the 3 hypothesis, in particular:

1. **In the Med Sea, the DOM pool is constituted by a relevant fraction of allocthonous molecules.** The CDOM and FDOM data collected in a large open sea area of the Wetesrn Med Sea and Ionian Sea (Chapter 1) supports that:
   - The Mediterranean DOM pool is dominated by humic-like substances with a terrestrial origin. Our data are in agreement with both the values of $\Delta^{14}C$ and $\delta^{13}C$ and the blue shade of the Med Sea waters. The parallel factorial analysis (PARAFAC) applied to the EEMs showed the presence of 4 humic-like components, 2 with a clear terrestrial signature. One component showed an emission spectrum with a maximum at 516 nm overlapping that of Pahokee peat humic-acid. None similar component was found in the open ocean.
   - Only one protein-like component was found in open sea waters of the Med Sea. It can represent an autochthonous fraction of CDOM, even if a similar component was observed in atmospheric deposition, suggesting that it could also have an allocthonous origin. The comparison with the oceans indicates that the Med Sea has a different protein-like composition, this observation can be explained by the different bacterial and archaeal ecotypes present in this basin.
2. **The atmosphere is the predominant source of allocthonous DOM to the Med Sea.** The time series of DOC, CDOM and FDOM in atmospheric deposition collected at the Lapedusa island (Chapter 2) showed that:
   - DOC fluxes from the atmosphere can be up to 6 times larger than river input. Atmosphere is a relevant source of both humic-like and protein-like substances to the surface waters of the Med Sea. Atmospheric input has an impact to the Med Sea larger than to the oceans. Atmospheric input may play a crucial role in determining CDOM composition in open sea waters as supported by the comparison among optical properties of CDOM in marine and atmospheric samples. Atmospheric input can therefore explain the occurrence of humic-substances with a terrestrial signatures in all the marine samples analyzed.

- Different sources, both natural and anthropogenic, contribute to the organic matter pool in the aerosol. The processes affecting atmospheric DOC dynamics are various and complexes. Saharan dust events may cause a relevant DOC input to the Mediterranean Sea. However, the load of DOC associated with dust is highly variable and large DOC fluxes were observed also in absence of dust deposition events.
- DOC, DOP and DON fluxes show a high annual and interannual variability indicating that marine ecosystem in surface waters undergoes to input of variable amount of DOM with a different quality from the atmosphere. DON and DOP were relevant contributors of nitrogen and phosphorous deposition, representing more than 30% of total dissolved atmospheric N and P.
- Atmospheric C:N:P molar ratios are in good agreement with data observed in atmospheric DOM collected in the North-Western Med Sea (Frioul island, Marseille, France). Good relationship between DOC and DOP values were obtained in two different sampling sites (Lampedusa and Frioul).

3. **Atmospheric deposition impacts the DOM dynamics in the surface ocean affecting the function of marine ecosystem.** The mesocosm experiment and the data from Central Med Sea showed that:

- In the mesocosm experiment (Eilat, Israel) the deposition of dust did not lead to an enrichment of DOM and CDOM. However, a marked increase of DOC, 20 hours after the addition of Saharan dust, was observed. One hypothesis to explain this observation is that the dust is rich in chemical elements that could stimulate chemosynthesis.
- Atmospheric DOC deposition can fulfill part of the bacterial carbon demand in the Central Med Sea during spring and summer. A fraction of atmospheric DOM may be recalcitrant, and it can be accumulated and exported in depth.

Future perspectives

1. A network of stations to assess the main sources and deposition regimes of DOC over the Mediterranean basin

The work, carried out during my PhD, stresses the need of a network of stations for continuous measurements of DOC, in order to obtain a robust estimate of atmospheric deposition of DOC to the Med Sea. A similar approach was used for nutrients (Markaki et al., 2010), but no such information is still available for DOC. There are areas such as the Tyrrhenian Sea, where no information about DOM deposition is available. This area could be crucial for studying atmospheric DOM deposition, since it is halfway between the North-Western Med Sea (Frioul and Cap Ferrat) and Lampedusa (Central Med Sea) and it is strongly affected by the Saharan dust deposition. Few information about atmospheric input of DOC is available for the easternmost part of the Med Sea, where DOC accumulation in the surface layer is observed.

It would be also interesting to compare the atmospheric input of DOC in remote areas (such as Lampedusa) and in coastal areas strongly affected by anthropic actives (e.g. Barcelona, Marseille, Genoa, Naples in the western basin, TelAviv and Athens in the eastern basin) in order to compare the impact of atmospheric deposition in clear and polluted waters.

2. Atmospheric DOC deposition and Saharan dust

Further studies are needed to better understand how the Saharan dust deposition impacts marine DOC dynamics and what are the main processes leading to DOC enrichment in the atmosphere. A longer time series of data at the same location can give additional information about the link between dust deposition and peak in DOC input. Our study suggests that when the aerosol is rich in dust and flows above an area rich in emission of organic molecules, concentration of organic molecules in aerosol can be much higher than in aerosol without dust, since OC can adsorb to the dust creating a coat and allowing for transport and deposition of organic molecules to the oceans. Further study focusing on the reactions between dust and organic molecules are needed to support this hypothesis. Data on stable carbon ($\delta^{13}C$) and radiocarbon ($\Delta^{14}C$) on atmospheric DOM samples would be crucial in order to gain information about the

main sources and cycling of atmospheric DOC. The modern analytical chemistry (high performance liquid chromatography, mass-spectrometry and nuclear magnetic resonance spectroscopy) could help to obtain detailed information about the chemical composition and structure of atmospheric DOM.

3. The biological lability of atmospheric DOM

One of the biggest unresolved question is about the biological lability of atmospheric DOM and its impact on marine ecosystem. Incubation experiments should be carried out, both with aerosol rich in DOC and with aerosol poor, in order to better understand how the microbial community can respond to dust input. Atmospheric and marine DOM molar ratios (C:N:P) could also be measured over time in order to obtain information about changes in marine DOM pool. The biggest problems of these experiments are that the amount of dust that should be added to observe a measurable increase of DOC is much higher than natural deposition values and that even if a decrease in DOC concentration can be observed is not possible to discriminate if microbes removed the marine or atmospheric DOM. Further work is needed to support the hypothesis of chemosynthesis as the main process that may occur in some conditions and to estimate the impact that this process can have on marine ecosystem.

4. A modelling effort

One of the effect of climate change is expected to be a change in the frequency and intensity of dust deposition. It can be hypothesized that the increase in deposition events could lead to a larger transfer of terrigenous and anthropogenic DOM from the atmosphere to the sea, with consequences for DOM dynamics in the oceans and marine ecosystem. Longer time series, combined with a modelling effort, are highly recommended in order to assess the response of DOM dynamics in the Med Sea to the change in aerosol deposition pattern.

Appendix I

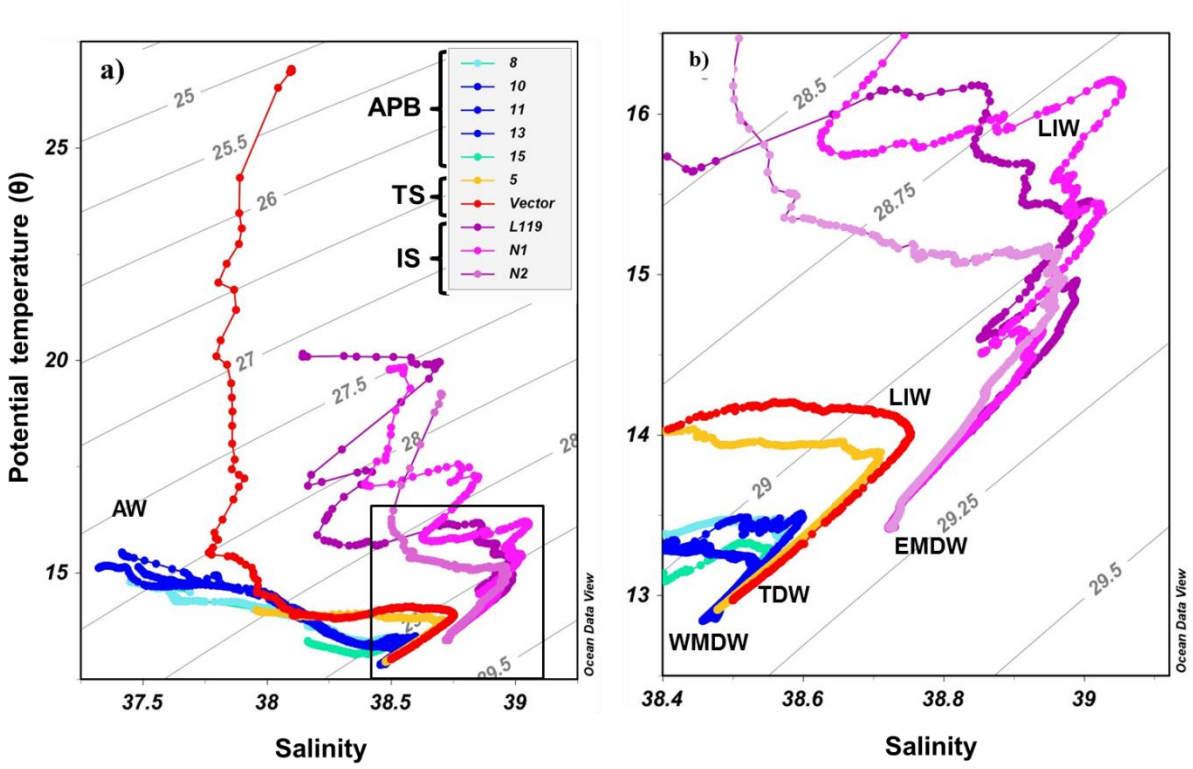

Figure A1. Potential temperature vs. Salinity (θ/S) diagram of all the sampling stations (a); a zoom of the θ/S diagram for the intermediate and deep waters (b). The 3 groups of stations are clearly identified: APB, Algero-Provençal Basin; TS, Tyrrhenian Sea; IS, Ionian Sea. The water masses are identified with their abbreviations: AW: Atlantic Water; LIW: Levantine Intermediate Water; TDW: Tyrrhenian Deep Water; EMDW Eastern Mediterranean Deep Water; WMDW: Western Mediterranean Deep Water.

Appendix II

Dissolved organic matter dynamics in surface waters affected by oil spill pollution: Results from the Serious Game exercise

M. Gonnelli[a] Y. Galletti[a] E. Marchetti[a] L. Mercadante[a] S. RetellettiBrogi[a] A. Ribotti[b] R. Sorgente[b] S. Vestri[a] C. Santinelli[a]

[a]Consiglio Nazionale delle Ricerche, IBF, Pisa, Italy
[b]Consiglio Nazionale delle Ricerche, IAMC, Oristano, Italy

Abstract

Dissolved organic carbon (DOC), chromophoric and fluorescent dissolved organic matter (CDOM and FDOM, respectively) surface distribution was studied during the Serious Game exercise carried out in the Eastern Ligurian Sea, where an oil spill was localized by using satellite images and models. This paper reports the first DOC, CDOM and FDOM data for this area together with an evaluation of fluorescence as a fast and inexpensive tool for early oil spill detection in marine waters. The samples collected in the oil spill showed a fluorescence intensity markedly higher (~5 fold) than all the other samples. The excitation–emission matrixes, coupled with parallel factor analysis (PARAFAC), allowed for the identification in the FDOM pool of a mixture of polycyclic aromatic hydrocarbons, humic-like and protein-like fluorophores.

https://doi.org/10.1016/j.dsr2.2016.05.027

Appendix III

Airborne Microbes Contribute to N_2 Fixation in Surface Water of the Northern Red Sea

E. Rahav, A. Paytan, E. Mescioglu, Y. Galletti, S. Rosenfeld, O. Raveh, C. Santinelli, T.-Y. Ho, B. Herut

Abstract

Desert dust storms are frequent in the Northern Red Sea region, providing nutrients (i.e., PO4) and trace-metals (i.e., Fe) that may stimulate dinitrogen (N_2) fixation. Dust also carries a high diversity of airborne microbes (bacteria and archaea), including diazotrophs, that may remain viable during transport and upon deposition. Here we evaluate the impact of atmospheric deposition and its associated airborne diazotrophs on N_2 fixation in the surface water of the low-nutrient Northern Red Sea, using mesocosm bioassay experiments. We compared the chemical (nutritional) and sole airborne microbial impact of aerosol additions on N_2 fixation using “live-dust” (release nutrients/trace metals and viable airborne microorganisms) and “UV-killed dust” (release only chemicals). Airborne diazotrophy accounted for about one third of the measured N_2 fixation (0.35 ± 0.06 nmol $N \cdot L^{-1} \cdot day^{-1}$ and 0.29 ± 0.06 nmol $N \cdot L^{-1} \cdot day^{-1}$, for “February 2017” and “May 2017,” “live-dust” additions, respectively). Two *nifH* sequences related to cluster III diazotrophs were amplified from the dust samples, consistent with the N_2 fixation measurement results. We postulate that the deposition of viable airborne diazotrophs may enhance N_2 fixation, especially in marine provinces subjected to high aerosol loads. We speculate that the relative contribution of airborne N_2 fixation may increase in the future with the predicted increase in dust deposition.

Plain Language Summary

Aerosols and dust are regularly transported across the oceans supplying nutrients and trace metals to the surface water. In addition, aerosols may also contain a wide array of different airborne microorganisms (heterotrophic bacteria, virus, cyanobacteria, and fungi) that can be easily transported for thousands of kilometers away from their place of origin within a few days. Here we examined the role of airborne N_2 fixers (diazotrophs) in the surface water of the low-nutrient Northern Red Sea during the summer. To this end, we compared the chemical (nutritional) and sole airborne microbial impact of aerosol additions on N_2 fixation using “live-dust” (release nutrients/trace metals and viable airborne microorganisms) and “UV-killed dust” (release only chemicals). Our results demonstrate that airborne N_2 fixation may be an important source of new bioavailable N in the Northern Red Sea, fueling primary production. In accordance with these measurements, two *nifH* sequences related to cluster III diazotrophs were amplified from the dust samples. Our results suggest that airborne N_2 fixation may play an important role in marine environments subjected to high aerosol loads. We further suggest that the role of airborne diazotrophs may likely increase in the future due to global desertification processes and thus an increase in dust deposition. https://doi.org/10.1029/2018GL077132.

References

Abdulla, H.A., Minor, E.C., Dias, R.F., Hatcher, P. G., 2010a. Changes in the compound classes of dissolved organic matter along an estuarine transect: a study using FTIR and ^{13}C NMR. Geochimica et Cosmochimica Acta, 74(13), 3815-3838. https://doi.org/10.1016/j.gca.2010.04.006.

Abdulla, H.A., Minor, E.C., Hatcher, P.G., 2010b. Using two-dimensional correlations of ^{13}C NMR and FTIR to investigate changes in the chemical composition of dissolved organic matter along an estuarine transect. Environmental science & technology, 44(21), 8044-8049. https://doi.org/ 10.1021/es100898x.

Aluwihare, L.I., Repeta, D.J., Chen, R.F., 1997. A major biopolymeric component to dissolved organic carbon in surface sea water. Nature, 387(6629), 166. https://doi.org/10.1038/387166a0.

Amon, R.M., Benner, R., 1996. Bacterial utilization of different size classes of dissolved organic matter. Limnology and Oceanography, 41(1), 41-51. https://doi.org/10.4319/lo.1996.41.1.0041.

Aminot, A., Kérouel, R., 2007. Dosage automatique des nutriments dans les eaux marines: méthodes en flux continu. Editions Quae.

Anderson, K., Peters, G., 2016. The trouble with negative emissions. Science, 354(6309), 182-183. https://doi.org/10.1126/science.aah4567.

Andreae, M.O., Rosenfeld, D., 2008. Aerosol–cloud–precipitation interactions. Part 1. The nature and sources of cloud-active aerosols. Earth-Science Reviews, 89(1-2), 13-41. https://doi.org/10.1016/j.earscirev.2008.03.001.

Antoine, D., d'Ortenzio, F., Hooker, S. B., Bécu, G., Gentili, B., Tailliez, D., Scott, A.J., 2008. Assessment of uncertainty in the ocean reflectance determined by three satellite ocean color sensors (MERIS, SeaWiFS and MODIS-A) at an offshore site in the Mediterranean Sea (BOUSSOLE project). Journal of Geophysical Research: Oceans, 113(C7). https://doi.org/10.1029/2007JC004472.

Armstrong, F.A.J., Williams, P.M., Strickland, J.H., 1966. Photo-oxidation of organic matter in sea water by ultra-violet radiation, analytical and other applications. Nature, 211(5048), 481. https://doi.org/10.1038/211481a0.

Arnosti, C., 2011. Microbial extracellular enzymes and the marine carbon cycle. Annual review of marine science, 3, 401-425. https://doi.org/10.1146/annurev-marine-120709-142731.

Arrigo, K.R., & Brown, C.W., 1996. Impact of chromophoric dissolved organic matter on UV inhibition of primary productivity in the sea. Marine Ecology Progress Series, 207-216.

Artuso, F., Chamard, P., Piacentino, S., Di Sarra, A., Meloni, D., Monteleone, F., Sferlazzo, D., Thiery, F., 2007. Atmospheric methane in the Mediterranean: analysis of measurements at the island of Lampedusa during 1995–2005. Atmospheric Environment, 41(18), 3877-3888. https://doi.org/10.1016/j.atmosenv.2007.01.024.

Artuso, F., Chamard, P., Piacentino, S., Sferlazzo, D. M., De Silvestri, L., Di Sarra, A., Meloni, D., Monteleone, F., 2009. Influence of transport and trends in atmospheric CO2 at Lampedusa. Atmospheric Environment, 43(19), 3044-3051. https://doi.org/10.1016/j.atmosenv.2009.03.027.

Astrahan, P., Herut, B., Paytan, A., Rahav, E., 2016. The impact of dry atmospheric deposition on the sea-surface microlayer in the SE Mediterranean Sea: an experimental approach. Frontiers in Marine Science, 3, 222. https://doi.org/10.3389/fmars.2016.00222.

Aurin, D., Mannino, A., 2012. A database for developing global ocean color algorithms for colored dissolved organic material, CDOM spectral slope, and dissolved organic carbon. In Paper presented at Ocean Optics XXI, 8–12 October, 2012, The Oceanography Society, Glasgow, UK.

Avery Jr, G.B., Willey, J.D., Kieber, R.J., 2006. Carbon isotopic characterization of dissolved organic carbon in rainwater: Terrestrial and marine influences. Atmospheric Environment, 40(39), 7539-7545. https://doi.org/10.1016/j.atmosenv.2006.07.014.

Avila, A., Queralt-Mitjans, I., Alarcón, M., 1997. Mineralogical composition of African dust delivered by red rains over northeastern Spain. Journal of Geophysical Research: Atmospheres, 102(D18), 21977-21996. https://doi.org/10.1029/97JD00485.

Aymoz, G., Jaffrezo, J. L., Jacob, V., Colomb, A., George, C., 2004. Evolution of organic and inorganic components of aerosol during a Saharan dust episode observed in the French Alps. Atmospheric Chemistry and Physics, 4(11/12), 2499-2512. https://doi.org/10.5194/acp-4-2499-2004.

Bakker, D.C.E., Pfeil, B., Smith, K., Hankin, S., Olsen, A., Alin, S.R., Cosca, C., Harasawa, S., Kozyr, A., Nojiri, Y., O'Brien, K.M., Schuster, U., Telszewski, M., Tilbrook, B., Wada, C., Akl, J., Barbero, L., Bates, N.R., Boutin, J., Bozec, Y., Cai, W.-J., Castle, R.D., Chavez, F.P., Chen, L., Chierici, M., Currie, K., de Baar, H.J.W., Evans, W., Feely, R.A., Fransson, A., Gao, Z., Hales, B., Hardman-Mountford, N.J., Hoppema, M., Huang, W.-J., Hunt, C. W., Huss, B., Ichikawa, T., Johannessen, T., Jones, E.M., Jones, S.D., Jutterström, S., Kitidis, V., Körtzinger, A., Landschützer, P., Lauvset, S.K., Lefèvre, N., Manke, A.B., Mathis, J. T., Merlivat, L., Metzl, N., Murata, A., Newberger, T., Omar, A. M., Ono, T., Park, G.-H., Paterson, K., Pierrot, D., Ríos, A.F., Sabine, C.L., Saito, S., Salisbury, J., Sarma, V.V.S.S., Schlitzer, R., Sieger, R., Skjelvan, I., Steinhoff, T., Sullivan, K. F., Sun, H., Sutton, A.J., Suzuki, T., Sweeney, C., Takahashi, T., Tjiputra, J., Tsurushima, N., van Heuven, S.M.A.C., Vandemark, D., Vlahos, P., Wallace, D.W.R., Wanninkhof, R., and Watson, A.J., 2014. An update to the Surface Ocean CO2 Atlas (SOCAT version 2), Earth Syst. Sci. Data, 6, 69-90. https://doi.org/10.5194/essd-6-69-2014.

Becagli, S., Sferlazzo, D. M., Pace, G., Sarra, A. D., Bommarito, C., Calzolai, G., Ghedini, C., Lucarelli, F, Meloni, D., Monteleone, F., Severi, M., Trasversi, R., Udisti, R., 2012. Evidence for heavy fuel oil combustion aerosols from chemical analyses at the island of Lampedusa: a possible large role of ships emissions in the Mediterranean. Atmospheric Chemistry and Physics, 12(7), 3479-3492. https://doi.org/10.5194/acp-12-3479-2012.

Becagli, S., Lazzara, L., Fani, F., Marchese, C., Traversi, R., Severi, M., di Sarra, A., Sferlazzo, D., Piacentino, S., Bommarito, C., Dayan, U., Udisti, R., 2013. Relationship between methanesulfonate (MS−) in atmospheric particulate and remotely sensed phytoplankton activity in oligo-mesotrophic central Mediterranean Sea. Atmospheric Environment, 79, 681-688. https://doi.org/10.1016/j.atmosenv.2013.07.032.

Becagli, S., Anello, F., Bommarito, C., Cassola, F., Calzolai, G., Iorio, T. D., di Sarra, A., Gómez-Amo, J.-L., Lucarelli, F., Marconi, M., Meloni, D., Monteleone, F., Nava, S., Pace, G., Severi, M., Sferlazzo, D.M., Traversi, R., Udisti, R., 2017. Constraining the ship contribution to the aerosol of the central Mediterranean. Atmospheric Chemistry and Physics, 17(3), 2067-2084. https://doi.org/10.5194/acp-17-2067-2017.

Benner, R., 2002. Chemical composition and reactivity. Biogeochemistry of marine dissolved organic matter, 3, 56-90.

Benson, B.B., Krause Jr, D., 1984. The concentration and isotopic fractionation of oxygen dissolved in freshwater and seawater in equilibrium with the atmosphere 1. Limnology and oceanography, 29(3), 620-632. https://doi.org/10.4319/lo.1984.29.3.0620.

Bergametti, G., Dutot, A.L., Buat-Menard, P., Losno, R., Remoudaki, E., 1989. Seasonal variability of the elemental composition of atmospheric aerosol particles over the northwestern Mediterranean. Tellus B, 41(3), 353-361. https://doi.org/10.1111/j.1600-0889.1989.tb00314.x.

Bergametti, G., Remoudaki, E., Losno, R., Steiner, E., Chatenet, B., Buat-Menard, P., 1992. Source, transport and deposition of atmospheric phosphorus over the northwestern Mediterranean. Journal of Atmospheric Chemistry, 14(1-4), 501-513.

Bergquist, B.A., Blum, J.D., 2007. Mass-dependent and-independent fractionation of Hg isotopes by photoreduction in aquatic systems. Science, 318(5849), 417-420. https://doi.org/ 10.1126/science.1148050.

Berman-Frank, I., Cullen, J.T., Shaked, Y., Sherrell, R.M., Falkowski, P.G., 2001. Iron availability, cellular iron quotas, and nitrogen fixation in Trichodesmium. Limnology and Oceanography, 46(6), 1249-1260. https://doi.org/10.4319/lo.2001.46.6.1249.

Biddanda, B., Benner, R., 1997. Carbon, nitrogen, and carbohydrate fluxes during the production of particulate and dissolved organic matter by marine phytoplankton. Limnology and Oceanography, 42(3), 506-518. https://doi.org/10.4319/lo.1997.42.3.0506.

Bigg, G.R., Jickells, T.D., Liss, P.S., Osborn, T.J., 2003. The role of the oceans in climate. International Journal of Climatology, 23(10), 1127-1159. https://doi.org/10.1002/joc.926.

Boyd, P.W., Doney, S.C., 2003. The impact of climate change and feedback processes on the ocean carbon cycle. In Ocean biogeochemistry (pp. 157-193). Springer, Berlin, Heidelberg.

Bonnet, S., Guieu, C., 2004. Dissolution of atmospheric iron in seawater. Geophysical Research Letters, 31(3). https://doi.org/10.1029/2003GL018423.

Bonnet, S., Guieu, C., Chiaverini, J., Ras, J., Stock, A., 2005. Effect of atmospheric nutrients on the autotrophic communities in a low nutrient, low chlorophyll system. Limnology and Oceanography, 50(6), 1810-1819. https://doi.org/10.4319/lo.2005.50.6.1810.

Bonnet, S., Guieu, C., 2006. Atmospheric forcing on the annual iron cycle in the western Mediterranean Sea: A 1-year survey. Journal of Geophysical Research: Oceans, 111(C9). https://doi.org/10.1029/2005JC003213.

Bracchini, L., Tognazzi, A., Dattilo, A.M., Decembrini, F., Rossi, C., Loiselle, S.A., 2010. Sensitivity analysis of CDOM spectral slope in artificial and natural samples: an application in the central eastern Mediterranean Basin. Aquatic sciences, 72(4), 485-498. https://doi.org/10.1007/s00027-010-0150-y.

Breitbart, M., 2012. Marine viruses: truth or dare. https://doi.org/10.1146/annurev-marine-120709-142805.

Bro, R., 1997. PARAFAC. Tutorial and applications. Chemometrics and intelligent laboratory systems, 38(2), 149-171. https://doi.org/10.1016/S0169-7439(97)00032-4.

Bronk, D.A., 2002. Dynamics of DON. Biogeochemistry of marine dissolved organic matter, 384, p153-247.

Buseck, P.R., Pósfai, M., 1999. Airborne minerals and related aerosol particles: Effects on climate and the environment. Proceedings of the National Academy of Sciences, 96(7), 3372-3379. https://doi.org/10.1073/pnas.96.7.3372.

Calzolai, G., Nava, S., Lucarelli, F., Chiari, M., Giannoni, M., Becagli, S., Trasversi, R., Marconi, M., Frosini, D., Severi, M., Udisti, R., di Sarra, A., Pace, G., Meloni, D., Bommarito, C., Monteleone, F., Anello, F., Sferlazzo, D.M., 2015. Characterization of PM 10 sources in the central Mediterranean. Atmospheric Chemistry and Physics, 15(24), 13939-13955. https://doi.org/10.5194/acp-15-13939-2015.

Cárdenas, C.S., Gerea, M., Garcia, P.E., Pérez, G.L., Diéguez, M.C., Rapacioli, R., Reissig, M., Queimaliños, C., 2017. Interplay between climate and hydrogeomorphic features and their effect on the seasonal variation of dissolved organic matter in shallow temperate lakes of the Southern Andes (Patagonia, Argentina): a field study based on optical properties. Ecohydrology. https://doi.org/10.1002/eco.1872.

Carlson, C.A., Hansell, D.A., Nelson, N.B., Siegel, D.A., Smethie, W.M., Khatiwala, S., Meyers, M.M., Halewood, E., 2010. Dissolved organic carbon export and subsequent remineralization in the mesopelagic and bathypelagic realms of the North Atlantic basin. Deep Sea Research Part II: Topical Studies in Oceanography 57(16), 1433-1445. https://doi.org/10.1016/j.dsr2.2010.02.013.

Carlson, C.A., Hansell, D.A., 2015. DOM sources, sinks, reactivity, and budgets. In Biogeochemistry of Marine Dissolved Organic Matter (Second Edition) (pp. 65-126). https://doi.org/10.1016/B978-0-12-405940-5.00003-0.

Castro-Jiménez, J., Berrojalbiz, N., Wollgast, J., Dachs, J., 2012. Polycyclic aromatic hydrocarbons (PAHs) in the Mediterranean Sea: Atmospheric occurrence, deposition and decoupling with settling fluxes in the water column. Environmental Pollution 166, 40-47. https://doi.org/10.1016/j.envpol.2012.03.003.

Catalá, T.S., Reche, I., Álvarez, M., Khatiwala, S., Guallart, E.F., Benítez-Barrios, V.M., Fuentes-Lema, A., Romera-Castillo, C., Nieto-Cid, M., Pelejero, C., Fraile-Nuez, E., Ortega-Retuerta, E., Marrasé, C., Álvarez-Salgado, X.A., 2015. Water mass age and aging driving chromophoric dissolved organic matter in the dark global ocean. Glob.Biogeochem. Cycles 29 (7), 917–934. https://doi.org/10.1002/2014GB005048.

Catalá, T.S., Álvarez-Salgado, X.A., Otero, J., Iuculano, F., Companys, B., Horstkotte, B., Romera-Castillo, C., Nieto-Cid, M., Latasa, M., Moràn, X.A.G., Gasol, J.M., Marrasé, C., Stedmon, C.A., Reche, I., 2016. Drivers of fluorescent dissolved organic matter in the global epipelagic ocean. Limnology and Oceanography, 61(3), 1101-1119. https://doi.org/10.1002/lno.10281.

Catalá, T.S., Marenez–Pérez, A. M., Nieto–Cid, M., Álvarez, M., Otero, J., Emelianov, M., Reche, I., Arístegui, J., Álvarez–Salgado, X.A., 2018. Dissolved Organic Matter (DOM) in the open Mediterranean Sea. I. Basin–wide distribution and drivers of chromophoric DOM. Progress in Oceanography, 165, 35–51. https://doi.org/10.1016/j.pocean.2018.05.002.

Cauwet, G., 2002. DOM in the Coastal Zone, in: Hansell D.A, Carlson C.A. (Eds.), Biogeochemestry of Marine Dissolved Organic Matter (First edition), Academic Press, San Diego, pp. 579–609. https://doi.org/10.1016/B978-012323841-2/50014-2.

Cawley, K.M., Ding, Y., Fourqurean, J., Jaffé, R., 2012. Characterising the sources and fate of dissolved organic matter in Shark Bay, Australia: a preliminary study using optical properties and stable carbon isotopes. Marine and Freshwater Research 63(11), 1098-1107. https://doi.org/10.1071/MF12028.

Chance, R., Jickells, T.D., Baker, A.R., 2015. Atmospheric trace metal concentrations, solubility and deposition fluxes in remote marine air over the south-east Atlantic. Marine Chemistry, 177, 45-56. https://doi.org/10.1016/j.marchem.2015.06.028.

Chase, Z., Paytan, A., Johnson, K.S., Street, J., Chen, Y., 2006. Input and cycling of iron in the Gulf of Aqaba, Red Sea. Global Biogeochemical Cycles, 20(3). https://doi.org/10.1029/2005GB002646.

Chavez, F.P., Messié, M., & Pennington, J.T., 2010. Marine primary production in relation to climate variability and change. https://doi.org/10.1146/annurev.marine.010908.163917.

Chen, R.F., Bada, J.L., 1992. The fluorescence of dissolved organic matter in seawater. Marine Chemistry, 37(3-4), 191-221. https://doi.org/10.1016/0304-4203(92)90078-O.

Chen, W., Westerhoff, P., Leenheer, J.A., Booksh, K., 2003. Fluorescence excitation−emission matrix regional integration to quantify spectra for dissolved organic matter. Environmental science & technology, 37(24), 5701-5710. https://doi.org/10.1021/es034354c.

Chen, Y., Paytan, A., Chase, Z., Measures, C., Beck, A.J., Sañudo-Wilhelmy, S.A., Post, A.F., 2008. Sources and fluxes of atmospheric trace elements to the Gulf of Aqaba, Red Sea, J. Geophys. Res. Atmos., 113(5), 1–13. https://doi.org/10.1029/2007JD009110.

Chester, R., Sharples, E.J., Sanders, G.S., Saydam, A.C., 1984. Saharan dust incursion over the Tyrrhenian Sea. Atmospheric Environment (1967), 18(5), 929-935. https://doi.org/10.1016/0004-6981(84)90069-6.

Chester, R., Keyse, S., Nimmo, M., 1996. The influence of Saharan and Middle Eastern desert-derived dust on the trace metal composition of Mediterranean aerosols and rainwaters: an overview. In The impact of desert dust across the Mediterranean (pp. 253-273). Springer, Dordrecht.

Chester, R., 2009. Marine geochemistry. John Wiley & Sons.

Church, M.J., Ducklow, H.W., Karl, D.M., 2002. Multiyear increases in dissolved organic matter inventories at Station ALOHA in the North Pacific Subtropical Gyre. Limnology and Oceanography, 47(1), 1-10. https://doi.org/10.4319/lo.2002.47.1.0001.

Christensen, J.P., Packard, T.T., Dortch, F.Q., Minas, H.J., Gascard, J.C., Richez, C., Garfield, P.C., 1989. Carbon oxidation in the deep Mediterranean Sea: evidence for dissolved organic carbon source. Global Biogeochemical Cycles, 3(4), 315-335. https://doi.org/10.1029/GB003i004p00315.

Claustre, H., Morel, A., Hooker, S.B., Babin, M., Antoine, D., Oubelkheir, K., Maritorena, S., 2002. Is desert dust making oligotrophic waters greener? Geophysical Research Letters 29(10), 107-1–107-4. https://doi.org/10.1029/2001GL014056.

Coble P.G., 1996. Characterization of marine and terrestrial DOM in seawater using excitation-emission matrix spectroscopy. Marine Chemistry 51, 325-346. https://doi.org/10.1016/0304-4203(95)00062-3.

Coble, P.G., 2007. Marine optical biogeochemistry: the chemistry of ocean color. Chemical reviews, 107(2), 402-418. https://doi.org/10.1021/cr050350+.

Coble, P.G., Lead, J., Baker, A., Reynolds, D. M., Spencer, R. G. (Eds.), 2014. Aquatic organic matter fluorescence. Cambridge University Press.

Crutzen, P.J., Stoermer, E.F., 2000. The “Anthropocene.” Global Change Newsletter 41, 17–18. International Geosphere–Biosphere Programme (IGBP).

Crutzen, P.J., 2006. The “anthropocene”. In Earth system science in the anthropocene (pp. 13-18). Springer, Berlin, Heidelberg.

D’Sa, E. J., Overton, E. B., Lohrenz, S. E., Maiti, K., Turner, R. E., & Freeman, A., 2016. Changing dynamics of dissolved organic matter fluorescence in the northern Gulf of Mexico following the Deepwater Horizon oil spill. Environmental science & technology, 50(10), 4940-4950. https://doi.org/ 10.1021/acs.est.5b04924.

D'Ortenzio, F., Iudicone, D., de Boyer Montegut, C., Testor, P., Antoine, D., Marullo, S., Santoleri, R., Madec, G., 2005. Seasonal variability of the mixed layer depth in the Mediterranean Sea as derived from in situ profiles. Geophysical Research Letters, 32(12). https://doi.org/10.1029/2005GL022463.

D'Ortenzio, F., Ribera d'Alcalà, M., 2009. On the trophic regimes of the Mediterranean Sea: a satellite analysis. Biogeosciences, 6(2), 139-148. https://doi.org/10.5194/bg-6-139-2009.

Dai, M., Yin, Z., Meng, F., Liu, Q., Cai, W.J., 2012. Spatial distribution of riverine DOC inputs to the ocean: An updated global synthesis. Curr. Opin. Environ. Sustain. 4(2), 170-178. https://doi.org/10.1016/j.cosust.2012.03.003.

Dat, N.D., Chang, M.B., 2017. Review on characteristics of PAHs in atmosphere, anthropogenic sources and control technologies. Science of the Total Environment, 609, 682-693. https://doi.org/10.1016/j.scitotenv.2017.07.204.

de Leeuw, G., Guieu, C., Arneth, A., Bellouin, N., Bopp, L., Boyd, P.W., Denier van der Gon, H.A.C., Desboeufs, K.V., Dulac, F., Facchini, M.C., Gantt, B., Langmann, B., Mahowald, N.M., Marañón E., O’Dowd, C., Olgun, N., Pulido-Villena, E., Rinaldi, M., Stephanou, E.G., Wagener, T., 2014. Ocean–Atmosphere Interactions of Particles. In: Liss P., Johnson M. (eds) Ocean-Atmosphere Interactions of Gases and Particles. Springer Earth System Sciences. Springer, Berlin, Heidelberg. https://doi.org/10.1007/978-3-642-25643-1_4.

De Vicente, I., Ortega-Retuerta, E., Morales-Baquero, R., Reche, I., 2012. Contribution of dust inputs to dissolved organic carbon and water transparency in Mediterranean reservoirs. Biogeosciences 9, 5049-5060. https://doi.org/10.5194/bg-9-5049-2012.

Del Vecchio, R., Blough, N.V., 2004. Spatial and seasonal distribution of chromophoric dissolved organic matter and dissolved organic carbon in the Middle Atlantic Bight. Marine Chemistry, 89(1-4), 169-187. https://doi.org/10.1016/j.marchem.2004.02.027.

Decina, S.M., Templer, P.H., Hutyra, L.R., 2018. Atmospheric Inputs of Nitrogen, Carbon, and Phosphorus across an Urban Area: Unaccounted Fluxes and Canopy Influences. Earth's Future, 6(2), 134-148. https://doi.org/10.1002/2017EF000653.

Després V.R., Huffman J.A., Burrows S.M., Hoose C., Safatov A.S., Buryak G., Fröhlich-Nowoisky J., Elbert W., Andreae M.O., Pöschl U., Jaenicke R., 2012. Primary biological aerosol particles in the atmosphere: a review, Tellus 64, 15598. https://doi.org/10.3402/tellusb.v64i0.15598.

di Sarra, A., Di Biagio, C., Meloni, D., Monteleone, F., Pace, G., Pugnaghi, S., Sferlazzo, D., 2011. Shortwave and longwave radiative effects of the intense Saharan dust event of 25–26 March 2010 at Lampedusa (Mediterranean Sea). Journal of Geophysical Research: Atmospheres, 116(D23). https://doi.org/10.1029/2011JD016238.

di Sarra, A., Sferlazzo, D., Meloni, D., Anello, F., Bommarito, C., Corradini, S., De Silvestri, L., Di Iorio, T., Monteleone, F., Pace, G., Piacentino, S., Pugnaghi, S., 2015. Empirical correction of multifilter rotating shadowband radiometer (MFRSR) aerosol optical depths for the aerosol forward scattering and development of a long-term integrated MFRSR-Cimel dataset at Lampedusa. Applied optics, 54(10), 2725-2737. https://doi.org/10.1364/AO.54.002725.

Dinar, E., Riziq, A.A., Spindler, C., Erlick, C., Kiss, G., Rudich, Y., 2008. The complex refractive index of atmospheric and model humic-like substances (HULIS) retrieved by a cavity ring down aerosol spectrometer (CRD-AS). Faraday Discussions, 137, 279-295.

Dittmar, T., Paeng, J., 2009. A heat-induced molecular signature in marine dissolved organic matter. Nature Geoscience, 2(3), 175. https://doi.org/10.1038/ngeo440.

Djaoudi, K., Van Wambeke, F., Barani, A., Hélias-Nunige, S., Sempéré, R., Pulido-Villena, E., 2018. Atmospheric fluxes of soluble organic C, N, and P to the Mediterranean Sea: Potential biogeochemical implications in the surface layer. Progress in Oceanography, 163, 59-69. https://doi.org/10.1016/j.pocean.2017.07.008.Draxler, R.R., Rolph, G.D., 2003. HYSPLIT (HYbrid single-particle Lagrangian integrated trajectory) model access via NOAA ARL READY. NOAA Air Resources Laboratory, Silver Spring, MD. Dostupno na: http://ready. arl. noaa. gov/HYSPLIT. php (06. 06. 2010.).

Duarte, R.M., Santos, E.B., Pio, C.A., Duarte, A.C., 2007. Comparison of structural features of water-soluble organic matter from atmospheric aerosols with those of aquatic humic substances. Atmospheric Environment, 41(37), 8100-8113. https://doi.org/10.1016/j.atmosenv.2007.06.034.

Duce, R.A., 1986. The impact of atmospheric nitrogen, phosphorus, and iron species on marine biological productivity. In The role of air-sea exchange in geochemical cycling (pp. 497-529). Springer, Dordrecht.

Duce, R.A., Liss, P.S., Merrill, J.T., Atlas, E.L., Buat-Menard, P., Hicks, B.B., Miller, J.M., Prospero, J.M., Arimoto, R., Church, T.M., Ellis, W., Galloway, J.N., Hansen, L., Jickells, T.D., Knap, A.H., Reinhardt, K.H., Schneider, B., Soudine, A., Tokos, J.J., Tsunogai, S., Wollast, R., Zhou, M., 1991. The atmospheric input of trace species to the world ocean. Global biogeochemical cycles, 5(3), 193-259. https://doi.org/10.1029/91GB01778.

Duce, R.A., LaRoche, J., Altieri, K., Arrigo, K.R., Baker, A.R., Capone, D.G., Cornell, S., Geider, R. J., Dentener, F., Galloway, J., Ganeshram, R.S., Geider, C.M., Jickells, T.D., Kuypers, M.M., Langlois, R., Liss, P.S., Liu, S.M., Middelburg, J.J., Moore, C.M., Nickovic, S., Oschlies, A., Pedersen, T., Prospero, J., Schlitzer, R., Seitzinger, S., Sorensen, L.L., Uematsu, M., Ulloa, O., Voss, M., Ward, B., Zamora, L., 2008. Impacts of atmospheric anthropogenic nitrogen on the open ocean. science, 320(5878), 893-897. https://doi.org/10.1126/science.1150369.

Ducklow, H.W., Carlson, C.A., Bates, N.R., Knap, A.H., Michaels, A.F., 1995. Dissolved organic carbon as a component of the biological pump in the North Atlantic Ocean. Phil. Trans. R. Soc. Lond. B, 348(1324), 161-167. https://doi.org/10.1098/rstb.1995.0058.

Dunne, J.P., Sarmiento, J.L., Gnanadesikan, A., 2007. A synthesis of global particle export from the surface ocean and cycling through the ocean interior and on the

seafloor. Global Biogeochemical Cycles, 21(4). https://doi.org/10.1029/2006GB002907.
Dzierzbicka-Glowacka, L., Zmijewska, I. M., Mudrak, S., Jakacki, J., Lemieszek, A., 2010. Population modelling of Acartia spp. in a water column ecosystem model for the South-Eastern Baltic Sea. Biogeosciences, 7(7), 2247. https://doi.org/10.5194/bg-7-2247-2010.
Economou, C., Mihalopoulos, N., 2002. Formaldehyde in the rainwater in the eastern Mediterranean: occurrence, deposition and contribution to organic carbon budget. Atmospheric Environment 36(8), 1337-1347. https://doi.org/10.1016/S1352-2310(01)00555-6.
Eyring, V., Köhler, H.W., Van Aardenne, J., Lauer, A., 2005. Emissions from international shipping: 1. The last 50 years. Journal of Geophysical Research: Atmospheres, 110(D17). https://doi.org/10.1029/2004JD005619.
Elderfield, H., 2002. Carbonate mysteries. Science, 296(5573), 1618-1621. https://doi.org/10.1126/science.1072079.
Ellis, E., Maslin, M., Boivin, N., Bauer, A., 2016. Involve social scientists in defining the Anthropocene. Nature News, 540(7632), 192. https://doi.org/10.1038/540192a.
Emerson, S., Hedges, J., 2008. Chemical oceanography and the marine carbon cycle. Cambridge University Press.
Escudero, M., Stein, A., Draxler, R.R., Querol, X., Alastuey, A., Castillo, S., Avila, A., 2006. Determination of the contribution of northern Africa dust source areas to PM10 concentrations over the central Iberian Peninsula using the Hybrid Single-Particle Lagrangian Integrated Trajectory model (HYSPLIT) model. Journal of Geophysical Research: Atmospheres, 111(D6). https://doi.org/10.1029/2005JD006395.
Escudero, M., Stein, A. F., Draxler, R.R., Querol, X., Alastuey, A., Castillo, S., Avila, A., 2011. Source apportionment for African dust outbreaks over the Western Mediterranean using the HYSPLIT model. Atmospheric Research, 99(3-4), 518-527. https://doi.org/10.1016/j.atmosres.2010.12.002.
Facchini, M.C., Decesari, S., Mircea, M., Fuzzi, S., Loglio, G., 2000. Surface tension of atmospheric wet aerosol and cloud/fog droplets in relation to their organic carbon content and chemical composition. Atmospheric Environment, 34(28), 4853-4857. https://doi.org/10.1016/S1352-2310(00)00237-5.
Falkovich, A.H., Ganor, E., Levin, Z., Formenti, P., Rudich, Y., 2001. Chemical and mineralogical analysis of individual mineral dust particles. Journal of Geophysical Research: Atmospheres, 106(D16), 18029-18036. https://doi.org/10.1029/2000JD900430.
Falkowski, P.G., Barber, R.T., Smetacek, V., 1998. Biogeochemical controls and feedbacks on ocean primary production. Science, 281(5374), 200-206. https://doi.org/ 10.1126/science.281.5374.200.
Fasham, M.J.R., Balino, B.M., Bowles, C.(Editors), 2001. A new vision of ocean biogeochemistry after a decade of the Joint Global Ocean Flux Study (JGOFS). Ambio Special Report 10,May 2001, pp.4–31.
Feely, R.A., Sabine, C.L., Lee, K., Berelson, W., Kleypas, J., Fabry, V.J., Millero, F.J., 2004. Impact of anthropogenic CO_2 on the $CaCO_3$ system in the oceans. Science, 305(5682), 362-366. https://doi.org/10.1126/science.1097329.
Ferretto, N., Tedetti, M., Guigue, C., Mounier, S., Redon, R., Goutx, M., 2014. Identification and quantification of known polycyclic aromatic hydrocarbons and pesticides in complex mixtures using fluorescence excitation–emission matrices and parallel factor analysis. Chemosphere 107, 344-353. https://doi.org/10.1016/j.chemosphere.2013.12.087.
Fichot, C.G., Benner, R. 2012. The spectral slope coefficient of chromophoric dissolved organic matter (S275-295) as a tracer of terrigenous dissolved organic carbon in river-influenced ocean margins. Limnology and Oceanography 57, 1453-1466. https://doi.org/10.4319/lo.2012.57.5.1453.

Floge, S.A., Wells, M.L., 2007. Variation in colloidal chromophoric dissolved organic matter in the Damariscotta Estuary, Maine. Limnology and oceanography, 52(1), 32-45. https://doi.org/10.4319/lo.2007.52.1.0032.

Formenti, P., Elbert, W., Maenhaut, W., Haywood, J., Osborne, S., Andreae, M.O., 2003. Inorganic and carbonaceous aerosols during the Southern African Regional Science Initiative (SAFARI 2000) experiment: Chemical characteristics, physical properties, and emission data for smoke from African biomass burning. Journal of Geophysical Research: Atmospheres, 108(D13). https://doi.org/10.1029/2002JD002408.

Freudenthal, T., Wagner, T., Wenzhöfer, F., Zabel, M., & Wefer, G., 2001. Early diagenesis of organic matter from sediments of the eastern subtropical Atlantic: evidence from stable nitrogen and carbon isotopes. Geochimica et Cosmochimica Acta, 65(11), 1795-1808. https://doi.org/10.1016/S0016-7037(01)00554-3.

Fu, P.Q., Kawamura, K., Chen, J., Charrière, B., Sempéré, R., 2013. Organic molecular composition of marine aerosols over the Arctic Ocean in summer: contributions of primary emission and secondary aerosol formation. Biogeosciences, 10(2), 653-667. https://doi.org/10.5194/bg-10-653-2013.

Fu, P., Kawamura, K., Chen, J., Qin, M., Ren, L., Sun, Y., Wang, Z., Barrie, L.A., Tachibana, E., Ding, A., Yamashita, Y., 2015. Fluorescent water-soluble organic aerosols in the High Arctic atmosphere. Scientific reports, 5, 9845.

Gachon, C.M., Küpper, H., Küpper, F.C., Šetlík, I., 2006. Single-cell chlorophyll fluorescence kinetic microscopy of Pylaiella littoralis (Phaeophyceae) infected by Chytridium polysiphoniae (Chytridiomycota). European Journal of Phycology, 41(4), 395-403. https://doi.org/10.1080/09670260600960918.

Gallisai, R., Peters, F., Volpe, G., Basart, S., Baldasano, J.M., 2014. Saharan dust deposition may affect phytoplankton growth in the Mediterranean Sea at ecological time scales. PloS one, 9(10), e110762. https://doi.org/10.1371/journal.pone.0110762.

Garbe, C.S., Rutgersson, A., Boutin, J., De Leeuw, G., Delille, B., Fairall, C.W., Gruber, N., Hare, J., Ho, D.T., Johnson, M.T., Nightingale, P.D., Pettersson, H., Piskozub, J., Sahlée, E., Tsai, W.T., Ward, B., Woolf, D.K., Zappa, C.J., 2014. Transfer across the air-sea interface. In Ocean-Atmosphere interactions of gases and particles (pp. 55-112). Springer, Berlin, Heidelberg.

Garcia, H.E., Gordon, L.I., 1992. Oxygen Solubility in Seawater: Better Fitting Equations. Limnology and Oceanography 37(6):1307–12. https://doi.org/10.4319/lo.1992.37.6.1307.

Gardner, W.D., Mishonov, A.V., & Richardson, M.J., 2006. Global POC concentrations from in-situ and satellite data. Deep Sea Research Part II: Topical Studies in Oceanography, 53(5-7), 718-740. https://doi.org/10.1016/j.dsr2.2006.01.029.

Genin, A., Lazar, B., Brenner, S., 1995. Vertical mixing and coral death in the Red Sea following the eruption of Mount Pinatubo. Nature, 377(6549), 507. https://doi.org. 10.1038/377507a0.

Gentry-Shields, J., Wang, A., Cory, R.M., Stewart, J.R., 2013. Determination of specific types and relative levels of QPCR inhibitors in environmental water samples using excitation–emission matrix spectroscopy and PARAFAC. Water research, 47(10), 3467-3476. https://doi.org/10.1016/j.watres.2013.03.049.

Ginoux, P., Prospero, J. M., Gill, T.E., Hsu, N.C., Zhao, M., 2012. Global-scale attribution of anthropogenic and natural dust sources and their emission rates based on MODIS Deep Blue aerosol products. Reviews of Geophysics, 50(3). https://doi.org/10.1029/2012RG000388.

Giovagnetti V., Brunet C., Conversano F., Tramontano F., Obernosterer I., Ridame C., Guieu C., 2013. Assessing the role of dust deposition on phytoplankton ecophysiology and succession in a low-nutrient low-chlorophyll ecosystem: a mesocosm experiment in the Mediterranean Sea. Biogeosciences, 10: 2973-2991. https://doi.org/10.5194/bg-10-2973-2013.

Goldberg, S.J., C.A. Carlson, D.A. Hansell, N.B. Nelson, and D.A. Siegel. 2009. Temporal dynamics of dissolved combined neutral sugars and the quality of dissolved organic

matter in the northwestern Sargasso Sea. Deep Sea Research Part I 56:672–685. https://doi.org/10.1016/j.dsr.2008.12.013.
Gonnelli, M., Galletti, Y., Marchetti, E., Mercadante, L., Brogi, S.R., Ribotti, A., Sorgente, R., Vestri, S., Santinelli, C., 2016. Dissolved organic matter dynamics in surface waters affected by oil spill pollution: Results from the Serious Game exercise. Deep Sea Research Part II: Topical Studies in Oceanography 133, 88-99. https://doi.org/10.1016/j.dsr2.2016.05.027.
Goss, K.U., Schwarzenbach, R.P., 1999. Quantification of the effect of humidity on the gas/mineral oxide and gas/salt adsorption of organic compounds. Environmental science & technology, 33(22), 4073-4078. https://doi.org/10.1021/es990502g.
Graeber, D., Gelbrecht, J., Pusch, M. T., Anlanger, C., von Schiller, D., 2012. Agriculture has changed the amount and composition of dissolved organic matter in Central European headwater streams. Science of the Total Environment, 438, 435-446. https://doi.org/10.1016/j.scitotenv.2012.08.087.
Granskog, M.A., Nomura, D., Müller, S., Krell, A., Toyota, T., Hattori, H., 2015. Evidence for significant protein-like dissolved organic matter accumulation in Sea of Okhotsk sea ice. Annals of Glaciology, 56(69), 1-8. https://doi.org/10.3189/2015AoG69A002.
Green, S.A., Blough, N.V., 1994. Optical absorption and fluorescence properties of chromophoric dissolved organic matter in natural waters. Limnology and Oceanography, 39(8), 1903-1916. https://doi.org/10.4319/lo.1994.39.8.1903.
Grossart, H.P., Ploug, H., 2001. Microbial degradation of organic carbon and nitrogen on diatom aggregates. Limnology and oceanography, 46(2), 267-277. https://doi.org/10.4319/lo.2001.46.2.0267.
Guéguen, C., Cuss, C.W., 2011. Characterization of aquatic dissolved organic matter by asymmetrical flow field-flow fractionation coupled to UV–Visible diode array and excitation emission matrix fluorescence. Journal of Chromatography A, 1218(27), 4188-4198. https://doi.org/10.1016/j.chroma.2010.12.038.
Guéguen, C., Kowalczuk, P., 2013. Colored dissolved organic matter in frontal zones.
Guerzoni, S., Molinaroli, E., Chester, R., 1997. Saharan dust inputs to the western Mediterranean Sea: depositional patterns, geochemistry and sedimentological implications. Deep Sea Research Part II: Topical Studies in Oceanography, 44(3), 631-654. https://doi.org/10.1016/S0967-0645(96)00096-3.
Guerzoni, S., Chester, R., Dulac, F., Herut, B., Loÿe-Pilot, M. D., Measures, C., Migon, C., Molinaroli, E., Moulin, C., Rossini, P., Saydam, C., Soudine, A., Ziveri, P., 1999. The role of atmospheric deposition in the biogeochemistry of the Mediterranean Sea. Progress in Oceanography, 44(1), 147-190. https://doi.org/10.1016/S0079-6611(99)00024-5.
Guieu, C., Thomas, A.J., 1996. Saharan aerosols: From the soil to the ocean. In The impact of desert dust across the Mediterranean (pp. 207-216). Springer, Dordrecht.
Guieu, C., Bozec, Y., Blain, S., Ridame, C., Sarthou, G., Leblond, N., 2002. Impact of high Saharan dust inputs on dissolved iron concentrations in the Mediterranean Sea. Geophysical Research Letters, 29(19). https://doi.org/10.1029/2001GL014454.
Guieu C., Aumont O., Paytan A., Bopp L., Law C.S., Mahowald N., Achterberg E.P., Marañón E., Salihoglu B., Crise A., Wagener T., Herut B., Desboeufs K., Kanakidou M., Olgun N., Peters F., Pulido-Villena E., Tovar-Sanchez A., Völker C., 2014. The significance of the episodic nature of atmospheric deposition to Low Nutrient Low Chlorophyll regions. Global Geochemical Cycles. https://doi.org/10.1002/2014GB004852.
Guitart, C., García-Flor, N., Miquel, J.C., Fowler, S.W., Albaigés, J., 2010. Effect of the accumulation of polycyclic aromatic hydrocarbons in the sea surface microlayer on their coastal air–sea exchanges. Journal of Marine Systems, 79(1-2), 210-217. https://doi.org/10.1016/j.jmarsys.2009.09.003.
Guo, W., He, M., Yang, Z., Lin, C., Quan, X., Wang, H., 2007. Distribution of polycyclic aromatic hydrocarbons in water, suspended particulate matter and sediment from Daliao River watershed, China. Chemosphere, 68(1), 93-104. https://doi.org/10.1016/j.chemosphere.2006.12.072.

Haas, A., El-Zibdah, M., Wild, C., 2010. Seasonal monitoring of coral–algae interactions in fringing reefs of the Gulf of Aqaba, Northern Red Sea. Coral Reefs, 29(1), 93-103.

Hallquist, M., Wenger, J.C., Baltensperger, U., Rudich, Y., Simpson, D., Claeys, M., Dommen, J., Donahue, N.M., George, C., Goldstein, A.H., Hamilton, J.F., Herrmann, H., Hoffmann, T., Iinuma, Y., Jang, M., Jenkin, M.E., Jimenez, J.L., Kiendler-Scharr, A., Maenhaut, W., McFiggans, G., Mentel, Th.F., Monod, A., Prévôt, A.S.H., Seinfeld, J.H., Surratt, J.D., Szmigielski, R., Wildt, J., 2009. The formation, properties and impact of secondary organic aerosol: current and emerging issues. Atmospheric chemistry and physics, 9(14), 5155-5236. https://doi.org/10.5194/acp-9-5155-2009.

Hansell, D.A., 2002. DOC in the global ocean carbon cycle, in: Hansell D.A, Carlson C.A. (Eds.), Biogeochemestry of Marine Dissolved Organic Matter (First edition), Academic Press, San Diego, pp. 685-714. https://doi.org/10.1016/B978-012323841-2/50017-8.

Hansell, D.A., 2005. Dissolved organic carbon reference material program. Eos, Transactions American Geophysical Union 86(35), 318-318. https://doi.org/10.1029/2005EO350003.

Hansell, D.A., Carlson, C.A., Repeta, D.J., Schlitzer, R. 2009. Dissolved organic matter in the ocean: A controversy stimulates new insights. Oceanography, 22(4), 202-211.

Hansell, D.A., 2013. Recalcitrant dissolved organic carbon fractions. Annual Review of Marine Science 5 (2013), 421-445. https://doi.org/10.1146/annurev-marine-120710-100757.

Hansell, D.A., Carlson, C.A., 2013. Localized refractory dissolved organic carbon sinks in the deep ocean. Global Biogeochemical Cycles 27(3), 705-710. https://doi.org/10.1002/gbc.20067.

Hayase, K., Shinozuka, N., 1995. Vertical distribution of fluorescent organic matter along with AOU and nutrients in the equatorial Central Pacific. Marine Chemistry, 48(3-4), 283-290. https://doi.org/10.1016/0304-4203(94)00051-E.

Havers, N., Burba, P., Lambert, J., Klockow, D., 1998. Spectroscopic characterization of humic-like substances in airborne particulate matter. Journal of Atmospheric Chemistry, 29(1), 45-54.

Hedges, J.I., Keil, R.G., Benner, R., 1997. What happens to terrestrial organic matter in the ocean?. Organic geochemistry, 27(5-6), 195-212. https://doi.org/10.1016/S0146-6380(97)00066-1.

Hedges, J.I., 2002. Why dissolved organics matter. Biogeochemistry of marine dissolved organic matter, 1-33.

Helms, J.R., Stubbins, A., Ritchie, J.D., Minor, E.C., Kieber, D.J., Mopper, K., 2008. Absorption spectral slopes and slope ratios as indicators of molecular weight, source, and photobleaching of chromophoric dissolved organic matter. Limnology and Oceanography 53(3), 955-969. https://doi.org/10.4319/lo.2008.53.3.0955.

Hertkorn, N., Benner, R., Frommberger, M., Schmitt-Kopplin, P., Witt, M., Kaiser, K., Kettrup, A., Hedges, J.I., 2006. Characterization of a major refractory component of marine dissolved organic matter. Geochimica et Cosmochimica Acta, 70(12), 2990-3010. https://doi.org/10.1016/j.gca.2006.03.021.

Herut, B., Krom, M.D., Pan, G., & Mortimer, R., 1999. Atmospheric input of nitrogen and phosphorus to the Southeast Mediterranean: Sources, fluxes, and possible impact. Limnology and Oceanography, 44(7), 1683-1692. https://doi.org/10.4319/lo.1999.44.7.1683.

Herut B., Collier R., Krom M.D., 2002. The role of dust in supplying nitrogen and phosphorus to the South East Mediterranean. Limnology and Oceanography, 47:870-878. https://doi.org/10.4319/lo.2002.47.3.0870.

Herut, B., Rahav, E., Tsagaraki, T.M., Giannakourou, A., Tsiola, A., Psarra, S., Lagaria, A., Papageorgiou, N., Mihalopoulos, N., Theodosi, C.N., Violaki, K., Stathopoulou, E., Scoullos, M., Krom, M.D., Stockdale, A., Shi, Z., Berman-Frank, I., Meador, T.B., Tanaka, T., Paraskevi, Pi., 2016. The potential impact of Saharan dust and polluted aerosols on microbial populations in the east Mediterranean Sea, an overview of a

mesocosm experimental approach, Front. Mar. Sci., 3, 1–16. https://doi.org/10.3389/fmars.2016.00226.
Honjo, S., Manganini, S.J., Krishfield, R.A., & Francois, R., 2008. Particulate organic carbon fluxes to the ocean interior and factors controlling the biological pump: A synthesis of global sediment trap programs since 1983. Progress in Oceanography, 76(3), 217-285. https://doi.org/10.1016/j.pocean.2007.11.003.
Hopkinson Jr, C.S., Vallino, J.J., 2005. Efficient export of carbon to the deep ocean through dissolved organic matter. Nature, 433(7022), 142. https://doi.org/ 10.1038/nature03191.
Hutchins, D.A., Boyd, P.W., 2016. Marine phytoplankton and the changing ocean iron cycle. Nature Climate Change, 6(12), 1072. https://doi.org/10.1038/nclimate3147.
Iavorivska, L., Boyer, E.W., DeWalle, D.R., 2016. Atmospheric deposition of organic carbon via precipitation. Atmospheric Environment, 146, 153-163. https://doi.org/10.1016/j.atmosenv.2016.06.006.
IPCC, 2014: Climate Change 2014: Synthesis Report. Contribution of Working Groups I, II and III to the Fifth Assessment Report of the Intergovernmental Panel on Climate Change [Core Writing Team, R.K. Pachauri and L.A. Meyer (eds.)]. IPCC, Geneva, Switzerland, 151 pp. https://doi.org/10013/epic.45156.d001.
Jiao, N., Herndl, G. J., Hansell, D. A., Benner, R., Kattner, G., Wilhelm, S.W., Kirchman, D.L., Weinbauer M.G., Luo, T., Chen, F., Azam, F., 2010. Microbial production of recalcitrant dissolved organic matter: long-term carbon storage in the global ocean. Nature Reviews Microbiology, 8(8), 593. https://doi.org/10.1038/nrmicro2386.
Jiao, N., Herndl, G.J., Hansell, D.A., Benner, R., Kattner, G., Wilhelm, S.W., Kirchman, D.L., Weinbauer M.G., Luo, T., Chen, F., Azam, F., 2011. The microbial carbon pump and the oceanic recalcitrant dissolved organic matter pool. Nature Reviews Microbiology, 9(7), 555. https://doi.org/10.1038/nrmicro2386-c5.
Jiao, N., Azam, F., 2011. Microbial carbon pump and its significance for carbon sequestration in the ocean. Microbial Carbon Pump in the Ocean, 10, 43-45.
Jiao, N., Robinson, C., Azam, F., Thomas, H., Baltar, F., Dang, H., Hardman-Mountford, N.J., Johnson, M., Kirchman, D.L., Koch, B.P., Legendre, L., Li, C., Liu, J., Luo, T., Luo, Y.W., Mitra, A., Romanou, A., Tang, K., Wang, X., Zhang, C., Zhang, R., 2014. Mechanisms of microbial carbon sequestration in the ocean–future research directions. Biogeosciences, 11(19), 5285-5306. https://doi.org/10.5194/bg-11-5285-2014.
Jickells, T.D., 2005. External inputs as a contributor to eutrophication problems. Journal of Sea Research, 54(1), 58-69. https://doi.org/10.1016/j.seares.2005.02.006.
Jickells, T.D., An, Z.S., Andersen, K.K., Baker, A.R., Bergametti, G., Brooks, N., Cao, J.J., Boyd, P.W., Duce, R.A., Hunter, K.A., Kawahata, H., Kubilay, N., laRoche, J., Liss, P.S., Mahowald, N., Prospero, J.M., Ridgwell, A.J., Tegen, I., Torres, R., 2005. Global iron connections between desert dust, ocean biogeochemistry, and climate. science, 308(5718), 67-71. https://doi.org/10.1126/science.1105959.
Jickells, T., Moore, C.M., 2015. The importance of atmospheric deposition for ocean productivity. Annual Review of Ecology, Evolution, and Systematics, 46, 481-501. https://doi.org/10.1146/annurev-ecolsys-112414-054118
Jickells, T.D., Buitenhuis, E., Altieri, K., Baker, A.R., Capone, D., Duce, R.A., Dentener, F., Fennel, K., Kanakidou, M., LaRoche, J., Lee, K., Liss, P., Middelburg, J.J., Moore, J.K., Okin, G., Oschlies, A., Sarin, M., Seitzinger, S., Sharples, J., Singh, A., Suntharalingam, P., Uematsu, M., Zamora, L.M., 2017. A reevaluation of the magnitude and impacts of anthropogenic atmospheric nitrogen inputs on the ocean. Global Biogeochemical Cycles, 31(2), 289-305. https://doi.org/10.1002/2016GB005586.
Jish Prakash, P., Stenchikov, G., Kalenderski, S., Osipov, S., Bangalath H., 2015. The impact of dust storms on the Arabian Peninsula and the Red Sea, Atmos. Chem. Phys., 15(1), 199–222, https://doi.org/10.5194/acp-15-199-2015.
Jordi A., Basterretxea G., Tovar-Sanchez A., Alastuey A., Querol X., 2012. Copper aerosols inhibit phytoplankton growth in the Mediterranean Sea. Proceedings of the

National Academy of Sciences of the United States of America, 109:21246-21249. https://doi.org/10.1073/pnas.1207567110.
Jørgensen, L., Stedmon, C.A., Kragh, T., Markager, S., Middelboe, M., Søndergaard, M., 2011. Global trends in the fluorescence characteristics and distribution of marine dissolved organic matter. Marine Chemistry 126, 139-148. https://doi.org/10.1016/j.marchem.2011.05.002.
Jørgensen, L., Stedmon, C.A., Granskog, M.A., Middelboe, M., 2014. Tracing the long-term microbial production of recalcitrant fluorescent dissolved organic matter in seawater. Geophysical Research Letters, 41(7), 2481-2488. https://doi.org/10.1002/2014GL059428.
Jurado, E., Dachs, J., Duarte, C. M., Simo, R., 2008. Atmospheric deposition of organic and black carbon to the global oceans. Atmospheric Environment, 42(34), 7931-7939. https://doi.org/10.1016/j.atmosenv.2008.07.029.
Kanakidou, M., Seinfeld, J.H., Pandis, S.N., Barnes, I., Dentener, F. J., Facchini, M.C., Van Dingenen, R., Ervens, B., Nenes, A., Nielsen, C.J., Swietlicki, E., Putaud, J.P., Balkanski, Y., Fuzzi, S., Horth, J., Moortgat, G.K., Winterhalter, R., Myhre, C.E.L., Tsigaridis, K., Vignati, E., Stephanou, E.G., Wilson, J., 2005. Organic aerosol and global climate modelling: a review. Atmospheric Chemistry and Physics, 5(4), 1053-1123.
Kanakidou, M., Duce, R.A., Prospero, J.M., Baker, A.R., Benitez-Nelson, C., Dentener, F.J., Hunter, K.A., Liss, P.S., Mahowald, N., Okin, G.S., Sarin, M., Tsigaridis, K., Uematsu, M., Zamora, L.M., Zhu, T., 2012. Atmospheric fluxes of organic N and P to the global ocean. Global Biogeochemical Cycles 26(3). https://doi.org/10.1029/2011GB004277.
Karl, D.M., Björkman, K.M., 2015. Dynamics of dissolved organic phosphorus. In Biogeochemistry of Marine Dissolved Organic Matter (Second Edition) (pp. 233-334). https://doi.org/10.1016/B978-0-12-405940-5.00005-4.
Kieber, R.J., Whitehead, R.F., Reid, S.N., Willey, J.D., Seaton, P.J., 2006. Chromophoric dissolved organic matter (CDOM) in rainwater, southeastern North Carolina, USA. Journal of Atmospheric Chemistry, 54(1), 21-41.
Kieber, R.J., Willey, J.D., Whitehead, R.F., Reid, S.N., 2007. Photobleaching of chromophoric dissolved organic matter (CDOM) in rainwater. Journal of Atmospheric Chemistry, 58(3), 219-235.
Kim, K.H., Jahan, S.A., Kabir, E., Brown, R.J., 2013. A review of airborne polycyclic aromatic hydrocarbons (PAHs) and their human health effects. Environment international, 60, 71-80. https://doi.org/10.1016/j.envint.2013.07.019.
Kiss, G., Tombácz, E., Hansson, H.C., 2005. Surface tension effects of humic-like substances in the aqueous extract of tropospheric fine aerosol. Journal of Atmospheric Chemistry, 50(3), 279-294.
Klein Goldewijk, K., Beusen, A., Van Drecht, G., De Vos, M., 2011. The HYDE 3.1 spatially explicit database of human-induced global land-use change over the past 12,000 years. Global Ecology and Biogeography, 20(1), 73-86. https://doi.org/10.1111/j.1466-8238.2010.00587.x.
Korak, J.A., Dotson, A.D., Summers, R.S., Rosario-Ortiz, F.L., 2014. Critical analysis of commonly used fluorescence metrics to characterize dissolved organic matter. Water research, 49, 327-338. https://doi.org/10.1016/j.watres.2013.11.025.
Koulouri, E., Saarikoski, S., Theodosi, C., Markaki, Z., Gerasopoulos, E., Kouvarakis, G., Makela, T., Hillamo, R., Mihalopoulos, N., 2008. Chemical composition and sources of fine and coarse aerosol particles in the Eastern Mediterranean. Atmospheric Environment, 42(26), 6542-6550. https://doi.org/10.1016/j.atmosenv.2008.04.010.
Kowalczuk, P., Durako, M.J., Young, H., Kahn, A.E., Cooper, W.J., Gonsior, M., 2009. Characterization of dissolved organic matter fluorescence in the South Atlantic Bight with use of PARAFAC model: Interannual variability. Marine Chemistry 113, 182-196. https://doi.org/10.1016/j.marchem.2009.01.015
Kowalczuk, P., Tilstone, G.H., Zabłocka, M., Röttgers, R., Thomas, R., 2013. Composition of dissolved organic matter along an Atlantic Meridional Transect from fluorescence

spectroscopy and Parallel Factor Analysis. Marine Chemistry, 157, 170-184. https://doi.org/10.1016/j.marchem.2013.10.004.

Kress, N., Herut, B., 2001. Spatial and seasonal evolution of dissolved oxygen and nutrients in the Southern Levantine Basin (Eastern Mediterranean Sea): chemical characterization of the water masses and inferences on the N: P ratios. Deep Sea Research Part I: Oceanographic Research Papers, 48(11), 2347-2372. https://doi.org/10.1016/S0967-0637(01)00022-X.

Krishnamurthy, A., Moore, J.K., Mahowald, N., Luo, C., Zender, C.S., 2010. Impacts of atmospheric nutrient inputs on marine biogeochemistry. Journal of Geophysical Research: Biogeosciences, 115(G1). https://doi.org/10.1029/2009JG001115.

Krom, M.D., Kress, N., Brenner, S., Gordon, L.I., 1991. Phosphorus limitation of primary productivity in the eastern Mediterranean Sea. Limnology and Oceanography, 36(3), 424-432. https://doi.org/10.4319/lo.1991.36.3.0424.

Krom, M.D., Cliff, R.A., Eijsink, L. M., Herut, B., Chester, R., 1999. The characterisation of Saharan dusts and Nile particulate matter in surface sediments from the Levantine basin using Sr isotopes. Marine Geology, 155(3-4), 319-330. https://doi.org/10.1016/S0025-3227(98)00130-3.

Krom, M.D., Herut, B., Mantoura, R.F.C., 2004. Nutrient budget for the Eastern Mediterranean: Implications for phosphorus limitation. Limnology and Oceanography, 49(5), 1582-1592. https://doi.org/10.4319/lo.2004.49.5.1582.

Krom, M.D., Woodward, E.M.S., Herut, B., Kress, N., Carbo, P., Mantoura, R.F.C., Spyres, G., Thingstad, T.F., Wassmann, P., Wexels-Riser, C., Kitidis, V., Law, C.S., Zodiatis, G., 2005. Nutrient cycling in the south east Levantine basin of the eastern Mediterranean: Results from a phosphorus starved system. Deep Sea Research Part II: Topical Studies in Oceanography, 52(22-23), 2879-2896. https://doi.org/10.1016/j.dsr2.2005.08.009.

Krom M.D., Shi Z., Stockdale A., Berman-Frank I., Giannakourou A., Herut B., Lagaria A., Papageorgiou N., Pitta P., Psarra S., Rahav E., Scoullos M., Stathopoulou E., Tsiola A., Tsagaraki, T.M., 2016. Response of the Eastern Mediterranean microbial ecosystem to dust and dust affected by acid processing in the atmosphere. Frontiers in Marine Science 3: 133. https://doi.org/10.3389/fmars.2016.00133.

Labiosa, R.G., Arrigo, K.R., Genin, A., Monismith, S.G., van Dijken, G., 2003. The interplay between upwelling and deep convective mixing in determining the seasonal phytoplankton dynamics in the Gulf of Aqaba: Evidence from SeaWiFS and MODIS. Limnology and oceanography, 48(6), 2355-2368. https://doi.org/10.4319/lo.2003.48.6.2355.

Lacowicz, J.R., 2006. Principles of Fluorescence Spectroscopy. Springer, Baltimore.

Lamarque, J. F., Bond, T. C., Eyring, V., Granier, C., Heil, A., Klimont, Z., Lee, D., Liousse, C., Mieville, A., Owen, B., Schultz, M.G., Shindell, D., Smith, S.J., Stehfest, E., Van Aardenne, J., Cooper, O.R., Kainuma, M., Mahowald, N., McConnell, J.R., Naik, V., Riahi, K., van Vuuren, D.P., 2010. Historical (1850–2000) gridded anthropogenic and biomass burning emissions of reactive gases and aerosols: methodology and application. Atmospheric Chemistry and Physics, 10(15), 7017-7039. https://doi.org/10.5194/acp-10-7017-2010.

Lambert, T., Teodoru, C. R., Nyoni, F. C., Bouillon, S., Darchambeau, F., Massicotte, P., Borges, A.V., 2016. Along-stream transport and transformation of dissolved organic matter in a large tropical river. Biogeosciences, 13(9), 2727. https://doi.org/10.5194/bg-13-2727-2016.

Law, B., 2013. Biogeochemistry: nitrogen deposition and forest carbon. Nature, 496(7445), 307.

Lawaetz, A.J., Stedmon, C.A., 2009. Fluorescence intensity calibration using the Raman scatter peak of water. Applied spectroscopy 63(8), 936-940. https://doi.org/10.1366/000370209788964548.

Leck C., Bigg E., 2008. Comparison of sources and nature of the tropical aerosol with the summer high Arctic aerosol. Tellus B, 60:118-126. https://doi.org/10.1111/j.1600-0889.2007.00315.x.

Lechtenfeld, O.J., Hertkorn, N., Shen, Y., Witt, M., Benner, R., 2015. Marine sequestration of carbon in bacterial metabolites. Nature communications, 6, 6711. https://doi.org/10.1038/ncomms7711.

Legendre, L., Rivkin, R.B., Weinbauer, M.G., Guidi, L., Uitz, J., 2015. The microbial carbon pump concept: Potential biogeochemical significance in the globally changing ocean. Progress in Oceanography, 134, 432-450. https://doi.org/10.1016/j.pocean.2015.01.008.

Lin, H., Guo, W., Hu, M., Lin, C., Ji, W., 2012. Spatial and temporal variability of colored dissolved organic matter absorption properties in the Taiwan Strait. Acta oceanologica sinica 31(5), 98-106. https://doi.org/10.1007/s13131-012-0240-x.

Lindell, D., Post, A.F., 1995. Ultraphytoplankton succession is triggered by deep winter mixing in the Gulf of Aqaba (Eilat), Red Sea. Limnology and Oceanography, 40(6), 1130-1141. https://doi.org/10.4319/lo.1995.40.6.1130.

Lis, H., Shaked, Y., 2009. Probing the bioavailability of organically bound iron: a case study in the Synechococcus-rich waters of the Gulf of Aqaba. Aquatic Microbial Ecology, 56(2-3), 241-253. https://doi.org/10.3354/ame01347.

Liu, F., Xu, Y., Liu, J., Liu, D., Li, J., Zhang, G., Li, X., Zou, S., Lai, S., 2013. Atmospheric deposition of polycyclic aromatic hydrocarbons (PAHs) to a coastal site of Hong Kong, South China. Atmospheric environment, 69, 265-272. https://doi.org/10.1016/j.atmosenv.2012.12.024.

Loh, X.J., Lee, T. C., Dou, Q., Deen, G.R., 2016. Utilising inorganic nanocarriers for gene delivery. Biomaterials science, 4(1), 70-86. https://doi.org. 10.1039/C5BM00277J.

Lomas, M.W., Burke, A.L., Lomas, D.A., Bell, D.W., Shen, C., Dyhrman, S.T., Ammerman, J.W., 2010. Sargasso Sea phosphorus biogeochemistry: an important role for dissolved organic phosphorus (DOP). Biogeosciences, 7(2), 695-710. https://doi.org/10.5194/bg-7-695-2010.

Lønborg, C., Yokokawa, T., Herndl, G.J., Álvarez-Salgado, X.A., 2015. Production and degradation of fluorescent dissolved organic matter in surface waters of the eastern north Atlantic ocean. Deep Sea Research Part I: Oceanographic Research Papers, 96, 28-37. https://doi.org/10.1016/j.dsr.2014.11.001.

Lord, N.S., Ridgwell, A., Thorne, M. C., Lunt, D. J., 2016. An impulse response function for the “long tail” of excess atmospheric CO2 in an Earth system model. Global Biogeochemical Cycles, 30(1), 2-17. https://doi.org/10.1002/2014GB005074.

Loÿe-Pilot, M.D., Martin, J.M., 1996. Saharan dust input to the western Mediterranean: an eleven years record in Corsica. In The impact of desert dust across the Mediterranean (pp. 191-199). Springer, Dordrecht.

Louis, J., Pedrotti, M.L., Gazeau, F., Guieu, C., 2017. Experimental evidence of formation of Transparent Exopolymer Particles (TEP) and POC export provoked by dust addition under current and high pCO2 conditions. PloS one, 12(2), e0171980. https://doi.org/10.1371/journal.pone.0171980.

Luna, G.M., 2015. Diversity of marine microbes in a changing Mediterranean Sea. Rend. Fis. Acc. Lincei 26, 49-58. https://doi.org/10.1007/s12210-014-0333-x.

Luo, C., Mahowald, N., Bond, T., Chuang, P. Y., Artaxo, P., Siefert, R., Chen, Y., Schauer, J., 2008. Combustion iron distribution and deposition. Global Biogeochemical Cycles, 22(1). https://doi.org/10.1029/2007GB002964.

Mahowald, N., Jickells, T. D., Baker, A. R., Artaxo, P., Benitez-Nelson, C. R., Bergametti, G., Bond, T.C., Chen, Y., Cohen, D.D., Herut, B., Kubilay, N., Losno, R., Luo, C., Maenhaut, W., McGee, K.A., Okin, G.S., Siefert, R.L., Tsukuda, S., 2008. Global distribution of atmospheric phosphorus sources, concentrations and deposition rates, and anthropogenic impacts. Global biogeochemical cycles, 22(4). https://doi.org/10.1029/2008GB003240.

Mahowald, N., 2011. Aerosol indirect effect on biogeochemical cycles and climate. Science, 334(6057), 794-796. https://doi.org/10.1126/science.1207374.

Mahowald, N., Albani, S., Kok, J. F., Engelstaeder, S., Scanza, R., Ward, D. S., & Flanner, M. G., 2014. The size distribution of desert dust aerosols and its impact on

the Earth system. Aeolian Research, 15, 53-71. https://doi.org/10.1016/j.aeolia.2013.09.002.
Maqbool, T., Cho, J., Hur, J., 2017. Spectroscopic descriptors for dynamic changes of soluble microbial products from activated sludge at different biomass growth phases under prolonged starvation. Water research, 123, 751-760. https://doi.org/10.1016/j.watres.2017.07.033.
Mannino, A., Harvey, H.R., 2000. Biochemical composition of particles and dissolved organic matter along an estuarine gradient: Sources and implications for DOM reactivity. Limnology and Oceanography, 45(4), 775-788. https://doi.org/10.4319/lo.2000.45.4.0775.
Manodori, L., Gambaro, A., Piazza, R., Ferrari, S., Stortini, A.M., Moret, I., Capodaglio, G., 2006. PCBs and PAHs in sea-surface microlayer and sub-surface water samples of the Venice Lagoon (Italy). Marine Pollution Bulletin, 52(2), 184-192. https://doi.org/10.1016/j.marpolbul.2005.08.017.
Maranon, E., Fernandez, A., Mourino-Carballido, B., Martinez-Garcia, S., Teira, E., Cermeno, P., Choucino, P., Huete-Ortega, M., Fernandez, E., Calvo-Diaz, A., Anxelu, X., Moran, G., Bode, A., Moreno-Ostos, E., Varela, M. M., Patey, M. D., and Achterberg, E. P., 2010. Degree of oligotrophy controls the response of microbial plankton to Saharan dust, Limnol. Oceanogr., 55, 2339–2352.
Marconi, M., Sferlazzo, D. M., Becagli, S., Bommarito, C., Calzolai, G., Chiari, M., di Sarra, A., Ghedini, C., Gómez-Amo, J.L., Lucarelli, F., Meloni, D., Monteleone, F., Nava, S., Pace, G., Piacentino, S., Rugi, F., Severi, M., Traversi, R., and Udisti, R., 2014. Saharan dust aerosol over the central Mediterranean Sea: PM10 chemical composition and concentration versus optical columnar measurements, Atmos. Chem. Phys., 14, 2039–2054. https://doi.org/10.5194/acp-14-2039-2014.
Margolin, A.R., Gerringa, L.J., Hansell, D.A., Rijkenberg, M.J., 2016. Net removal of dissolved organic carbon in the anoxic waters of the Black Sea. Marine Chemistry, 183, 13-24. https://doi.org/10.1016/j.marchem.2016.05.003.
Margolin, A.R., Gonnelli, M., Hansell, D.A., Santinelli, C., 2018. Black Sea dissolved organic matter dynamics: Insights from optical analyses. Limnology and Oceanography. https://doi.org/10.1002/lno.10791.
Markaki, Z., Oikonomou, K., Kocak, M., Kouvarakis, G., Chaniotaki, A., Kubilay, N., Mihalopoulos, N., 2003. Atmospheric deposition of inorganic phosphorus in the Levantine Basin, eastern Mediterranean: Spatial and temporal variability and its role in seawater productivity. Limnology and Oceanography, 48(4), 1557-1568. https://doi.org/10.4319/lo.2003.48.4.1557.
Markaki, Z., Loÿe-Pilot, M. D., Violaki, K., Benyahya, L., Mihalopoulos, N., 2010. Variability of atmospheric deposition of dissolved nitrogen and phosphorus in the Mediterranean and possible link to the anomalous seawater N/P ratio. Marine Chemistry, 120(1-4), 187-194. https://doi.org/10.1016/j.marchem.2008.10.005.
Martin, J.H., Gordon, M., Fitzwater, S.E., 1991. The case for iron. Limnology and Oceanography, 36(8), 1793-1802. https://doi.org/10.4319/lo.1991.36.8.1793.
Martínez-Pérez, A.M., Osterholz, H., Nieto-Cid, M., Álvarez, M., Dittmar, T., Álvarez-Salgado, X.A., 2017a. Molecular composition of dissolved organic matter in the Mediterranean Sea. Limnology and Oceanography, 62(6), 2699-2712. https://doi.org/10.1002/lno.10600.
Martínez-Pérez, A.M., Nieto-Cid, M., Osterholz, H., Catalá, T.S., Reche, I., Dittmar, T., Álvarez-Salgado, X.A., 2017b. Linking optical and molecular signatures of dissolved organic matter in the Mediterranean Sea. Scientific Reports, 7(1), 3436. https://doi.org/10.1038/s41598-017-03735-4.
Mayol, E., Arrieta, J. M., Jiménez, M. A., Martínez-Asensio, A., Garcias-Bonet, N., Dachs, J., González-Gaya, B., Royer, S.-J., Benítez-Barrios, V.M., Fraile-Nuez, E., Duarte, C. M. (2017). Long-range transport of airborne microbes over the global tropical and subtropical ocean. Nature Communications, 8(1), 201.
Medeiros, P.M., Seidel, M., Ward, N.D., Carpenter, E.J., Gomes, H.R., Niggemann, J., Krusche, A.V., Richey, J.E., Yager, P.L., Dittmar, T., 2015. Fate of the Amazon

River dissolved organic matter in the tropical Atlantic Ocean. Global Biogeochemical Cycles, 29(5), 677-690. https://doi.org/10.1002/2015GB005115.

Meloni, D., Di Sarra, A., Di Iorio, T., Fiocco, G., 2005. Influence of the vertical profile of Saharan dust on the visible direct radiative forcing. Journal of Quantitative Spectroscopy and Radiative Transfer, 93(4), 397-413. https://doi.org/10.1016/j.jqsrt.2004.08.035.

Meloni, D., Di Sarra, A., Monteleone, F., Pace, G., Piacentino, S., Sferlazzo, D.M., 2008. Seasonal transport patterns of intense Saharan dust events at the Mediterranean island of Lampedusa. Atmospheric Research, 88(2), 134-148. https://doi.org/10.1016/j.atmosres.2007.10.007.

Meloni, D., Di Biagio, C., Di Sarra, A., Monteleone, F., Pace, G., Sferlazzo, D.M., 2012. Accounting for the solar radiation influence on downward longwave irradiance measurements by pyrgeometers. Journal of Atmospheric and Oceanic Technology, 29(11), 1629-1643. https://doi.org/10.1175/JTECH-D-11-00216.1.

Meloni, D., Junkermann, W., Sarra, A., Cacciani, M., De Silvestri, L., Di Iorio, T., Estellés, V., Gómez-Amo, J.L., Sferlazzo, D.M., 2015. Altitude-resolved shortwave and longwave radiative effects of desert dust in the Mediterranean during the GAMARF campaign: Indications of a net daily cooling in the dust layer. Journal of Geophysical Research: Atmospheres, 120(8), 3386-3407. https://doi.org/10.1002/2014JD022312.

Meng, F., Dai, M., Cao, Z., Wu, K., Zhao, X., Li, X., Chen, J., Gan, J., 2017. Seasonal dynamics of dissolved organic carbon under complex circulation schemes on a large continental shelf: The Northern South China Sea. Journal of Geophysical Research: Oceans, 122(12), 9415-9428. https://doi.org/10.1002/2017JC013325.

Mermex group: White book of Mermex program, 2011. Progress in Oceanography, 91, 97-166. https://doi.org/10.1016/j.pocean.2011.02.003.

Middelboe, M., 2008. Microbial disease in the sea: effects of viruses on carbon and nutrient cycling (pp. 242-259). Princeton, NJ, USA: Princeton University Press.

Migon, C., Copin-Montegut, G., Elegant, L., Morelli, J., 1989. Atmospheric input of nutrients to the coastal Mediterranean area. Biogeochemical implications. Oceanologica acta. Paris, 12(2), 187-191.

Migon, C., Sandroni, V., 1999. Phosphorus in rainwater: Partitioning inputs and impact on the surface coastal ocean. Limnology and Oceanography, 44(4), 1160-1165. https://doi.org/10.4319/lo.1999.44.4.1160.

Mills M.M., Ridame C., Davey M., La Roche J., Geider R.J., 2004. Iron and phosphorus co-limit nitrogen fixation in the eastern tropical North Atlantic. Nature, 429:292-295. https://doi.org/10.1038/nature02550.

Mladenov, N., Sommaruga, R., Morales-Baquero, R., Laurion, I., Camarero, L., Dieguez, M. C., Camacho, A., Delgado, A., Torres, O., Chen, Z., Felip, M., Reche, I., 2011. Dust inputs and bacteria influence dissolved organic matter in clear alpine lakes. Nature Communications, 2, 405. https://doi.org/10.1038/ncomms1411.

Moore, C.M., Mills, M.M., Arrigo, K.R., Berman-Frank, I., Bopp, L., Boyd, P.W., Galbraith, E.D., Geider, R.J., Guieu, C., Jaccard, S.L., Jickells, T.D., La Roche, J., Lenton, T.M., Mahowald, N.M., Marañón E., Marinov, I., Moore, J.K., Nakatsuka, T., Oschlies, A., Saito, M.A., Thingstad, T.F., Tsuda, A., Ulloa, O., 2013. Processes and patterns of oceanic nutrient limitation. Nature Geoscience, 6(9), 701. https://doi.org/10.1038/ngeo1765.

Mopper, K., Schultz,C.A., 1993. Fluorescence as a possible tool for studying the nature and water column distribution of DOC components. Marine Chemistry, 41, 229–238. https://doi.org/10.1016/0304-4203(93)90124-7.

Mopper, K., Kieber, D.J., 2002. Photochemistry and the cycling of carbon, sulfur, nitrogen and phosphorus. In Biogeochemistry of marine dissolved organic matter (Vol. 455). San Diego, CA: Academic Press.

Morel, A., Claustre, H., Antoine, D., Gentili, B., 2007. Natural variability of bio-optical properties in Case 1 waters: attenuation and reflectance within the visible and near-UV spectral domains, as observed in South Pacific and Mediterranean waters. Biogeosciences Discussions, 4(4), 2147-2178.

Morel, A., Gentili, B., 2009. The dissolved yellow substance and the shades of blue in the Mediterranean Sea. Biogeosciences, 6(11), 2625-2636. https://doi.org/10.5194/bg-6-2625-2009.

Moulin, C., Lambert, C.E., Dulac, F., Dayan, U., 1997. Control of atmospheric export of dust from North Africa by the North Atlantic Oscillation. Nature, 387(6634), 691. https://doi.org/ 10.1038/42679.

Müller, M.N., Schulz, K.G., Riebesell, U., 2010. Effects of long-term high CO 2 exposure on two species of coccolithophores. Biogeosciences, 7(3), 1109-1116. https://doi.org/10.5194/bg-7-1109-2010.

Murphy, J., Riley, J.P., 1962. A modified single solution method for the determination of phosphate in natural waters. Analytica chimica acta, 27, 31-36. https://doi.org/10.1016/S0003-2670(00)88444-5.

Murphy, K.R., Ruiz, G.M., Dunsmuir, W.T., Waite, T.D., 2006. Optimized parameters for fluorescence-based verification of ballast water exchange by ships. Environmental science & technology 40(7), 2357-2362. https:/doi.org/10.1021/es0519381.

Murphy, K.R., Stedmon C.A., Waite T.D., Ruiz G.M., 2008. Distinguishing between terrestrial and autochthonous organic matter in marine environments using fluorescence spectroscopy. Marine Chemistry 108, 40-58. https://doi.org/10.1016/j.marchem.2007.10.003.

Murphy, K.R., Hambly, A., Singh, S., Henderson, R.K., Baker, A., Stuetz, R., Khan, S.J., 2011. Organic matter fluorescence in municipal water recycling schemes: toward a unified PARAFAC model. Environmental Science & Technology 45(7), 2909-2916. https://doi.org/10.1021/es103015e.

Murphy, K.R., Stedmon, C.A., Wenig, P., Bro, R., 2014. OpenFluor–an online spectral library of auto-fluorescence by organic compounds in the environment. Analytical Methods 6(3), 658-661. https:/doi.org/10.1039/C3AY41935E.

Nakatsuka, T., Toda, M., Kawamura, K., Wakatsuchi, M., 2004. Dissolved and particulate organic carbon in the Sea of Okhotsk: Transport from continental shelf to ocean interior. Journal of Geophysical Research: Oceans, 109(C9). https://doi.org/10.1029/2003JC001909.

Nebbioso, A., Piccolo, A., 2013. Molecular characterization of dissolved organic matter (DOM): a critical review. Analytical and Bioanalytical Chemistry, 405(1), 109-124. https://doi.org/10.1007/s00216-012-6363-2.

Nelson, N.B., Carlson, C.A., Steinberg, D.K., 2004. Production of chromophoric dissolved organic matter by Sargasso Sea microbes. Marine Chemistry, 89(1-4), 273-287. https://doi.org/10.1016/j.marchem.2004.02.017.

Nelson, N.B., Siegel, D.A., Carlson, C.A., Swan, C., Smethie Jr, W.M., Khatiwala S., 2007. Hydrography of chromophoric dissolved organic matter in the North Atlantic. Deep-Sea Reasearch I 54, 710-731. https://doi.org/10.1016/j.dsr.2007.02.006.

Nelson, N.B., Siegel, D.A., Carlson, C.A., Swan, C.M., 2010. Tracing global biogeochemical cycles and meridional overturning circulation using chromophoric dissolved organic matter. Geophysical Research Letters 37(3). https://doi.org/10.1029/2009GL042325.

Nelson, N.B., Siegel, D.A., 2013. The global distribution and dynamics of chromophoric dissolved organic matter. Annual Review Marine Science 5, 447-476. https://doi.org/10.1146/annurev-marine-120710-100751.

Nelson, N.B., Gauglitz, J.M., 2016. Optical signatures of dissolved organic matter transformation in the global ocean. Frontiers in Marine Science 2, 118. https://doi.org/10.3389/fmars.2015.00118.

Nickovic, S., Vukovic, A., Vujadinovic, M., 2013. Atmospheric processing of iron carried by mineral dust. Atmospheric Chemistry and Physics, 13(18), 9169. https://doi.org/10.5194/acp-13-9169-2013.

Nieto-Cid, M., Álvarez-Salgado, X.A., Gago, J., Pérez, F.F., 2005. DOM fluorescence, a tracer for biogeochemical processes in a coastal upwelling system (NW Iberian Peninsula). Marine Ecology Progress Series 297, 33-50. https://doi.org/10.3354/meps297033.

Nieto-Cid, M., Álvarez-Salgado, X.A., Pérez, F.F., 2006. Microbial and photochemical reactivity of fluorescent dissolved organic matter in a coastal upwelling system. Limnology and Oceanography, 51(3), 1391-1400. https://doi.org/10.4319/lo.2006.51.3.1391.

Nimptsch, J., Woelfl, S., Osorio, S., Valenzuela, J., Ebersbach, P., von Tuempling, W., Palma, R., Encina, F., Figueroa, D., Kamjunke, N., Graeber, D., 2015. Tracing dissolved organic matter (DOM) from land-based aquaculture systems in North Patagonian streams. Science of the Total Environment, 537, 129-138. https://doi.org/10.1016/j.scitotenv.2015.07.160.

Nyaga, J.M., Cramer, M.D., Neff, J.C., 2013. Atmospheric nutrient deposition to the west coast of South Africa. Atmospheric environment, 81, 625-632. https://doi.org/10.1016/j.atmosenv.2013.09.021.

Ogawa, H., Amagai, Y., Koike, I., Kaiser, K., Benner, R., 2001. Production of refractory dissolved organic matter by bacteria. Science, 292(5518), 917-920. https://doi.org/10.1126/science.1057627.

Organelli, E., Bricaud, A., Antoine, D., Matsuoka, A., 2014. Seasonal dynamics of light absorption by chromophoric dissolved organic matter (CDOM) in the NW Mediterranean Sea (BOUSSOLE site). Deep Sea Research 91, 72-85. https://doi.org/10.1016/j.dsr.2014.05.003.

Osburn, C.L., Stedmon, C.A., 2011. Linking the chemical and optical properties of dissolved organic matter in the Baltic–North Sea transition zone to differentiate three allochthonous inputs. Marine chemistry 126(1-4), 281-294. https://doi.org/10.1016/j.marchem.2011.06.007.

Osburn, C.L., Handsel, L.T., Mikan, M.P., Paerl, H.W., Montgomery, M.T., 2012. Fluorescence tracking of dissolved and particulate organic matter quality in a river-dominated estuary. Environmental science & technology, 46(16), 8628-8636. https://doi.org/10.1021/es3007723.

Osburn, C.L., Boyd, T.J., Montgomery, M.T., Bianchi, T.S., Coffin, R.B., Paerl, H.W., 2016. Optical proxies for terrestrial dissolved organic matter in estuaries and coastal waters. Frontiers in Marine Science, 2, 127. https://doi.org/10.3389/fmars.2015.00127.

Painter, S.C., Lapworth, D.J., Woodward, E.M.S., Kroeger, S., Evans, C.D., Mayor, D.J., Sanders, R.J., 2018. Terrestrial dissolved organic matter distribution in the North Sea. Science of the Total Environment, 630, 630-647. https://doi.org/10.1016/j.scitotenv.2018.02.237.

Para, J., Coble, P.G., Charrière, B., Tedetti, M., Fontana, C., Sempéré, R., 2010. Fluorescence and absorption properties of chromophoric dissolved organic matter (CDOM) in coastal surface waters of the northwestern Mediterranean Sea, influence of the Rhône River. Biogeosciences 7(12), 4083-4103. https://doi.org/10.5194/bg-7-4083-2010.

Park, J.S., Wade, T.L., Sweet, S., 2001. Atmospheric distribution of polycyclic aromatic hydrocarbons and deposition to Galveston Bay, Texas, USA. Atmospheric Environment, 35(19), 3241-3249. https://doi.org/10.1016/S1352-2310(01)00080-2.

Paytan, A., Mackey, K.R., Chen, Y., Lima, I.D., Doney, S.C., Mahowald, N., Labiosa, R., Post, A.F., 2009. Toxicity of atmospheric aerosols on marine phytoplankton. Proceedings of the National Academy of Sciences, 106(12), 4601-4605. https://doi.org/10.1073/pnas.0811486106.

Pérez, G.L., Galí, M., Royer, S.J., Sarmento, H., Gasol, J.M., Marrasé, C., Simó, R., 2016. Bio-optical characterization of offshore NW Mediterranean waters: CDOM contribution to the absorption budget and diffuse attenuation of downwelling irradiance. Deep Sea Research Part I: Oceanographic Research Papers, 114, 111-127. https://doi.org/10.1016/j.dsr.2016.05.011.

Perkins, S., 2001. Dust, the Thermostat How tiny airborne particles manipulate global climate. Science News, 160(13), 200-2002.

Pitta, E., Zeri, C., Tzortziou, M., Mousdis, G., Scoullos, M., 2017. Seasonal variations in dissolved organic matter composition using absorbance and fluorescence

spectroscopy in the Dardanelles Straits–North Aegean Sea mixing zone. Continental Shelf Research 149, 82-95. https://doi.org/10.1016/j.csr.2016.07.013.

Placenti, F., Azzaro, M., Artale, V., La Ferla, R., Caruso, G., Santinelli, C., Maimone, G., Monticelli, L.S., Quinci, E., Sprovieri, M., 2018. Biogeochemical patterns and microbial processes in the Eastern Mediterranean Deep Water of Ionian Sea. Hydrobiologia 815, 97-112. https://doi.org/10.1007/s10750-018-3554-7.

Pongkiatkul, P., Oanh, N.T.K., 2007. Assessment of potential long-range transport of particulate air pollution using trajectory modeling and monitoring data. Atmospheric Research, 85(1), 3-17. https://doi.org/10.1016/j.atmosres.2006.10.003.

Pósfai, M., Li, J., Anderson, J.R., Buseck, P.R., 2003. Aerosol bacteria over the southern ocean during ACE-1. Atmospheric Research, 66:231-240. https://doi.org/10.1016/S0169-8095(03)00039-5.

Pósfai, M., Buseck, P.R., 2010. Nature and climate effects of individual tropospheric aerosol particles. Annual Review of Earth and Planetary Sciences, 38. https://doi.org/10.1146/annurev.earth.031208.100032.

Prospero, J.M., Ginoux, P., Torres, O., Nicholson, S.E., Gill, T.E., 2002. Environmental characterization of global sources of atmospheric soil dust identified with the Nimbus 7 Total Ozone Mapping Spectrometer (TOMS) absorbing aerosol product. Reviews of geophysics, 40(1). https://doi.org/10.1029/2000RG000095.

Pulido-Villena, E., Wagener, T., Guieu, C., 2008a. Bacterial response to dust pulses in the western Mediterranean: Implications for carbon cycling in the oligotrophic ocean. Global Biogeochemical Cycles, 22(1). https://doi.org/10.1029/2007GB003091.

Pulido-Villena, E., Reche, I., Morales-Baquero, R., 2008b. Evidence of an atmospheric forcing on bacterioplankton and phytoplankton dynamics in a high mountain lake. Aquatic sciences, 70(1), 1-9. https://doi.org/10.1007/s00027-007-0944-8.

Pulido-Villena, E., Rerolle, V., Guieu, C., 2010. Transient fertilizing effect of dust in P-deficient LNLC surface ocean. Geophysical Research Letters, 37(1). https://doi.org/10.1029/2009GL041415.

Pulido-Villena, E., Baudoux, A.C., Obernosterer, I., Landa, M., Caparros, J., Catala, P., Georges, C., Harmand, J., Guieu, C., 2014. Microbial food web dynamics in response to a Saharan dust event: results from a mesocosm study in the oligotrophic Mediterranean Sea. Biogeosciences, 5607. https://doi.org/10.5194/bg-11-5607-2014.

Pujo-Pay, M., Conan, P., Oriol, L., Cornet-Barthaux, V., Falco, C., Ghiglione, J.F., Goyet, C., Moutin T., Prieur, L., 2011. Integrated survey of elemental stoichiometry (C, N, P) from the western to eastern Mediterranean Sea. Biogeosciences 8(4), 883-899. https://doi.org/10.5194/bg-8-883-2011.

Rahav, E., Shun-Yan, C., Cui, G., Liu, H., Tsagaraki, T.M., Giannakourou, A., Tsiola, A., Psarra, S., Lagaria, A., Mulholland, M.R., Stathopoulou, E., Paraskevi, P., Herut, B., Berman-Frank, I., 2016a. Evaluating the impact of atmospheric depositions on springtime dinitrogen fixation in the Cretan Sea (Eastern Mediterranean), a mesocosm approach. Frontiers in Marine Science 3:1–13. https://doi.org/10.3389/fmars.2016.00180.

Rahav, E., Ovadia, G., Paytan, A., Herut, B., 2016b. Contribution of airborne microbes to bacterial production and N2 fixation in seawater upon aerosol deposition. Geophysical Research Letter 43:1–9. https://doi.org/10.1002/2015GL066898.

Rahav, E., Bar-Zeev, E., 2017. Sewage outburst triggers Trichodesmium bloom and enhance N2 fixation rates, Sci. Rep., 7(1), 4367. https://doi.org/10.1038/s41598-017-04622-8.

Rahav, E., Paytan, A., Mescioglu, E., Galletti, Y., Rosenfeld, S., Raveh, O., Santinelli, C., Ho, T.-Y. Herut, B., 2018. Airborne microbes contribute to N2 fixation in surface water of the Northern Red Sea. Geophysical Research Letters, 45(12), 6186-6194. https://doi.org/10.1029/2018GL077132.

Raven, J. A., & Falkowski, P. G. (1999). Oceanic sinks for atmospheric CO2. Plant, Cell & Environment, 22(6), 741-755. https://doi.org/10.1046/j.1365-3040.1999.00419.x.

Raven, J., Caldeira, K., Elderfield, H., Hoegh-Guldberg, O., Liss, P., Riebesell, U., Watson, A., 2005. Ocean acidification due to increasing atmospheric carbon dioxide. The Royal Society.

Raymond, P. A., 2005. The composition and transport of organic carbon in rainfall: Insights from the natural (13C and 14C) isotopes of carbon. Geophysical Research Letters, 32(14). https://doi.org/10.1029/2005GL022879.

Reche, I., Ortega-Retuerta, E., Romera, O., Villena, E.P., Baquero, R.M., Casamayor, E.O., 2009. Effect of Saharan dust inputs on bacterial activity and community composition in Mediterranean lakes and reservoirs. Limnology and Oceanography, 54(3), 869-879. https://doi.org/10.4319/lo.2009.54.3.0869.

Remoudaki, E., Bergametti, G., Buat-Ménard, P., 1991. Temporal variability of atmospheric lead concentrations and fluxes over the northwestern Mediterranean Sea. Journal of Geophysical Research: Atmospheres, 96(D1), 1043-1055. https://doi.org/10.1029/90JD00111.

Repeta, D.J., 2015. Chemical characterization and cycling of dissolved organic matter. In Biogeochemistry of Marine Dissolved Organic Matter (Second Edition) (pp. 21-63). https://doi.org/10.1016/B978-0-12-405940-5.00002-9.

Retelletti Brogi, S., Gonnelli, M., Vestri, S., Santinelli, C., 2015. Biophysical processes affecting DOM dynamics at the Arno river mouth (Tyrrhenian Sea). Biophysical chemistry, 197, 1-9. https://doi.org/10.1016/j.bpc.2014.10.004.

Ribera d'Alcalà, M., Civitarese, G., Conversano, F., Lavezza, R., 2003. Nutrient ratios and fluxes hint at overlooked processes in the Mediterranean Sea. Journal of Geophysical Research: Oceans, 108(C9). https://doi.org/10.1029/2002JC001650.

Ridame, C., Guieu, C., 2002. Saharan input of phosphate to the oligotrophic water of the open western Mediterranean Sea. Limnology and Oceanography, 47(3), 856-869. https://doi.org/10.4319/lo.2002.47.3.0856.

Ridgwell, A., Arndt, S. 2015. Why Dissolved Organics Matter: DOC in Ancient Oceans and Past Climate Change. In: Hansell, D., Carlson (2nd ed.) 2015. Biogeochemistry of Marine Dissolved Organic Matter, pp 1–20.

Romera-Castillo, C., Sarmento, H., Álvarez-Salgado, X.A., Gasol, J.M., Marrasé, C., 2011. Net production and consumption of fluorescent colored dissolved organic matter by natural bacterial assemblages growing on marine phytoplankton exudates. Applied and environmental microbiology, 77(21), 7490-7498. https://doi.org/10.1128/AEM.00200-11.

Romero, E., Peters, F., Marrasé, C., Guadayol, Ò., Gasol, J.M., Weinbauer, M.G., 2011. Coastal Mediterranean plankton stimulation dynamics through a dust storm event: An experimental simulation. Estuarine, Coastal and Shelf Science, 93(1), 27-39. https://doi.org/10.1016/j.ecss.2011.03.019.

Rowe, O.F., Dinasquet, J., Paczkowska, J., Figueroa, D., Riemann, L., Andersson, A., 2018. Major differences in dissolved organic matter characteristics and bacterial processing over an extensive brackish water gradient, the Baltic Sea. Marine Chemistry, 202, 27-36. https://doi.org/10.1016/j.marchem.2018.01.010.

Rubino, A., Hainbucher, D., 2007. A large abrupt change in the abyssal water masses of the eastern Mediterranean. Geophysical Research Letters 34(23). https://doi.org/10.1029/2007GL031737.

Rullkötter, J., 2006. Organic matter: the driving force for early diagenesis. In Marine geochemistry (pp. 125-168). Springer Berlin Heidelberg.

Sánchez-Pérez, E.D., Marín, I., Nunes, S., Fernández-González, L., Peters, F., Pujo-Pay, M., Conan, P., Marrasé, C, 2016. Aerosol inputs affect the optical signatures of dissolved organic matter in NW Mediterranean coastal waters. Scientia Marina 80(4), 437-446. https://doi.org/10.3989/scimar.04318.20B.

Santinelli, C., Ribotti, A., Sorgente, R., Gasparini, G.P., Nannicini, L., Vignudelli, S., Seritti, A., 2008. Coastal dynamics and dissolved organic carbon in the western Sardinian shelf (Western Mediterranean). Journal of Marine Systems, 74(1-2), 167-188. https://doi.org/10.1016/j.jmarsys.2007.12.005.

Santinelli, C., Nannicini, L., Seritti, A., 2010. DOC dynamics in the meso and bathypelagic layers of the Mediterranean Sea. Deep Sea research II 57, 1446-1459. https://doi.org/10.1016/j.dsr2.2010.02.014.

Santinelli, C., Hansell, D.A., d'Alcalà, M.R., 2013. Influence of stratification on marine dissolved organic carbon (DOC) dynamics: The Mediterranean Sea case. Progress in oceanography, 119, 68-77. https://doi.org/10.1016/j.pocean.2013.06.001.

Santinelli, 2015. DOC in the Mediterranean Sea. In: Hansell D.A, Carlson C.A. (Eds.), Biogeochemestry of Marine Dissolved Organic Matter (Second edition), Academic Press, San Diego, pp. 579-608. https://doi.org/10.1016/B978-0-12-405940-5.00013-3.

Santinelli, C., Follett, C., Brogi, S.R., Xu, L., Repeta, D., 2015. Carbon isotope measurements reveal unexpected cycling of dissolved organic matter in the deep Mediterranean Sea. Marine Chemistry 177, 267-277. https://doi.org/10.1016/j.marchem.2015.06.018.

Sarmiento, J.L., Gruber, N., 2006. Ocean biogeochemical cycles. Princeton University.

Sarthou, G., Jeandel, C., 2001. Seasonal variations of iron concentrations in the Ligurian Sea and iron budget in the Western Mediterranean Sea. Marine Chemistry, 74(2), 115-129. https://doi.org/10.1016/S0304-4203(00)00119-5.

Saxena, P., Hildemann, L.M., McMurry, P.H., Seinfeld, J.H., 1995. Organics alter hygroscopic behavior of atmospheric particles. Journal of Geophysical Research: Atmospheres, 100(D9), 18755-18770. https://doi.org/10.1029/95JD01835.

Schroeder, K., Ribotti, A., Borghini, M., Sorgente, R., Perilli, A., Gasparini, G.P., 2008. An extensive western Mediterranean deep water renewal between 2004 and 2006. Geophysical Research Letters, 35(18). https://doi.org/10.1029/2008GL035146.

Sciare, J., Bardouki, H., Moulin, C., Mihalopoulos, N., 2003. Aerosol sources and their contribution to the chemical composition of aerosols in the Eastern Mediterranean Sea during summertime. Atmospheric Chemistry and Physics, 3(1), 291-302. https://doi.org/10.5194/acp-3-291-2003.

Seinfeld, J.H., Pandis, S.N., 2016. Atmospheric chemistry and physics: from air pollution to climate change. John Wiley & Sons.

Sempéré, R., Kawamura, K., 2003. Trans-hemispheric contribution of C2–C10 α, ω-dicarboxylic acids, and related polar compounds to water-soluble organic carbon in the western Pacific aerosols in relation to photochemical oxidation reactions. Global Biogeochemical Cycles, 17(2). https://doi.org/10.1029/2002GB001980.

Senesi, N., Miano, T.M., Provenzano, M.R., Brunetti, G., 1989. Spectroscopic and compositional comparative characterization of IHSS reference and standard fulvic and humic acids of various origin. Science of the total environment 81, 143-156. https://doi.org/10.1016/0048-9697(89)90120-4.

Seritti, A., Russo, D., Nannicini, L., Del Vecchio, R., 1998. DOC, absorption and fluorescence properties of estuarine and coastal waters of the Northern Tyrrhenian Sea. Chemical Speciation & Bioavailability 10(3), 95-106. https://doi.org/10.3184/095422998782775790.

Shulman, M.L., Jacobson, M.C., Carlson, R.J., Synovec, R.E., Young, T.E., 1996. Dissolution behavior and surface tension effects of organic compounds in nucleating cloud droplets. Geophysical Research Letters, 23(3), 277-280. https://doi.org/10.1029/95GL03810.

Siegel, D.A., Maritorena, S., Nelson, N.B., Hansell, D.A., Kayser-Lorenzi, M., 2002. Global distributions and dynamics of colored dissolved and detrital organic materials. Journal of Geophysical Research 107 (C12), 3228. https://doi.org/10.1029/2001JC000965.

Siegel, D.A., Maritorena, S., Nelson, N.B., Behrenfeld, M.J., McClain, C.R., 2005. Colored dissolved organic matter and its influence on the satellite-based characterization of the ocean biosphere. Geophysical Research Letters, 32(20). https://doi.org/10.1029/2005GL024310.

Simon, M., Alldredge, A., Azam F., 1990. Bacterial carbon dynamics on marine snow, Mar. Ecol. Prog. Ser., 65(3), 205–211.

Simon, M., Grossart, H.P., Schweitzer, B., Ploug, H., 2002. Microbial ecology of organic aggregates in aquatic ecosystems. Aquatic microbial ecology, 28(2), 175-211. https://doi.org/10.3354/ame028175.

Simoneit, B.R., 2002. Biomass burning—a review of organic tracers for smoke from incomplete combustion. Applied Geochemistry, 17(3), 129-162. https://doi.org/10.1016/S0883-2927(01)00061-0.

Simoneit, B.R., Elias, V.O., 2000. Organic tracers from biomass burning in atmospheric particulate matter over the ocean. Marine Chemistry, 69(3-4), 301-312. https://doi.org/10.1016/S0304-4203(00)00008-6.

Simoneit, B.R., Kobayashi, M., Mochida, M., Kawamura, K., Lee, M., Lim, H. J., Turpin, B.J., Komazaki, Y, 2004. Composition and major sources of organic compounds of aerosol particulate matter sampled during the ACE-Asia campaign. Journal of Geophysical Research: Atmospheres, 109(D19). https://doi.org/10.1029/2004JD004598.

Simoneit, B.R., 2006. Atmospheric transport of terrestrial organic matter to the sea. In Marine Organic Matter: Biomarkers, Isotopes and DNA (pp. 165-208). Springer, Berlin, Heidelberg. https://doi.org/10.1007/698_2_006.

Singh, N., Abiven, S., Torn, M.S., Schmidt, M.W.I., 2012. Fire-derived organic carbon in soil turns over on a centennial scale. Biogeosciences, 9(8), 2847. https://doi.org/10.5194/bg-9-2847-2012.

Sipler, R.E., Bronk, D.A., 2015. Dynamics of dissolved organic nitrogen. In Biogeochemistry of Marine Dissolved Organic Matter (Second Edition) (pp. 127-232). https://doi.org/10.1016/B978-0-12-405940-5.00004-2.

Søndergaard, M., Stedmon, C.A., Borch, N.H., 2003. Fate of terrigenous dissolved organic matter (DOM) in estuaries: aggregation and bioavailability. Ophelia, 57(3), 161-176. https://doi.org/10.1080/00785236.2003.10409512.

Speicher, E.A., Moran, S.B., Burd, A.B., Delfanti, R., Kaberi, H., Kelly, R.P., Papucci, C., Smith, J.N., Stavrakakis, S., Torricelli, L., Zervakis, V., 2006. Particulate organic carbon export fluxes and size-fractionated POC/234Th ratios in the Ligurian, Tyrrhenian and Aegean Seas. Deep Sea Research Part I: Oceanographic Research Papers, 53(11), 1810-1830. https://doi.org/10.1016/j.dsr.2006.08.005.

Stedmon, C.A., Markager, S., Bro, R., 2003. Tracing dissolved organic matter in aquatic environments using a new approach to fluorescence spectroscopy. Marine Chemistry 82, 239-254. https://doi.org/10.1016/S0304-4203(03)00072-0.

Stedmon, C.A., Markager, S., 2005a. Resolving the variability in dissolved organic matter fluorescence in a temperate estuary and its catchment using PARAFAC analysis. Limnology and Oceanography 50, 686-697. https://doi.org/10.4319/lo.2005.50.2.0686.

Stedmon, C.A., Markager, S., 2005b. Tracing the production and degradation of autochthonous fractions of dissolved organic matter by fluorescence analysis. Limnology and Oceanography 50, 1415-1426. https://doi.org/10.4319/lo.2005.50.5.1415.

Stedmon, C.A., Markager, S., Tranvik, L., Kronberg, L., Slätis, T., Martinsen, W., 2007. Photochemical production of ammonium and transformation of dissolved organic matter in the Baltic Sea. Marine Chemistry 104(3), 227-240. https://doi.org/10.1016/j.marchem.2006.11.005.

Stedmon, C.A., Bro, R., 2008. Characterizing dissolved organic matter fluorescence with parallel factor analysis: a tutorial. Limnology and Oceanography: Methods 6(11), 572-579. https://doi.org/10.4319/lom.2008.6.572.

Stedmon, C.A., Álvarez-Salgado, X.A., 2011. Shedding light on a black box: UV–visible spectroscopic characterization of marine dissolved organic matter. Jiao, N. and Azam, F., Senders, 62-63.

Stedmon, C.A., Thomas, D.N., Papadimitriou, S., Granskog, M.A., & Dieckmann, G.S., 2011. Using fluorescence to characterize dissolved organic matter in Antarctic sea ice brines. Journal of Geophysical Research: Biogeosciences, 116(G3). https://doi.org/10.1029/2011JG001716.

Stedmon, C.A., Nelson, N.B., 2015. The optical properties of DOM in the ocean. In Biogeochemistry of Marine Dissolved Organic Matter (Second Edition) (pp. 481-508). https://doi.org/10.1016/B978-0-12-405940-5.00010-8.

Steffen, W., Sanderson, R. A., Tyson, P. D., Jäger, J., Matson, P. A., Moore III, B., Oldfield, F., Richardson, K., Schellnhuber, H.J., Turner, B.L., Wasson, R. J., 2006. Global change and the earth system: a planet under pressure. Springer Science & Business Media.

Steffen, W., Persson, Å., Deutsch, L., Zalasiewicz, J., Williams, M., Richardson, K., Crumley, C., Crutzen, P., Folke, C., Gordon, L., Molina, M., Ramanathan, V., Rockström, J., Scheffer, M., Schellnhuber, H.J., Svedin, U., 2011. The Anthropocene: From global change to planetary stewardship. AMBIO: A Journal of the Human Environment, 40(7), 739-761. https://doi.org/10.1007/s13280-011-0185-x.

Stein, R., Macdonald, R.W., 2004. Organic carbon budget: Arctic Ocean vs. global ocean. In The organic carbon cycle in the Arctic Ocean (pp. 315-322). Springer, Berlin, Heidelberg. https://doi.org/10.1007/978-3-642-18912-8_8.

Stubbins, A., Lapierre, J.F., Berggren, M., Prairie, Y.T., Dittmar, T., del Giorgio, P.A., 2014. What's in an EEM? Molecular signatures associated with dissolved organic fluorescence in boreal Canada. Environmental science & technology, 48(18), 10598-10606. https://doi.org/10.1021/es502086e.

Sun, J., Ariya, P.A., 2006. Atmospheric organic and bio-aerosols as cloud condensation nuclei (CCN): A review. Atmospheric Environment, 40(5), 795-820. https://doi.org/10.1016/j.atmosenv.2005.05.052.

Suttle, C.A., 1994. The significance of viruses to mortality in aquatic microbial communities. Microbial Ecology, 28(2), 237-243.

Suttle, C.A., 2007. Marine viruses—major players in the global ecosystem. Nature Reviews Microbiology, 5(10), 801. https://doi.org/10.1038/nrmicro1750.

Tan, J., Xiang, P., Zhou, X., Duan, J., Ma, Y., He, K., Cheng, Y., Yu, J., Querol, X., 2016. Chemical characterization of humic-like substances (HULIS) in PM2. 5 in Lanzhou, China. Science of the Total Environment, 573, 1481-1490. https://doi.org/10.1016/j.scitotenv.2016.08.025.

Tanaka, T., Thingstad, T.F., Christaki, U., Colombet, J., Cornet-Barthaux, V., Courties, C., Grattepanche, J.,-D., Lagaria, A., Nedoma, J., Oriol, L., Psarra, S., Pujo-Pay, M., Van Wambeke, F., 2011. Lack of P-limitation of phytoplankton and heterotrophic prokaryotes in surface waters of three anticyclonic eddies in the stratified Mediterranean Sea. Biogeosciences, 8(2), 525-538. https://doi.org/10.5194/bg-8-525-2011.

Tedetti, M., Sempéré, R., 2006. Penetration of ultraviolet radiation in the marine environment. A review. Photochemistry and photobiology, 82(2), 389-397. https://doi.org/10.1562/2005-11-09-IR-733.

Tedetti, M., Longhitano, R., Garcia, N., Guigue, C., Ferretto, N., Goutx, M., 2012. Fluorescence properties of dissolved organic matter in coastal Mediterranean waters influenced by a municipal sewage effluent (Bay of Marseilles, France). Environmental Chemistry, 9(5), 438-449. https://doi.org/10.1071/EN12081.

Ternon, E., Guieu, C., Loÿe-Pilot, M. D., Leblond, N., Bosc, E., Gasser, B., Miquel, J.-C., Martín, J., 2010. The impact of Saharan dust on the particulate export in the water column of the North Western Mediterranean Sea. Biogeosciences, 7(3), 809-826. https://doi.org/10.5194/bg-7-809-2010.

Theodosi, C., Panagiotopoulos, C., Nouara, A., Zarmpas, P., Nicolaou, P., Violaki, K., Kanakidou, M., Sempéré, R., Mihalopoulos, N., 2017. Sugars in atmospheric aerosols over the Eastern Mediterranean. Progress in Oceanography. https://doi.org/10.1016/j.pocean.2017.09.001.

Thingstad, T.F., Zweifel, U.L., Rassoulzadegan, F., 1998. P limitation of heterotrophic bacteria and phytoplankton in the northwest Mediterranean. Limnology and Oceanography, 43(1), 88-94. https://doi.org/10.4319/lo.1998.43.1.0088.

Tipping, E., Benham, S., Boyle, J. F., Crow, P., Davies, J., Fischer, U., Guyatt, H., Helliwell, R., Jackson-Blake, L., Lawlor, A.J., Monteith, D.T., Roweg, E.C., Tobermanac, H., 2014. Atmospheric deposition of phosphorus to land and freshwater. Environmental Science: Processes & Impacts, 16(7), 1608-1617.

Tomasi, C., Lupi, A., 2017. Coagulation, Condensation, Dry and Wet Deposition, and Cloud Droplet Formation in the Atmospheric Aerosol Life Cycle. Atmospheric Aerosols: Life Cycles and Effects on Air Quality and Climate, 1.

Torfstein, A., Teutsch, N., Tirosh, O., Shaked, Y., Rivlin, T., Zipori, A., Stein, M., Lazar, B., Erel, Y., 2017. Chemical characterization of atmospheric dust from a weekly time series in the north Red Sea between 2006 and 2010. Geochimica et Cosmochimica Acta, 211, 373-393. https://doi.org/10.1016/j.gca.2017.06.007.

Trochkine, D., Iwasaka, Y., Matsuki, A., Yamada, M., Kim, Y. S., Nagatani, T., Zhang D., Shi, G.-Y. Shen, Z., 2003. Mineral aerosol particles collected in Dunhuang, China, and their comparison with chemically modified particles collected over Japan. Journal of Geophysical Research: Atmospheres, 108(D23). https://doi.org/10.1029/2002JD003268.

Tsagaraki, T.M., Herut, B., Rahav, E., Berman Frank, I.R., Tsiola, A., Tsapakis, M., Giannakourou, A., Gogou, A., Panagiotopoulos, C., Violaki, K., Psarra, S., Lagaria, A., Christou, E., Papageorgiou, N., Zervoudaki, S., Fernandenz de Puelles, M.L., Nikolioudakis, N., Meador, T.B., Tanaka, T., Pedrotti, M.L. Krom, M.D., Pitta, P., 2017. Atmospheric Deposition Effects on Plankton Communities in the Eastern Mediterranean: A Mesocosm Experimental Approach. Frontiers in Marine Science, 4, 210. https://doi.org/10.3389/fmars.2017.00210.

Tsiola, A., Pitta, P., Giannakourou, A., Bourdin, G., Marro, S., Maugendre, L., Pedrotti, M.L., Gazeau, F., 2017. Ocean acidification and viral replication cycles: frequency of lytically infected and lysogenic cells during a mesocosm experiment in the NW Mediterranean Sea. Estuarine, Coastal and Shelf Science, 186, 139-151. https://doi.org/10.1016/j.ecss.2016.05.003.

Usher, C.R., Michel, A.E., Grassian, V.H., 2003. Reactions on mineral dust. Chemical Reviews, 103(12), 4883-4940. https://doi.org/10.1021/cr020657y.

Ussher, S.J., Achterberg, E.P., Powell, C., Baker, A.R., Jickells, T.D., Torres, R., Worsfold, P.J., 2013. Impact of atmospheric deposition on the contrasting iron biogeochemistry of the North and South Atlantic Ocean. Global Biogeochemical Cycles, 27(4), 1096-1107. https://doi.org/10.1002/gbc.20056.

Vähätalo, A.V., Zepp, R.G., 2005. Photochemical mineralization of dissolved organic nitrogen to ammonium in the Baltic Sea. Environmental Science & Technology, 39(18), 6985-6992. https://doi.org/10.1021/es050142z.

Van Wambeke, F., Heussner, S., Diaz, F., Raimbault, P., Conan, P., 2002. Small-scale variability in the coupling/uncoupling of bacteria, phytoplankton and organic carbon fluxes along the continental margin of the Gulf of Lions, Northwestern Mediterranean Sea. Journal of Marine Systems, 33, 411-429. https://doi.org/10.1016/S0924-7963(02)00069-6.

Vignudelli, S., Santinelli, C., Murru, E., Nannicini, L., Seritti, A., 2004. Distributions of dissolved organic carbon (DOC) and chromophoric dissolved organic matter (CDOM) in coastal waters of the northern Tyrrhenian Sea (Italy). Estuarine, Coastal and Shelf Science 60(1), 133-149. https://doi.org/10.1016/j.ecss.2003.11.023.

Vincent, J., Laurent, B., Losno, R., Bon Nguyen, E., Roullet, P., Sauvage, S., Chevaillier, S., Coddeville, P., Ouboulmane, N., di Sarra, A.G., Tovar-Sánchez, A., Sferlazzo, D., Massanet, A., Triquet, S., Morales Baquero, R., Fornier, M., Coursier, C., Desboeufs, K., Dulac, F., Bergametti, G., 2016. Variability of mineral dust deposition in the western Mediterranean basin and south-east of France. Atmospheric Chemistry and Physics, 16(14), 8749-8766. https://doi.org/10.5194/acp-16-8749-2016.

Violaki, K., Bourrin, F., Aubert, D., Kouvarakis, G., Delsaut, N., Mihalopoulos, N., 2017. Organic phosphorus in atmospheric deposition over the Mediterranean Sea: An

important missing piece of the phosphorus cycle. Progress in Oceanography. https://doi.org/10.1016/j.pocean.2017.07.009.
Visschedijk, A.H.J., Denier vanderGon, H.A.C., Hulskotte, J.H.J., Quass, U., 2013, January). Anthropogenic Vanadium emissions to air and ambient air concentrations in North-West Europe. In E3S Web of Conferences (Vol. 1). EDP Sciences. https://doi.org/10.1051/ e3sconf/ 20130103004.
Vodacek, A., Blough, N.V., DeGrandpre, M.D., Peltzer, E.T., Nelson, R.K., 1997. Seasonal variation of CDOM and DOC in the Middle Atlantic Bight: terrestrial inputs and photooxidation. Limnology and Oceanography 42, 674-686. https://doi.org/10.4319/lo.1997.42.4.0674.
Volpe, G., Banzon, V.F., Evans, R.H., Santoleri, R., Mariano, A.J., Sciarra, R., 2009. Satellite observations of the impact of dust in a low-nutrient, low-chlorophyll region: Fertilization or artifact?. Global Biogeochemical Cycles, 23(3). https://doi.org/10.1029/2008GB003216.
Walker, S.A., Amon, R.M., Stedmon, C., Duan, S., Louchouarn, P., 2009. The use of PARAFAC modeling to trace terrestrial dissolved organic matter and fingerprint water masses in coastal Canadian Arctic surface waters. Journal of Geophysical Research 114(G4). https://doi.org/10.1029/2009JG000990.
Wang, X., Ge, T., Xu, C., Xue, Y., Luo, C., 2016. Carbon isotopic (14C and 13C) characterization of fossil-fuel derived dissolved organic carbon in wet precipitation in Shandong Province, China. Journal of Atmospheric Chemistry, 73(2), 207-221.
Weinbauer, M.G., Chen, F., Wilhelm, S.W., 2011. Virus-mediated redistribution and partitioning of carbon in the global oceans. Microbial carbon pump in the ocean, 54-56.
Weishaar, J.L., Aiken, G.R., Bergamaschi, B.A., Fram, M.S., Fujii, R., Mopper, K., 2003. Evaluation of specific ultraviolet absorbance as an indicator of the chemical composition and reactivity of dissolved organic carbon. Environmental science & technology, 37(20), 4702-4708. https://doi.org/ 10.1021/es030360x.
Willey, J.D., Kieber, R.J., Eyman, M.S., Avery, G.B., 2000. Rainwater dissolved organic carbon: concentrations and global flux. Global Biogeochemical Cycles 14(1), 139-148. https://doi.org/10.1029/1999GB900036.
Williams, C.J., Frost, P.C., Xenopoulos, M.A., 2013. Beyond best management practices: pelagic biogeochemical dynamics in urban stormwater ponds. Ecological Applications, 23(6), 1384-1395. https://doi.org/10.1890/12-0825.1.
Williams, C. J., Frost, P. C., Morales-Williams, A. M., Larson, J. H., Richardson, W. B., Chiandet, A. S., & Xenopoulos, M. A., 2016. Human activities cause distinct dissolved organic matter composition across freshwater ecosystems. Global change biology, 22(2), 613-626. https://doi.org/10.1111/gcb.13094.
Womack, A.M., Bohannan, B.J., Green, J.L., 2010. Biodiversity and biogeography of the atmosphere. Philosophical Transactions of the Royal Society B: Biological Sciences, 365(1558), 3645-3653. https://doi.org/10.1098/rstb.2010.0283.
Yahel, G., Sharp, J.H., Marie, D., Häse, C., Genin, A., 2003. In situ feeding and element removal in the symbiont-bearing sponge Theonella swinhoei: Bulk DOC is the major source for carbon. Limnology and Oceanography, 48(1), 141-149. https://doi.org/10.4319/lo.2003.48.1.0141.
Yamashita, Y., Tsukasaki, A., Nishida, T., Tanoue, E., 2007. Vertical and horizontal distribution of fluorescent dissolved organic matter in the Southern Ocean. Marine Chemistry, 106(3-4), 498-509. https://doi.org/10.1016/j.marchem.2007.05.004.Yamashita, Y., Tanoue, E., 2008. Production of bio-refractory fluorescent dissolved organic matter in the ocean interior. Nature Geoscience, 1(9), 579. https://doi.org/10.1038/ngeo279.
Yamashita, Y., Tanoue, E., 2009. Basin scale distribution of chromophoric dissolved organic matter in the Pacific Ocean. Limnology and Oceanography, 54(2), 598-609. https://doi.org/10.4319/lo.2009.54.2.0598.
Yamashita, Y., Scinto, L.J., Maie, N., Jaffé, R., 2010a. Dissolved organic matter characteristics across a subtropical wetland's landscape: application of optical

properties in the assessment of environmental dynamics. Ecosystems 13(7), 1006-1019. https://doi.org/10.1007/s10021-010-9370-1.

Yamashita Y., Cory R.M., Nishioka J., Kuma., Tanoue E., Jaffé R., 2010b. Fluorescence characteristics of dissolved waters of the Okhotsk Sea and northwestern North Pacific Ocean. Deep-sea Research II 57, 1478-1485. https://doi.org/10.1016/j.dsr2.2010.02.016.

Yamashita Y., Boyer J.N., Jaffé R., 2013. Evaluating the distribution of terrestrial dissolved organic matter in a complex coastal ecosystem using fluorescence spectroscopy. Continental Shelf Research 66, 136-144. https://doi.org/10.1016/j.csr.2013.06.010.

Yan, G., Kim, G., 2012. Dissolved organic carbon in the precipitation of Seoul, Korea: implications for global wet depositional flux of fossil-fuel derived organic carbon. Atmospheric environment, 59, 117-124. https://doi.org/10.1016/j.atmosenv.2012.05.044.

Xing, X., Claustre, H., Wang, H., Poteau, A., D'Ortenzio, F., 2014. Seasonal Dynamics in Colored Dissolved Organic Matter in the Mediterranean Sea: Patterns and Drivers. Deep-Sea Research Part I: Oceanographic Research Papers, 93–101. https://doi.org/10.1016/j.dsr.2013.09.008.

Zalasiewicz, J., Williams, M., Haywood, A., Ellis, M., 2011. The Anthropocene: a new epoch of geological time?. https.//doi.org/10.1098/rsta.2010.0339.

Zappoli, S., Andracchio, A., Fuzzi, S., Facchini, M.C., Gelencser, A., Kiss, G.Y., Krivàcsy, Z., Molnàr, A., Mèzsàros, E., Hansson, H.-C., Rosman, K., Zebühr, Y., 1999. Inorganic, organic and macromolecular components of fine aerosol in different areas of Europe in relation to their water solubility. Atmospheric Environment, 33(17), 2733-2743. https://doi.org/10.1016/S1352-2310(98)00362-8.

Zepp, R.G., Erickson Iii, D.J., Paul, N.D., Sulzberger, B., 2007. Interactive effects of solar UV radiation and climate change on biogeochemical cycling. Photochemical & Photobiological Sciences, 6(3), 286-300.

Zeri, C., Beşiktepe, Ş., Giannakourou, A., Krasakopoulou, E., Tzortziou, M., Tsoliakos, D., Pavlidou, A., Mousdis, G., Pitta, E., Scoullos, M., Papathanassiou, E., 2014. Chemical properties and fluorescence of DOM in relation to biodegradation in the interconnected Marmara–North Aegean Seas during August 2008. Journal of Marine Systems, 135, 124-136. https://doi.org/10.1016/j.jmarsys.2013.11.019.

Zhao, Y., Song, K., Shang, Y., Shao, T., Wen, Z., Lv, L., 2017. Characterization of CDOM of river waters in China using fluorescence excitation-emission matrix and regional integration techniques. Journal of Geophysical Research: Biogeosciences, 122(8), 1940-1953. https://doi.org/10.1002/2017JG003820.

Zhou, Z., Guo, L., Shiller, A.M., Lohrenz, S.E., Asper, V.L., Osburn, C.L., 2013. Characterization of oil components from the Deepwater Horizon oil spill in the Gulf of Mexico using fluorescence EEM and PARAFAC techniques. Marine Chemistry, 148, 10-21. https://doi.org/10.1016/j.marchem.2012.10.003.

Zhou, F., Gao, X., Song, J., Chen, C.T.A., Yuan, H., Xing, Q., 2018. Absorption properties of chromophoric dissolved organic matter (CDOM) in the East China Sea and the waters off eastern Taiwan. Continental Shelf Research, 159, 12-23. https://doi.org/10.1016/j.csr.2018.03.005.

Zhu, W.Z., Zhang, H.H., Zhang, J., Yang, G.P., 2018. Seasonal variation in chromophoric dissolved organic matter and relationships among fluorescent components, absorption coefficients and dissolved organic carbon in the Bohai Sea, the Yellow Sea and the East China Sea. Journal of Marine Systems, 180, 9-23. https://doi.org/10.1016/j.jmarsys.2017.12.003.

Ziolkowski, L.A., Druffel, E.R., 2010. Aged black carbon identified in marine dissolved organic carbon. Geophysical Research Letters, 37(16). https://doi.org/10.1029/2010GL043963.